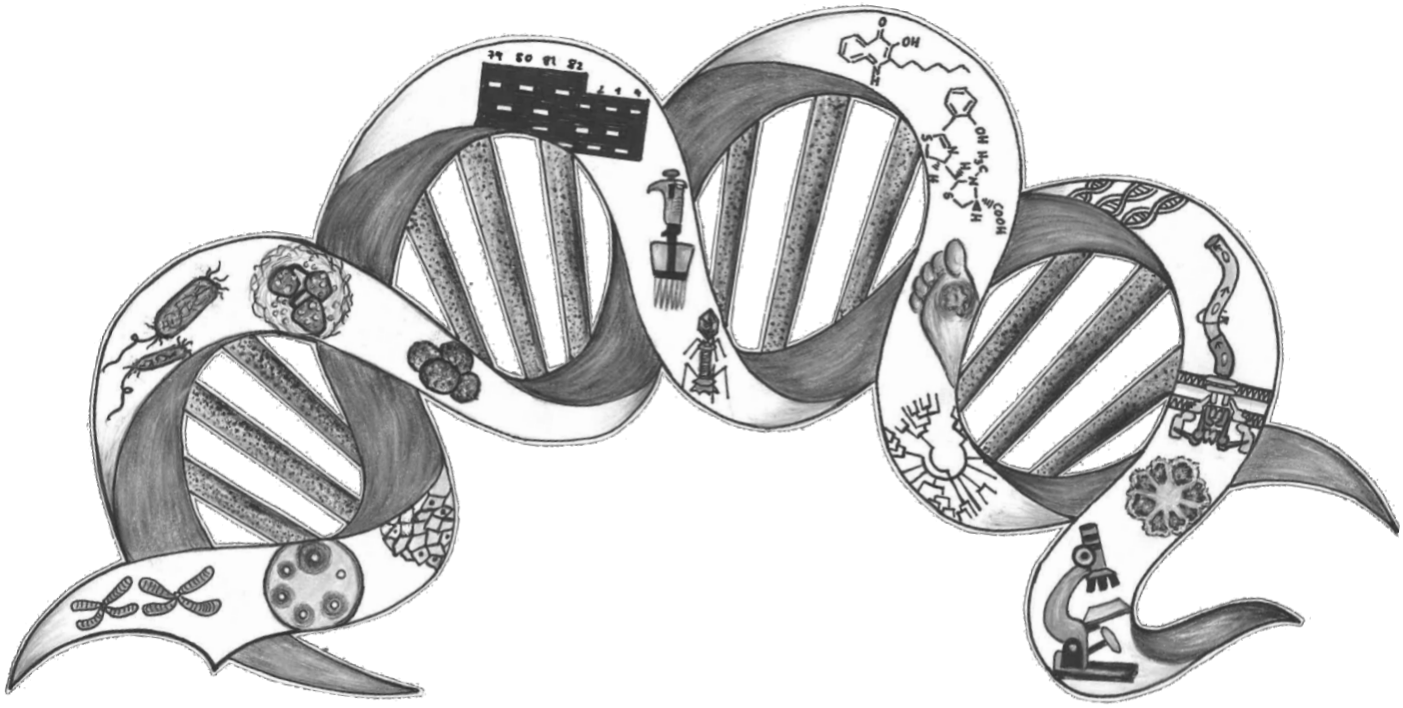
University of Nottingham
UK | CHINA | MALAYSIA

Understanding the diversity and evolution of complex wound infections



Ana Catarina da Silva

Thesis submitted to the University of Nottingham

for the degree of Doctor of Philosophy

November 2018

Declaration

I hereby declare that this thesis has not been and will not be submitted in whole or in part to another University for the award of any other degree.

Ana Catarina da Silva

Abstract

Chronic wounds (CW) are a common complication of diabetic ulcers (DUs), which are a major burden to health care systems worldwide and can result in lower limb amputation due to the intractability of the infection. DUs appear because of underlying causes such as peripheral neuropathy, peripheral vascular disease and trauma and often become colonized with multiple microbial species including *Staphylococcus aureus* and *Pseudomonas aeruginosa*. Such polymicrobial infections have been suggested to be more virulent, antibiotic resistant and result in worse patient outcomes but the reasons why remain unclear.

In a long-term infections such as DUs, there is a high probability of the infecting bacteria evolving considerable phenotypic and genetic diversity, as has previously been shown for chronic lung infections of cystic fibrosis patients. However, it is not known whether this is also the case for chronic DUs, and whether diversity and/or interactions between strains or species impacts on virulence and antibiotic resistance. To study this, bacterial populations were isolated from bone and soft tissue samples from five patients and six chronic wounds (CWs) from diabetic foot or leg ulcers. Initially phenotypic diversity was investigated in *P. aeruginosa* CW populations through the analysis of phenotypes traditionally associated with pathogenicity, and through a whole genome study.

Phenotypic variation in *P. aeruginosa* isolates taken from different patients was observed, but little variation within the same chronic wound (with exception of one patient with a diabetic leg ulcer). Antibiotic resistance was found to increase

during the course of infection, and with the genomic analysis it became apparent that *P. aeruginosa* colonisation in a diabetic CW is via a single strain per ulcer, and potentially per patient, even though some sample-specific phenotypic profiles can arise from a homogenous population, as happened in one of the patients.

For this patient, two distinct phenotypic profiles were found, so a detailed genomic analysis between isolates was done, including a full characterisation of the single nucleotide polymorphisms and a comparison of their transcriptomes using RNAseq. The results suggest that the loss of flagellum due to a *fliJ* mutation facilitated evasion of the innate immune system, and blood isolates were able to go undetected and were able to spread systemically causing the rapid decline in the patient's health.

Furthermore, *S. aureus* isolates from two of the CWs were used to investigate interactions between strains of both species that co-evolved in the same or different ulcers. We observed that *S. aureus* and *P. aeruginosa* strains isolated from the same wound can often co-exist when grown together in synthetic wound fluid. In contrast, when such strains were isolated from different wounds, *P*. a*eruginosa* often outcompeted *S. aureus*, possibly because of differences in alkyl quinolone levels. The data presented in this thesis furthers aids our understanding of how ecology influences the evolution of different species within wound infections and how this contributes to virulence and antibiotic resistance in polymicrobial infections.

Acknowledgements

First of all, my most sincere thanks to my supervisors, Steve Diggle and Paul Williams. I could not have asked for more supportive and patient guidance. I am really grateful for all the conversations about science and life, your invaluable biological insight, and overall support during these years, which for sure has enriched my academic career as well as my personal life.

I must also thank the other mentors, particularly Stephan Heeb, but also Steve Atkinson and Miguel Cámara. I feel really grateful to have been able to learn with you all. Furthermore, a word of appreciation to the three amazing researchers and excellent teachers who helped me to settle in and supported me in many ways, in and out of the lab: Freya Harrison, Sheyda Azimi, and Jeni Luckett. Without your teachings and discussions, this thesis would be undoubtedly poorer! Thanks also to Thomas Bjarnsholt at the University of Copenhagen who hosted me in his laboratory for three months, to Stephanie Crone who was more than willing to share her biofilm secrets, and help me get my head around Denmark, and to Klaus Kirketerp-Møller for allowing me to visit the Bispebjerg Hospital, guide me around and answer my million questions. I'm also grateful to Kendra Rumbaugh and Rebecca Gabrilska for their help with the infection models, and to Tim Sloan for his discussions and availability to share wound samples.

In addition, a word of gratitude towards those with whom I have shared the last four years in Nottingham, especially Daniella, Paolo, Victoria, Scott, Ale, Ronni, Carol, Michelle, and all the other fantastic members of the Pseudomonas lab and

inhabitants of CBS labs. A special thanks to my lovely students, Jia and Bhumin, for their dedication and for being able to surpass themselves – you really helped with my project!

Moreover, to all the amazing people from flat 112: Fernando, Nalu, Yago, Fernanda and Leo, and to all you cheerful bunch from the University of Sussex, Lucía, Ridwan, Dániel, Alex, Michaela, Anthony, Daisy, Jamie, Paul (and the list goes on!), it was a pleasure to meet all of you; a big thanks for everything.

Finally, to my brother, thank you for all the laugher, and to my mother, thanks is an empty word considering how very grateful I am for your love and support – the distance in nothing diminishes your presence at my side! Thank you for doing the amazing drawing summarising my research that I used in the cover – this way my accomplishment will be forever yours as well. And to complete my support system, my sincerest thanks to Pedro, much more than my partner, you are the core pillar in every aspect of my life, and I could not have done this without you.

Table of Contents

Declaration i

Abstract ii

Acknowledgements iv

Table of Contents vi

List of Figures x

List of Tables xvii

List of Abbreviations xxi

1 Chapter 1: Chronic Wounds 1

1.1 What is a chronic wound? 1

1.2 Wound healing process 1

1.2.1 Haemostasis 2

1.2.2 Inflammation 3

1.2.3 Proliferation 4

1.2.4 Remodelling 5

1.3 Types of chronic wounds 6

1.3.1 Chronic wound pathology 7

1.4 Chronic wounds and diabetes 9

1.4.1 Pathophysiology of diabetes 10

1.4.2 Prevalence and classification of diabetic foot ulcers 12

1.4.3 Dysregulated inflammation 14

1.4.4 Diabetic foot infections 18

1.5 Chronic wound management 24

1.5.1 Advances in wound care and current treatment 26

1.5.2 Adjunctive treatments and future perspectives 29

1.6 Microbiology of wound infections 30

1.6.1 Bacterial diversity and polymicrobial infections 32

1.6.2 Sampling technique dilemma 36

1.6.3 Antibiotic resistance 39

1.7 Project overview 43

2 Chapter 2: Methods 45

2.1 Chronic wound sampling 45
2.1.1 Colony PCR 46
2.1.2 Bacterial isolate maintenance 47
2.2 Bacterial growth and preparation 47
2.3 *P. aeruginosa* phenotypic assays 49
2.3.1 Identification of colony morphologies on Congo Red agar plates 49
2.3.2 AHL biosensor assay 49
2.3.3 Qualitative protease assay using 15 % skim milk agar plates 50
2.3.4 Quantification of siderophore production 50
2.3.5 Pyocyanin quantitation 51
2.4 Determination of antibiotic susceptibility (BSAC method) 51
2.5 Quantification of AQ molecules by LC-MS/MS 52
2.6 Motility assays 53
2.6.1 Swarming 53
2.6.2 Swimming 54
2.6.3 Twitching 54
2.7 Microscopy 54
2.7.1 Flagella staining 55
2.7.2 Transmission electron microscopy 55
2.8 Infection assays 56
2.8.1 Larvae assay 56
2.8.2 Murine assay 56
2.9 Genomic analysis 57
2.10 RNAseq 60
2.11 *P. aeruginosa* vs *S. aureus* spot assay 62
2.12 *P. aeruginosa* vs *S. aureus* cell-free interaction assay 63
2.13 Semi-solid biofilm model 64
2.13.1 Set-up and adaptations of the semi-solid *in vitro* biofilm model 65
2.13.2 Quantification of viable cells after co-culture 67
2.13.3 Microscopy 68
2.14 Identification of *P. aeruginosa* and *S. aureus* metabolites by LC-MS/MS 68
2.14.1 Sample preparation 68
2.14.2 Liquid chromatography-mass spectrometry (LC-MS/MS) 70
2.14.3 Metabolite identification 71
3 Chapter 3: Phenotypic Diversity of *P. aeruginosa* in Chronic Diabetic Ulcers 72

3.1 Introduction & Objectives 72
3.2 Results 76
3.2.1 Phenotypic characterisation of chronic wound isolates 76
3.2.2 Determination of antibiotic susceptibility 89
3.2.3 Quantification of QS signalling AQ molecules by LCMS/MS 91
3.2.4 Summary of *P. aeruginosa* phenotypic results 92
3.2.5 Genomic analysis of *P. aeruginosa* chronic wound isolates 92
3.3 Discussion 105
3.3.1 Phenotypic diversity in populations from DFUs is low 107
3.3.2 High phenotypic diversity in a population taken from a DLU 112
3.3.3 Genomic analysis of *P. aeruginosa* chronic wound isolates 116
3.4 Conclusions 124
4 Chapter 4: Rise of a Blood-invasive *P. aeruginosa* Isolate in a Patient with a Chronic Diabetic Foot Ulcer 126
4.1 Introduction & Objectives 126
4.2 Results 133
4.2.1 Patient medical history 133
4.2.2 Overview of the phenotypic analysis 135
4.2.3 Genome analysis 139
4.2.4 Motility assays 149
4.2.5 Microscopy 150
4.2.6 Pilot infection assays 152
4.2.7 Transcriptome analysis 154
4.3 Discussion 167
4.3.1 Antibiotic susceptibility 168
4.3.2 Lack of AQ production 170
4.3.3 Siderophore production, iron metabolism and CSS systems 171
4.3.4 *fliJ* mutation – effect on motility 175
4.3.5 Infection pilot assays 178
4.4 Conclusion 180
5 Chapter 5: *P. aeruginosa* and *S. aureus*: Ecologic Interactions and Evolution in Chronic Diabetic Foot Ulcers 182
5.1 Introduction 182
5.2 Results 186
5.2.1 P. aeruginosa vs S. aureus colony drop assays 187
5.2.2 *P. aeruginosa* vs *S. aureus* cell-free interaction assays 189

5.2.3 *P. aeruginosa* and *S. aureus* interactions in a semi-solid biofilm model 192

5.2.4 Identification of *P. aeruginosa* and *S. aureus* metabolites by LC-MS/MS 198

5.3 Discussion and Conclusion 201

6 Chapter 6: Conclusions and Future Work 205

7 References..... 210

8 List of Appendices 241

List of Figures

Figure 1: Stages of normal wound healing..... 2

Figure 2: First phase of wound healing. 3

Figure 3: Second phase of wound healing. 3

Figure 4: Third phase of wound healing. 4

Figure 5: Fourth and last phase of wound healing..... 5

Figure 6: Common pathway of diabetic foot ulcer occurrence and recurrence 10

Figure 7: M1 and M2 polarisation of macrophages (MØ)..... 15

Figure 8: Biofilms hijack the host immune response 17

Figure 9: Most studied biofilm-related infections in humans..... 19

Figure 10: Development and structure of a bacterial biofilm..... 20

Figure 11: Flow diagram of chronic wound management 25

Figure 12: The wound care cycle in the TIME framework 28

Figure 13: The clinical spectrum of microbial wound colonisation and infection 32

Figure 14: Development of the microbiology of the diabetic foot ulcer over time.. 35

Figure 15: Protocol overview from sample collection to storage of filter-sterilised supernatants (FSNs) that will later be used in *P. aeruginosa* phenotypic assays. 48

Figure 16: Set-up for the *P. aeruginosa* vs *S. aureus* cell-free interaction assay 64

Figure 17: Example of the semi-solid *in vitro* wound biofilm model 64

Figure 18: Optimisation of the semi-solid *in vitro* biofilm model protocol to study *P. aeruginosa* and *S. aureus* interactions 66

Figure 19: Summary of the adaptations made in the semi-solid *in vitro* wound biofilm model. 67

Figure 20: Summary of virulence factors produced by *P. aeruginosa* and their main targets in epithelial cells 74

Figure 21: Schematic representation of the QS signalling networks in *P. aeruginosa*, including reporter/receptor genes, effectors and regulons 75

Figure 22: The *P. aeruginosa* virulence regulatory network 75

Figure 23: *P. aeruginosa* isolates used in this work. 77

Figure 24: Panel with 4 plates displaying the phenotypes of each representative isolate streaked on LB agar plates 77

Figure 25: Colony morphologies of representative *P. aeruginosa* isolates on Congo Red agar plates 80

Figure 26: Example of AHL biosensor detection assay in *P. aeruginosa* chronic wound isolates 81

Figure 27: Qualitative protease assay in chronic wound isolates using 15% skim milk agar plates..... 83

Figure 28: Categories used in the quantification of siderophore production..... 83

Figure 29: Pyoverdine (PVD) and pyochelin (PCH) production by isolates from one batch from each chronic wound studied 85

Figure 30: Growth curves for isolates of diabetic foot ulcer..... 88

Figure 31: Antibiotic susceptibility assay for a chronic wound isolate (CW5 T1)..... 90

Figure 32: LC-MS/MS quantification of AQs produced by *P. aeruginosa* taken from diabetic foot ulcers of patients V, W, and X and the PAO1 lab strain..... 91

Figure 33: Whole genome sequence comparison of *P. aeruginosa* PAO1 reference with chronic wound (CW) *P. aeruginosa* clinical isolates..... 95

Figure 34: Whole genome sequence comparison of *P. aeruginosa* PAO1 reference with CW7 *P. aeruginosa* clinical isolates taken from a diabetic leg ulcer..... 96

Figure 35: Synteny of the *las* operon region between patient X isolates and PAO1 reference..... 99

Figure 36: Multiple sequence alignment analysis of RhlI trough PATRIC platform 100

Figure 37: Polar tree layout of the phylogenetic relationship between the 23 genomes of the *P. aeruginosa* chronic wound isolates sequenced..... 105

Figure 38: Siderophore and haem iron uptake systems in *P. aeruginosa*..... 128

Figure 39: Model for regulation of AmpC β-lactamase induction in *P. aeruginosa.* 131

Figure 40: Timeline of hospital visits for patient X 134

Figure 41: Colony morphology of patient X *P. aeruginosa* morphotypes on Congo Red Agar plate..... 137

Figure 42: Pyoverdine (PVD) and pyochelin (PCH) production by all *P. aeruginosa* isolates from patient X..... 137

Figure 43: Antibiotic susceptibility assay in chronic wound isolates from patient X 138

Figure 44: Quantification of AQs produced by clinical strains of *P. aeruginosa* from patient X, and the lab strain PAO1..... 139

Figure 45: Whole genome sequence comparison of *P. aeruginosa* chronic wound isolates from patient X with PAO1..... 140

Figure 46: Multiple sequence alignment analysis of *fliJ* via PATRIC platform..... 143

Figure 47: Partial structure of the flagellar type III export apparatus in Gram-negative bacteria. 144

Figure 48: Primary amino acid sequence of the FliJ proteins in *S. typhimurium* and *P. aeruginosa* 145

Figure 49: Multiple sequence alignment analysis of *pvdS* trough PATRIC platform 145

Figure 50: Predicted structure of the PvdS protein 146

Figure 51: Multiple sequence alignment analysis of *amn* trough PATRIC platform 147

Figure 52: Multiple sequence alignment analysis of *mexZ* trough PATRIC platform 148

Figure 53: Three-dimensional illustration of MexZ mutations, localized on the MexZ/DNA model 148

Figure 54: *P. aeruginosa* PAO1 and representative CW5 isolate motility..... 150

Figure 55: Frames of a video of a clinical *P. aeruginosa* strain isolated from bone of patient X (CW5 bone) stained with Alexa Fluor 488 151

Figure 56: Transmission electron microscopy images of two clinical *P. aeruginosa* strains isolated from bone (left) and blood (right) of patient X..... 151

Figure 57: Detailed transmission electron microscopy images of two clinical *P. aeruginosa* strains isolated from bone (left) and blood (right) of patient X 152

Figure 58: Pilot infection experiment in a *G. mellonella* larval infection model using patient X's bone and blood isolates..... 153

Figure 59: Pilot infection experiments in a murine chronic wound model using patient X's bone and blood isolates 154

Figure 60: Siderophore production measured over time in the lab strain PAO1 ... 155

Figure 61: Principal component analysis of the distribution of gene-level expression 156

Figure 62: MA-plot providing a global view of the differential genes with the log2 fold change over the mean of normalized counts 157

Figure 63: Venn diagram showing the genes whose expression significantly changes between CW5 bone (B) and CW5 blood (S) at 18h and at 8h. 158

Figure 64: A 30 kbp region consisting of type III secretion systems genes that are downregulated in the CW5 blood when compared to the CW5 bone 164

Figure 65: A 25 kbp region consisting of PCH-related genes that are upregulated in the CW5 blood when compared with the CW5 bone isolates 165

Figure 66: Confocal laser scanning microscopy images of *S. aureus* and *P. aeruginosa* in chronic wounds 184

Figure 67: Growth curves for *P. aeruginosa* and *S. aureus* chronic wound isolates and lab adapted strains (PAO1 and *S. aureus* Newman) 187

Figure 68: *P. aeruginosa* and *S. aureus* colony drop interaction assays. 188

Figure 69: Cell-free interactions between *P. aeruginosa* and *S. aureus* grown in SWF 190

Figure 70: Monocultures of *S. aureus* and *P. aeruginosa* in the cell-free interaction assay after 24 h incubation. 191

Figure 71: Cell-free interactions between *P. aeruginosa* and *S. aureus* grown in SWF for 24h..... 191

Figure 72: Semi-solid *in vitro* biofilm model of *P. aeruginosa* and *S. aureus* polymicrobial infection 193

Figure 73: *P. aeruginosa* and *S. aureus* interactions in a semi-solid biofilm model 194

Figure 74: Example of fluorescent Gram stain in chronic wound isolates of *S. aureus* and *P. aeruginosa* 195

Figure 75: *P. aeruginosa* and *S. aureus* suspended aggregates in a semi-solid *in vitro* biofilm model 196

Figure 76: *P. aeruginosa* and *S. aureus* interaction in SCW semi-solid biofilm model 197

List of Tables

Table 1: Major types of chronic wounds..... 6

Table 2: Worldwide prevalence of diabetic foot ulcer..... 12

Table 3: Infectious Diseases Society of America classifications of diabetic foot infection..... 21

Table 4: Changes in the microbiological knowledge and antimicrobial treatment of diabetic foot infections in the last 30 years..... 41

Table 5: Patient information, chronic wound characteristics and sampling details from the biopsy specimens supplied by the Clinical Microbiology Department, Nottingham University Hospitals NHS Trust Laboratory..... 45

Table 6: Description of sequenced *P. aeruginosa* isolates from patient X 59

Table 7: Conditions used for the metabolomic analysis 69

Table 9: Colony morphotypes shown by *P. aeruginosa* chronic wound isolates on Congo Red agar plates 79

Table 10: Presence of QS signal molecules C4-HSL and 3-oxo-C12-HSL in different chronic wound isolates, assessed by *E. coli ahyRI'::lux* and *lasRI'::lux* biosensor strains 81

Table 11: Presence and type of halo formed on skim milk plates by the action of exoproteases produced by bacteria from chronic wound samples..... 82

Table 12: Correlation of both siderophores production in chronic wound isolates . 84

Table 13: Quantification of pyocyanin production by chronic wound isolates 87

Table 13: Description of representative isolates used in this work 88

Table 14: Antibiotic susceptibility profiles for chronic diabetic foot ulcer isolates .. 89

Table 15: Antibiotic susceptibility profiles for chronic diabetic leg ulcer isolates 89

Table 16: Summary of the characterization results for *P. aeruginosa* phenotypes .. 92

Table 17: Genome assembly information for the 23 *P. aeruginosa* isolates sequenced 93

Table 18: List of amino acid substitutions in genes of the *las*/*rhl* systems 97

Table 19: Position and frequency of amino acid substitutions in Las and Rhl proteins 98

Table 20: List of amino acid substitutions in genes of the *pqs* operon 101

Table 21: Position and frequency of amino acid substitutions in Pqs and Phn proteins 102

Table 22: Summary table associating phenotypic with genotypic data 125

Table 23: Summary of the phenotypic assays of *P. aeruginosa* CW4 and CW5 isolates sampled from the diabetic foot ulcer of patient X at two different time points 136

Table 24: List of amino acid substitutions in genes of the *gyr*, *trp* and *kyn* pathways 141

Table 25: SNPs identified through PATRIC variation analysis service in CW5 phenotypic profile 2 genomes (C, D, and G) that are not present in phenotypic profile 1 genomes (E, F, and H) 142

Table 26: Summary of differentially expressed genes in the CW5 blood isolate when compared with the CW5 bone isolate after 18 h growth 159

Table 27: Biological processes associated with genes that are significantly downregulated in CW5 blood when compared to CW5 bone after 18 h growth 160

Table 28: Biological processes associated with genes that are significantly upregulated in CW5 blood when compared with CW5 bone after 18 h growth 161

Table 29: Biological processes associated with genes that significantly change in CW5 blood when compared with CW5 bone after 18 h growth 162

Table 30: Genes that have > 25 fold difference in expression in the CW5 blood when compared with the CW5 bone isolate after 18 h growth, using PAO1 genome as mapping reference..... 163

Table 31: Genes involved with cell-surface signalling (CSS) systems in *P. aeruginosa* that are differentially expressed in CW5 blood when compared to CW5 bone isolates after 18 h growth. 165

Table 32: *P. aeruginosa* flagellar assembly genes that are differentially expressed in the CW5 blood when compared with the CW5 bone isolates after 18 h growth 166

Table 33: Metabolites identified in interactions with *P. aeruginosa* and *S. aureus* isolated from the same ulcer 199

Table 34: Metabolites identified in interactions with *P. aeruginosa* and *S. aureus* isolated from different ulcers 200

Table 35: Adaptations made in the semi-solid *in vitro* wound biofilm model. 202

List of Abbreviations

3-oxo-C12-HSL	*N*-3-oxododecanoyl-homoserine lactone
aa	amino acids
ABC	ATP-binding cassette
Abs_{691}	absorbance at 691 nm
AHL	*N*-acyl-homoserine lactone
AMP	adenosine monophosphate
AMR	antimicrobial resistance
AQ	2-alkyl-4-quinolone
AS	antimicrobial susceptibility
ATCC	American Type Culture Collection
ATM	Aztreonam
ATP	adenosine triphosphate
BLAST	Basic Logic Alignment Search Tool
BLASTn	nucleotide BLAST
bp	base pair
BPA	Baird Parker Agar
BRIG	BLAST Ring Image Generator
BSAC	British Society for Antimicrobial Chemotherapy
C4-HSL	*N*-butanoyl-homoserine lactone
C9-PQS	2-hydroxy-2-nonyl-4(1H)-quinolone
CAZ	ceftazidime
CF	cystic fibrosis
CFU	colony forming units
CIP	ciprofloxacin
CLSI	American Clinical and Laboratory Standards Institute
CM	cytoplasmic membrane
CN	gentamicin
CRA	Congo Red agar
CSS	cell-surface signalling
CW	chronic wounds
d_4-PQS	5,6,7,8-tetradeutero-3,4-dihydroxy-2-heptylquinoline
DFI	diabetic foot infections
DFU	diabetic foot ulcers
DNA	deoxyribonucleic acid
DNase	deoxyribonuclease
DU	diabetic ulcers
E. coli	*Escherichia coli*
ECF σ	extra cytoplasmic sigma factor
ECM	extracellular matrix
EPM	extracellular polymeric matrix
ESBL	extended-spectrum beta-lactamase
EUCAST	European Committee on Antimicrobial Susceptibility Testing

FC	fold-change
FSNs	filter-sterilised supernatants
HHQ	2-heptyl-4-hydroxyquinolone
HILIC	hydrophilic interaction liquid chromatography
HPLC	high performance liquid chromatography
HQNO	2-heptyl-4-hydroxyquinoline N-oxide
HTP	haem-transport protein
I/R	ischaemia-reperfusion
IDSA	Infectious Disease Society of America
ISA	Iso-Sensitest agar
IWGDF	International Working Group on the Diabetic Foot
LB	lysogeny broth
LC-MS/MS	liquid chromatography-mass spectrometry
LEA	lower extremity amputation
LES	Liverpool epidemic strain
LPS	lipopolysaccharides
LU	leg ulcers
MEM	meropenem
MFS	major facilitator superfamily
MØ	macrophages
MRSA	methicillin-resistant *S. aureus*
MS	mass spectrometry
MS/MS	high-resolution tandem mass spectrometry
MW	Meggitt-Wagner
NCBI	National Centre for Biotechnology Information
NCTC	National Collection of Type Cultures
NHQ	2-nonyl-4-hydroxyquinolone
NQNO	2-nonyl-4-hydroxyquinoline *N*-oxide
O/N	overnight cultures
OD_{600}	optical density at 600 nm
P. aeruginosa	*Pseudomonas aeruginosa*
PATRIC	Pathosystems Resource Integration Center
PBP	periplasmic binding protein
PBS	phosphate buffered saline
PCH	pyochelin
PCR	polymerase chain reaction
PIA	*Pseudomonas* Isolation Agar
PQS	2-heptyl-3-hydroxy-4(1H)-quinolone
PU	pressure ulcers
PVD	pyoverdine
PYO	pyocyanin
QC	quality control
QS	quorum-sensing
RASTtk	RAST tool kit
RFU	relative fluorescence units
RNA	ribonucleic acid

RNAseq	RNA sequencing
RND	resistance-nodulation-division
ROS	reactive oxygen species
rRNA	ribosomal RNA
rpm	revolutions per minute
S. aureus	*Staphylococcus aureus*
SNP	single nucleotide polymorphism
spp.	species
SCW	synthetic chronic wound
SWF	synthetic wound fluid
TBDT	TonB-dependent transporter
TEM	transmission electron microscopy
TIRF	total internal reflection fluorescence
TnSS	Type *n* (where *n* is 1 to 6) secretion system
TOF-SIMS	time of flight-secondary-ion mass spectrometry
TPM	Transcripts Per Kilobase Million
TZP	piperacillin/tazobactam
UT	University of Texas
WLM	wound-like medium

Chapter 1: Chronic Wounds

1.1 What is a chronic wound?

A wound is usually defined as an injury to any tissue that is the result of trauma made by a cut or some other impact, typically involving the skin being breached. Sometimes, however, a wound starts as a minor traumatic penetrating injury but the repair process halts before the last stage. In such cases, when inflammation persists for over three months, it is considered a chronic wound [1].

Chronic wounds are a major health problem, impacting the lives of more than 50 million people worldwide [2]. The physical stress and the emotional damage they entail are translated into cumulative impairments that significantly reduce the quality of life of affected patients [3]. Moreover, they constitute a major economic burden, corresponding to between 3% and 5.5% of the budget of health services of developed countries [4].

1.2 Wound healing process

Our bodies have a predictable process of physiological wound healing that deals with damage and involves four stages: haemostasis; inflammation; proliferation; and remodelling. In a healthy individual, when a trauma causes a wound, this process is immediately triggered. Normal wound healing has been extensively described, for example in [5], and is mainly controlled by the immune system, involving a plethora of cell types and cellular events (Figure 1).

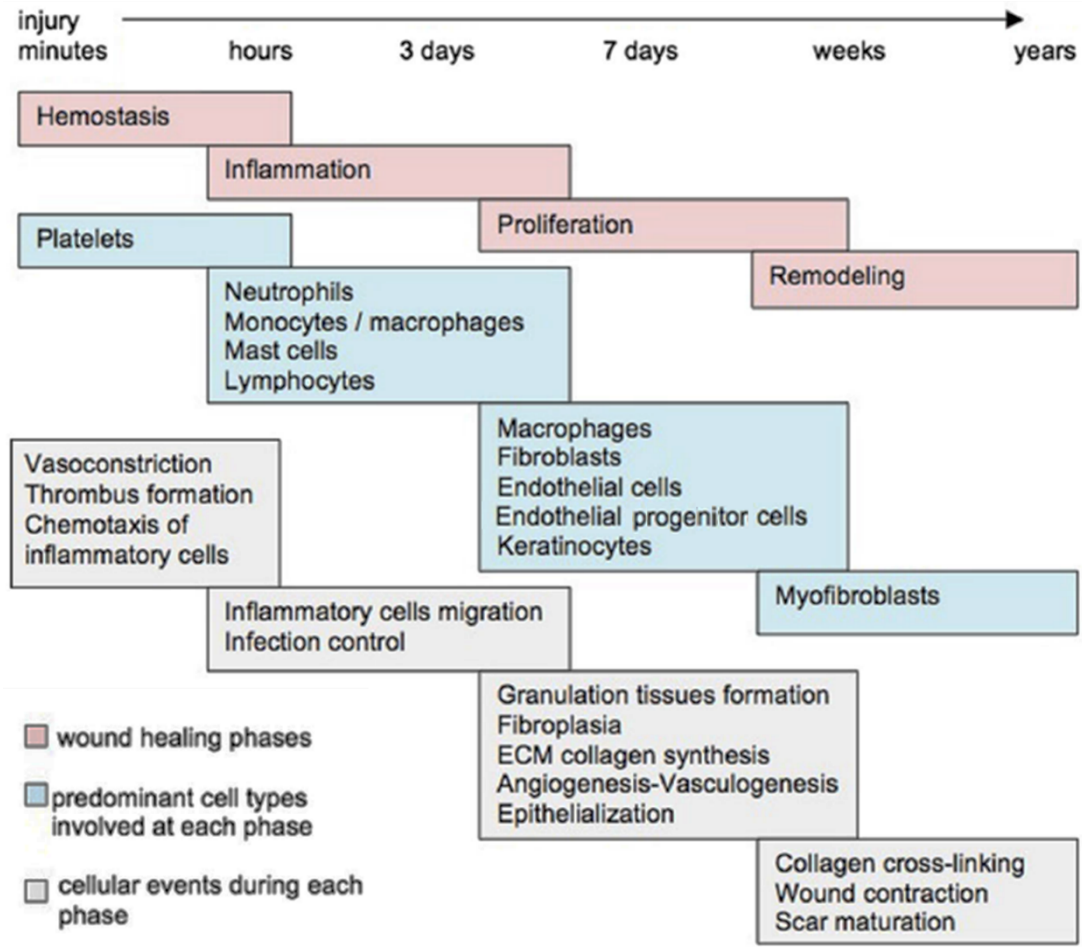


Figure 1: Stages of normal wound healing. Note that healing phases overlap in time and remodelling (scar formation and healing) can take weeks or years depending on the severity of the trauma sustained; ECM - extracellular matrix; adapted from [6].

The next sections will summarise the main points in each phase, highlighting the mechanisms that have been correlated with the development of chronic wounds.

1.2.1 Haemostasis

After trauma, the body immediately tries to close the breach by forming a blood clot. This is part of the haemostasis phase when a provisional wound matrix is formed. This acts like a scaffold for the migration and proliferation of other cells involved in wound healing (Figure 2).

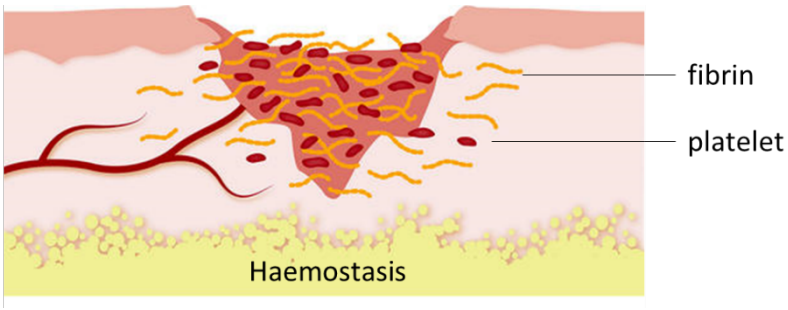


Figure 2: First phase of wound healing.

Initially this is achieved by activating circulating platelets that flood the injury site and undergo adhesion and aggregation. Thrombin converts fibrinogen to fibrin and these molecules assemble into long fibrils that together with the platelets form a mesh that completes the clot.

1.2.2 Inflammation

Once the damaged tissue is stabilised by the fibrin-platelet clot, the extrinsic and intrinsic coagulation pathways are activated and there is an increase in the accumulation of cytokines and growth factors. This triggers the most important phase of wound healing: inflammation. It encompasses a non-specific innate immune response that is responsible for the clean-up of cellular, extra-cellular, and pathogen debris. Vasodilation combined with an increased permeability of local capillaries allows neutrophils and then macrophages to accumulate in the wound site (Figure 3).

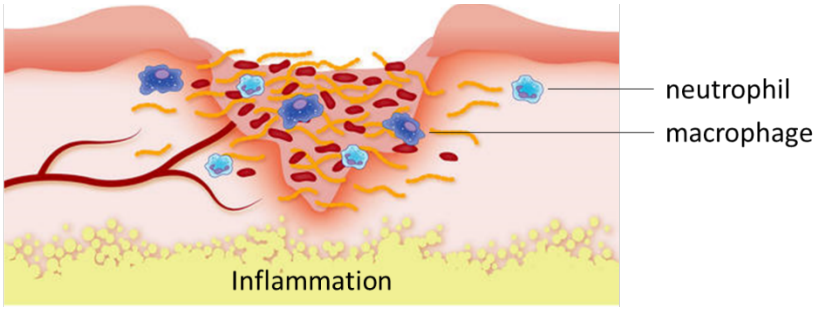


Figure 3: Second phase of wound healing.

Inflammation is the key factor that differentiates between normal and chronic wounds. If this phase is resolved after one to two weeks, the body can continue the healing process. However, if the inflammation is disturbed in any way and does not subside, the wound will likely develop into an ulcer that can persist for years. This arrested phase prevents the adequate transmission of the signals that trigger wound healing. In section 1.4.3, examples of the main dysregulation factors will be given. The transition between inflammatory and proliferative phases depends on the action of activated macrophages that phagocytise debris and release growth factors to stimulate the formation of granulation tissue.

1.2.3 Proliferation

When the concentration of anti-inflammatory molecules surpasses the level of pro-inflammatory molecules, the process of re-epithelialization begins. The main focus of this phase is to allow epithelial cells to migrate across the wound surface to close it (Figure 4). Additionally, the formation of granulation tissue and restoration of the vascular network are important checkpoints before the last phase can take place.

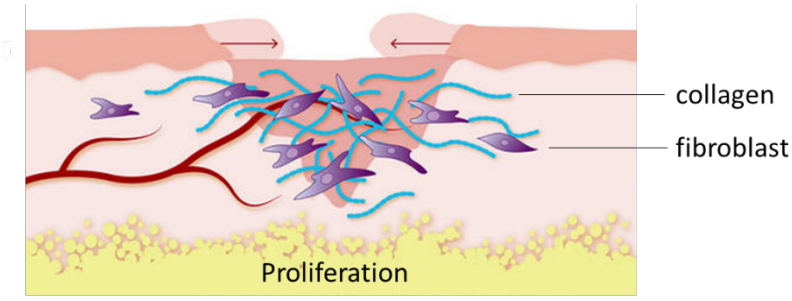


Figure 4: Third phase of wound healing.

Fibroblasts are the cells responsible for the synthesis of collagen and other substances that form the basis for a new matrix of connective tissue. Angiogenesis and fibroplasia occur simultaneously, providing oxygen and nutrients to sustain high levels of cellular activity. The formation of this rich and hydrated extracellular matrix allows the closure of tissue gaps and the restoration of the mechanical strength of the wound tissue.

1.2.4 Remodelling

In the last phase of wound healing the objective is to enhance tissue strength and decrease wound thickness. Fibroblasts modify their gene expression to assume a myofibroblast phenotype that facilitates contraction of the forming scar (Figure 5).

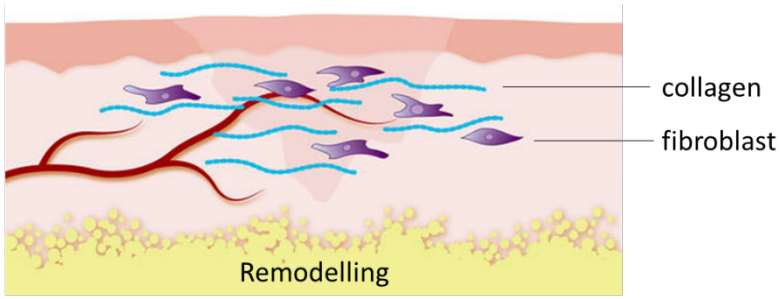


Figure 5: Fourth and last phase of wound healing.

The components of the extracellular matrix (ECM) undergo changes and the formation of granulation tissue stops through apoptosis. Tight control between synthesis and metabolism of collagen results in the development of a normal scar where collagen fibres are rearranged in small parallel bundles along tension lines. However, the majority of the tissue will never fully recover its tensile strength after wound closure, as its composition is going to be altered. In deep wounds, for example, hair follicles or sweat glands have no potential to heal or grow back.

1.3 Types of chronic wounds

In chronic wounds, the healing process is halted in the inflammatory and proliferative stages of healing [7] but, in addition, there is normally an underlying cellular dysfunction and dysregulation that results in over-production of matrix molecules [8]. As the epidermis in the wound margins is unable to respond to reparative stimuli and cannot migrate to cover the wound bed, it remains open and susceptible to infection [9-11].

Patients are admitted to hospitals with chronic wounds from different aetiologies but they can generally be assigned to one of three clinical categories: pressure ulcers (PU); leg ulcers (LU) that involve venous and arterial ulcers; and diabetic foot ulcers (DFU) (Table 1).

Table 1: Major types of chronic wounds, adapted from [12].

Wound type	Relevant pathology	No of affected patients	Estimated annual cost (£)
Pressure ulcer	Immobility; excessive pressure	~ 15 million	2 to 5 billion
Leg ulcer	Venous / arterial insufficiency; thrombosis; atherosclerosis	~ 20 million	1.4 to 1.9 billion
Diabetic foot ulcer	Neuropathy; ischaemia; hyperglycaemia	~ 30 million	9 to 13 billion

Table presents worldwide data (2017) for number of affected patients and estimated annual cost, based on the "Worldwide Wound Management, Forecast to 2026" report [2].

Pressure ulcers develop as a result of a combination of physiological events – such as conditions that lead to prolonged immobility and malnutrition – and external conditions like poor skin hygiene and lying on hard surfaces. These wounds occur over predictable pressure points where bony protuberances are more likely to

compress tissues over time, and treatment is necessary for patient comfort and to decrease the risk of systemic infection, reviewed in [13].

Leg ulcers are usually caused by an increase of pressure due to circulatory problems in the veins (venous ulcer) or arteries (arterial insufficiency ulcer). Venous ulcers are more frequent (up to 80% of total) due to risk factors such as obesity, previous deep vein thrombosis, or varicose veins. This high pressure causes inflammation of the skin and swelling that if left untreated can result in the development of chronic wounds, reviewed in [14].

Diabetic foot ulcers – the most common cause of diabetes-related hospital admissions – will be described in detail in section 1.4. It is relevant to point out that identifying the underlying cause of the wound is invaluable for categorizing the ulcer, but it is also fundamental for treatment as the type of wound bed care implemented may vary with ulcer type. For example, sharp debridement is common in the management of patients with DFUs; while compression therapy is the recommended treatment for patients with venous LUs [15]. Further chronic wound treatments will be described in section 1.5.1.

1.3.1 Chronic wound pathology

Although the pathologies underlying each wound are different, many chronic wounds progress similarly. This uniformity was explained by the presence of several key pathophysiologic phenomena [16] that result in the failure of these wounds to follow the normal healing process described in section 1.2. These common factors are the co-existence of cellular and systemic changes of ageing, hypoxia caused by

repeated ischaemia-reperfusion injury, and the inflammatory environment of protease and oxidant excess induced by bacteria colonisation.

Longstanding clinical observations and many studies have identified a slower wound healing in the elderly, specifically when subjected to stress, and this is very relevant when we consider that the majority of chronic wounds occur in individuals aged over 60 [17]. Specific age-related impairments in inflammation include alterations in cell-adhesion and migration, as well as in many functional responses such as phagocytic capacity of both neutrophils and macrophages [18].

One of the key substances for cell metabolism and energy production is oxygen. Several studies associated the appearance of hypoxic wounds with vascular and circulatory diseases. Typically, a tissue that has been depleted of blood supply for a significant amount of time becomes ischaemic. Poor oxygen supply leads to ischaemia-reperfusion (I/R) injuries – cycles of blood reperfusion to previously ischaemic tissue – that were identified as one of the precipitating events in all types of chronic wounds [16]. I/R injury triggers a cascade of harmful events such as downregulation of nitric oxide and overproduction of reactive oxygen species (ROS), which induce a pro-inflammatory state [19].

Bacterial colonisation is another common occurrence in chronic wounds and is extremely relevant as the association of biofilms with chronic wounds is widely accepted. The action of typical wound pathogens increases the production of proteases and ROS, further exacerbating the oxidative damage while maintaining inflammatory cascades [20]. In section 1.4.3, we will address the role of biofilms in

the chronic inflammation loop and discuss how bacteria can obtain a sustainable nutrient source in the form of inflammatory exudate.

These common causality factors generally lead to an altered inflammation and thus delay or prevent progression to the proliferative phase, impairing wound healing. The healing process eventually resumes if good care is provided, but the rates and speed of healing in chronic wounds are generally measured in weeks and months rather than days as for acute wounds. Moreover, other underlying mechanisms such as immunosuppression or acquired immunodeficiency, and metabolic diseases such as diabetes, will also have a major effect on wound healing. The effects of diabetes in the chronicity of ulcers will be explored in detail in the section below.

1.4 Chronic wounds and diabetes

Diabetes mellitus is a group of chronic metabolic disorders with severe health consequences. A 2016 World Health Organization report on diabetes stated that in 2014 an estimated 422 million adults were living with diabetes worldwide, compared to just 108 million in 1980 [21]. The common denominator in diabetes is the inadequate secretion or utilization of insulin, caused by a combination of hereditary and environmental factors. It is mainly characterized by excessive amounts of glucose in the blood and urine, and can cause a wide range of metabolic abnormalities [22].

1.4.1 Pathophysiology of diabetes

Researchers describe the precipitating and predisposing factors for the appearance of chronic wounds in diabetic patients as the triad of neuropathy, ischaemia, and trauma (Figure 6) [23].

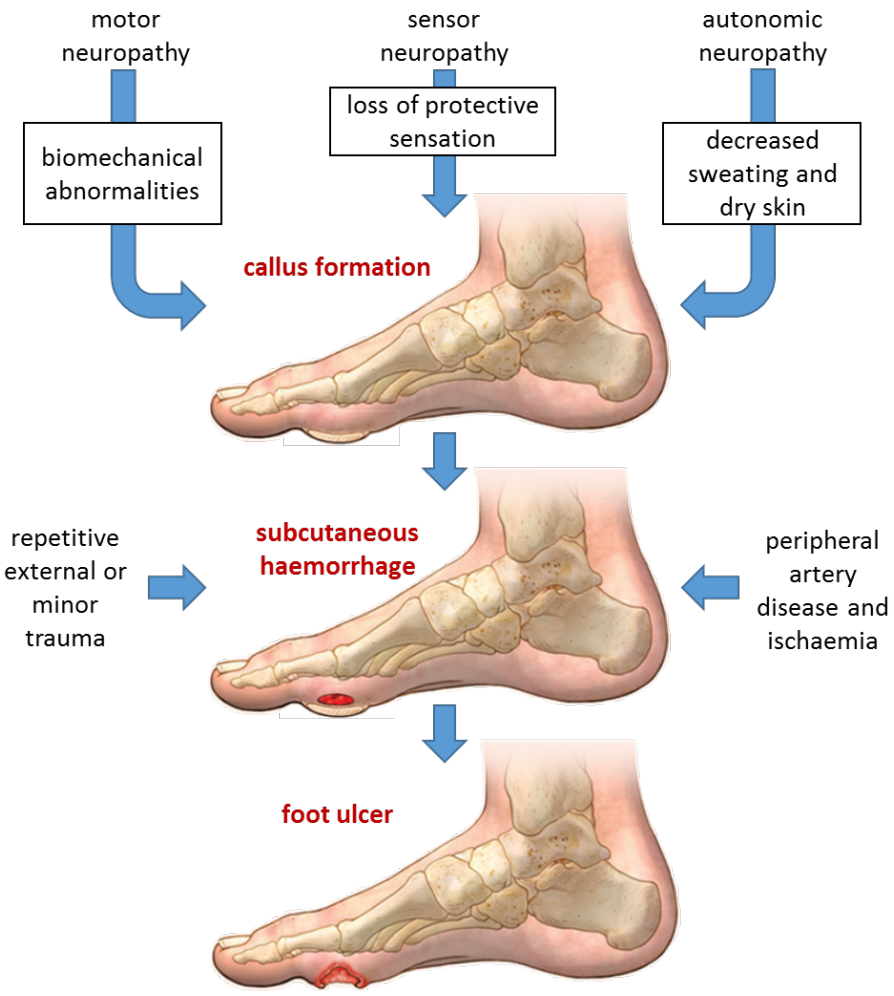


Figure 6: Common pathway of diabetic foot ulcer occurrence and recurrence (adapted from [24]).

Diabetic neuropathy is the term used for nerve damage as a result of diabetes. The symptoms depend on which types of nerves are affected, and can be categorised as: motor neuropathy – foot deformities and impaired balance; sensory neuropathy – loss of pain and sense of touch; and autonomic neuropathy – reduction of

autonomic functions like sweating. These factors combined lead to a lack of awareness in cases of trauma with rupture of the skin [25]. Diabetic neuropathy is also associated with a decreased and even absent vasodilation that affects microcirculation – resulting in functionally ischaemic tissues, regardless of the presence of macrovascular disease [26].

Diabetic patients have circulatory dysfunctions, encompassing micro- and macrovascular diseases, for example thrombosis. The accumulation of plaques of fatty deposits typical of atherosclerosis leads to a narrowing of arteries that not only damages the heart but also reduces the blood flow to the limbs, causing peripheral arterial disease that eventually leads to ischaemia induced by hypoxia [27].

However, one of the most important underlying pathologies of diabetes is hyperglycaemia. The presence of high levels of glucose in the blood activates a myriad of biochemical pathways, reviewed in detail by [28], that involve, for instance: the formation of advanced glycation end-products and their receptors, the activation of the diacylglycerol-protein kinase C pathway [29], and the inducible nitric oxide synthase.

The overall effect of diabetes on the healing process is complex. The underlying pathologies affect not only the inflammation phase but also the proliferation and remodelling phases. A more detailed review, highlighting the different molecular changes that occur, is presented by Baltzis and collaborators [6].

1.4.2 Prevalence and classification of diabetic foot ulcers

Several studies have shown that a diabetic patient can have a lifetime risk of developing chronic wounds between 19% and 34% [24, 30]. In 2015, the International Diabetes Federation estimated that between 9.1 million and 26.1 million people with diabetes across the world are diagnosed with a chronic foot ulcer every year (IDF Diabetes Atlas 7th Edition 2015). A recent epidemiological study calculated a global diabetic foot ulcer prevalence of 6.3% (mostly in hospital based diabetic population), but this varies greatly from country to country as we can see in Table 2 [31].

Table 2: Worldwide prevalence of diabetic foot ulcer, adapted from [31].

Country	No. of studies	Prevalence (%)
USA	3	13
India	2	11.6
Cameroon	3	9.9
Thailand	2	8.8
Pakistan	4	7.4
UK	4	6.3
France	1	5.6
China	10	4.1
Spain	5	3
Germany	2	2.8
Korea	2	1.7
Australia	2	1.5

An important step to facilitate intra- and inter- communication between clinical practices, in order to better treat chronic wounds, is the classification of diabetic foot ulcers into categories and grades. Theoretically, this should facilitate clinical judgement and management planning, but several attempts have been unsuccessful because classification fails to predict wound outcome [32]. Nevertheless, two classification systems are widely used: the Meggitt-Wagner (MW) classification, that has six grades of lesions and looks at the depth of the ulcers and

the extent of gangrene and loss of perfusion in the foot [33]; and the University of Texas (UT) classification, that is similar to the MW system but uses four instead of six grades, as well as four stages that evaluate the presence of ischaemia and infection [34].

These 2 classifications have been compared in an international study that combined UK and US populations in 2001 [34]. The authors concluded that although both systems predicted lower extremity amputation (LEA) to a certain degree, the UT classification was thought to be more descriptive, and also showed a better association with increased amputation risk and prediction of ulcer healing when compared to the MW classification. However, the UT system does not include neuropathy – a typical diabetic risk factor, as discussed before – and as such it lacks the universality needed for a clinical classification. For classification purposes it is extremely important to recognise all the underlying pathologies, since diabetic patients with co-existing neuropathy and ischaemia may remain asymptomatic.

A recent study [35] tried to assess the inter-observer reliability of the MW and the UT systems and found that both of these systems are only moderately reliable when scored by multiple clinicians, thus not appearing very useful as single instruments to determine treatment options. When used for research purposes, these classifications should always be used in combination with additional clinical information to ensure reliable handover.

In summary, there is currently no single classification system that is universally applicable in clinical care. However, this problem has been prioritised over the years and has been tackled by organizations such as the International Working

Group on the Diabetic Foot, so that a system that can be easily remembered and applied may be developed. Several systems have been introduced localy even though none is consistently used and most have not been robustly validated within and between centres. Dr Game wrote a detailed review about the classification systems currently in use and suggested an algorithm for choosing the adequate system for either research, clinical care, or audit [36].

1.4.3 Dysregulated inflammation

Apart from the many overlapping pathologies inherent to diabetes that lead to foot ulceration, there is also impairment in the immune response due to a reduction in the recruitment of inflammatory cells into the damaged tissues. This slows down healing and increases the risk of infection [32], particularly with multi-drug resistance bacteria that form biofilms – communities of bacterial cells embedded in an extracellular polymeric matrix [37, 38].

In the early stage of the inflammatory phase, macrophages derived predominantly from circulatory monocytes are recruited to the wound site [39]. Their main task is to phagocytose neutrophils that have engulfed bacteria, in a process known as efferocytosis [40]. A considerable amount of research has been performed on monocytes, and 2 phenotypes have been identified: the M1 phenotype is pro-inflammatory, phagocytic, and bactericidal, while the M2 macrophages act to switch off inflammation and regulate re-vascularisation and wound closure (Figure 7) [41]. Typically, there is a continuum of phenotypes from M1 to M2 that changes over time as the wound heals; i.e., the M1 macrophage that regulates the early inflammatory

response then smoothly transitions to an M2 macrophage with reparative functions [42].

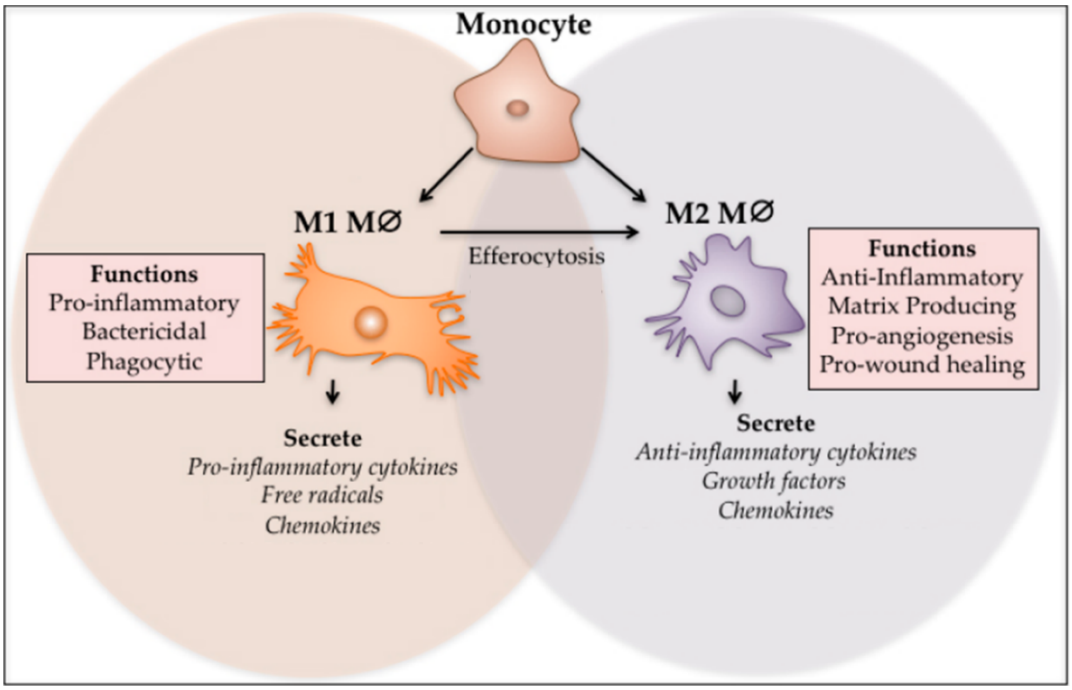


Figure 7: M1 and M2 polarisation of macrophages (MØ). Monocytes can be classically or alternatively activated to form M1 and M2 macrophages respectively. M1 macrophages can also differentiate into M2 macrophages through local cues and after efferocytosis (adapted from [41]).

Studies have shown that hyperglycaemia and the associated glycation end-products alter macrophages such that they present an impaired ability to efferocytose neutrophils, which effectively impairs the M1 to M2 transition and results in the alteration of the M1 to M2 ratio in chronic wounds [43, 44]. These findings suggest that wound macrophages probably control wound neutrophils, and that a partial loss of this control on macrophage-mediated depletion of neutrophils changes the inflammatory balance in wounds toward pro-inflammatory responses with increased action of neutrophils as a consequence [45]. A logical conjecture would then be that increasing M2 macrophages in wounds could trigger the

proliferative phase and resume wound healing. However, studies that investigated the action of artificially activated M2 macrophages in the wound bed found that there was no effect on wound closure rates [46, 47]. Thus, data from chronic diabetic wounds suggests that the timing and manner of the transition between M1 and M2 macrophages is crucial for wound healing.

Disruption of the host external surface allows bacteria that are part of the commensal skin populations to colonize the wound. Phenotypic and genotypic reorganisation of commensal bacteria facilitates successful colonisation of environmentally derived bacterial species that are usually more virulent. Combined with the inefficiency of the initial immune system response, this enables colonisers to establish a biofilm community and trigger disease states such as chronic wounds. Biofilms are associated with inflammation in a multitude of diseases such as cystic fibrosis, periodontal disease, and inflammatory bowel disease [48-50].

Wolcott and collaborators were the first to hypothesise that the wound biofilm might commandeer the host immune response in order to achieve a steady state of hyper-inflammation, which is out of the host's control, and establish a valuable nutrient source [37]. In patients with poorly managed diabetes, the underlying pathologies lead to ulcers that are colonized, and then the accumulation of virulence factors produced by the biofilm results in a chronic inflammation loop that prevents the normal healing of wounds (Figure 8).

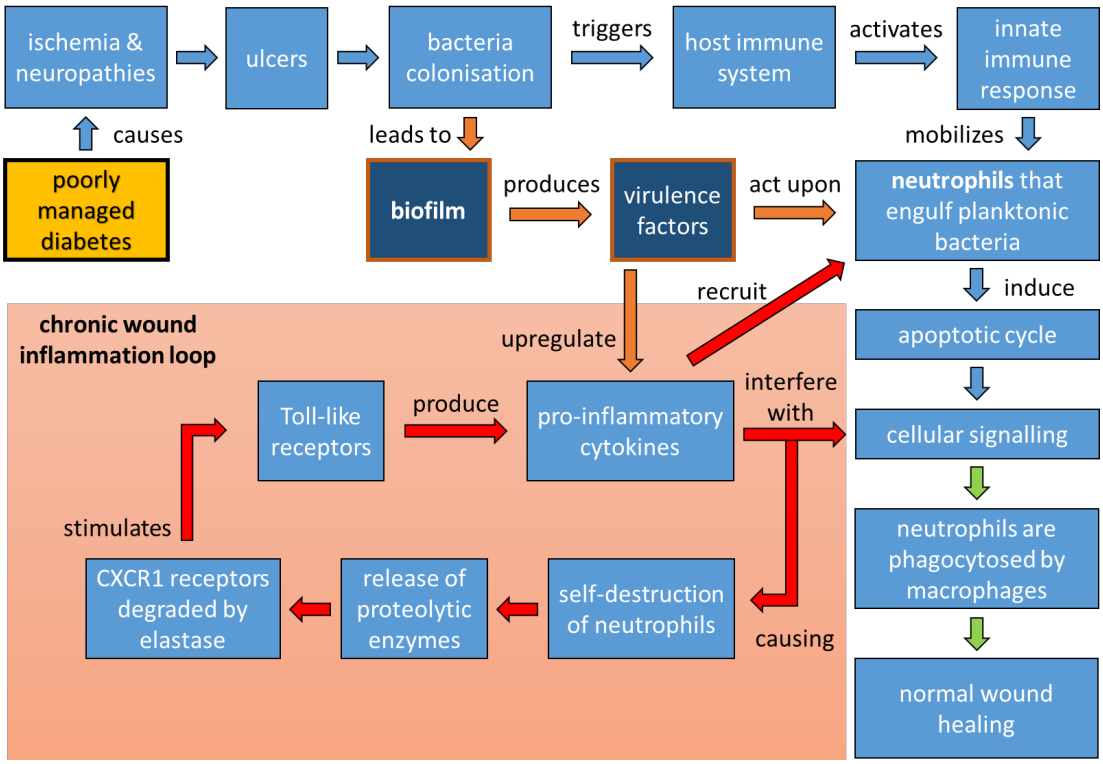


Figure 8: Biofilms hijack the host immune response. Blue arrows represent the development that leads to normal wound healing (green arrows); orange arrows highlight the pathway when infection is not recognized and treated early; red arrows identify the part of the mechanism responsible for the maintenance of an inflammatory loop (pink square) in chronic wounds.

The M1 to M2 macrophage imbalance discussed above results in an overabundance of neutrophils, which is typical of diabetes and many other chronic infections [51-55]. A common trait across all types of chronic wounds is the high concentration of pro-inflammatory cytokines and mediators in the wound fluid, which contributes to the overall non-healing phenotype [56-58]. Moreover, this effect is further heightened by the up-regulation of cytokines caused by the action of virulence factors produced by the biofilm. The increased levels of cytokines interrupt the normal cell signalling that controls efferocytosis and instead leads the bacteria-filled neutrophils to self-destruct. Upon dying, these cells release large amounts of proteolytic enzymes, such as proteases, that later degrade the wound site. Bacteria

use this damaged tissue particularly the amino acids as a nutrient source to multiply, spreading the infection. Moreover, elastase degrades the CXCR1 receptors (large transmembrane proteins specific for cytokines) of the remnant neutrophils, producing fragments that stimulate the Toll-like receptors expressed in different cells of the innate immune system, which further increases the production of pro-inflammatory cytokines so closing the loop.

In summary, neutrophils appear to be critical and act as biological markers of the extent of inflammation, even in non-colonized wounds [59]. Bacteria, particularly after a biofilm is established, stimulate the accumulation of neutrophils leading to the over-production of ROS that cause direct damage to the cell membrane and, subsequently, premature cell senescence [12]. This stalemate between bacterial biofilms and the host immune system perpetuates inflammation, which promotes wound chronicity.

1.4.4 Diabetic foot infections

The relevance of biofilms for human health is unquestionable since they are known to be associated with 65% to 80% of human infections [60]. This enormous potential to cause diseases that are hard to treat or frequently relapsing can be explained by the fact that biofilms can not only develop in tissues but, importantly, also form on medical devices such as joint prostheses or catheters despite host immune defences (Figure 9). If we also consider the fact that the bacterial species in the majority of these biofilms have been described as critical and high priority in a recent WHO news release due to their high levels of antibiotic resistance, it is easy to understand the huge impact of infection in high-concern scenarios like chronic ulcers.

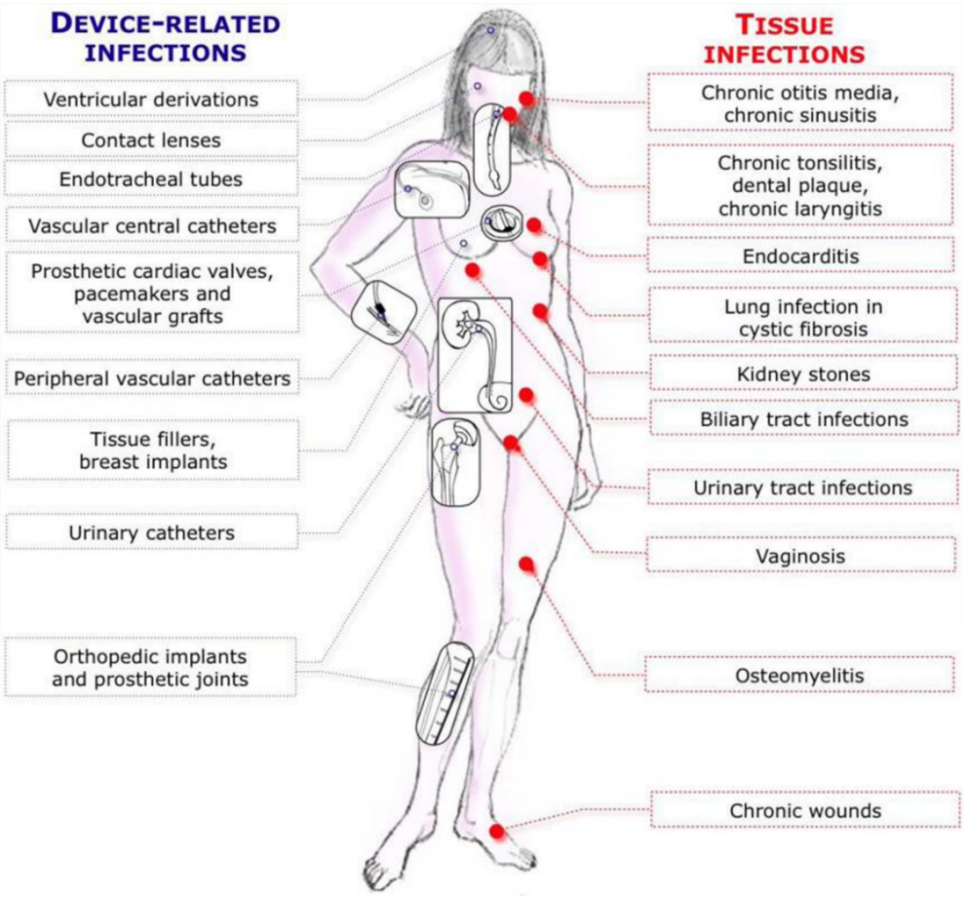


Figure 9: Most studied biofilm-related infections in humans [60].

The process by which free-living planktonic bacteria transform into surface-attached biofilms has been studied in detail for several pathogenic species, such as *Staphylococcus aureus* (responsible for most of the device-related infections) and *Pseudomonas aeruginosa* (responsible for chronic infections in, for example, cystic fibrosis patients). This process starts with a switch from reversible to irreversible attachment and involves several key stages that result in a microcolony that matures into a three-dimensional structure as a result of the increased production of an extracellular polymeric matrix (EPM). Biofilms are able to disperse actively via detachment of single cells or passively by the release of small aggregates that become suspended biofilms, and can themselves disseminate and attach elsewhere to create a new mature biofilm (Figure 10).

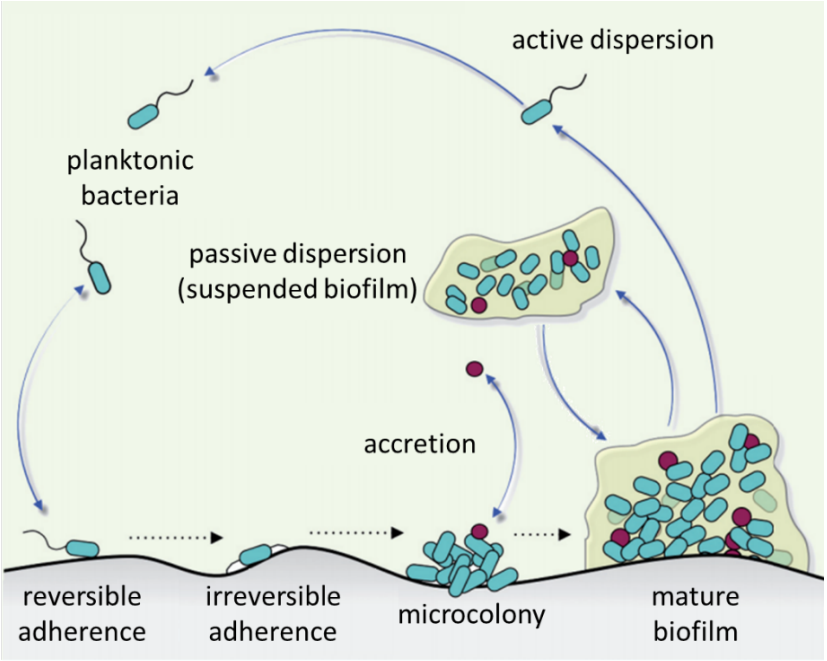


Figure 10: Development and structure of a bacterial biofilm (adapted from [61]).

The biofilm lifestyle, unlike that of free-living microorganisms, facilitates intrinsic tolerance to desiccation and antimicrobials, even if the latter are present in very high concentrations. In mono- and poly- microbial infections, bacteria are able to communicate by employing quorum-sensing – a population density-dependent mechanism that regulates gene expression in different species and allows, for example, a coordinated attack against the host immune system. The incorporation of bacteria within an EPM protects the cells and bolsters tolerance towards antibiotics, and the immune system.

Studies have found that around half of all DFUs are clinically infected at presentation, mainly because patients do not seek care in a timely manner due to missing the traditional first signs of infection – particularly pain, absent as a result of the loss of protective sensations. In 2004, two of the most recognized authorities in DFU diagnosis and management – the International Working Group on the Diabetic

Foot (IWGDF) and the Infectious Disease Society of America (IDSA) – developed a set of guidelines to serve as guidance in the diagnostic of diabetic foot infections (DFI). Early detection of infection and adequate treatment can prevent the development of biofilm and help the wound avoid the inflammatory loop that leads to chronicity. Since the majority of wounds are colonised by commensal microorganisms that are not pathogenic, DFI should not be diagnosed microbiologically but clinically. In order to do this, doctors should determine the presence of at least 2 of the following symptoms around the diabetic foot ulcer: erythema; swelling or induration; tenderness or pain; warmth; and purulent discharge that is thick, opaque to white or sanguineous. The severity of the infection should then be classified using one of the scales developed for it, such as the IDSA infection severity scale (Table 3).

Table 3: Infectious Diseases Society of America classifications of diabetic foot infection (adapted from [62]).

Clinical manifestation of infection	**Infection Severity**
No symptoms or signs of infection.	Uninfected
Local infection involving only the skin and the subcutaneous tissue (without involvement of deeper tissues and without systemic signs as described below). If erythema is present, it must be >0.5 cm to ≤2 cm around the ulcer. Other causes of an inflammatory response of the skin (e.g. fracture or thrombosis) must be excluded.	Mild
Local infection with erythema > 2 cm, or involving structures deeper than skin and subcutaneous tissues (e.g. abscess or osteomyelitis) **and** no systemic inflammatory response signs (as described below).	Moderate
Local infection with the signs of systemic inflammatory response syndrome, as manifested by more than 2 of the following: ○ Temperature >38°C or <36°C ○ Heart rate >90 beats/min ○ Respiratory rate >20 breaths/min ○ White blood cell count >12 000 or < 4000 cells/µL or ≥10% immature (band) forms	Severe

Assessing the severity of infection in DFUs is fundamental to good patient management, especially when selecting the antibiotic regimen and route of administration. A mild DFI can be treated with oral antibiotics in an outpatient setting without the need for hospitalization, whereas a moderate to severe infection will probably require intravenous antibiotics since it can be limb- or even life-threatening [63]. However, antibiotic treatment may fail because the compounds might never reach the bacteria due to poor blood supply resulting from ischaemia [64]. Note that experts state that the presence of peripheral arterial disease and ischemia (both risk-factors for the appearance of DFUs, as previously discussed) increases the severity of any infection. Therefore, this condition should be diagnosed alongside infection [65].

Compared with patients with an uninfected DFU, the presence of infection increases the risk of a minor amputation by 50% [66]. Furthermore, systemic infection can manifest by other symptoms in diabetic patients, such as severe hyperglycaemia or hypotension, so blood tests should be prescribed if a severe infection is suspected. IWGDF and IDSA highlight, however, that their guidelines cannot always account for individual variation among patients, and its application has to be made by the physician in light of each patient's individual circumstances. Nonetheless, this approach helps clinicians decide which procedures to follow (either imaging, hospitalization, or surgical interventions).

Most DFIs require some level of surgical intervention, ranging from minor debridement to major resection. It is also common for patients to have different types of ulcers in the same limb. Often, the infection spreads from the soft tissues surrounding the ulcer to the adjacent bone and patients develop osteomyelitis (bone

infections). Moreover, when the infection progresses, it usually results in lower extremity amputation (LEA), which is one of the most feared and costly consequences of a DFU. For example, in diabetics with osteomyelitis, the risk of amputation is 4 times higher than in those with soft tissue infections alone [67] – contributing to the frightening reality that every 20 s a lower limb is lost due to diabetes somewhere in the world. Globally, many studies have reported that approximately 85% of all LEA performed in diabetic patients are preceded by DFI [68], meaning that amputations occur up to 30 times more often in people with diabetes than in the general population [69].

Surprisingly, two independent studies in France and Denmark have confirmed that the incidence of LEA in diabetic people is underestimated, with around 15% of patients being undiagnosed when admitted to the hospital for amputation [70, 71]. After limb loss, the patients often become dependent on the care and support of others, which entails a high psychological cost since it is hard to maintain the same level of social contact. In addition to poor quality of life, diabetic patients who undergo LEA face a 5-year survival rate of roughly 40%, which is similar to that of some of the deadliest cancers [72, 73]. However, decreasing this amputation rate can be achieved with a change in the care strategy offered. Several studies point out that solutions are clear and affordable: having better-organised multidisciplinary care for patients with DFU and, most importantly, improving diabetic care – not only combining close monitoring and education of people with diabetes, but also informing healthcare professionals.

1.5 Chronic wound management

Today, ulcers are a massive public health problem that, despite sometimes being overlooked, should be prioritised in order to minimize the probability of inducing chronic wounds, and avoiding other severe consequences such as amputations or clinical removal of toe bones, which happens for 15% to 27% of all ulcers [74].

Large multi-centre trials have shown that, even with good management, healing rates for diabetic ulcers caused by neuropathy were 24% at 12 weeks and 31% at 20 weeks [75], and these rates may be lower for generalised ulcers. In a study from Nottingham City Hospital involving 389 ulcers in 179 patients, only 33% healed within 3 months. In patients followed after 6 months, the healing rate increased slightly to 48% when no surgery was performed, but nevertheless 40% of the ulcers remained unhealed and ten patients died [76]. It is therefore of the utmost importance that appropriate screening and intervention measures should be implemented.

As a management approach, clinicians should screen all patients with diabetes to identify those at risk of foot ulceration and prevent further development of DFI. This should include a detailed assessment of relevant past history – that should include details such as nutritional and smoking habits, and the identification of foot deformities, especially early detection of loss of protective sensation. This screening will allow the patient to be categorised by risk, which will dictate both the type and frequency of interventions needed [77].

The IWGDF and other international organizations have established guidelines for an adequate chronic wound management. Initially, the wound should be classified and doctors should try to discern its aetiology, signalling all risk-factors and co-morbidities discussed so far. A multidisciplinary team should then envision a treatment plan that ought to be updated as time passes and the wound develops (Figure 11). The treatment should primarily focus on preventing infection or treating it before it spreads further [78].

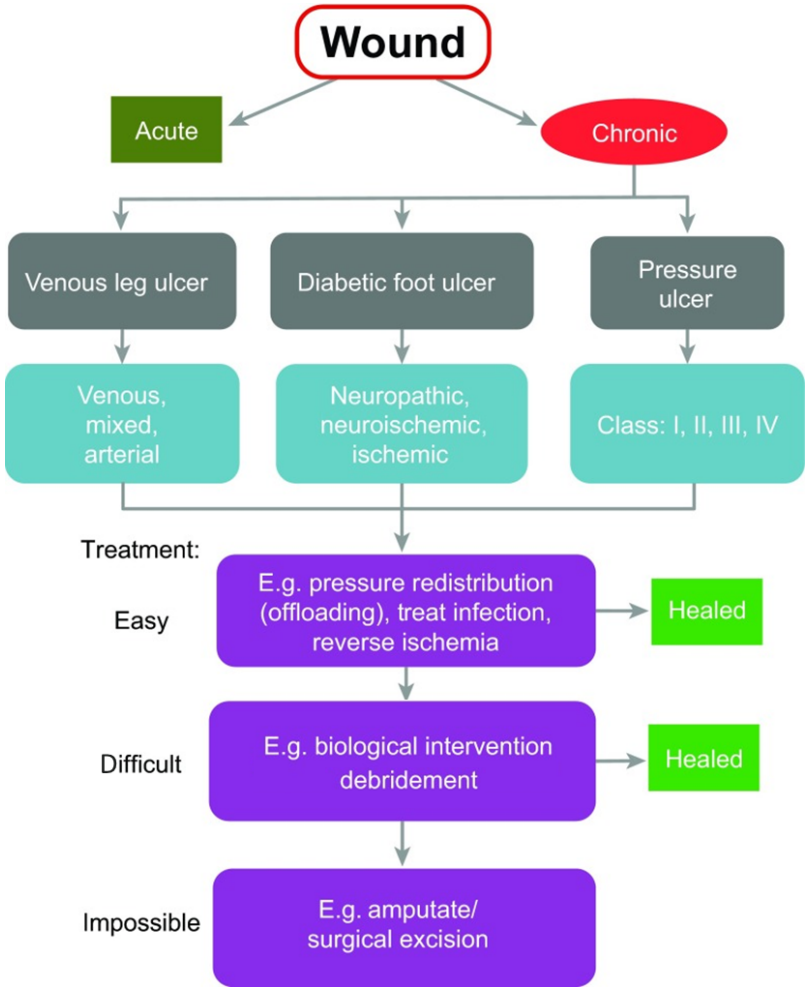


Figure 11: Flow diagram of chronic wound management (adapted from [64]).

Depending of the ulcer type, this first step should include strategies that reduce the pressure on the wound. For PUs, methods that alleviate persistent or

repetitive cycles of pressure are used, such as using appropriate mattresses and turning immobile patients [79]. For venous LUs, the most common technique is the utilization of compression bandaging in order to control swelling and limit venous hypertension in the limb. This approach results in healing rates of around 70%; however, the ulcer recurrence is very high since the pathophysiological factors are still present and mostly not tackled [80].

Finally, for DFUs, offloading mechanisms are frequently used such as specific shoes or casts in order to redistribute the pressure on the plantar region around the injury sites. When ischaemia is present, it should be treated with drugs or surgery in order to improve arterial flow to the foot [81]. When the wound persists for longer, more aggressive treatment is needed with, for instance, biological intervention with maggot therapy to help removal of dead tissue, or surgical debridement via scraping with a scalpel to remove necrotic areas. Nevertheless, in cases where treatment is impossible, the last resort is amputation, especially when infection is present and is endangering the patient's life. As it can be easily understandable by the number of steps this process requires, a direct consequence of the longer healing period of chronic wounds is the higher cost in treating these wounds, and the main cost driver is the amount of nursing time needed.

1.5.1 Advances in wound care and current treatment

In most countries, chronic wounds are typically managed as a co-morbidity with other conditions, thus limiting the impact of efforts to overcome the growing challenge they represent. In health centres, ulcers are assessed by general practitioners that often lack specialised training in the diagnosis and treatment of

chronic wounds. However, the Danish model showed the benefits of having a team of different specialists – such as podiatrists, endocrinologists, and vascular surgeons – gathered in multidisciplinary wound care centres [82]. The development of specialised educational programmes is fundamental for the establishment of a healthcare structure within wound management, which would not only reduce the economic costs for wound management by up to 30% but also the human and social burden on society as a whole [83].

Several years ago, as the underlying cellular and biological mechanisms of chronic wounds began to be understood, a new approach was developed that allows clinicians to recognise the cause of the problem through the identification of the critical components of a non-healing wound. The "TIME" acronym has been designed to help remember the observable characteristics of a chronic wound: T – Tissue (non-viable or deficient); I – infection or inflammation; M – Moisture imbalance; E – Edge of the wound (non-advancing or undermining). The TIME framework has the aim of implementing a care programme that assesses the patient as a whole (Figure 12). This includes a wound bed preparation care cycle that strives to achieve a stable wound, with particular emphasis on the healthy granulation of the tissue and a well-vascularised wound bed [84]. As more healthcare professionals are aware of the nefarious consequences of chronic wounds, this simple tool can be used as a treatment guide. Patients can then be referred to a team that can identify the barriers to healing and develop a care plan aimed at removing these obstacles.

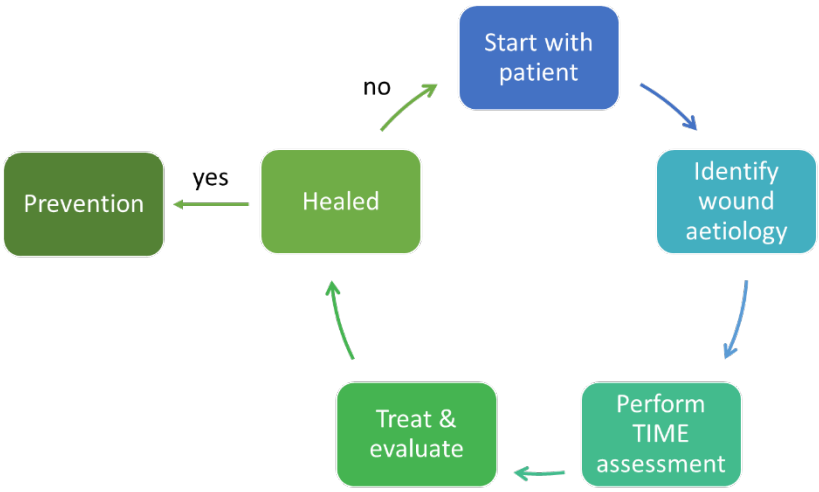


Figure 12: The wound care cycle in the TIME framework; T – Tissue, I – infection or inflammation; M – Moisture imbalance; E – Edge of the wound (adapted from [85]).

As an example, the treatment for diabetic ulcers always encompasses 5 key stages: wound debridement – that is extensive and regular and includes treatment of calluses, since one of the most consistent obstacles in the healing of many chronic wounds is a build-up of necrotic debris at the wound edge; wound dressing – that should offer protection from infections while keeping a moist environment that promotes tissue regeneration and removes wound exudates; pressure off-loading – to remove pressure and trauma; revascularization – that is essential to preserve adequate blood flow and can prevent up to 80% of amputations [86]; and infection management – to avoid infection and treat biofilms. Regarding this latter stage, usually an agent active against Gram-positive cocci is given as empirical treatment in the UK because infections with *Staphylococcus aureus* are the most common in patients with DFU. However, in severe or recurrent DFI, treatment should also include extended coverage for Gram-negative bacilli and enterococci.

Several studies have concluded that the use of prophylactic medication is not helpful in preventing infection, but a reasonable amount of prevention could be

achieved with patient education. A detailed explanation of good foot hygiene, proper protection of pressure points and early local care of shallow ulcers could prevent the formation of chronic wounds [32]. Thus, the ideal scenario would be to deliver a mass educational campaign in all health centres with a large population of diabetic patients.

1.5.2 Adjunctive treatments and future perspectives

As the medical and research communities are aware of the impact of non-healing wounds, there has been an immense drive to develop research aimed at improving the clinical outcome of patients with CW. While the golden standard in, for instance, DFU treatment is considered to be sharp debridement – particularly involving callus removal, since it can reduce pressure by up to 30% [87], nowadays there are more sophisticated treatments that, when used synergistically, can increase the rate of wound healing.

Wound care has become increasingly important not only because of the rise of chronic wounds, but also because of the morbidity associated with them and the billion-dollar industry that they create. High-tech wound dressings that can be made from hydrogels, alginate, polyurethane films or foams, and can be impregnated with therapeutic substances ranging from natural products like honey or silver, to topical antiseptics and antibiotics, are very commonly used in different settings to help manage CW. These serve a myriad of functions, among which keeping the wound sterile or reducing the wound bioburden are the most relevant to prevent infection and development of biofilms. More advanced surgical skin grafts, either allogenic

(from the same person) or using modern synthetic skin substitutes, can be used as a treatment option in patients with recalcitrant ulcers (reviewed by [88]).

Nonetheless, therapies like hyperbaric oxygen and negative pressure treatments have occasionally been used as adjuncts to standard wound care. Both are based on the observation that hypoxia negatively impacts the normal healing course. However, they have been associated with potential adverse effects, such as oxygen toxicity to brain and lungs, so their use is tightly regulated, and doctors should only apply these when a favourable treatment response is most likely [89].

Since inflammation and remodelling are partially controlled by the level of different growth factors, a lot of research has been done on its application to CW treatment. Application of exogenous growth factors to ulcers is already authorized in some countries, but this procedure shows better results in well-perfused and properly debrided DFU [90]. However, due to their global action as stimulators of angiogenesis, cellular proliferation, and migration, concerns have been raised over its security since some studies reported an increased mortality rate from systemic malignancies after treatment with recombinant human platelet-derived growth factor. Future perspectives in care involve fine-tuned treatments like gene therapies, use of stem cells, inhibition of cytokines and application of bacteriophages [6].

1.6 Microbiology of wound infections

A key decisive factor in whether the wound heals is the presence of infection, as previously discussed. Infection happens when the balance between

microorganisms and the host immune system is altered, and bacteria invade viable tissue and disseminate, leading to local and systemic host responses [91]. If we aim to prevent or halt infections in chronic wounds, our top priority should be to understand wound microbiology, with special focus on wound pathogens.

In healthy individuals the skin microbiota is formed by a diverse collection of bacteria and fungi. With the advance of 16S ribosomal RNA (rRNA) Polymerase Chain Reaction (PCR) typing and gene sequencing, it has been possible to characterise the diversity of commensal and pathogenic bacteria and address their role in both health and disease [92]. When the skin integrity is compromised, a wound is formed and bacteria easily contaminate it. Moreover, the nutritious and moist wound environment is conducive to rapid colonisation and proliferation.

Colonisation is usually defined by the existence of replicating microorganisms and the absence of tissue damage [93], and nowadays it is thought to occur as a normal process in open wounds. Nonetheless, as mentioned in section 1.4.4, it is the presence of clinical signs of infection that allows clinicians to diagnose infections in chronic wounds. When there is an increased bioburden in a wound and a critical point of bacteria colonisation is reached, there is a shift in host-microbe interactions that has been identified as the start of local infection [94]. This process is marked by the establishment of biofilms, whose development encompasses adherence to wound bed tissue and aggregation as seen in Figure 10. This critical colonisation is a state of transition to scenarios where there is a marked delay in the wound healing process (Figure 13). From the local infection stage, if bacteria are left unchecked, they will actively invade the adjacent tissue and continue spreading until they reach the

circulatory system and cause major systemic infection, leading to amputation and even death.

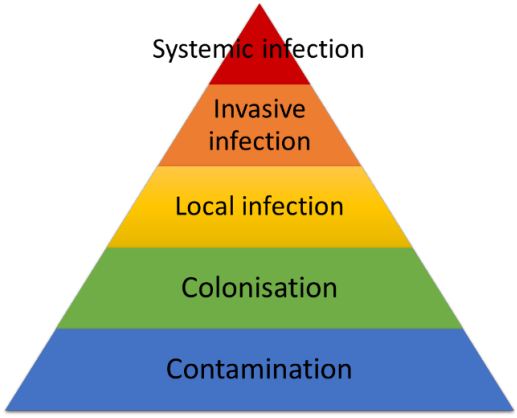


Figure 13: The clinical spectrum of microbial wound colonisation and infection (adapted from [9]).

Most of the work initially done in microbiology of CW, particularly in DFUs, was centred on the identification of bacterial species present in wounds, either colonised or showing clinical signs of infection. Later, the organization and ecology of bacteria started to be explored, with special focus on the differences in the results of different sampling techniques. Now, research has evolved into trying to understand how infection adversely affects wound healing and the specific role of pathogenic bacteria in disease. It is important to comprehend how biofilm formation influences bacteria-host interactions and, most importantly, antibiotic resistance, since it is relevant to know why antibiotic treatment often fails and patients eventually need to be amputated.

1.6.1 Bacterial diversity and polymicrobial infections

Between 1970 and 2000, the majority of microbiology studies in chronic wounds were conducted in Europe and North America. Characteristically, these

studies suggested that more than one type of organism was involved, including Gram-positive, Gram-negative, aerobic, and anaerobic species. Results suggested that, despite some degree of stability, ulcers are a dynamic environment and microbial interactions probably cause an enhanced pathogenic effect [95].

In a wound microbiology review in 2001, Bowler and collaborators highlighted that it was usual to find a correlation between normal flora species in close proximity and microorganisms present in wounds [91]. Since non-healing ulcers that are hypoxic are considered more prone to infection than wounds involving well-perfused tissue, it was hypothesised that this would likely facilitate colonisation of endogenous micro-organisms. Research then focused on identifying bacteria that were likely to interfere with wound healing and tried to differentiate these pathogens from the skin flora.

As researchers became aware that most of the sampling methods and traditional culturing techniques excluded fastidious and mostly anaerobic bacteria, there was an increase in interest in this group. A 1999 study that surveyed infected vs non-infected leg ulcers showed that anaerobic bacteria (particularly *Peptostreptococcus* spp. and *Prevotella* spp.) were much more frequent in the first group, representing 49% of the total microbial composition, compared with 36% in non-infected leg ulcers [96]. Later, a study supported the view that anaerobes are very common – even representing more than half of the total number of organisms found in chronic wounds – and could have a competitive advantage because of their ability to impair host immune cell function [97]. It was agreed, however, that either type of bacteria could not individually explain all the pathogenic potential of

microorganisms, but together the aerobic-anaerobic interactions were viewed as a critical component of the pathogenicity of chronic wound infections [91].

There was also a consensus that aerobic Gram-positive cocci, especially *S. aureus,* were the most common pathogens. In a long-term non-healing ulcer, particularly if it was previously submitted to antibiotic treatment, a polymicrobial infection with Gram-negative bacilli and anaerobes was also very common [98]. A widespread opinion at the time was that empiric treatment against *S. aureus* was very cost-effective and thus microbiology sampling should be used to exclude dangerous pathogens, like methicillin-resistant *S. aureus* (MRSA) [78]. Moreover, the presence of *P. aeruginosa* or beta-haemolytic streptococci was viewed as a sign of a complicated long-term infection that needed high doses of antimicrobial therapy [99]. In fact, ulcers with *P. aeruginosa* were usually described as larger and harder to treat [100]. Identifying these main pathogens was then the key to define the antibiotic treatment and help the management of the various types of chronic ulcers.

Conversely, another school of thought defended that, since ulcers (particularly DFUs) are polymicrobial, there was no need to precisely identify the causative microorganisms [101], and that all species associated with chronic infection should be considered potentially synergistic [102]. These and others contended that repetitive cultures following an initial test culture were a waste of resources since they would not change the initial treatment. Further support for this view came from a different study whose results suggested that antibiotic testing followed by a long course of antibiotics had the same effectiveness as culture-guided empiric treatment [103]. Albeit less consistent with more recent data [104, 105], these ideas were

relevant for the decision to diagnose chronic ulcers based on clinical grounds and not only on microbiology cultures [106].

In summary, the idea that a significantly lower probability of healing is associated with the interaction of bacteria in polymicrobial infections has been around for more than 20 years. When infections are present in chronic wounds, polymicrobial infections are found in 27.2% (32) to 52.2% (33) of infected ulcers and are mainly constituted by co-infections of *S. aureus* and *P. aeruginosa*. Co-infections with these species were suggested to be more virulent and result in worse patient outcomes than single-species infections (34). There is also an understanding that the wound microbiota changes over time, and surface aerobic bacteria can create adequate conditions that favour the growth of anaerobic bacteria, or produce by-products that support the growth of other cohabiting microorganisms (Figure 14).

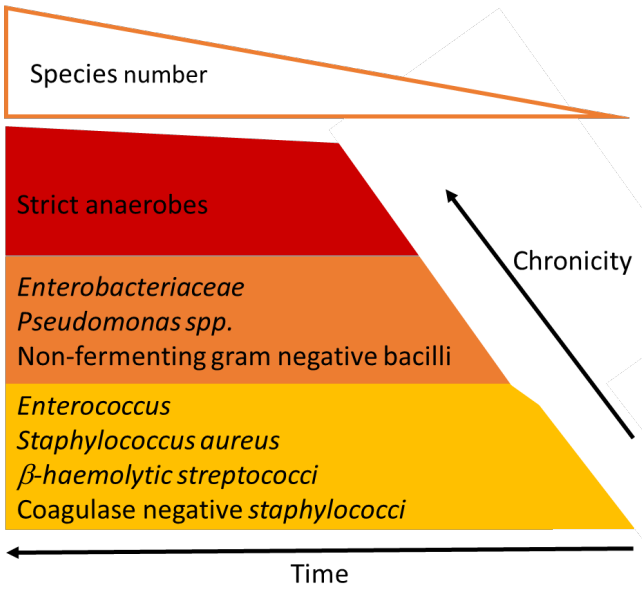


Figure 14: Development of the microbiology of the diabetic foot ulcer over time. The colonising bacterial species are dependent on the chronicity of the ulcer and the age of the wound. Species number increases resulting in the evolution of a polymicrobial community (adapted from [107]).

However, to date there are no definitive studies of bacterial succession within chronic wounds, the influence of antibiotics on this succession, or of the interactions between bacterial succession and healing [108]. And even though the majority of studies seem to agree that *S. aureus* is universally present in chronic wounds, the bacterial diversity depends mostly of the geographical and climate conditions.

In recent years, the prevalence in chronic wounds of other species like *Streptococcus*, *Enterococcus*, *Enterobacteriaceae,* and *Pseudomonas* has been on the rise. In Africa, the Mediterranean (particularly Turkey), and in Eastern countries like India and China, there is a predominance of Gram-negative bacteria over Gram-positive bacteria [109, 110]. The reasons for this have been suggested to be climate-related – for instance increased foot sweating due to the hot climate and increased humidity, but also important is the poor sanitation and the sewage that is disposed untreated and contaminates rivers with antibiotic residues, increasing the appearance of antibiotic-resistant organisms. However, over-the-counter availability of antibiotics and poor control over self-medication seem to play a bigger role [111].

1.6.2 Sampling technique dilemma

One aspect that remained controversial for a long period was which method was more appropriate for culturing microorganisms from chronic wounds. Initially, most reports defended that swab sampling should be used because it was cheap and some later studies showed a good correlation with deep tissue samples or aspirates. However, evidence accumulated in the opposite direction and, in the span of a decade, the general opinion changed towards the current guidelines, which state that a tissue specimen should always be used when obtaining cultures from ulcers.

What was argued was that even though sampling techniques based on surface cultures differ from tissue biopsies, it is agreed that wound contamination will occur from sources external to the wound and that both techniques haven proven valid in identifying these contaminants. However, with the emergence of sequencing techniques, the amount of information that superficial tissue is likely to harbour, including huge diversity of aerobic and anaerobic bacteria, can prove to be misleading when trying to identify microorganisms that may invade deeper tissue and aggravate the patient's health.

Analysing data reported in several studies, the percentage of polymicrobial infections found in wounds tends to be lower when a swab method is used to collect the samples compared with tissue biopsy. Nowadays some authors still suggest that these differences are not significant [112, 113] but, according to Bjarnsholt and collaborators the swab method is not completely accurate because it only surveys the surface of the wound [114]. Indeed, using fluorescence in situ hybridization combined with confocal laser scanning microscopy, Fazli and collaborators [115] showed that there is a different spatial structure in the colonisation of *P. aeruginosa* and *S. aureus* in chronic wounds: *S. aureus* has a tendency to colonize the surface of the wound while *P. aeruginosa* is mainly found in the deepest part of the tissues, thus explaining why testing through swab culture techniques probably underestimates the presence of *P. aeruginosa* in chronic wounds.

As in most real-life scenarios, the majority of health care providers lack the necessary funds to systematically do deep tissue biopsies. A compromise between sampling cost and patient care (particularly focusing on avoiding invasive and

potentially painful procedures) is the use of curettage. This is done through the aseptic scraping of tissue at the base of the ulcer after it has been cleansed and thoroughly debrided. This technique, which can be performed using a scalper blade or a dermal curette, has been demonstrated to yield better results than traditional wound swabs. In combination with this, it is also very important to assure an adequate transport of the samples to the microbiology lab. Specimens for culture should be transported in sterile containers in appropriate transport media adequate to the culture type [62].

A point that has been debated is whether ulcers that are clinically uninfected should be subjected to culturing. While this is currently not recommended, it is allowed for epidemiological studies. Additionally, cultures should not be repeated unless the patient is not clinically responding to treatment – except in cases of infection control surveillance of multidrug-resistant bacteria. Nonetheless, with the advancement of new non-invasive techniques to diagnose the presence of bacteria, like the MolecuLight device [116], it seems apparent that even ulcers with no clinical signs of infection (see Table 3) can have an elevated bacterial load – that will most likely affect the healing rate of the wound.

Another relevant issue that has to be taken into consideration is that bacteria are not evenly distributed within the wound. This fact has been known since the 80's, when a study by Sapico et al. reported only a 63% concordance between biopsy specimens taken from the periphery and the centre of pressure ulcers [117]. At the end of the day, it is still essential to quantify and determine the causative invasive

bacteria in wound infection, and investigate how pathogens are likely to interfere with wound healing and cause infection.

1.6.3 Antibiotic resistance

The development and worsening of an infection in chronic wounds is often more feared than the increase of antibiotic resistance in the microbial community. Consequently, clinicians choose to administer prolonged courses of antibiotics to high-risk patients in an attempt to eradicate or at least control the infection [118]. In general, antibiotic prescription is recommended for the treatment of established infections in chronic wounds, although guidelines clearly state that an antimicrobial susceptibility (AS) test should be performed beforehand [119]. Nevertheless, when infections are severe, doctors usually start empiric treatment as soon as possible, based on the results of antimicrobial resistance profiles for the geographical area of the clinic, and change the treatment if need be, when results specific for each patient are available [120].

Until January 2016, the common practice in clinical microbiology laboratories in the UK was using the British Society for Antimicrobial Chemotherapy (BSAC) disc diffusion method for AS testing. However, with an increased awareness of the importance of comparing resistance rates in surveillance studies in different countries, there has been an international effort to harmonize different protocols for AS testing. The European Committee on Antimicrobial Susceptibility Testing (EUCAST) launched a standardized disc diffusion AS method that has been implemented across all European countries. Additionally, they established a joint working group with the American Clinical and Laboratory Standards Institute (CLSI) in order to develop

reference breakpoint tables that can be used by laboratories worldwide. This effort has led to the publication of zone diameter quality control criteria for several non-fastidious and fastidious reference strains for each phenotype: R – resistant; I – intermediate; and S – sensitive [121]. These strains are available worldwide from several type culture collections, but the most commonly used are the American Type Culture Collection (ATCC) strains, and the National Collection of Type Cultures (NCTC) strains.

Nevertheless, even these new AS protocols are limited to the analysis of only a few isolates per patient per time point, so there is a high risk of intra-sample phenotypic diversity being underestimated [122]. The validity of these tests has been challenged by several studies performed on bacterial strains isolated from lungs with chronic infections due to cystic fibrosis which highlighted the importance of phenotypic diversity and heterogeneity in the context of the treatment of chronic infections [123, 124]. Consequently, the clinical community should be aware that diversity can complicate microbiological analyses performed on patient samples [124, 125].

The treatment of chronic wounds like DFIs has changed over the past 30 years with the development of new microbiological diagnosis, but also with the increased knowledge about pathogens in general, and specifically wound microbiology – as described in the previous section. The wider community is aware that the development of new antibiotics, with only a few exceptions, has been stagnant. So our general awareness for the need to fine-tune the duration and spectrum of

antibiotic therapy in the treatment of infections is of the utmost importance in order to find a sustainable solution for the threat of antimicrobial resistance (Table 4).

Table 4: Changes in the microbiological knowledge and antimicrobial treatment of diabetic foot infections in the last 30 years (adapted from [110]).

Research field	1985	2015
Pathogens	Methicillin-susceptible *Staphylococcus aureus*, streptococci, Enterobacteriaceae	More multidrug-resistant organisms (MRSA, ESBL); predominance of Gram-negative pathogens in (sub)tropical climates
Microbiological diagnosis	Standard cultures, usually of swab specimens	Aerobic and anaerobic cultures of tissue specimens (soft tissue and bone); molecular microbiology (e.g. PCR); metagenomics
Antibiotic agents	Penicillins; 1st to 3rd generation cephalosporins; some 2nd generation fluoroquinolones	4th/5th generation cephalosporins; carbapenems; 3rd/4th generation fluoroquinolones; linezolid; daptomycin
Route of administration and site of treatment	Initial (sometimes prolonged) intravenous administration, usually in hospital	Mostly oral (sometimes after a brief intravenous course), even in the presence of vascular disease or osteomyelitis; some topical; outpatient except for severe infections or complex treatments
Spectrum of antibiotic therapy	Relatively broad (directed at Gram-positive and Gram-negative pathogens)	Very broad empiric treatment for severe infections; more targeted for mild / moderate infections and definitive therapy
Duration of antibiotic therapy	Many weeks for soft tissue infections; ≥6-12 weeks for osteomyelitis	1-2 weeks for soft tissue infections; 4-6 weeks for osteomyelitis

MRSA methicillin-resistant *Staphylococcus aureus*; ESBL extended-spectrum beta-lactamase

In the UK, there has been an effort to implement an antimicrobial stewardship programme – that consists of limiting antibiotic use to when it is absolutely needed – and to develop good infection control to prevent the spread of antibiotic resistance. The IWGDF guidelines for the choice of empirical antibiotic treatment, specifically for chronic wounds like DFIs, are widely used in Europe with good results. However,

recent studies in other regions highlighted the importance of having nationwide epidemiology studies to identify critical pathogens [109]. As treatment depends on which pathogens and antibiotic resistance are more common in each specific area, in order to reduce the inappropriate and unnecessary use of antibiotics in DFIs, it is necessary to know which bacteria the patient is most likely to have [126]. Although positive identification of specific microorganisms isolated from chronic wounds and the associated resistance profiles may be interpreted by clinicians as an infection that requires antibiotic therapy, it is important to highlight that without clinical signs of infection, the patient should not be treated with systemic antibiotics. It is therefore suggested that microbiological information and clinical observations be taken into consideration before a treatment is decided [91].

Alongside antimicrobial testing to check for resistance, a more detailed investigation of other molecules produced by the microorganisms that infect chronic wounds could be done. In a clinical set-up this is almost impossible to do routinely because it is costly and time consuming. Nonetheless, in an academic set-up, this type of research could provide invaluable information that would lead to a better understanding of how infection develops in chronic wounds. With this, we could aim to achieve a reduction of the overall time needed to properly heal these wounds and avoid amputations, as solve the infection is a starting point for healing the wound.

1.7 Project overview

The initial goal of this project is to assess *P. aeruginosa* diversity in chronic wounds and its implications for antibiotic treatment. The question of whether phenotypic variability impacts the validity of antimicrobial susceptibility testing has been studied in chronic infections in patients with cystic fibrosis [124, 125, 127, 128], but not in wounds. Thus, this work will help to fill that gap by investigating *P. aeruginosa* phenotypic diversity in chronic diabetic ulcers. This will facilitate a comparison with chronic infection in the cystic fibrosis lung to determine whether diversity is a mechanism that arises universally as a response to a prolonged and non-healing infection, or simply specific to certain environments.

As discussed in this introductory chapter, chronic wounds are a common complication of diabetic ulcers, which are a major burden to health care systems worldwide [129], and can frequently result in lower limb amputation due to the intractability of the infection [68]. Diabetic ulcers often become chronically colonized with polymicrobial communities that include *S. aureus* and *P. aeruginosa* [119]. Polymicrobial infections have been suggested to be more virulent, antibiotic resistant and result in worse patient outcomes [119, 130, 131], but the reasons why remain unclear. With this in mind, the polymicrobial context of chronic wounds will also be investigated through the study of *P. aeruginosa* and *S. aureus* interactions.

To achieve the above goals, bacterial populations isolated from bone, blood, and soft tissue from five patients and six chronic diabetic ulcers will be investigated. Initially, the research will focus on understanding whether phenotypic diversity is present in *P. aeruginosa* populations through the analysis of antibiotic susceptibility

and phenotypes traditionally associated with pathogenicity in chronic wound infections. If phenotypic diversity occurs in chronic wounds, whether this correlates with the clinical status of a patient will also be evaluated. This will enable a new set of protocols to be devised that can be used to facilitate better and more effective treatment regimens. Furthermore, *S. aureus* isolates from two chronic wounds will be used to examine the polymicrobial context of chronic diabetic foot ulcers through the study of *S. aureus* – *P. aeruginosa* interactions using isolates that either co-evolved in the same ulcer or originated from different ulcers. This information will be invaluable in our attempts to understand how ecology influences the evolution of different species within wound infections and how this contributes to antibiotic resistant polymicrobial infections. In summary, this work will advance knowledge in this field by elucidating mechanisms that could be essential for the adequate treatment of patients in order to reduce the prevalence of chronic wound infections.

Chapter 2: Methods

2.1 Chronic wound sampling

Five patients diagnosed with chronic diabetic ulcers (V-Z) and aged between 49-78 years old were included in the study – four with foot ulcers and one with a leg ulcer – see Table 5 for full patient information and CW characteristics. Patients V, W, and Z had short-term ulcers, defined by the presence in the wound of *P. aeruginosa* for less than 6 months, while patients X and Y had long-term ulcers. Patients V, W, and X had osteomyelitis at the time of sampling, while patient Y had previously had it, and patient Z never had it. From the different wounds, 3 types of samples were collected: soft tissue (T), bone (B), or blood (S), and sampling methods varied between bone or tissue biopsy, blood culture, swab on soft tissue, and aspirate of tissue exudate. Ulcers of patients V and X contained both *S. aureus* and *P. aeruginosa* at the time of sampling. Specimens grown on blood agar plates were provided by Dr Tim Sloan (Clinical Microbiology Department, Nottingham University Hospitals).

Table 5: Patient information, chronic wound characteristics and sampling details from the biopsy specimens supplied by the Clinical Microbiology Department, Nottingham University Hospitals NHS Trust Laboratory.

Patient code	Age	Wound location	OM	Duration (months)	LT	Sample		
						Code	Type	Method
V	78	big toe	Yes	3	No	CW2	Bone	biopsy
W	78	calcaneal ulcer first metatarsal	Yes	5	No	CW3	Tissue Bone	biopsy biopsy
X	55	calcaneal ulcer	Yes	25	Yes	CW4	Tissue Blood	biopsy culture
		calcaneal ulcer	Yes	26		CW5	Tissue Bone	biopsy biopsy
Y	49	heel ulcer	No	36	Yes	CW6	Tissue	aspirate
Z	77	leg ulcer	No	3	No	CW7	Tissue	swab

Age: patient age at sampling time, OM: osteomyelitis at sampling time, Duration: time since first recorded identification of *P. aeruginosa* or *S. aureus* in the ulcer, LT: long-term ulcer defined by the presence in the wound of *P. aeruginosa* for more than 6 months.

Bacteria on blood agar plates were mixed with 2 mL of phosphate buffered saline pH 7.4 (PBS) (Oxoid). This mix was serially diluted to 10^{-8} in PBS, and 100 µL of each dilution was plated, spread and incubated overnight at 37 °C. *Pseudomonas* Isolation Agar (PIA) (Sigma-Aldrich) was used to isolate *P. aeruginosa* and Baird Parker Agar (BPA) with egg yolk tellurite emulsion (Sigma-Aldrich) was used to isolate *S. aureus*. 40 colonies, thought to be *P. aeruginosa*, from each chronic wound population (CW2 to CW7) and type of sample (B, T, and S) were selected from PIA plates (usually dilutions of 10^{-5} and 10^{-6}).

2.1.1 Colony PCR

Colony PCR was performed to amplify the 16S rRNA gene to confirm whether each individual isolate was *P. aeruginosa*. For each 50 µL PCR reaction, 25 µL 2X OneTaq PCR master mix, 2 µL 16S specific primer (5'-GGCTGGATCACCTCCTT), 2 µL 23S specific primer (5'-TGCCAAGGCATCCACCG) and 21 µL molecular biology grade water (Hyclone) were used. PCR conditions were as follows: 95 °C for 5 min (cell lysis), 95 °C for 30 s (denaturation to single-stranded DNA), 60 °C for 30 s (primers anneal), and 72°C for 1 min (extension of DNA). PCR fragments were then purified using the QIAQuick PCR Purification kit (Qiagen) according to the manufacturer's protocol, and sent to the University of Nottingham DeepSeq Facility, for sequencing. The colonies were confirmed to be *P. aeruginosa* by homology comparison against sequenced microbial genomes using the National Centre for Biotechnology Information (NCBI) Basic Logic Alignment Search Tool (BLAST) programme [132].

2.1.2 Bacterial isolate maintenance

Each confirmed *P. aeruginosa* colony was mixed with 1 mL of Lysogeny Broth (LB) in wells of 24-well microplates, and grown overnight on a shaking platform at 37 °C. 600 µL of each isolate was transferred to 2 mL sterile cryotubes with 400 µL of glycerol (50% w/v) and stored at -80 °C until needed. In total, 360 *P. aeruginosa* isolates from different sample types and different wounds were stored. 20 probable *S. aureus* colonies from CW2 and CW4 were selected from BPA plates and transferred to DNase agar plates (Oxoid). These plates were used to check the production of deoxyribonuclease (DNase), and a positive result confirmed the presence of *S. aureus*. One confirmed colony from each chronic wound was kept at -80 °C as described above.

2.2 Bacterial growth and preparation

When a protocol refers to samples grown O/N, it means that glycerol stocks of bacterial wound isolates stored at -80 °C were streaked onto LB agar plates and left incubating overnight at 37 °C. Then each isolate was transferred to 50 mL tubes with 10 mL of filter sterilized synthetic wound fluid (SWF) – made of 50 % peptone water, and 50 % foetal bovine serum (Gibco) – which has previously been describe to mimic the conditions of chronic wounds [133]. Tubes were incubated at 37 °C for 18 h with shaking at 200 rpm.

For the phenotypic assays, due to space limitations, isolates from each chronic wound and sample type were divided into batches of 10 isolates with the

P. aeruginosa PAO1 Nottingham subline strain [134] as control (referred as PAO1 from here on). Each batch consisted of three biological replicates per sample, in a total of 33 tubes per batch. After 18 h, OD_{600} was measured using an Infinite Pro200 (Tecan) plate reader, by transferring 100 µL of culture to a 96-well flat-bottom transparent plate (Greiner Cellstar) and SWF was used as a blank. The cultures were centrifuged at 4,300 rpm for 10 min, and the supernatants filtered using a 10 mL syringe and a 0.2 µm filter (Minisart). The filter-sterilised supernatants (FSNs) were aliquoted in 2 mL and 5 mL tubes and stored at -20 °C until required (Figure 15).

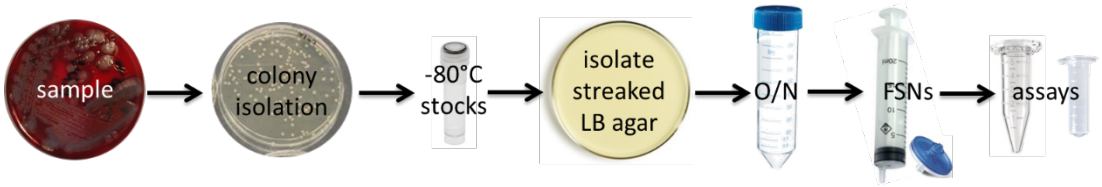


Figure 15: Protocol overview from sample collection to storage of filter-sterilised supernatants (FSNs) that will later be used in *P. aeruginosa* phenotypic assays.

Cell growth was monitored over time on *P. aeruginosa* representative isolates from each diabetic foot ulcer, on two *S. aureus* isolates isolated from CW2 B and CW4 T diabetic foot ulcer samples, and on two widely used lab strains PAO1 (*P. aeruginosa*) and Newman (*S. aureus*) [135]. The inoculum for each isolate was standardised to OD_{600} = 0.1 in 10 mL of SWF and 50 mL tubes were incubated at 37 °C for 20 h with shaking at 200 rpm. Every 2 h, 100 µL were transferred to a 96-well flat-bottom transparent plate (Greiner) and serial diluted to 10^{-7}. 10 µL (*P. aeruginosa*) or 5 µL (*S. aureus*) of 10^{-3} to 10^{-7} dilutions were spotted in LB agar (in duplicate), incubated overnight at 37 °C and then CFU was scored.

2.3 *P. aeruginosa* phenotypic assays

2.3.1 Identification of colony morphologies on Congo Red agar plates

Congo Red agar (CRA) plates were made using a protocol previously described [136] that was adapted to include 0.1 % casamino acids and 4 mM $CaCl_2$. Each -80 °C glycerol stocked isolate was streaked onto LB agar plates and incubated overnight at 37 °C. Bacteria were then transferred from LB plates to CRA using sterilized toothpicks, in duplicate. The plates were incubated overnight at 37 °C, and then left at 20 °C until the phenotype developed (usually 48 to 72 h). Control strains used were PAO1 as reference wild type (Nottingham substrain), a PAO1 *pel*/*psl* double mutant that produces smooth colonies, and a PAO1 *wspF* mutant that produces small and wrinkly colonies. The plates were inspected visually, the phenotype recorded, and pictures were taken using an EPSON Photo 2480 scanner.

2.3.2 AHL biosensor assay

The production of the QS signalling molecules *N*-butanoyl-homoserine lactone (C4-HSL) and *N*-3-oxododecanoyl-homoserine lactone (3-oxo-C12-HSL) was assessed using the *lux* based reporter strains *Escherichia coli* pSB1142 (*lasRI'::luxCDABE* for 3-oxo-C12-HSL) and *E. coli* pSB536 (*ahyRI'::luxCDABE* for C4-HSL) [137, 138]. These biosensor strains were plated onto LB + tetracycline 10 µg / mL and LB + ampicillin 50 µg / mL respectively, and incubated overnight at 37 °C. Each biosensor was grown in triplicate (per plate used) in 5 mL LB + antibiotics for 4 h at 37 °C and 200 rpm. Exponential cultures were standardised to OD_{600} = 1.0 in 1 mL of PBS and added to 19 mL of LB agar cooled to 40°C in a 50 mL tube. The mixture was

poured into a plate and left to dry by a Bunsen burner. Wells were made in the agar with the top of a yellow tip, and 90 µL of an FSN (obtained as described above) was added to each. Plates were incubated at 37 °C for 30 min to 1 h without being inverted, and luminescence was assessed using a light camera.

2.3.3 Qualitative protease assay using 15 % skim milk agar plates

3.6 g of Bacto agar was added to 255 mL of distilled water and autoclaved. When the agar temperature was at 40 °C, 45 mL of sterilized (5 min of UV light) skimmed UHT milk was mixed with the agar. 15 mL was dispensed to each plate and left to dry near a Bunsen burner for 15 min. Frozen bacterial FSNs (obtained as described above) were thawed and 10 µL of each was spotted, alongside 10 µL of proteinase K 10 µM (positive control) and SWF (negative control). Each batch (10 isolates + PAO1) and the controls were added to the same plate (in duplicate). Once dried, the plates were incubated at 37 °C for 18 h.

2.3.4 Quantification of siderophore production

Pyoverdine (PVD) and pyochelin (PCH) production was measured using a previously described assay [139]. Briefly, 100 µL of previously thawed bacterial FSN was transferred (in duplicate) to a 96-well flat-bottom black plate (Greiner) and the fluorescence was measured using an Infinite Pro200 (Tecan) plate reader. PVD production was measured as relative fluorescence units (RFU), at an excitation wavelength of 400 nm and an emission wavelength of 460 nm, with a gain of 61. PCH production was measured as RFU, at an excitation wavelength of 350 nm and an emission wavelength of 430 nm, with a gain of 82. Gains were optimised and

standardised to prevent fluorescence scans with readings outside the detection range. Because PVD is still excited at 350 nm and has ten times more fluorescence than PCH, a correction was used to obtain an unbiased estimate of PCH RFU at 350/430 nm (*z*), which is defined as $z=w-xy$, where *w* is the total RFU measured at 350/430 nm, *x* is the RFU measured at 400/460 nm and *y* is the fraction leakage, i.e., the amount of PVD measured in the PCH channel. According to [139], 5% leakage was estimated, and then RFU values were divided by the corresponding OD_{600} values.

2.3.5 Pyocyanin quantitation

Pyocyanin (PYO) was measured using a previously described assay [140]. Briefly, previously thawed bacterial FSNs were vortexed for 30 s to ensure complete oxidation of any PYO by ambient oxygen. The absorbance at 691 nm (Abs_{691}) was measured in 1-cm-pathlength cuvettes, using SWF as a blank. The Abs_{691} was divided by the OD_{600}, and the concentration of PYO was calculated according to the equation [PYO] (mM) = Abs_{691} cm^{-1}/ 4.31 mM^{-1} cm^{-1} and converted to µg/mL using MW_{PYO}= 210.24 g/L [141].

2.4 Determination of antibiotic susceptibility (BSAC method)

Isolates were grown O/N as described above. Each isolate was standardised to OD_{600} = 1.0 in 1 mL of PBS and vortexed gently. Each suspension was streaked onto Iso-Sensitest Agar (ISA) (Oxoid) using a sterile cotton swab in order to create a confluent bacterial lawn, and duplicate plates were prepared for each isolate. Antibiotic discs were placed onto the agar using a standard applicator (Oxoid). Five

antibiotics from the standard set to treat *Pseudomonas* were used: Ciprofloxacin CIP (1 µg), Gentamicin CN (10 µg), Piperacillin/Tazobactam TZP (85 µg), Ceftazidime CAZ (30 µg), and Meropenem MEM (10 µg) (Oxoid) plus one antibiotic from the extended set, Aztreonam ATM (30 µg) (Oxoid). Plates were incubated for 24 h, and afterwards the diameter of the zones of inhibition (mm) was measured and compared with standard breakpoints provided by the BSAC in tables available online (http://bsac.org.uk/wp-content/uploads/2012/02/Version-12-Apr-2013_final.pdf), and the isolates characterized as sensitive, intermediate or resistant. NCTC 10622, the *P. aeruginosa* strain used for this test in the Clinical Microbiology Department at Nottingham University Hospitals, was used as a positive control for each batch of samples tested.

2.5 Quantification of AQ molecules by LC-MS/MS

The production of six 2-alkyl-4-quinolone (AQ) signalling molecules [2-heptyl-4-hydroxyquinolone (HHQ), 2-nonyl-4-hydroxyquinolone (NHQ), 2-heptyl-4-hydroxyquinoline N-oxide (HQNO), 2-nonyl-4-hydroxyquinoline N-oxide (NQNO), 2-heptyl-3-hydroxy-4(1H)-quinolone (PQS), and 2-hydroxy-2-nonyl-4(1H)-quinolone (C9-PQS)] was quantified. Samples grown O/N were seeded at OD_{600} = 0.01 in 10 mL of SWF and incubated at 37 °C for 18 h with shaking at 200 rpm. They were centrifuged at 4000 rpm for 10 min and filtered using a 2 mL syringe with a 0.2 µm filter (Minisart). 10 µL of 10 µM 5,6,7,8-tetradeutero-3,4-dihydroxy-2-heptylquinoline (d_4-PQS) was used as an internal standard and was added in 500 µL of acidified (0.01% acetic acid) ethyl acetate (Sigma-Aldrich, UK) to 500 µL of the

filtered supernatant. The mixture was vortex-mixed for 2 min and the organic phase removed. The extraction procedure was repeated twice and the combined ethyl acetate extracts were evaporated in a speed vacuum (Jouan RC10 series, Thermo Scientific, UK) for 20 min at 45 °C. The dried samples were stored at −80 °C until further use. Samples were reconstituted in 50 µL methanol immediately prior to LC-MS/MS analysis that was carried out by Nigel Halliday (School of Life Sciences, University of Nottingham) according to a previously established protocol [142]. Only one sample per population was assayed (for CW2, CW3, CW4, and CW5) in triplicate and run twice. Standard calibration curves (R^2>0.995) were made using concentrations ranging from 0.5 µM to 10 µM of all AQs tested (Appendix A). For this assay we used PAO1 grown in SWF as a control.

2.6 Motility assays

P. aeruginosa PAO1 Nottingham subline (PAO1) was used as control and chronic wound isolates from blood (CW5 S1) and bone (CW5 B1) were grown O/N in triplicate and used in the assays described below [143]. For each assay, images were taken after incubation using a Nikon D40 camera, with a black background and indirect light reflected from the bottom. Note that for twitching assays, the agar was removed with twezzers before images were captured.

2.6.1 Swarming

A solution of 2.5% D-glucose was added to cooled down medium (0.5 % Bacto Agar and 0.8% Nutrient Broth #2). 20 mL were dispensed into Petri dishes, and plates

were allowed to settle for 15 min before drying for 30 min under laminar flow. 3 µL of O/N culture was spotted on the surface of each plate, and the plates incubated at 37 °C for 24 h.

2.6.2 Swimming

20 mL of medium (0.5 % yeast extract, 1 % tryptone, 1 % NaCl, and 0.3 % Bacto Agar) were dispensed into Petri dishes. Plates were allowed to settle for 15 min, 1 µL of O/N culture was inoculated into the agar, and plates incubated at 37 °C for 18 h.

2.6.3 Twitching

20 mL of medium (0.5 % yeast extract, 1 % tryptone, 1% NaCl and 1 % Agar Oxoid#1) were dispensed into Petri dishes. Plates were allowed to settle for 15 min before inoculation with 3 µL of O/N culture by stabbing through to the interface between the agar and plate bottom. Plates were incubated under high humidity conditions in a closed container at 37 °C for 48 h.

2.7 Microscopy

P. aeruginosa chronic wound isolates from bone (CW5 B1 – representative of the phenotypic profile 1) and blood (CW5 S1 – representative of the phenotypic profile 2) grown O/N were seeded at OD_{600} = 0.01 in 10 mL of SWF and incubated at 37 °C for 18 h with shaking at 200 rpm until they reached log phase.

2.7.1 Flagella staining

Samples were centrifuged at 4000 rpm for 10 min, and washed 3 times with PBS and stained with Alexa Fluor 488 NHS Ester (Invitrogen) for 1 h. After this, individual cells were observed in PBS with OD_{600} = 0.132 on borosilicate glass using Total Internal Reflection Fluorescence (TIRF) microscopy (60x, numerical aperture 1.4) with laser 488 nm at 10 Hz frequency [144, 145]. Images and videos were recorded for further analysis using a 2/3D multimode microscope with the help of Alessandro Carabelli (School of Pharmacy, University of Nottingham).

2.7.2 Transmission electron microscopy

600 µL 25% glutaraldehyde were mixed with 2.5 mL of 0.2M cacodylate buffer (pH 7.4) and 1.9 mL distilled water, and 1 mL aliquoted into each of 4 tubes. Samples were diluted to OD_{600} = 0.5 and 0.05, and 50 µL of each added to each tube. These were incubated for 1 h in an agitation wheel to allow for fixation. Afterwards they were centrifuged at 4000 rpm for 5 min and the supernatant was removed. 1 mL of 0.1ml of cacodylate buffer was added and after 10 min incubation with gently mixing, the samples were re-centrifuged. This was done twice to ensure that all fixation buffer had been removed. After the last wash, 100 µL of pure H_2O (Hyclone) were used to re-suspend the pellet. The tubes were left in the fridge overnight at 4 °C. Samples were placed on 200 mesh copper grids with carbon support and visualised on a Tecnai T12 Biotwin TEM, which runs at an accelerating voltage of 110kV. Images were captured using a Mega View SIS camera for analysis with the help of Denise McLean (Advanced Microscopy Unit, School of Life Sciences, University of Nottingham).

2.8 Infection assays

A pilot experiment on the effect of bone and blood isolates in two different infection models was investigated in collaboration with Prof. Kendra Rumbaugh and Rebecca Gabrilska (School of Medicine, Texas Tech University Health Sciences Center, Texas, U.S.). Both assays were performed using 3 individuals (larva or mouse) for each strain (bone and blood) and condition. Bacterial inocula used in larvae assays were either grown in LB or in wound-like medium (WLM) – constituted by 50% Bolton broth, 45% adult bovine plasma, and 5% laked horse blood [131] – which is similar to SWF, while bacterial inocula used in murine assay were grown in WLM only.

2.8.1 Larvae assay

A *Galleria mellonella* larvae infection was set up as described in [146]. Briefly, a 1 mL tuberculin syringe was used to inject 5 µL aliquots of bacteria or supernatant into *G. mellonella* larvae via the hindmost left proleg and the survival was assessed over a 7 day period.

2.8.2 Murine assay

A murine chronic wound infection was set up as described in [147]. Briefly, chronic wounds were induced by the surgical removal of a 1.5 × 1.5 cm full-thickness patch of skin from the shaved back of female Swiss Webster mice and covered with OPSITE dressing (Smith & Nephew IV3000) prior to inoculating the incision with 100 µL of bacteria (10^3 CFU). 4 days post-infection the mice were euthanized and wound, liver, and spleen sections from wounded mice were extracted, weighed and

homogenized in 1ml PBS. Homogenates were serially diluted and plated on LB agar to determine the number of CFU calculated per gram of tissue.

2.9 Genomic analysis

DNA was extracted from overnight cultures (O/N) of 10 *P. aeruginosa* chronic wound isolates (CW2 B1, CW3 T1, CW3 B1, CW4 T1, CW5 T1, CW5 T2, CW5 T34, CW5 T40, CW5 B1, and CW5 S1) using the GenElute Bacterial Genomic DNA Kit (Sigma-Aldrich) according to the manufacturers protocol. DNA concentration and purity were assessed using Nanodrop ND-1000 (Nanodrop Technologies). A single colony of each of the other 13 chronic wound isolates (CW2 B40, CW3 T40, CW3 B40, CW4 T40, CW6 T4, CW6 T25, CW6 T40, CW7 T1, CW7 T3, CW7 T11, CW7 T13, CW7 T17, and CW7 T36) was mixed in 100 µL PBS, and then re-streaked onto LB agar. After incubation at 37 °C overnight, bacteria were removed from the plates using a large sterile loop and mixed into barcode-labelled bead tubes provided by MicrobesNG (http://www.microbesng.uk). The tubes were mixed, sealed, and sent at room temperature to MicrobesNG.

At MicrobesNG, genomic DNA was purified and quantified before the preparation of libraries (see http://microbesng.uk/documents/5 for full protocol). Pooled libraries were quantified using the Kapa Biosystems Library Quantification Kit for Illumina on a Roche light cycler 96 qPCR machine. Libraries were sequenced on the Illumina HiSeq using a 250 bp paired end protocol. Reads were adapter trimmed using Trimmomatic 0.30 with a sliding window quality cut-off of Q15 [148].

Trimmed raw reads for all genomes were submitted to the comprehensive genome analysis service at the Pathosystems Resource Integration Center (PATRIC) online platform (https://www.patricbrc.org/) [149]. Based on the annotation statistics and on comparisons with other *P. aeruginosa* genomes in PATRIC, these 23 new chronic wound genomes were classed as of good quality. *De novo* assembly was performed using SPAdes version 3.7 [150], and contigs were annotated through MicrobesNG using Prokka 1.11 [151], and through PATRIC using RAST tool kit (RASTtk) [152].

Comparative genomics were performed by pairwise BLAST analysis using BLAST Ring Image Generator (BRIG) [153]. *P. aeruginosa* protein alignments were extracted from panX [154] and visualised by MEGA 7 [155]. Several services from PATRIC were used, particularly to construct a phylogenetic tree with the genomes of the 23 *P. aeruginosa* chronic wound isolates, and with the PAO1 (SAMN02603714), UCBPP-PA14 (SAMN02603591), LESB58 (SAMEA1705916), PASS2 (SAMN04041443), BWH035 (SAMN02584701), and M18 (SAMN02603849) strains, which were taken from Pseudomonas.com database [156]. Note that PATRIC's phylogenetic tree building algorithm pipeline makes use of BLAST [132], MCL [157], Muscle [158], hmmbuild and hmmsearch [159], Gblocks [160], FastTree [161] for progressive refinement support trees, and RAxML [162] for the main tree. Trees were edited using FigTree 1.4.3 [163].

For more detailed genomic analyses (Chapter 4) the eight genomes isolated from patient X namely CW4 T1, CW4 T40, CW5 T1, CW5 T2, CW5 T34, CW5 T40, CW5 B1, and CW5 S1 were used (see Table 17). Whole genome comparison was done with

8 isolates taken from patient X using BRIG as described previously. To facilitate the discussion, the genomes were named A to H according to the list in Table 6.

Table 6: Description of sequenced *P. aeruginosa* isolates from patient X.

Genome	Time point	Sample type	Isolate #	Phenotypic profile	% G+C content	Length (bp)
A	CW4	tissue	T1	1	66.43	6,452,696
B	CW4	tissue	T40	1	66.42	6,453,104
C	CW5	bone	B1	1	66.43	6,452,584
D	CW5	tissue	T1	1	66.43	6,452,401
E	CW5	tissue	T2	2	66.43	6,452,282
F	CW5	tissue	T34	2	66.43	6,452,473
G	CW5	tissue	T40	1	66.43	6,452,643
H	CW5	blood	S1	2	66.43	6,459,815

The PATRIC variation analysis service was used for single nucleotide polymorphism (SNP) typing of the 6 CW5 genomes (C to H) against CW4 genomes (A and B) and the PAO1 reference genome. Sequence variations were identified using a combination of four aligners – BWA-MEM and BWA-mem-strict [164], Bowtie2 [165], and LAST [166] – with Free-Bayes [167] as a SNP caller run with the default parameters. The raw SNPs were filtered by SNP quality (QUAL>10) and read depth (DP>5) to keep only the high-quality SNPs that were not due to sequencing errors. Moreover, SNPs not present in all genomes of the same phenotype (either profile1: C, D, and G or profile 2: E, F, and H) were not included, as they would not be associated with the phenotypic differences between profile 1 and profile 2 isolates.

After identification of the mutated genes, the corresponding nucleotide gene sequences extracted from Pseudomonas.com database [156] were inserted in the PATRIC BLAST service. Nucleotide BLAST (BLASTn) (default settings) was used to identify each gene in the genomes of the group that included the 8 *P. aeruginosa*

chronic wound isolates from patient X (Table 6). The results were checked through the multiple sequence alignment amino acid option that generates an alignment where each amino acid is represented by a different colour and logos at the top represent the amino acid conserved for each position (e.g. see Figure 36). The PanX database [154] was used to identify the frequency of the SNPs found in a group of 123 *P. aeruginosa* genomes from different sources. Gene sequences of *gyrA*/*B*, *trpE*/*G*, and *kynA*/*B* were also analysed as described above to identify mutations in ciprofloxacin resistance (*gyr*) and anthranilate synthesis (*trp* and *kyn*) genes.

2.10 RNAseq

Biological triplicates of *P. aeruginosa* chronic wound isolates from blood (CW5 S1) and bone (CW5 B1) grown O/N were seeded at OD_{600} = 0.01 in 10 mL of SWF and incubated at 37 °C for either 8 h or 18h with shaking at 200 rpm. A total of 6 samples per time point were used (12 in total).

1500 µL RNAprotect reagent was added to 500 µL of each culture, left for 5 min before centrifuging for 10 min at 4000 rpm. After removing the supernatant, the tubes were stored overnight at -80 °C. Tubes were thawed, and after addition of 200 µL TE + lysozyme were incubated for 10 min at room temperature. 20 µL of a 15 mg/mL stock of proteinase K was added and the tubes were incubated for another 10 min. After mixing with 700 µL of buffer RLT Plus the homogenate was transferred to a genomic DNA Eliminator spin column which was centrifuged for 30 s at 14,000 rpm. Protocols 4 and 7 of the RNeasy Mini Kit (QIAGEN) were followed, with the

exception of the DNase digestion step. Instead, the RNA samples were treated with Turbo DNase, and their concentrations were determined using a Nanodrop spectrophotometer. Afterwards RNA quality and integrety (RIN higher than 8) was checked using a Prokaryote Total RNA 6000 Nano kit on an Agilent 2100 BioAnalyzer.

RNA was sent to the University of Nottingham DeepSeq Facility, for library preparation and sequencing. Total RNA samples were processed for rRNA depletion using the Bacteria Ribo-Zero rRNA Removal Kit (Illumina), and then assessed for ribodepletion efficiency using the Agilent TapeStation 4200 and the High Sensitivity RNA ScreenTape assay (Agilent). mRNA-enriched samples were then used to generate libraries using the NEBNext Ultra Directional RNA Library Preparation Kit for Illumina (NEB) and NEBNext Multiplex Oligos for Illumina, Index Primers Set 4 (NEBNext). Libraries were quantified using the Qubit Fluorometer and the Qubit dsDNA HS Kit (ThermoFisher Scientific). Library fragment-length distributions were analysed using the Agilent TapeStation 4200 and the Agilent High Sensitivity D1000 ScreenTape Assay (Agilent). Libraries were pooled in equimolar amounts and final library quantification was performed using the KAPA Library Quantification Kit for Illumina (Roche). The library pool was multiplexed onto High Output NextSeq 150 cycle kit (Illumina) with 75 bp pair-end reads generating approximately 5-10 Mbp reads per sample with sequencing performed using Illumina NextSeq500 platform.

The filtering pipeline was used to filter reads with low sequencing scores as well as reads aligned to adaptor sequences using Skewer [168]. Trimmed reads were mapped onto the reference genome PAO1 (NCBI assembly ASM676v1) using the HISAT2 mapping tool [169]. Uniquely and correctly aligned reads were used to

generate read counts for each gene using HTSeq [170]. TPM (Transcripts Per Kilobase Million) counts for all genes were calculated to compare the proportion of reads that mapped to each gene in each sample and condition. Differentially expressed genes between conditions were detected in a pair-wise fashion by DESeq2 [171]. This analysis uses the gene counts, and corrects for dispersion using Bayes' theorem. The final values for differential expression were adjusted with a Benjamini-Hochberg false discovery rate procedure, with a P value < 0.05 deemed as significant. Note that genes from the pyoverdine and flagellar regions were also mapped onto the genome of CW5 B1 (genome C) as these regions had low similarity between CW4/CW5 isolates and PAO1. Expression levels were consistent even when different reference strains were used (maximum of ±0.25 FC difference), and as such fold-change (FC) values using genome C as reference will only be used for genes whose FC was not obtainable using PAO1 as reference.

2.11 *P. aeruginosa* vs *S. aureus* spot assay

Stationary phase cultures of *P. aeruginosa* and *S. aureus* grown O/N as previously described, were diluted to OD_{600} ~ 0.2 in 1 mL of PBS, and added as spots onto dry LB agar plates [172]. For each *P. aeruginosa* culture, 5 µL was spotted first, and after drying by a Bunsen burner, 5 µL of each *S. aureus* culture was spotted at a 5 mm distance from the *P. aeruginosa* spot. The experiments were carried out in triplicate, and the plates were incubated at 37 °C. After 16 h of incubation, the two bacterial colonies touched each other or had less than 0.1 mm distance between them. The interaction between *P. aeruginosa* and *S. aureus* was recorded, and the

plates were photographed using an EPSON Photo 2480 scanner. For this assay six *P. aeruginosa* isolates were used, namely the lab strain PAO1 (Nottingham subline) and five diabetic foot ulcer isolates (CW2 B1, CW3 T1, CW4 T1, CW5 B1, and CW5 S1), together with three *S. aureus* isolates, namely the lab strain Newman, Sa2, a methicillin sensitive (MSSA) strain isolated from the CW2 B population, and Sa4, a methicillin resistant (MRSA) strain isolated from the CW4 T population.

2.12 *P. aeruginosa* vs *S. aureus* cell-free interaction assay

Standard 6-well plates incorporating transwell® inserts with a polyester membrane with pore size 0.4 µm (Corning) were used to study cell-free interactions between *P. aeruginosa* and *S. aureus* isolates placed on either side of the membrane. 200 µL of LB agar were poured on the membrane to prevent bacteria from crossing and 2.5 mL of SWF was added to each well. Pairs of *P. aeruginosa* and *S. aureus* from the same wound (CW2 or CW4) grown O/N were diluted to OD_{600}=0.01 and inoculated into the transwell plate (in triplicates), with *S. aureus* in the top compartment and *P. aeruginosa* in the bottom compartment (see Figure 16) to mimic their distribution in a chronic wound setting (as discussed in the introduction). Plates were incubated for 48 h at 37 °C with gentle shaking (60 rpm). 100 µL from each compartment were transferred every 2 h (until 12 h), and at 24 and 48 h, to a sterile 96-well plate, OD_{600} was measured using an Infinite Pro200 (Tecan) plate reader with SWF as blank, and then each sample was serial diluted in PBS (20 µL bacteria + 180 µL PBS). 10 µL of 10^{-3} to 10^{-8} dilutions were plated (in duplicate) onto LB plates that were scored after overnight incubation at 37 °C.

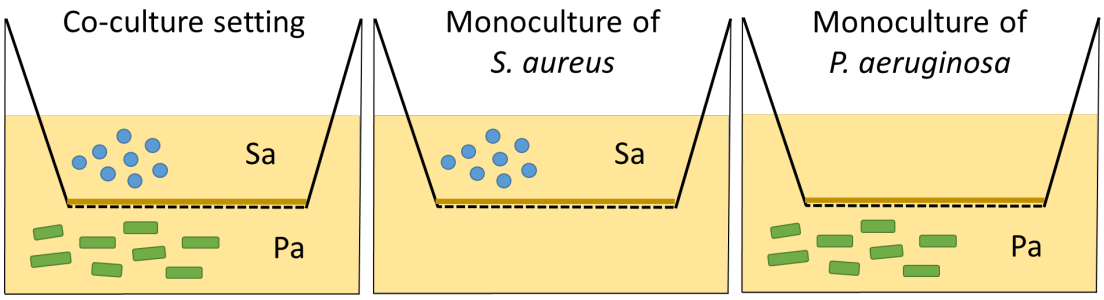


Figure 16: Set-up for the *P. aeruginosa* vs *S. aureus* cell-free interaction assay. In the co-culture setting (left) *S. aureus* (Sa) was inoculated in the top compartment and *P. aeruginosa* (Pa) in the bottom. For the monocultures, each species was inoculated in the same compartment, and the other was left empty.

2.13 Semi-solid biofilm model

A semi-solid *in vitro* wound biofilm model that mimics the non-surface attached spatial distribution of mature biofilms was used [173]. In this method biofilms are inoculated as individual bacteria in the middle of two agar layers in a semi-solid agar (0.5%) cast in a silicone mould (Figure 17). During maturation the bacteria grow into biofilms in the form of aggregates that are spatially distributed within the agar as found in wounds and other clinical settings (see Chapter 1).

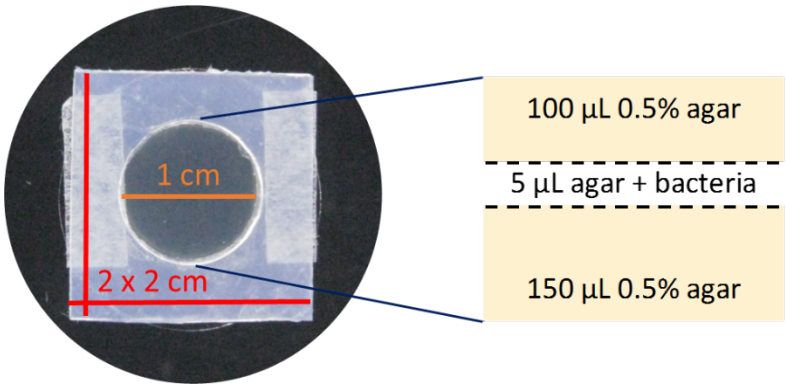


Figure 17: Example of the semi-solid *in vitro* wound biofilm model. The silicone mould can be mounted directly onto a glass slide or a coverslip for microscopy, or it can be removed after incubation for CFU counting. Bacteria are grown in a layered fashion in the inner compartment that has capacity for approximately 250 µL of medium.

Since agar is not a natural component of the wound environment, it was replaced with collagen, in an adaptation of the synthetic chronic wound model described previously [133]. For CFU counting the semi-solid model structure (two medium layers with bacteria between them) was used, while for microscopy a more realistic wound environment was also used (one layer of medium mixed with bacteria), and instead of using the silicone moulds, 8-well chamber slides with a coverslip bottom were used. In the sections below the protocol is described thoroughly, and "well" corresponds to either the centre of the silicone mould or an individual compartment of the chamber slide.

2.13.1 Set-up and adaptations of the semi-solid *in vitro* biofilm model

Bacteria were grown O/N as described above. Silicone moulds mounted in glass slides or 8-well chamber slides were placed in a sterile plastic box. 0.5% Bacto agar and a small sterile magnet were added to freshly autoclaved Bolton broth (enzymatic digest of animal tissue), and kept on a heated magnetic stirrer plate. After the agar dissolved completely, the temperature was reduced to 50 °C, and 150 µL were added to each well, and dried for 10 min in a sterile environment. Bacteria were adjusted to OD_{600}=0.5 in PBS and serial diluted to 10^{-2} in PBS, then to 10^{-3} in SWF, and finally to 10^{-4} in Bolton broth with 0.5% agar. To mimic polymicrobial infections, bacteria were either grown overnight together (two *S. aureus* colonies + one *P. aeruginosa* colony) or grown as monocultures (one colony of each strain per tube) and then 50 µL of 10^{-3} dilutions of either *P. aeruginosa* or *S. aureus* were added to the same 10^{-4} dilution tube (see Figure 18). 5 µL of bacteria encapsulated in Bolton broth agar (from the 10^{-4} dilution) were pipetted onto the top of the first agar layer

and after 5 min another layer of 100 µL was added and left to dry for another 10 min. Wet tissue was placed inside the plastic box, as further away as possible from the slides, to maintain a moist atmosphere, and the box was sealed and incubated at 37 °C for 18 h.

For microscopy, alongside Bolton broth agar, SWF solidified with collagen was used to create a synthetic chronic wound (SCW), following a protocol previously described [133]: 30/20 µL of rat tail collagen I 10 mg/mL (Corning), 15/10 µL of acetic acid 0.1%, 90/60 µL of SWF, and 15/10 µL of sodium hydroxide 0.1 M for 150/100 µL layers respectively. Briefly, the components were added to a chilled, sterile 15 mL tube in the order listed, and the change from acidic to basic pH triggered collagenase polymerisation. As the collagen solidifies quickly after polymerisation, the medium was prepared in small batches and used immediately. The SCW was used either in the layered structure as described above (150 µL + 5 µL + 100 µL), or 200 µL of medium previously mixed with bacteria (in the 10^{-4} dilution tube) were added to each well (see Figure 18). The alterations made in the semi-solid in vitro wound biofilm model described above are summarised in Figure 19.

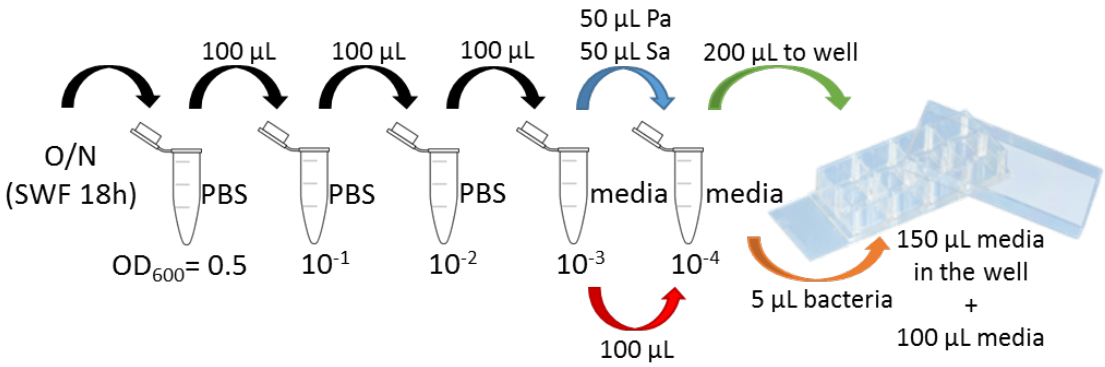


Figure 18: Optimisation of the semi-solid *in vitro* biofilm model protocol to study *P. aeruginosa* and *S. aureus* interactions. After O/N incubation bacteria were adjusted to OD_{600}=0.5 in PBS and then diluted to 10^{-2}. For co-culture (Pa+Sa) overnights 100 µL were transferred from the 10^{-3} dilution to the 10^{-4} dilution (red

arrow), for monoculture overnights 50 µL of *P. aeruginosa* (Pa) and *S. aureus* (Sa) individual 10^{-3} dilutions were added to the same 10^{-4} dilution tube (blue arrow). From here, either 200 µL of the 10^{-4} dilution were added to each well (green arrow), or a multilayer was made with 150 µL medium + 5 µL bacteria (from the 10^{-4} dilution) + 100 µL medium (orange arrow).

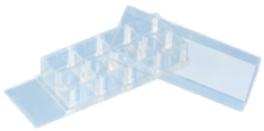
	semi-solid *in vitro* wound biofilm model	adapted model
Container:	silicone mould 	8-well chamber slides 
Structure:	multilayer model 100 µL medium 5 µL medium + bacteria 150 µL medium	more realistic model 200 µL medium + bacteria
Medium:	Bolton broth agar	synthetic chronic wound (SCW)

Figure 19: Summary of the adaptations made in the semi-solid *in vitro* wound biofilm model. Note that in this work we use all combinations of structure and media.

2.13.2 Quantification of viable cells after co-culture

Slides were taken from the plastic box, moulds were removed, and gels were transferred to 2 mL tubes containing 600 µL of PBS plus six 2.8 mm ceramic beads. Used silicone moulds were rinsed in ethanol for 24 h and then dried and autoclaved for re-use. Gels were disrupted in a FastPrep-24™ bead beater for 10 s. Tubes were centrifuged for 10 min at 7000 rpm and the supernatant removed. Pellets were resuspended in 1 mL of PBS and then biofilm aggregates were disrupted by 5 min of de-gassing followed by 5 min sonication in a water bath. 100 µL from each tube were transferred to a sterile 96-well plate and serial diluted in PBS (20 µL bacteria + 180 µL

PBS). 10 µL of 10^{-3} to 10^{-8} dilutions were plated (in duplicate) in either PIA/BPA plates for co-culture settings, or in LB plates for monocultures. CFU were counted after overnight incubation at 37 °C.

2.13.3 Microscopy

Slides were taken from the plastic box and each well was stained with 500 µL of a PBS solution with 20 µM of Syto13 (Invitrogen), for visualizing live cells via green fluorescence, and 10 mg/mL hexidium iodide (Invitrogen), for counter-staining Gram-positive cells via red fluorescence [174]. After 15 min of incubation in the dark, slides were imaged on a Zeiss LSM 700 confocal laser scanning microscope with a 10x objective, using a 488 nm laser with 2% intensity, and beam splitters set to 530 nm (green channel) and to 600 nm (red channel).

2.14 Identification of *P. aeruginosa* and *S. aureus* metabolites by LC-MS/MS

Untargeted metabolomic profiling using high-resolution mass spectrometry (MS) coupled with hydrophilic interaction liquid chromatography was used to identify low molecular mass metabolites differentially produced by clinical isolates of *P. aeruginosa* and *S. aureus* grown singly and in mixed cultures.

2.14.1 Sample preparation

Two DFU isolates of each species were used, namely *P. aeruginosa* PA2 (CW2 B1) and PA4 (CW4 T1), and *S. aureus* SA2 (isolated from CW2 B population) and SA4

(isolated from CW4 T population). Bacteria were either grown in a co-culture setting (one *P. aeruginosa* strain + one *S. aureus* strain – conditions 1 to 4; Table 7), or in monoculture (conditions 5 to 8; Table 7). Two control conditions were used: condition 9 as the growth medium control, where SWF was incubated without bacteria, and condition 10 as the growth medium control for incubation, where SWF was used directly from the fridge (4 °C). These controls will aid detection of background components from the growth medium before use and after 18 h incubation at 37 °C.

Table 7: Conditions used for the metabolomic analysis.

Condition	Strains
1	PA2 + SA2 co-culture
2	PA2 + SA4 co-culture
3	PA4 + SA2 co-culture
4	PA4 + SA4 co-culture
5	PA2 monoculture
6	SA2 monoculture
7	PA4 monoculture
8	SA4 monoculture
9	SWF control
10	SWF incubation control

Each -80 °C glycerol stocked isolate was streaked onto LB agar plates and incubated overnight at 37 °C. Single colonies (one colony of each for the monocultures and two *S. aureus* colonies + one *P. aeruginosa* colony for the co-culture) were transferred to 10 mL of SWF and incubated at 37 °C for 18 h. For conditions 1 to 8, six replicates were used. Tubes were centrifuged at 5000 rpm for 10 min at 4 °C and filtered using a 10 mL syringe and a 0.2 µm filter (Minisart). Then 250 µL of the filtered supernatants were transferred to pre-cooled 2 mL tubes, and 750 µL of cold LC-MS grade MeOH (pre-cooled at -20 °C) were added to each tube.

The mixture was vortex-mixed for 1 min to precipitate proteins, and the tubes were incubated at -20 °C for 20 min. The tubes were vortexed again for 15 s and centrifuged at 13,000 rpm for 10 min at 4 °C. The supernatants were transferred to new pre-cooled 2 mL tubes and stored at -80 °C overnight prior to the LC-MS/MS run.

2.14.2 Liquid chromatography-mass spectrometry (LC-MS/MS)

On the day of the LC-MS/MS run, the tubes were vortexed for 1 min and then centrifuged at 13,000 rpm for 10 min at 4 °C. Then 700 µL of supernatants were transferred to new pre-cooled 2 mL tubes, and vortexed for 5 s. 200 µL of the extracted supernatants corresponding to each sample were transferred to labelled high performance liquid chromatography (HPLC) vials, and for the quality control (QC) sample, 4 µL from each sample from test conditions (in this case conditions 1 to 8; Table 7, in a total of 48 samples corresponding to a total volume of192 µL were mixed in a separate HPLC vial.

LC-MS/MS was performed by Alvin Teo and Malak Jaber (School of Pharmacy, University of Nottingham) using a Dionex UHPLC system (Thermo Fisher Scientific, USA) coupled to a high-resolution quadrupole-orbitrap mass spectrometer (Q-Exactive) (Thermo Fisher Scientific, USA), as previously described [175, 176]. Liquid chromatography was performed on a SeQuant® ZIC®-pHILIC column (150 mm x 4.6 mm, 5 µm particle size) (Merck) with appropriate guard column, with a mobile phase consisted of A: 20 mM ammonium carbonate and B: acetonitrile. Compounds were separated by the following linear gradient: 80% to 5% B over 15 min, followed by a 2 min linear gradient from 5% B to 80% B, and 7 min re-equilibration with 80% B, at a flow rate of 300 µL/min and sample injection volume of 10 µL. The samples were

maintained at 4 °C, and the column was maintained at 45 °C. Tandem MS was acquired on the Q-Exactive MS, in the range of m/z 75-1100 and a resolution of 140,000 for full MS scan; 17,500 for data-dependant (top5) MS/MS scans, in both positive and negative modes. The capillary and probe temperatures were maintained at 275 °C and 150 °C, respectively. The MS/MS Isolation window was set to 2 Da, with a normalised collision energy of 30.

2.14.3 Metabolite identification

The raw data files of the test (conditions 1 to 4) and control (conditions 5 to 10) groups and blanks were imported into the Compound Discoverer software (v. 2.0; Thermo Fisher Scientific, Fremont, CA, USA) for metabolite identification. The processing workflow employed the "Unknown compound detection" node for untargeted profiling with the following settings: mass tolerance 5 ppm and retention time tolerance of 2 min. The blank samples were used for the subtraction of the background compounds. Based on the column characteristics, the retention time window within 3.9 min and 23.5 min was chosen.

The elemental compositions were predicted and ChemSpider Database, a chemical structure database, and mzCloud (HighChem LLC, Slovakia), a mass spectral database, were used for structural search. PAMDB, a comprehensive *P. aeruginosa* metabolome database [177] was also used. Scripts to compare the different test conditions and subtract the control conditions were written by José Vieira (School of Mathematical and Physical Sciences, University of Sussex).

Chapter 3: Phenotypic Diversity of *P. aeruginosa* in Chronic Diabetic Ulcers

3.1 Introduction & Objectives

As discussed in the previous chapter, diabetes is an endocrine disorder with severe consequences, ranging from metabolic abnormalities to limited joint mobility, and particularly interference with healing processes. Peripheral neuropathy and ischaemia are precipitating and predisposing factors for the appearance of chronic wounds [78], especially when diabetes is poorly controlled. Reduced sensation in the lower limbs and feet due to damage to nerves and muscles, as well as circulation problems, increases the likelihood of ulceration and amputation. Additionally, chronic wound patients are a high-risk group for the acquisition of antibiotic-resistant organisms, and their ulcers can act as a reservoir for cross-contamination and dissemination of resistance [108].

Pseudomonas aeruginosa is an important opportunistic Gram-negative pathogen found, for instance, in burn and chronic wounds and in the lungs of cystic fibrosis (CF) patients. Its ability to form biofilms and acquire multi-drug resistance makes it a frequent cause of hospital-acquired infections [114, 178]. *P. aeruginosa* has a relatively large genome (5.5–7 Mb), high G+C content (65–67%), and an extremely high proportion of regulatory genes (~10%) [179, 180]. It also has a large number of genes involved in the catabolism, transport and efflux of organic compounds, and in chemotaxis systems, providing the basis of its great nutritional versatility and environmental adaptability [181]. Generally classified as an aerobe,

P. aeruginosa can survive under hypoxic conditions and at a broad range of temperatures [182]. The size and complexity of its genome reflect an evolutionary adaptation designed to allow this bacterium to thrive in diverse environments and resist the effects of a variety of antimicrobial substances.

P. aeruginosa produces many virulence factors (Figure 20) that have been associated with its pathogenicity in the wound environment [183-185]. These include both cell-associated and extracellular products including exoproteases (such as LasA and AprA) and elastases (such as LasB) that are involved in connective tissue elastin degradation [186, 187] as well as extracellular polysaccharides (such as alginate, Pel and Psl) that comprise a major component of the biofilm matrix [188-190]. Other important virulence factors include phenazine pigments, such as the blue-green pyocyanin, that are involved in the evasion of the host immune system [191]. These have several toxic effects linked to their ability to modulate redox cycling and generate reactive oxygen species capable of causing significant oxidative stress and tissue destruction [192]. *P. aeruginosa* also produces two major siderophores, pyoverdine and pyochelin, involved in iron acquisition [193]. The export of these virulence factors is done via different types of secretion systems, from type I secretion system (T1SS) up to type VI secretion system (T6SS) – reviewed in detail by [183], that allow the translocation of proteins from the cytoplasm to the outside of the cell trough both inner and outer membrances and the peptidoglycan-containing periplasm.

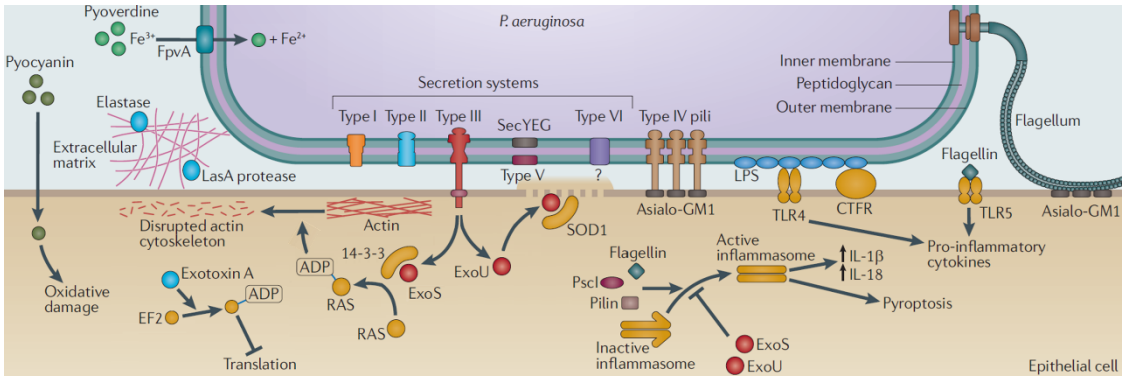


Figure 20: Summary of virulence factors produced by *P. aeruginosa* and their main targets in epithelial cells. This bacterium produces diverse adhesins and toxins, proteases, effector proteins and pigments that facilitate adhesion, modulate or disrupt host cell pathways and target the extracellular matrix (adapted from [194]).

Also important for *P. aeruginosa* pathogenesis is the population cell-density-dependent quorum-sensing (QS) system, viewed as a "network of networks" [195]. This system comprises three tightly interconnected regulatory networks: *las*, *rhl*, and *pqs* systems, reviewed in detail by [196] and by [197]. They are mediated by different signalling molecules including *N*-acyl-homoserine lactones (AHLs), especially C4-HSL (*rhl* system) and 3-oxo-C12-HSL (*las* system), and the AQs, PQS – also called the *Pseudomonas* quinolone signal (*pqs* system) – and its precursor HHQ, which control the expression of multiple virulence genes (Figure 21) [147, 198, 199]. Furthermore, the multiple virulence systems in *P. aeruginosa* are also regulated at different levels (transcriptionally, post-transcriptionally, and/or post-translationally) by an array of transcriptional regulators, reviewed by Balasubramanian et al. [200], which further increases the pathogenic potential of this bacterium (Figure 22).

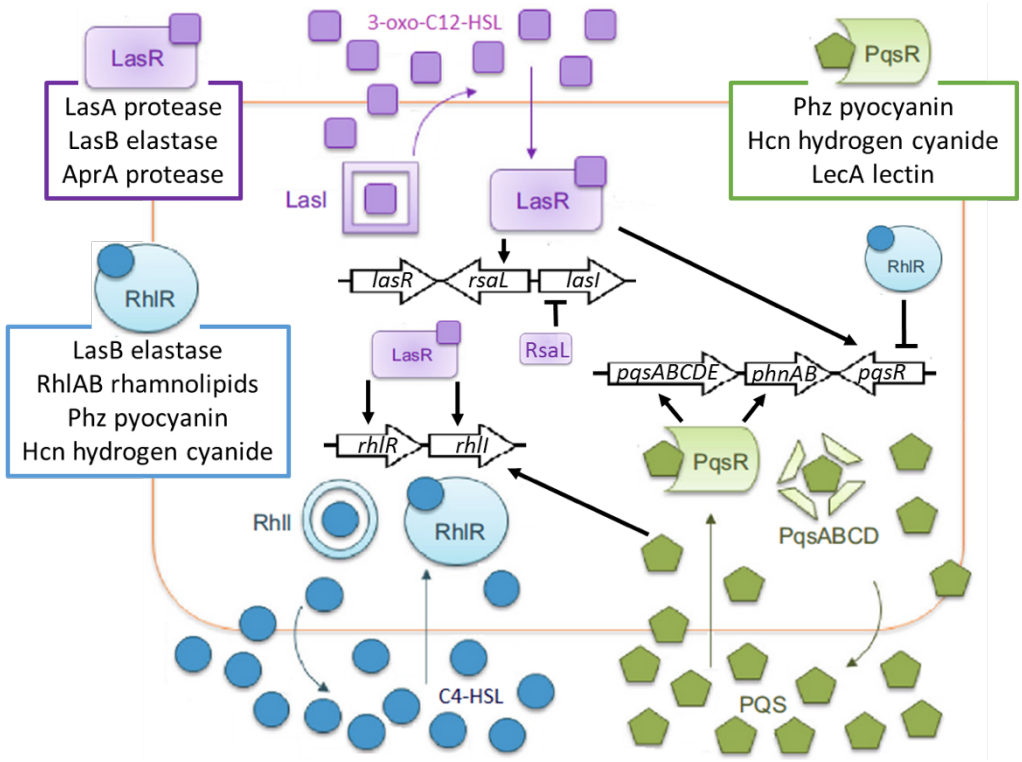


Figure 21: Schematic representation of the QS signalling networks in *P. aeruginosa*, including reporter/receptor genes, effectors and regulons, adapted from [201].

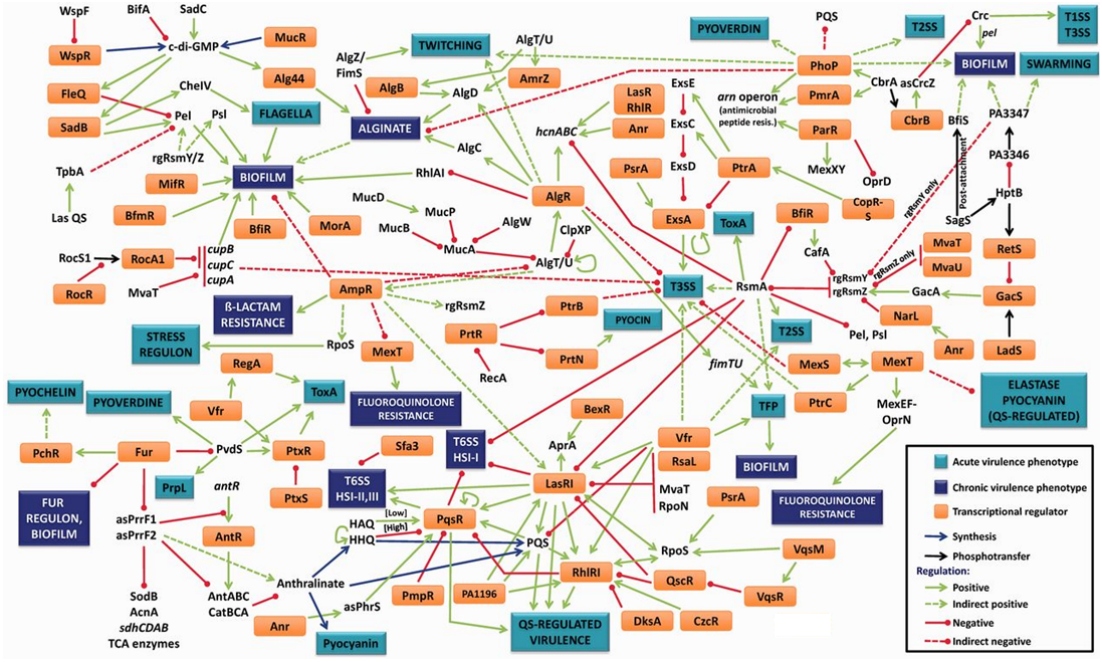


Figure 22: The *P. aeruginosa* virulence regulatory network. The central mechanism for *P. aeruginosa* virulence regulation involves quorum-sensing controlled transcriptional regulators such as LasR, RhlR, and PqsR that regulate numerous acute and chronic infection phenotypes (adapted from [200]).

Several studies have reported that the loci encoding the AHL-dependent QS systems accumulate mutations in bacteria isolated from CF patients chronically colonised with *P. aeruginosa*, which can result in extensive metabolic and phenotypic modifications of long-term host-evolved strains compared with those of environmental origin [202, 203]. Additionally, work on CF isolates has highlighted the importance of *P. aeruginosa* phenotypic diversity and heterogeneity for the treatment of chronic infections, challenging the validity of microbiological analysis done in patient samples, especially antibiotic susceptibility tests [123-125]. Moreover, several recent studies found that convergent evolution and adaptation alter *P. aeruginosa* regulatory networks and central metabolism, influencing the acquisition of antibiotic resistance and the loss of extracellular virulence factors [172, 204]. The diabetic ulcer environment is susceptible to chronic infections such as those encountered in individuals with CF, but is still mostly an uncharacterized setting. As such, a wide screen of the phenotypes associated with *P. aeruginosa* virulence would help to better understand the context of *P. aeruginosa* colonisation and infection, and the reason why infected ulcers are so resistant to antibiotics and difficult to treat.

3.2 Results

3.2.1 Phenotypic characterisation of chronic wound isolates

40 *P. aeruginosa* isolates were taken from each chronic wound population (CW2 to CW7) and type of sample – B: bone, T: tissue, and S: blood (Figure 23), and each isolate was tested in triplicate for the six phenotypes described in section 2.2.3.

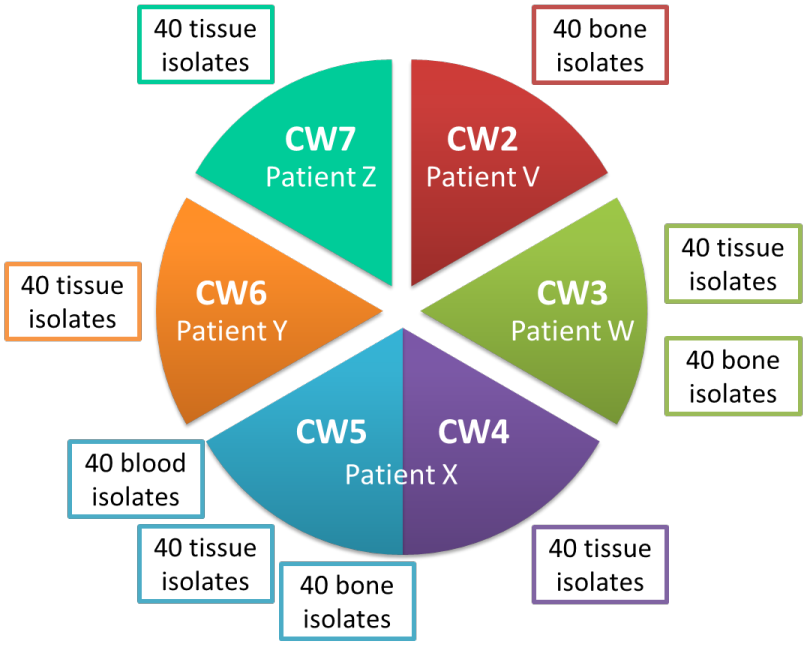


Figure 23: *P. aeruginosa* isolates used in this work. Note that patient X was sampled twice (CW4 and CW5).

Before doing the phenotypic assays, after incubating the *P. aeruginosa* chronic wound isolates on LB agar, characteristics such as colour and colony shape were distinct as illustrated in Figure 24.

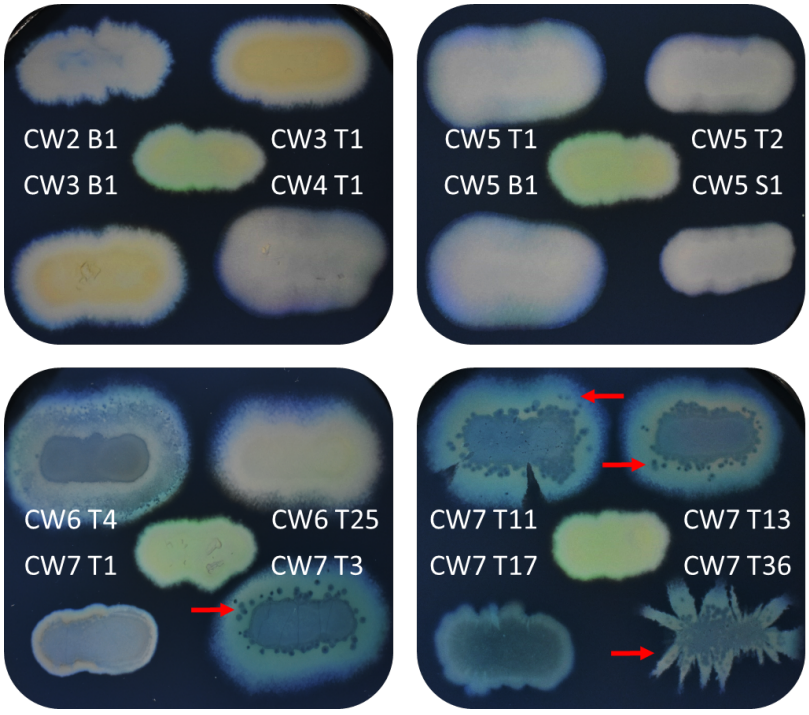


Figure 24: Panel with 4 plates displaying the phenotypes of each representative isolate streaked on LB agar plates. B: bone, T: tissue, S: blood – see Table 13 for

details. PAO1 in the middle of every plate. Red arrows point to plaques presumably caused by bacteriophage lysis.

Compared with PAO1 (in the middle of each plate in Figure 24), CW2 isolates were brownish and CW3 isolates were greener, with an iridescent dark yellow glow, and appeared to spread further. There were no obvious visual differences between the tissue and bone isolates from CW3, and when transferred, bacteria from CW2 isolates were stickier than PAO1. Tissue isolates from CW4 and bone isolates from CW5 were yellow and spread, while blood isolates from CW5 were whiter and did not spread. CW5 tissue isolates could be grouped into two profiles: either yellow like CW5 bone, represented by CW5 T1 (profile 1: 24 out of 40 isolates), or white like CW5 blood, represented by CW5 T2 (profile 2: 16 out of 40 isolates). All CW6 isolates were green like PAO1 except for T25 which was paler. Isolates from CW7, the leg ulcer sample, were different from each other, even though the majority were very green. A distinctive feature of the majority of CW7 isolates was the presence of autolysis plaques probably made by bacteriophages, which are highlighted by red arrows in Figure 24.

3.2.1.1 Colony morphologies on Congo Red agar plates

Groups of 10 isolates plus controls were grown on Congo Red agar plates (in triplicate), assessed visually and photographed after morphotype development. The majority of diabetic foot isolates taken from the same wound had the same colony morphology. For CW3 but not CW5, isolates from different sample types (bone and tissue) had the same morphology. CW5 isolates from bone and blood had different colony morphologies, even though within each sample type all 40 isolates were the

same. Moreover, CW5 tissue isolates could be grouped into two groups, with their colony morphologies either being like CW5 bone (profile 1), or like CW5 blood (profile 2). For the 40 leg ulcer isolates investigated from CW7, colony morphologies varied significantly. Nevertheless, isolates could be grouped in five different morphotypes. This information is summarised in Table 8, and Figure 25.

Table 8: Colony morphotypes shown by *P. aeruginosa* chronic wound isolates on Congo Red agar plates.

Sample	Isolates	Colour	Centre	Spreads	Edge
CW2 B	1-40	white	red	yes	fuzzy
CW3 T	1-40	red	red	yes	smooth
CW3 B	1-40	red	red	yes	smooth
CW4 T	1-40	orange	orange	yes	smooth
CW5 T	1, 5, 10-12, 18, 20-30, 32, 35-40	orange	orange	yes	smooth
	2-4, 6-9, 13-17, 19, 31, 33, 34	red	red	No	wrinkly
CW5 B	1-40	orange	orange	yes	smooth
CW5 S	1-40	red	red	No	wrinkly
CW6 T	1-24, 26-40	red	white	yes	smooth
	25	white	red	yes	smooth
CW7 T	1, 7-9, 27, 31	red	yellow	yes	wrinkly
	2, 12, 13, 18, 19, 23, 24, 26, 29, 32-34, 37, 38, 40	red	yellow	yes	smooth
	11, 17, 30	red	red	No	smooth
	3-6, 10, 14-16, 20-22, 25, 28, 35, 39	red	white	yes	smooth
	36	red	white	yes	spiky
PAO1	Nottingham reference	white	white	yes	smooth
Δ*wspF*	*wspF* mutant	red	red	no	wrinkly
Δ*pel*/*psl*	*pel*/*psl* double mutant	white	white	yes	Smooth

Note: Δ*wspF* and Δpel/psl mutants have a PAO1 background.

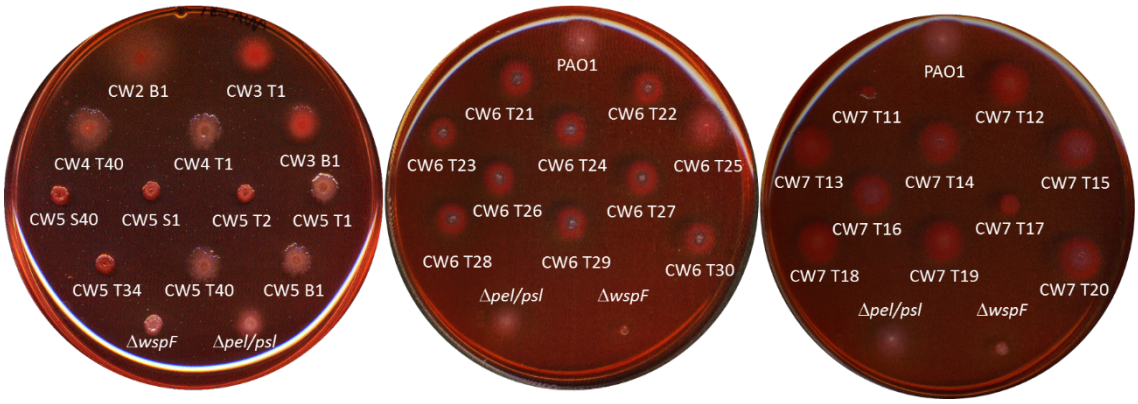


Figure 25: Colony morphologies of representative *P. aeruginosa* isolates on Congo Red agar plates. PAO1, Δ*wspF*, and Δ*pel/psl* mutants were used as controls in both plates for wrinkly and smooth phenotypes, respectively. Left plate: isolates from CW2, CW3, CW4 and CW5; middle plate: CW6 isolates from T21 to T30 (batch 3); right plate: CW7 isolates from T11 to T20 (batch 2).

3.2.1.2 Quantification of AHL quorum-sensing molecules

Induction of bioluminescence in *E. coli ahyRI'::lux* and *lasRI'::lux* AHL biosensor strains in response to cell free culture supernatants extracted from chronic wound isolates was used to estimate production of QS signal molecules C4-HSL and 3-oxo-C12-HSL respectively. All isolates produced C4-HSL at comparable levels with the exception of CW7 T17 whose bioluminescent response was much reduced. With respect to 3-oxo-C12-HSL, isolates from patient X (CW4 and CW5) did not induce bioluminescence, while all other isolates had a strong signal, with the exception of isolates CW7 T17, T22 and T36 whose bioluminescent response was lower than the average. Results are summarised in Table 9, and an example for CW5 T batch 1 (left) and CW7 batch 2 (right) can be seen in Figure 26.

Table 9: Presence of QS signal molecules C4-HSL and 3-oxo-C12-HSL in different chronic wound isolates, assessed by *E. coli ahyRI'::lux* and *lasRI'::lux* biosensor strains.

Samples	C4-HSL	3-oxo-C12-HSL
CW2 B	+	+
CW3 T / B	+	+
CW4 T	+	-
CW5 B / T / S	+	-
CW6 T	+	+
CW7 T	+ ±T17	+ ± T17, T22, T36
PAO1	+	+

– no production; ± low production; + production

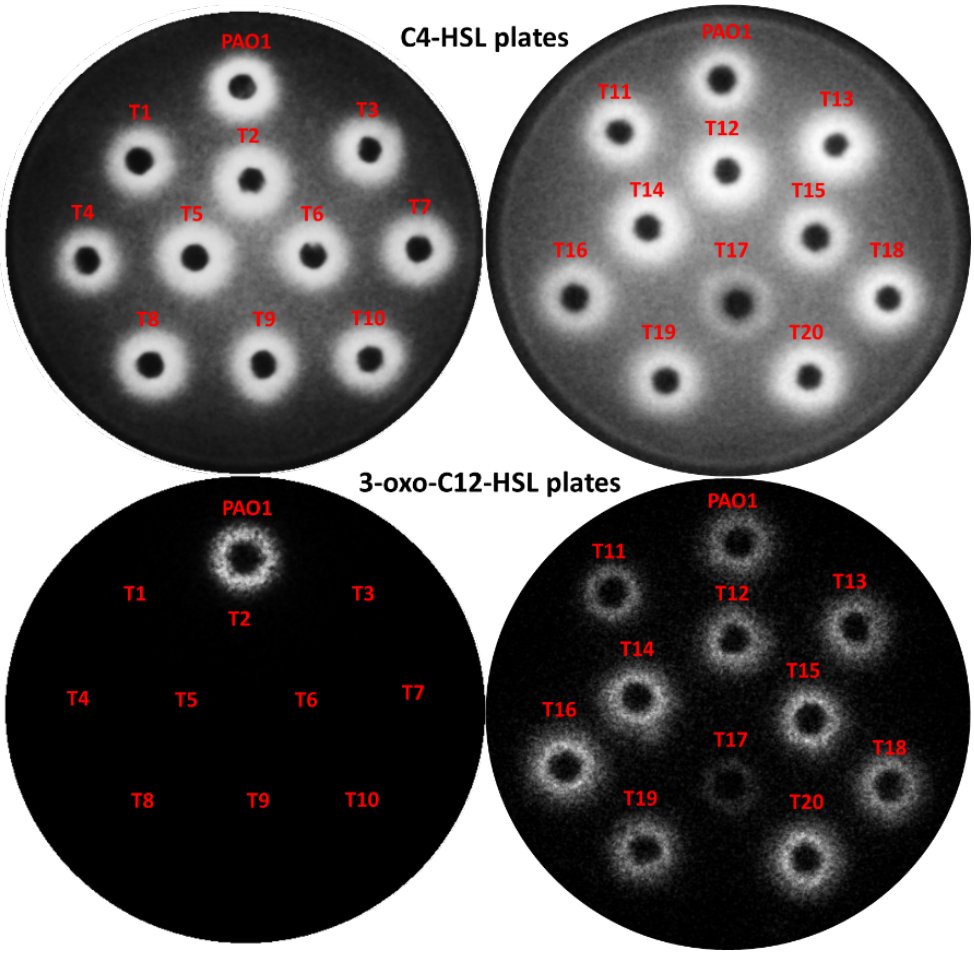


Figure 26: Example of AHL biosensor detection assay in *P. aeruginosa* chronic wound isolates. Bioluminescence response to C4-HSL on top and below to 3-oxo-C12-HSL. Left side: PAO1 as a positive control and isolates from CW5 T1 to T10 (batch 1); right side: PAO1 and isolates from CW7 T11 to T20 (batch 2).

3.2.1.3 Semi-quantification of protease production

15% skim milk agar plates were used for the detection of total exoprotease activity, since when a bacterial supernatant containing proteases is plated onto this medium, the enzymes will break down the casein protein producing halos. The results obtained are summarised in Table 10.

Table 10: Presence and type of halo formed on skim milk plates by the action of exoproteases produced by bacteria from chronic wound samples.

Samples	Clear halo	Faint halo	No halo
CW2 B	1-40	-	-
CW3 T	1-40	-	-
CW3 B	1-40	-	-
CW4 T	-	-	1-40
CW5 B	-	-	1-40
CW5 T	-	-	1-40
CW5 S	-	-	1-40
CW6 T	25	-	1-24, 26-40
CW7 T	11, 15, 16, 21-23, 25, 28, 30, 35, 38, 39	3-6, 10, 17, 20, 24, 26, 29, 31-34, 37, 40	1, 2, 7-9, 12-14, 18, 19, 27, 36

In each category the numbers correspond to the isolates that showed that characteristic. Each isolate was tested in triplicate, and an example of the categories is highlighted in Figure 27 by arrows with different colours (green: clear halo, yellow: faint halo, and red: no halo).

Regarding samples from diabetic foot ulcers (all except CW7), isolates from short-term ulcers (CW2 and CW3) were all protease positive, while isolates from long-term ulcers were all protease negative (CW4, CW5, and CW6) with the exception of CW6 T25 that was protease positive. On the other hand, isolates from the short-term leg ulcer (CW7) showed substantial variation: 30% (12/40 isolates) did not produce halos, 40% (16/40) produced faint halos, and the other 30% produced clear halos similar to PAO1. Examples of CW7 phenotypes are indicated by arrows in Figure 27.

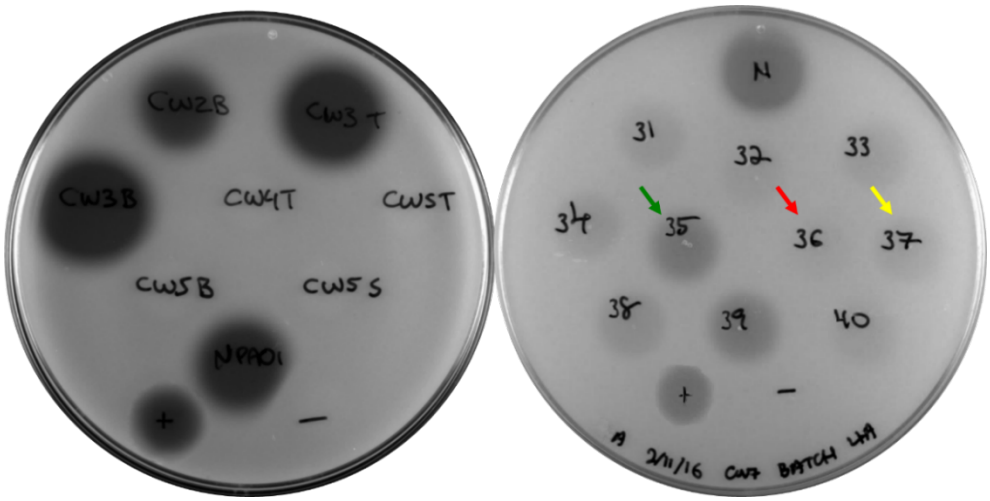


Figure 27: Qualitative protease assay in chronic wound isolates using 15% skim milk agar plates**.** In both plates: "NPAO1" and "N" corresponds to control Nottingham PAO1 strain, + to proteinase K as positive control, and – to SWF as negative control. On the right plate: representative isolates from CW2 to CW5; on the left plate: CW7 isolates T31 to T40. Categories in Table 10 are represented on the right by: green arrow (halo, +), yellow arrow (faint halo, ±), and red arrow (no halo, -).

3.2.1.4 Quantification of siderophore production

Pyoverdine (PVD) and pyochelin (PCH) production, in relative fluorescence units (RFU) per estimated bacterial density (OD_{600}), were quantified by fluorescence spectroscopy (Figure 29). Since there was high variability between values, to simplify the analysis the isolates were grouped into five categories, according to their RFU/OD_{600} values (Figure 28).

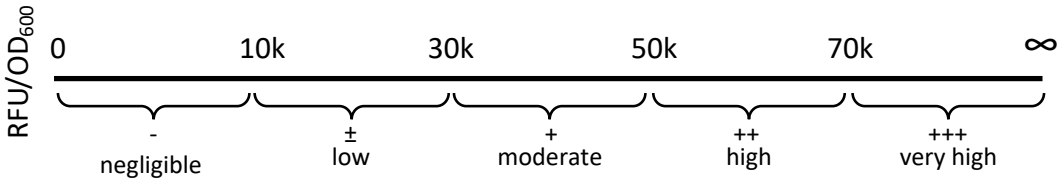


Figure 28: Categories used in the quantification of siderophore production

Isolates were classed as having: negligible production (–) if they had less than 10k RFU/OD_{600}; low production (±) if RFU/OD_{600} varied between 10k and 30k;

moderate production (+) if RFU/OD_{600} varied between 30k and 50k; high production (++) if RFU/OD_{600} varied between 50k and 70k; and very high production (+++) if they had more than 70k RFU/OD_{600} (Table 11). Isolates were tested in triplicate and, when standard deviation spanned more than one category, the category selected was that in which they were statistically more likely to fit.

Table 11: Correlation of both siderophores production in chronic wound isolates.

Sample	PVD	PCH	Isolates
CW2 B	± (40/40)	+ (40/40)	**PVD±∩PCH+: 1-40**
CW3 B	± (40/40)	+ (40/40)	**PVD±∩PCH+: 1-40**
CW3 T	± (40/40)	+ (40/40)	**PVD±∩PCH+: 1-40**
CW4 T	± (40/40)	± (40/40)	PVD±∩PCH±: 1-40
CW5 T	– (16/40) ± (24/40)	± (40/40)	PVD-∩PCH±: 2-4, 6-9, 13-17, 19, 31,33, 34 PVD±∩PCH±: 1, 5, 10-12, 18, 20-30, 32, 35-40
CW5 B	± (40/40)	± (40/40)	PVD±∩PCH±: 1-40
CW5 S	– (40/40)	± (40/40)	PVD-∩PCH±: 1-40
CW6 T	± (40/40)	+ (39/40) ++ (1/40)	**PVD±∩PCH+: 1-24, 26-40** PVD±∩PCH++: 25
CW7 T	– (22/40)	± (3/40)	PVD-∩PCH±: 7-9 PVD-∩PCH+: 1, 2, 12, 13, 18, 19, 23, 24, 26, 27, 29, 31-34, 37, 38, 40
	± (13/40)	+ (26/40)	PVD-∩PCH+++: 30
	+ (4/40)	++ (7/40)	**PVD±∩PCH+: 3-6, 10, 14, 16, 20** PVD±∩PCH++: 15, 22, 28, 35, 39 PVD+∩PCH++: 21, 25
	+++ (1/40)	+++ (4/40)	PVD+∩PCH+++: 11, 17 PVD+++∩PCH+++: 36

PVD: pyoverdine, PCH: pyochelin. Siderophore production measured in relative fluorescence units (RFU) by OD_{600} and grouped in the categories (see Figure 28): -, 0 to 10k; ±, 10k to 30k; +, 30k to 50k; ++, 50k to 70k; +++, > 70k. In the isolates column, values in bold represent the most common combination of PVD and PCH production (indicated by the intersection symbol, ∩).

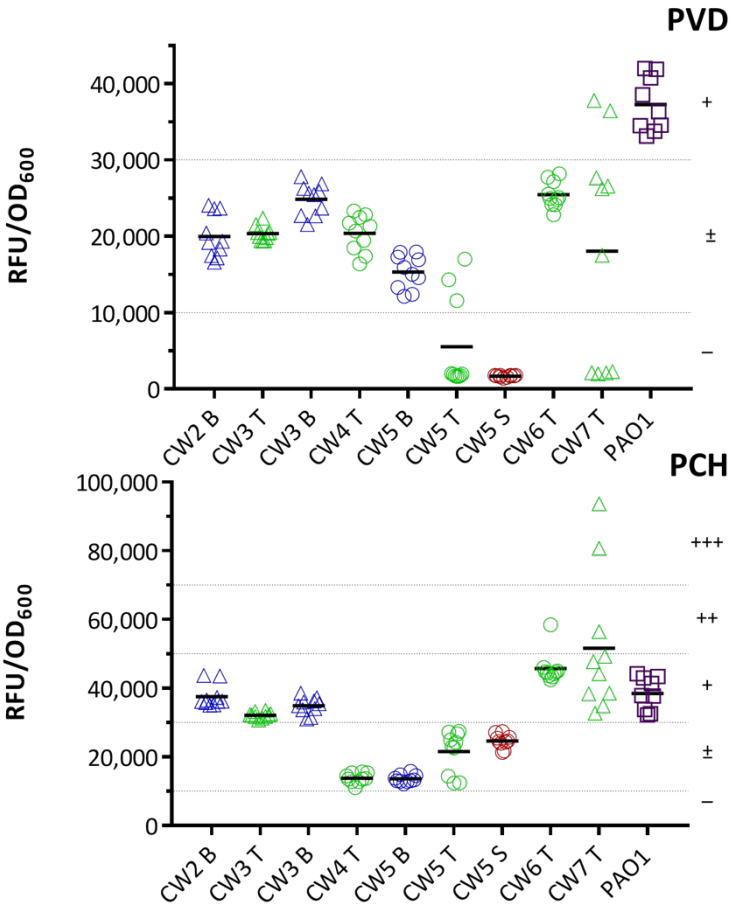


Figure 29: Pyoverdine (PVD) and pyochelin (PCH) production by isolates from one batch from each chronic wound studied. Triangles: isolates from short-term ulcers, circles: isolates from long-term ulcers, and squares: lab strain PAO1 (purple). Type of sample: B - bone (blue), T - tissue (green), and S - blood (red). Faint lines and signs on the right represent RFU/OD_{600} categories of Figure 28. CW5 T has two distinct groups that correspond to profile 1 isolates (like CW5 B), and profile 2 isolates (like CW5 S), while CW7 has more diversity than the other samples.

Overall, isolates taken from diabetic chronic wounds produce low (±) amounts of PVD and moderate (+) amounts of PCH. However, isolates from patient X (CW4 and CW5) have relatively low production of both siderophores, with RFU/OD_{600} values less than 30k.

For diabetic foot isolates, those taken from the ulcers of patients V and W (CW2 B, CW3 B, and CW3 T) produced low levels of PVD and moderate levels of PCH. Meanwhile, isolates taken from the ulcer of patient X could be grouped in two

different profiles: CW4 T, CW5 B, and CW5 T profile 1 (24 isolates represented by CW5 T1) had low levels of both PVD and PCH, whereas isolates from CW5 S (blood) and CW5 T profile 2 (16 isolates represented by CW5 T2) still had low levels of PCH but did not produce PVD. Moreover, all isolates taken from patient Y (CW6) produced low levels of PVD and moderate levels of PCH (similar to isolates from patients V and W), with the exception of isolate T25 that produced the highest levels of PCH in DFUs and can be easily identified as the separate circle in the CW6 T column in the PCH plot of Figure 29.

As for isolates taken from the diabetic leg ulcer (CW7) the production of PVD was mostly spread across the three lower categories (-, ±, and +), with the exception of T36 which produced very high levels of PVD (+++). In detail, 55% (22/40) produced negligible amounts of PVD, 32.5% (13/40) produced low levels of PVD, and only 10% (4/40) produced moderate levels of PVD. Regarding PCH production, 65% (26/40) of the isolates produced moderate levels (between 30k and 40k RFU/OD_{600}), and only three isolates produced low levels (7.5%). 17.5% (7/40) of the isolates produced high levels of PCH, and 10%, corresponding to isolates T11, T17, T30, and T36 produced very high levels of PCH (more than 70k RFU/OD_{600}). Note that siderophore production by PAO1 was measured alongside each batch of chronic wound isolates as an internal control, and it produced moderate (+) levels of both siderophores (Figure 29).

3.2.1.5 Quantitative analysis of pyocyanin production

Pyocyanin (PYO) was measured by reading the absorbance of FSNs at 691 nm and the results were converted in µg/mL and summarised in Table 12.

Table 12: Quantification of pyocyanin production by chronic wound isolates.

Pyocyanin (µg/mL)	CW2 B	CW3 B	CW3 T	CW4/5	CW6 T	CW7 T
Negligible (0 – 5)	-	-	-	1-40	-	1, 5, 8, 13
Low (5 – 10)	-	-	-	-	25	majority (25/40)
Moderate (10 – 15)	1-40	1-40	1-40	-	19, 20, 22, 26, 28, 30	16, 35, 38, 39
High (15 – 35)	-	-	-	-	majority (33/40)	11, 15, 22, 28, 30, 36
Very high (> 35)	-	-	-	-	-	17

Regarding diabetic foot ulcers, isolates from CW2 and CW3 (short-term ulcers) were all PYO positive, while isolates from patient X (CW4 and CW5) that had a long-term ulcer were all PYO negligible. Surprisingly, most isolates from patient Y (CW6), who also had a long-term ulcer, produced high levels of PYO, with the exception of isolate T25 that produced between 5 and 10 µg/mL of PYO. For the diabetic leg ulcer (CW7), isolates were spread across the entire range, however, the majority (25/40) produced low levels of PYO. Curiously, 6/40 isolates produced high levels of PYO, while isolate T17 produced the highest concentration, around 83 µg/mL.

3.2.1.6 Bacterial growth

Since most of the isolates showed the same phenotype within each CW sample, representative isolates were selected from each CW, according to the table below (Table 13). Note that for CW7 we selected multiple isolates in order to represent the variability found in the phenotypes investigated in this section.

Table 13: Description of representative isolates used in this work.

Patient	Sample	Representative	Code
V	CW2	Bone isolate 1	CW2B1
W	CW3	Tissue isolate 1	CW3T1
		Bone isolate 1	CW3B1
X	CW4	Tissue isolate 1	CW4T1
X	CW5	Bone isolate 1	CW5B1
		Blood isolate 1	CW5S1
		Tissue isolate 1	CW5T1
		Tissue isolate 2	CW5T2
Y	CW6	Tissue isolate 4	CW6T4
		Tissue isolate 25	CW6T25
Z	CW7	Tissue isolate 1	CW7T1
		Tissue isolate 3	CW7T3
		Tissue isolate 11	CW7T11
		Tissue isolate 13	CW7T13
		Tissue isolate 17	CW7T17
		Tissue isolate 36	CW7T36

Note: all isolates are from foot ulcers except CW7 which is from a leg ulcer.

The growth in SWF of representative isolates from diabetic foot samples (CW2 to CW6) was monitored over 20 h. The number of colonies in each dilution plate was then used to calculate the colony forming units (CFU) per mL at each time point for each sample (in triplicate) (Figure 30).

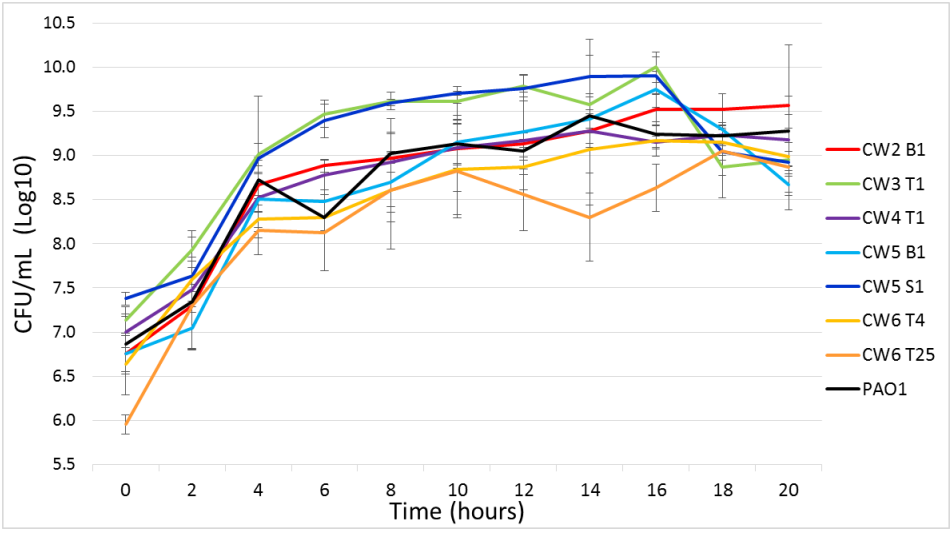


Figure 30: Growth curves for isolates of diabetic foot ulcer. Error bars represent the standard deviation between biological triplicates. B: bone, T: tissue, S: blood – see

Table 13 for details. Since CW3 T1 and CW3 B1 are identical, only CW3 T1 was used. CW5 T was not used as it was identical to either CW5 B (all isolates represented by CW5T1) or CW5 S (all isolates represented by CW5T2).

3.2.2 Determination of antibiotic susceptibility

Plates with a confluent bacterial lawn were incubated for 24 h with antibiotic disks, and afterwards the diameter of the zones of inhibition was measured, and the isolates characterized as sensitive, intermediate or resistant to each antibiotic according to BSAC breakpoint tables. The results are summarised in Tables 14 and 15.

Table 14: Antibiotic susceptibility profiles for chronic diabetic foot ulcer isolates.

Isolates	CIP	CN	TZP	CAZ	ATM	MEM
CW2 B1	S	S	S	S	I	S
CW3 T1/B1	S	S	S	S	I	S
CW4 T1	R	S	S	S	I	S
CW5 B1/T1	R	S	S	S	I	S
CW5 S1/T2	R	S	R	S	I	S
CW6 majority	I	R	R	R	R	R
CW6 T25	I	R	R	R	I	S
PAO1 / NTC 10662	S	S	S	S	I	S

Results represent average of 2 plates per isolate, according to BSAC breakpoint table version 12 (May 2013). CIP, Ciprofloxacin; CN, Gentamicin; TZP, Piperacillin-tazobactam; CAZ, Ceftazidime; ATM, Aztreonam; MEM, Meropenem; S sensitive (green); I intermediate (orange); R resistant (red). Note that 60 isolates were tested for CW6.

Table 15: Antibiotic susceptibility profiles for chronic diabetic leg ulcer isolates.

Isolates	CIP	CN	TZP	CAZ	ATM	MEM
CW7 majority	S	S	n.d.	S	I	S
CW7 T1-T3	S	S	n.d.	S	I	I
CW7 T10, 16, 17, 20, 35	I	S	n.d.	S	I	S
CW7 T13	S	S	n.d.	R	I	S
PAO1 / NTC 10662	S	S	n.d.	S	I	S

Results represent average of 2 plates per isolate (all 40 isolates of CW7 were tested), according to BSAC breakpoint table version 12 (May 2013). CIP, Ciprofloxacin; CN, Gentamicin; TZP, Piperacillin-tazobactam; CAZ, Ceftazidime; ATM, Aztreonam; MEM, Meropenem; S sensitive (green); I intermediate (orange); R resistant (red); n.d. – not defined as TZP disks did not work for the controls.

Note that all strains of *P. aeruginosa* tested have at least an intermediate resistance to aztreonam. The majority of isolates from patients with short-term ulcers (CW2, CW3 and CW7), were sensitive to all other antibiotics. There were exceptions in CW7: T1, T2, and T3 were intermediate for meropenem, T13 that was resistant to ceftazidime, and five isolates (T10, T16, T17, 20, and T35) were intermediate for ciprofloxacin (Table 15). Additionally, some isolates appear to be evolving resistance as results were not consistent between replicate plates, and no information on piperacillin-tazobactam susceptibility is given for CW7 since TZP disks did not work for the controls (n.d. Table 15). Isolates from patients with long-term ulcers (CW4, CW5, and CW6) exhibited higher levels of antibiotic resistance. Particularly, isolates from patient X (CW4 and CW5) showed 100% resistance to ciprofloxacin, and isolates from CW5 profile 2 (CW5 S and CW5 T2) were also resistant to piperacillin-tazobactam (Table 14). In some plates, colonies were found within the inhibition halo of aztreonam (Figure 31).



Figure 31: Antibiotic susceptibility assay for a chronic wound isolate (CW5 T1). Clockwise from the top: MEM, meropenem; CIP, ciprofloxacin; CN, gentamicin; TZP, piperacillin-tazobactam; CAZ, ceftazidime; and ATM, aztreonam. This isolate is 100% resistant to CIP and has a heterogeneous response to ATM.

Both CW6 isolates showed intermediate resistance to ciprofloxacin and were resistant to gentamicin, piperacillin-tazobactam and ceftazidime (Table 14). CW6 T4 is classed as resistant to aztreonam however the size of the diameter zone was in the limit between resistant / intermediate categories. The only difference between resistance profiles in CW6 isolates was in meropenem, where in average the diameter zone for CW6 T4 was 9 mm (resistant) while for CW6 T25 it was 34 mm (sensitive).

3.2.3 Quantification of QS signalling AQ molecules by LCMS/MS

The production of six AQ molecules (HHQ, NHQ, HQNO, NQNO, PQS, and C9-PQS) was measured in representative isolates from patients V to X (Figure 32).

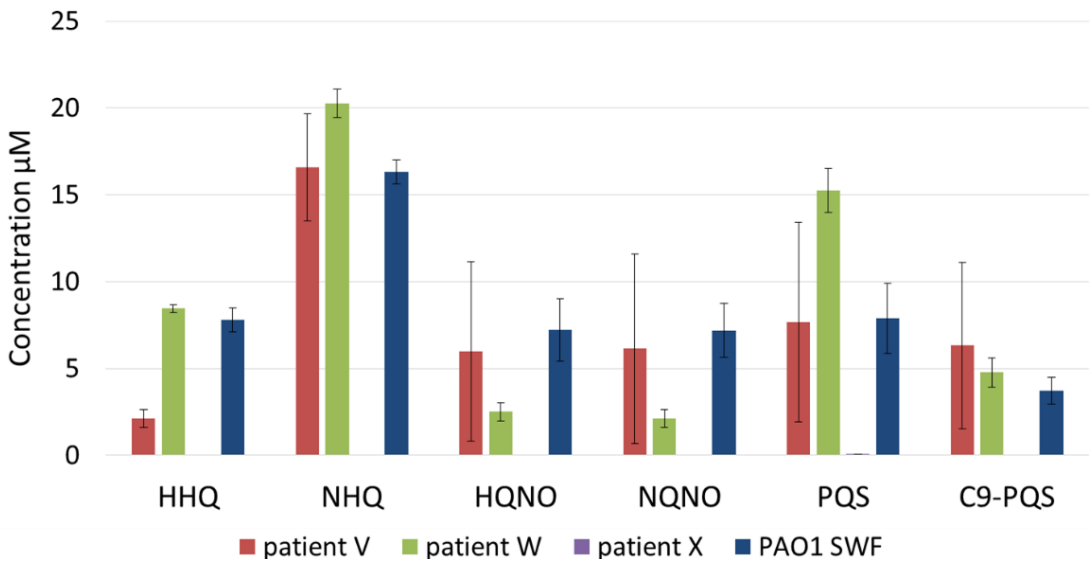


Figure 32: LC-MS/MS quantification of AQs produced by *P. aeruginosa* taken from diabetic foot ulcers of patients V, W, and X and the PAO1 lab strain.

Samples from patient V (CW2) produced similar levels of AQs to PAO1 with the exception of HHQ that was reduced, while samples from patient W (CW3) compared to PAO1 produced similar levels of HHQ and C9-PQS, higher levels of NHQ and PQS, and lower levels of HQNO and NQNO. Samples from patient X (CW4)

produced very small amounts of AQs – less than 0.5 µM for all AQs tested, which is the lowest calibration point used and a threshold for biological activity. Note that the production of these molecules is probably tightly regulated *in vivo* in *P. aeruginosa* from patient V as there was a big variation between the biological replicates.

3.2.4 Summary of *P. aeruginosa* phenotypic results

In order to facilitate discussion and comparison of the different phenotypic assays, the results presented in sections 3.2.1 and 3.2.2 are summarised in Table 16.

Table 16: Summary of the characterization results for *P. aeruginosa* phenotypes.

Sample	Siderophores		Pyocyanin	Total exo-proteases	QS signals		Antibiotic resistance
	PVD	PCH			C4	C12	
CW2 B	±	+	+	+	+	+	-
CW3 T	±	+	+	+	+	+	-
CW3 B	±	+	+	+	+	+	-
CW4 T	±	±	–	–	+	–	CIP
CW5 (1)	±	±	–	–	+	–	CIP
CW5 (2)	–	±	–	–	+	–	CIP, TZP
CW6 T	±	+ ++ T25	++ ± T25	– + T25	+	+	CN, TZP, CAZ, ATM, MEM
CW7 T	–	+	±	±	+	+	-

CW5 samples were divided into CW5 (1) – which includes CW5 B isolates and isolates with profile 1 represented by CW5 T1, and CW5 (2) – which includes CW5 S isolates and isolates with profile 2 represented by CW5 T2. For CW7 T only the result displayed by the majority of the isolates is represented. For siderophores and pyocyanin: – negligible, ± low, + average, ++ high, +++ very high. For exoproteases and QS signals: + production, ± low production, – no production. For antibiotic resistance, acronyms represent the antibiotics to which bacteria showed resistance: CIP, Ciprofloxacin; CN, Gentamicin; TZP, Piperacillin-tazobactam; CAZ, Ceftazidime; ATM, Aztreonam; MEM, Meropenem. Note that CW6 T25 is sensitive to MEM.

3.2.5 Genomic analysis of *P. aeruginosa* chronic wound isolates

The genomes of 16 representative *P. aeruginosa* isolates were sequenced alongside an additional isolate per chronic wound and sample type (Table 17; 23

isolates in total). The 6 isolates selected for CW7 are phenotypically very different from each other and between the other 34 isolates taken from this patient. However, these were selected with the objective of covering the maximum diversity possible. Nonetheless, they do not cover all of the variations observed in, for example, siderophore production (section 2.3.1.4) within the *P. aeruginosa* population of the diabetic leg ulcer of patient Z.

Table 17: Genome assembly information for the 23 *P. aeruginosa* isolates sequenced.

Samples	Isolates	GC Content (%)	Length (bp)	# Contigs
CW2	B1*	66.18	6,891,079	**128**
	B40	66.15	**6,936,598**	109
CW3	T1*	66.28	6,654,054	80
	T40	66.27	6,658,635	**25**
	B1*	66.29	6,656,317	68
	B40	66.27	6,655,387	79
CW4	T1*	**66.43**	6,452,696	92
	T40	66.42	6,453,104	49
CW5 (profile 1)	T1*	**66.43**	6,452,584	73
	T40*	**66.43**	6,452,401	82
	B1*	**66.43**	6,452,282	78
CW5 (profile 2)	T2*	**66.43**	6,452,473	90
	T34*	**66.43**	6,452,643	77
	S1*	**66.43**	6,459,815	142
CW6	T4	**66.06**	6,848,834	66
	T25	**66.06**	6,848,327	70
	T40	**66.06**	6,849,367	58
CW7	T1	66.42	6,367,587	95
	T3	66.42	6,366,936	90
	T11	**66.43**	6,358,853	101
	T13	66.42	6,367,462	66
	T17	**66.43**	**6,358,533**	81
	T36	**66.43**	6,359,666	90

Data obtained from the full genome report for each isolate, generated via the PATRIC comprehensive genome analysis service (using raw reads as input, auto as assembly strategy, and genetic code 11). Isolates marked with an asterisk (*) were sequenced using MiSeq, all others were sequenced using HiSeq (with a guaranteed minimum of 30x coverage for both). Values in bold correspond to the minimum and the maximum for each column.

Genome assemblies were used to construct a comparative genomics diagram using BRIG (Figures 33 and 34). With the information available in the Pseudomonas.com database on virulence factor annotations, regions shown to be associated with virulence in *P. aeruginosa* were selected. These included Hcp secretion islands encoded by the type VI secretion system (T4SS); regions that contained genes involved in the biosynthesis of the three major extracellular matrix polysaccharides (alginate, Pel, Psl) and the LPS O-antigen region; regions with motility genes (in particular operons related to type IV pili involved in twitching motility and flagella); and genes involved with type III secretion system (T3SS). The virulence-associated regions also included genes responsible for the phenotypes tested in section 2.3, such as the three quorum-sensing systems (*las*, *rhl* and *pqs*), the regions involved with production of both PVD and PCH, and the *phz* operons involved in biosynthesis of phenazines such as pyocyanin.

Additionally, regions with a skew in the GC content and that are associated with mobile elements were also highlighted, such as the Pf1 phage region and the different regions coding for pyocins (toxins which are distantly derived from phages). Regions that appear as blank spaces in each ring (zones with less than 75% identity) and that are common to the majority of the chronic wound isolates analysed here, were manually identified, checked and numbered R1 to R8. They mostly contain hypothetical proteins, but a description of the start and end positions, the total size of each region, and a detailed list of the corresponding genes and the predicted protein function was compiled and can be seen in the Appendix B.

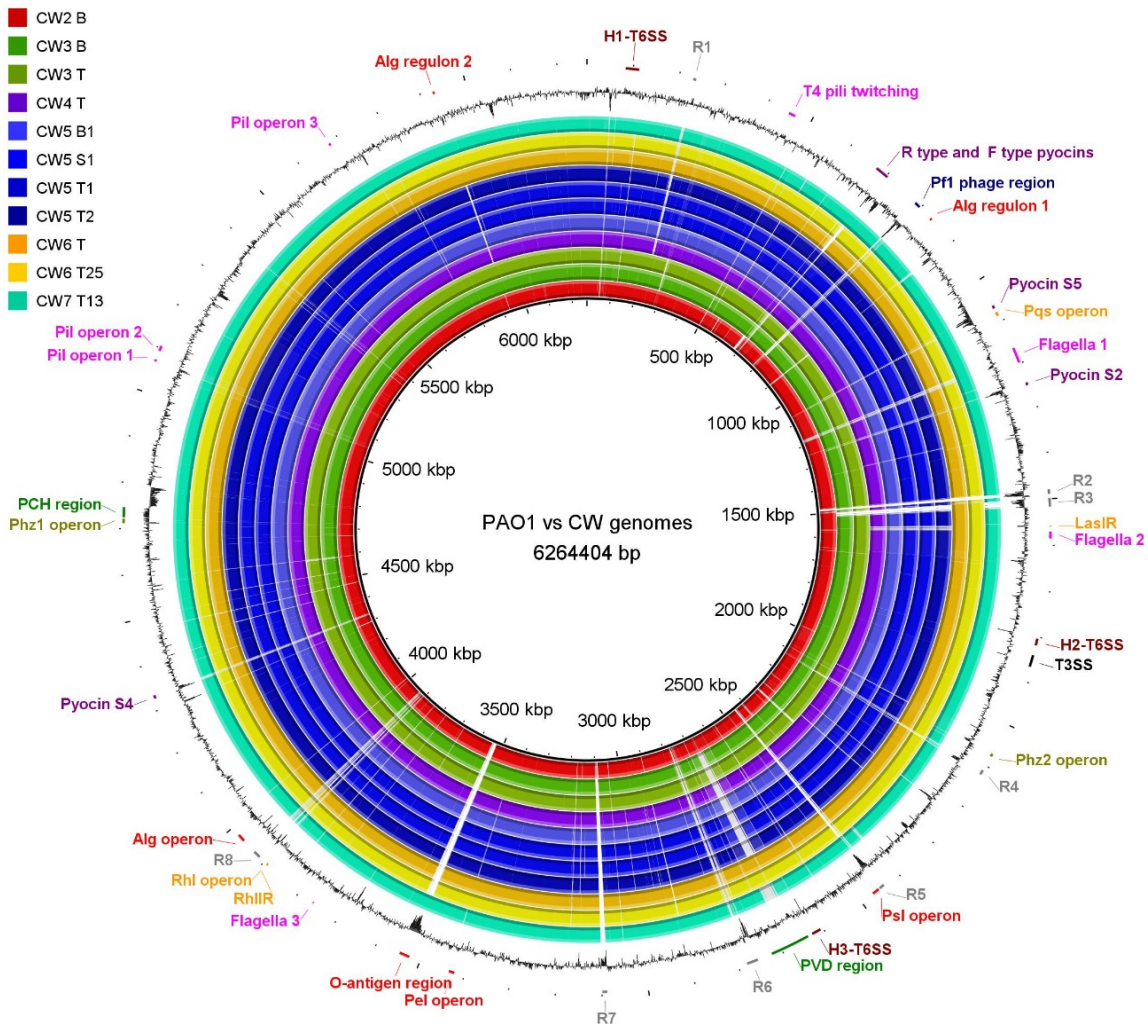


Figure 33: Whole genome sequence comparison of *P. aeruginosa* PAO1 reference with chronic wound (CW) *P. aeruginosa* clinical isolates. From inside out, this circular map shows PAO1 reference (thin black line), CW2 through CW7 genomes (refer to colour-coded legend: B – bone, T – tissue, S – blood), and percentage of G+C content for PAO1. If there is no number next to the sample type, it contains combined information from T1 and T40 isolates, except for CW6 T that combines data from T4 and T40 isolates. Ring shades denote different levels of nucleotide identity to PAO1 according to BLASTn, ranging from 75% (lightest) to 100% (darkest). Matches with less than 75% identity, or regions with no BLAST matches, appear as blank spaces in each ring. Low-identity regions common to most genomes are identified by grey arcs (R1 to R8) and mostly contain hypothetical proteins – see Appendix B. Virulence-associated regions are identified by colour-coded arcs: brown (Hcp secretion islands 1, 2 and 3 encoded by T6SS), pink (motility genes – type IV pili and flagellar operons), dark blue (phage regions), red (extracellular matrix polysaccharides – alginate, Pel, Psl operons and LPS O-antigen region), purple (pyocin regions), orange (quorum-sensing systems – *las*, *rhl*, and *pqs* operons), and black (genes involved with T3SS). Diagram generated using BRIG [153].

Since there was high phenotypic diversity in isolates from patient Z (diabetic leg ulcer), only CW7 T13 is included in Figure 33, and a separate diagram was made with the six sequenced *P. aeruginosa* representatives from CW7 (Figure 34).

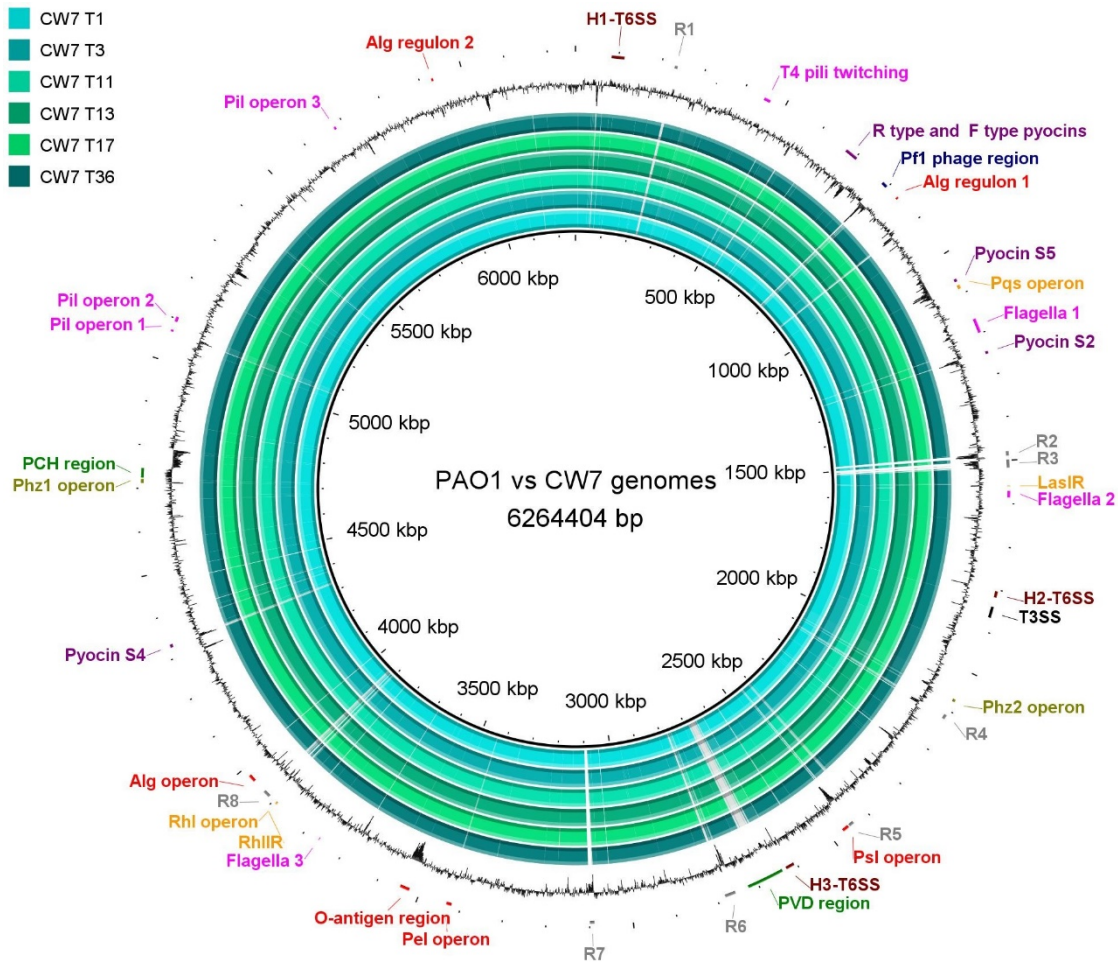


Figure 34: Whole genome sequence comparison of *P. aeruginosa* PAO1 reference with CW7 *P. aeruginosa* clinical isolates taken from a diabetic leg ulcer. From inside out, this circular map shows PAO1 reference (thin black line), CW7 genomes (T1, T3, T11, T13, T17, and T36), and percentage of G+C content for PAO1. Ring shades denote different levels of nucleotide identity to PAO1 according to BLASTn, ranging from 75% (lightest) to 100% (darkest). Matches with less than 75% identity, or regions with no BLAST matches, appear as blank spaces in each ring. Low-identity regions common to most genomes are identified by grey arcs (R1 to R8) and mostly contain hypothetical proteins – see Appendix B. Virulence-associated regions are identified by colour-coded arcs: brown (Hcp secretion islands 1, 2 and 3 encoded by T6SS), pink (motility genes – type IV pili and flagellar operons), dark blue (phage regions), red (extracellular matrix polysaccharides – alginate, Pel, Psl operons and LPS O-antigen region), purple (pyocin regions), orange (quorum-sensing systems – *las*, *rhl*, and *pqs* operons), and black (genes involved with T3SS). Diagram generated using BRIG [153].

Using the PATRIC BLAST service, mutations in the genes of the *las* and *rhl* QS systems were identified (Table 18). For each substitution, panX was used to analyse the frequency of the amino acids (aa) in other *P. aeruginosa* genomes (Table 19). PROVEAN was used to predict whether each amino acid substitution identified has an impact on the biological function of the protein. This software identifies closely related sequences by BLAST and computes an alignment score for each sequence. The scores are then averaged to generate a final score, and if this is equal to or below -2.5, the substitution is predicted to have a "deleterious" effect. Otherwise, if the score is above the threshold, the variant is predicted to have a "neutral" effect.

Table 18: List of amino acid substitutions in genes of the *las*/*rhl* systems.

Gene	CW2	CW3	CW4/CW5	CW6	CW7	Impact
lasR	-	-	G.N.F.	-	p.S204L	**-5.361**
	-	-		p.A231V[#]	-	**-3.717**
rsaL	-	-	G.N.F.	-	-	n.a.
lasI	-	-	G.N.F.	-	-	n.a.
lasA	p.P12S	-	-	-	-	-0.216
	-	p.L80V	p.L80V	p.L80V	p.L80V	0.122
	p.V111A	-	-	-	-	0.852
	p.V192A	p.V192A	p.V192A	p.V192A	p.V192A	0.620
	p.S223R	p.S223R	p.S223R	p.S223R	p.S223R	-0.592
lasB	-	-	-	-	p.S241G	-0.622
	-	-	-	-	p.S436L	-1.990
rhlR	-	-	-	-	-	n.a.
rhlI	-	-	p.R41K	-	-	-0.204
	-	-	p.S62G	p.S62G	-	-1.289
	p.D83E	p.D83E	p.D83E	p.D83E	p.D83E	0.275
rhlA	p.Q168P	p.Q168P	p.Q168P	p.Q168P	p.Q168P	0.372
rhlB	-	-	-	-	p.Y119H	-1.308
	-	-	p.A126T	-	-	-0.110
	-	-	-	-	p.K182N	-1.191
	-	-	p.S251N	-	-	-0.624

Data obtained through PATRIC BLAST service using BLASTn against the genomes in Table 17 (only substitutions present in all genomes corresponding to each column are indicated). G.N.F means gene not found, i.e., BLASTn did not yield results; p.X*n*Z indicates a substitution on protein position *n* where amino acid X was replaced by amino acid Z; – indicates the same sequence as the corresponding PAO1 gene; superscript # denotes a substitution not present in CW6 T25; Impact was calculated with PROVEAN and values in bold correspond to a predicted deleterious impact on the biological function of each protein; n.a. non applicable.

Table 19: Position and frequency of amino acid substitutions in Las and Rhl proteins.

Protein	Total	Position and frequency of amino acid substitutions											
		204		231									
LasR	94	S	L	A	V	-							
		94	0	92	1	1							
		12		80			111		**192**		**223**		
LasA	122	P	S	L	V	M	V	A	**V**	**A**	**S**	**R**	
		101	22	76	45	2	98	25	**3**	**120**	**3**	**120**	
		241		436									
LasB	122	S	G	S	L								
		59	63	116	6								
		41		62		83							
RhlI	122	R	K	S	G	D	E						
		116	6	20	102	31	91						
		168											
RhlA	123	**Q**	**P**										
		3	**120**										
		119		126			182		251				
RhlB	122	Y	H	A	T	V	K	N	S	N			
		122	0	113	5	4	122	0	115	7			

Position of the substitution is indicated by the number on top of each row, and the alternative amino acids found in that position are indicated below, as well as their frequency. Data was acquired from panX (http://pangenome.tuebingen.mpg.de/Pseudomonas_aeruginosa) filtering each protein in the gene cluster table. Total column corresponds to the number of isolates in panX that contained the queried protein (from 123 *P. aeruginosa* genomes available). Values in bold correspond to substitutions present only in 3 isolates closely related to PAO1.

With this analysis it is clear that the *las* operon (constituted by *lasR, rsaI,* and *lasI*) is not present in the genomes of *P. aeruginosa* isolates from patient X (CW4 and CW5, Figure 33 and Table 18). Actually in these isolates there is a deletion of approximately 10000 bp in this region between genes PA1429 and PA1438 (Figure 35). Other 29 *P. aeruginosa* isolates whose genomes have been sequenced and available in panX also lack the *lasR* gene (in Table 19 the "total" for LasR is 94 out of the 123 available on the database). Genes *rsaL* and *lasI* are present in all other chronic wound genomes analysed in this work, and do not have any have substitutions, as well as *rhlR* (Table 18).

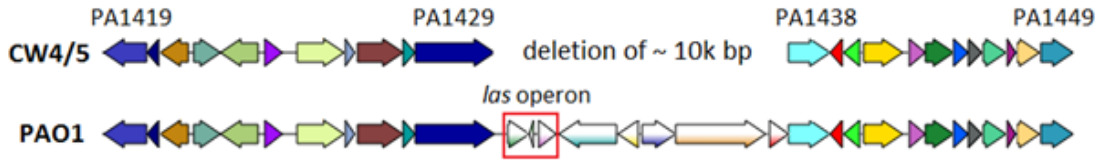


Figure 35: Synteny of the *las* operon region between patient X isolates and PAO1 reference. A deletion of around 10k bp was identified in isolates from patient X (CW4 and CW5) between genes PA1429 and PA1438, which explains the absence of the *las* operon (highlited by a red square) and other 5 genes in these clinical isolates.

The substitution p.S204L in *lasR* is unique to the six CW7 isolates tested and is predicted to negatively affect LasR protein function as it involves a chemical change from serine (S), a polar but uncharged aa, to a leucine (L), a non-polar, hydrophilic aa. This mutation in *lasR* and the substitutions p.Y119H and p.K182N in *rhlB* are the only changes unique to *P. aeruginosa* from the patient Z population (diabetic leg ulcer), since their frequencies in the other 123 *P. aeruginosa* genomes from panX are 0, as noted in Table 19.

The substitutions p.V192A and p.S223R (LasA), and p.Q168P (RhlA) are present in all isolates tested, however they are not true SNPs associated specifically with chronic wound genomes since only PAO1 (and two other PAO1-related isolates) have different aa in these positions (see bold values in Table 19). For the other three substitution found in LasA (p.P12S, p.L80V, p.V111A) mutations in codons 12 and 111 detected in CW2 isolates are not uncommon amongst other *P. aeruginosa* genomes, with frequencies of 17.9% and 20.3%, respectively. The mutation in position 80 however is more common, not only in our isolates (present in all samples except CW2), but also in other *P. aeruginosa* genomes (frequency of 36.6%).

For *lasB* mutations were only detected in CW7 isolates, and the substitution p.S436L was rare, only present in other 6 clinical isolates from panX, while glycine in

position 241 (p.S241G) was as common (51.6%) as the alternative serine (Table 19). For *rhlI*, a total of three substitutions were found and mutations in positions 41 and 62 are highlighted in Figure 36. Substitution p.K41R, which is only found in the isolates of patient X (CW4 and CW5), is very rare since its frequency is below 5% in *P. aeruginosa* genomes on panX, whereas p.S62G, even though only present in isolates from patient X and Y (CW6), is extremely common (frequency of 86.3%) in other *P. aeruginosa* genomes on panX. The substitution p.D83E entails a change from aspartate (D) to glutamate (E), and is common in all chronic wound genomes. However, it is glutamate that is more common in other *P. aeruginosa* strains and not aspartate, as observed by their unbalanced aa frequency: D – 31 vs E – 91 (Table 19).

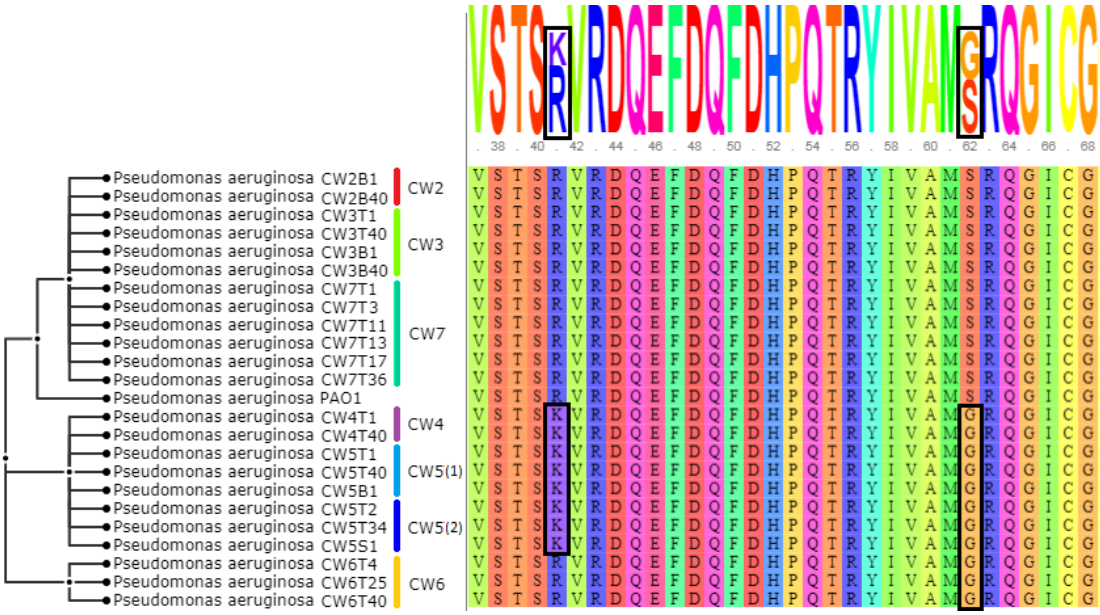


Figure 36: Multiple sequence alignment analysis of RhlI trough PATRIC platform. Nucleotide gene sequences extracted from Pseudomonas.com were inserted in the PATRIC BLAST service (https://www.patricbrc.org/app/BLAST). BLASTn was used against the genome group that included 23 *P. aeruginosa* chronic wound isolates and the reference genome *P. aeruginosa* PAO1. Results were observed through the MSA amino acid option that generates a phylogenetic tree (on the left, with each CW group highlighted) and the corresponding alignment on the right; each amino acid is represented by a different colour and logos at the top represent the amino acid conserved for each position. Black boxes highlight the p.R41K mutation in CW4 and CW5, and the p.S62G mutation in CW4, CW5 and CW6.

In general, substitutions which are only present in isolates from patient X, such as p.A126T and p.S251 in *rhlB*, are very rare in the genomes of *P. aeruginosa* available on panX. For *rhlB*, the frequency of T at position 126 is only 4%, even though there is also another variant (A→V) which is even less common (3.2%). The frequency of N at position 251 is 5.7%.

As described in the introduction to this chapter, the QS network in *P. aeruginosa* incorporates three systems: *las*, *rhl*, and *pqs*. As such, substitutions in genes of the *pqs* system were also annotated using the PATRIC BLAST service (Table 20). For each substitution, panX was used to analyse the frequency of the aa in other *P. aeruginosa* genomes (Table 21).

Table 20: List of amino acid substitutions in genes of the *pqs* operon.

Gene	CW2	CW3	CW4/CW5	CW6	CW7	Impact
pqsA	-	-	p.P360L	-	-	-2.013
	-	-	-	-	p.G375D	**-3.746**
pqsB	p.D47N	-	-	-	-	-1.999
	-	p.A50V	-	-	-	-2.346
	-	-	-	p.P200L	-	-1.170
pqsC	-	-	-	-	p.A7T	-0.279
	-	p.K277R	-	-	-	-0.534
pqsD	p.E176D	-	p.E176D	p.E176D	-	-0.460
	-	p.A243V	p.A243V	-	-	-1.367
pqsE	-	p.A179V	-	-	-	-2.467
phnA	-	p.S79A	-	-	-	-0.591
	p.D91A	p.D91A	p.D91A	p.D91A	p.D91A	0.907
	-	p.S114P	-	-	-	0.071
	-	p.G143E	-	-	-	2.448
	p.V145A	p.V145A	p.V145A	-	p.V145A	-1.541
	-	-	-	-	p.H171Y	-1.525
	-	-	p.A197G	-	-	-1.420
phnB	-	p.A73V	-	-	-	0.968
	-	p.R116H	-	-	-	-0.668
	p.F143S	-	-	-	-	-2.299
pqsR	-	-	p.H176P	-	-	**-8.989**
	p.V215A	-	-	-	-	-1.976
	-	p.A314V	-	-	-	-0.004

Data obtained through PATRIC BLAST service using BLASTn against the genomes in Table 17 (only substitutions present in all genomes corresponding to each column are indicated). p.X*n*Z indicates a substitution on protein position *n* where amino acid X was replaced by amino acid Z; – indicates same sequence as corresponding PAO1 gene; Impact was calculated with PROVEAN and values in bold correspond to a predicted deleterious impact on the biological function of each protein.

Table 21: Position and frequency of amino acid substitutions in Pqs and Phn proteins.

Samples	Protein, position and frequency of amino acid substitutions											
only in CW2	PqsB 47		PhnB 143		PqsR 215							
	D	N	F	S	V	A						
	119	4	118	4	118	1						
only in CW3	PqsB 50			PqsC 277			**PqsE 179**		PhnA 79			
	A	V	S	K	N		**A**	**V**	S	A	P	
	113	6	4	119	4		**122**	**0**	73	43	4	
	PhnA 114		PhnA 143			PhnB 73		PhnB 116		PqsR 314		
	S	P	G	E	R	A	V	R	H	A	V	
	107	13	78	38	4	121	1	93	29	89	30	
only in CW4/5	PqsA 360		PhnA 197		**PqsR 176**							
	P	L	A	G	**H**	**P**						
	117	5	115	5	**119**	**0**						
only in CW6	PqsB 200											
	P	L										
	121	2										
only in CW7	PqsA 375		PqsC 7		PhnA 171							
	G	D	A	T	H	Y	Q					
	118	4	117	6	110	6	4					
mixed	PqsD 176		PqsD 243		PhnA 145		PhnA 91					
	E	D	A	V	V	A	D	A				
	59	63	80	42	16	104	8	112				

Protein name and substitution position are indicated on top of each row, and the alternative amino acids found in that position are indicated below, as well as their frequency. Data was taken from panX (http://pangenome.tuebingen.mpg.de/Pseudomonas_aeruginosa) filtering each protein in the gene cluster table. "mixed" identifies substitutions present in more than one sample. Values in bold correspond to unique substitutions in the corresponding sample. Note that the number of strains in panX that contained the queried protein (from 123 *P. aeruginosa* genomes available) corresponds to the sum of the frequencies.

The substitutions present only in CW2, p.D47N (PqsB), p.F143S (PhnB), and p.V215A (PqsR), are not common in other *P. aeruginosa* isolates, as their frequencies are very low (3.3%, 3.3%, and 0.8% respectively), nonetheless they are not predicted to impact the function of the proteins.

For patient W (CW3), all genes in this region except pqsA had mutations, however none was predicted to impact the function of the proteins. The gene with more substitutions was phnA, but the substitutions in positions 79, 114, and 143 are relatively common when compared with other *P. aeruginosa* isolates (frequencies of 35.8%, 10.8%, and 31.6% respectively). Other substitutions in the CW3 isolates, particularly in PqsB (p.A50V), PqsC (p.K277N), PqsE (p.A179V), and PhnB (p.A73V) are rare in the 123 *P. aeruginosa* genomes from panX, as seen in Table 21 by the low frequencies of the substituted aa (4.9%, 3.3%, 0%, and 0.8% respectively). Meanwhile, substitutions p.R116H (PhnB) and p.A313V (PqsR) are relatively more common with frequencies of 23.8% and 25.2% respectively.

In isolates from patient X (CW4 and CW5), substitutions in PqsA (p.P360L) and PhnA (p.A197G) are rare, with frequencies of ~ 4.1% in the *P. aeruginosa* strains from panX. Moreover, the substitution of histidine (H) by proline (P) at position 176 of PqsR is unique to these isolates, and predicted to negatively affect protein function and consequently AQ biosynthesis. For CW6 isolates the substitution p.P200L in PqsB is very uncommon (1.6% in other *P. aeruginosa* genomes). For CW7 isolates, all of the unique substitutions identified (p.G375D in PqsA, p.A7T in PqsC, and p.H171Y in PhnA) have very low frequencies (below 5%) in other *P. aeruginosa* genomes, however only the mutation in *pqsA* is predicted to negatively effect the protein.

The substitution p.D91A in PhnA is present in all chronic wound isolates, however it does not correlate with a true adaptive SNP since alanine (A, 93.3% frequency) is much more common at that position than aspartate (D, 6.7% frequency) (Table 21). In the same predicted protein, p.V145A is slightly less common (86.7%),

and is also not present in the CW6 isolates analysed. Mutations in positions 176 and 243 of PqsD, have high frequencies (51.6% and 34.4% respectively), so there is a low probability of them being associated with adaptation to the chronic wound setting.

A phylogenetic tree was constructed with the *P. aeruginosa* diabetic isolates using the phylogenetic tree building service at the PATRIC platform (Figure 37). Besides the isolates from the chronic wounds studied in this work, the phylogenetic tree also includes six other well-characterized *P. aeruginosa* strains (taken from Pseudomonas.com database) namely the PAO1 (reference) and PA14 strains originally isolated from human wounds (now lab adapted); LESB58 – a cystic fibrosis Liverpool epidemic strain that is hyper virulent; PASS2 – a cystic fibrosis strain from an adult; BWH035 – a strain isolated from a human ear infection; and M18 – a strain originated from the rhizosphere.

From the phylogenetic analysis, it can be concluded that chronic wound isolates cluster according to the patient they were isolated from, and that they are very distinct from well characterised lab strains like PAO1 and PA14. This supports the hypothesis that only one strain of *P. aeruginosa* colonises a given ulcer at a particular time.

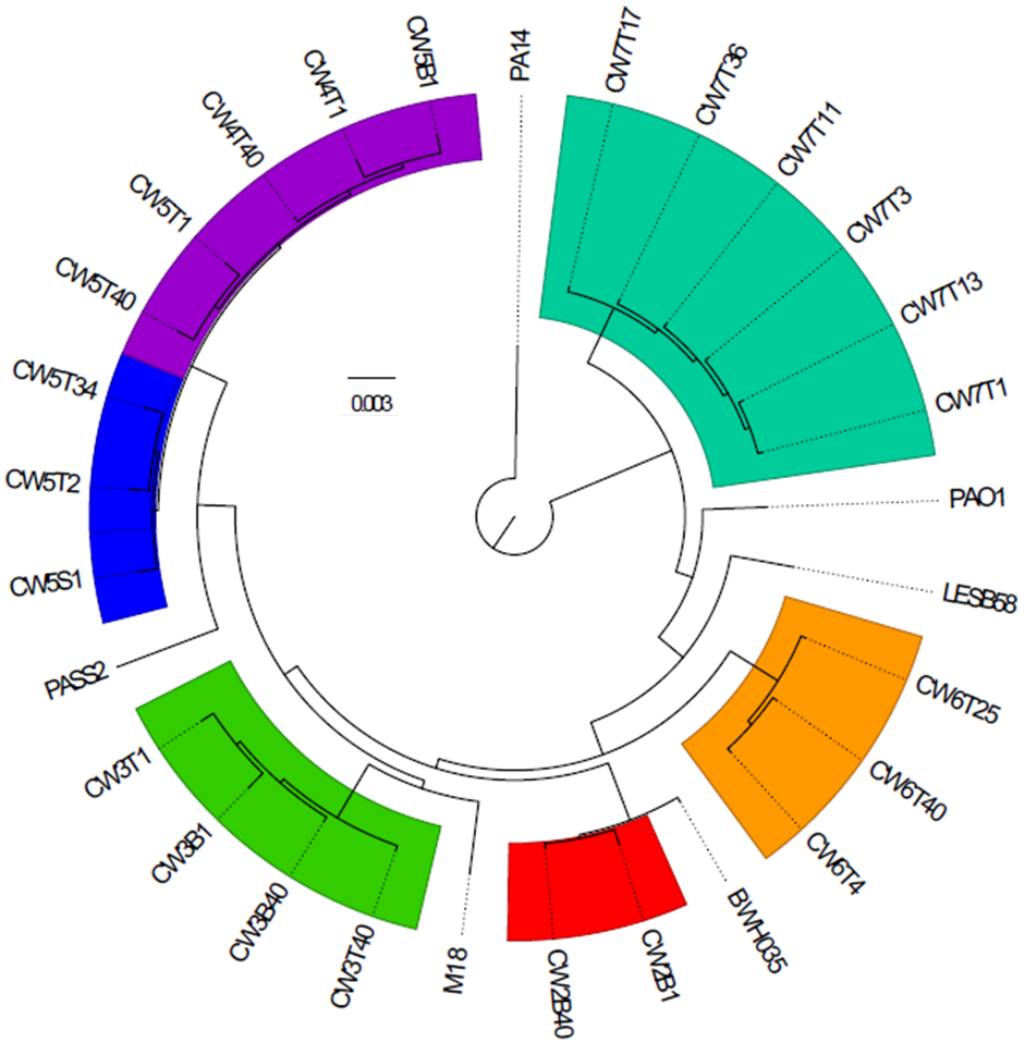


Figure 37: Polar tree layout of the phylogenetic relationship between the 23 genomes of the *P. aeruginosa* chronic wound isolates sequenced. Isolates cluster by patient, as can be observed by the coloured regions (teal: CW7 patient Z, orange: CW6 patient Y, red: CW2 patient V, green: CW3 patient W, and from patient X blue: CW5 profile 2 and purple: CW5 profile 1 and CW4. Sequences of another six *P. aeruginosa* strains where included in this analysis: PAO1 and PA14 lab strains (the last one used as outgroup), BWH035 from an ear infection, LESB58 (Liverpool Epidemic Strain) and PASS2 from cystic fibrosis patients, and M18 a rhizosphere originating strain.

3.3 Discussion

The phenotypic diversity present in *P. aeruginosa* chronic diabetic wound populations was explored through the analysis of colony morphology and of phenotypes traditionally associated with *Pseudomonas* pathogenicity in the wound

environment. This was followed by genomic analysis of *P. aeruginosa* chronic wound isolates, with special focus on (i) whole genome sequence comparisons of virulence-associated regions, (ii) a detailed analysis of the three QS systems, and (iii) their phylogeny.

In general, *P. aeruginosa* populations taken from diabetic foot ulcers (DFUs) had very low phenotypic diversity, in contrast to the single population taken from a diabetic leg ulcer (DLU). In particular, for DFUs no diversity was found within *P. aeruginosa* isolates from each population taken from patients V (CW2 - 40 isolates tested) and W (CW3 - 80 isolates tested); whereas the 160 *P. aeruginosa* isolates taken from patient X could be grouped into just 2 profiles. Here, there was a clear association with the type of sample: tissue isolates from the first biopsy (earlier time point – CW4) and bone isolates from the second biopsy (later time point – CW5) displayed the same phenotypic profile, while isolates sampled from blood (CW5) displayed a different phenotypic profile. Tissue isolates from CW5 constituted one or the other, in a proportion similar to the global profile 1 / profile 2 ratio (65% and 35% respectively). Differences between bone and blood Isolate profiles will be further explored in Chapter 4.

In the *P. aeruginosa* population taken from patient Y, there were also 2 phenotypic profiles; however, one was common and observed in 39 out of 40 isolates, whilst the other was only found in a single isolate. In the *P. aeruginosa* population taken from patient Z, that corresponds to the only DLU tested in this work, the analysis of 40 isolates showed a high degree of phenotypic diversity.

3.3.1 Phenotypic diversity in populations from DFUs is low

Globally, the results show differences in colony morphology in isolates taken from different patients but not from within the same chronic wound. Isolates from CW2 and CW3 stain red on CRA plates because of Congo red adsorption. Congo red binds to exopolysaccharides, the major extracellular matrix component, in several bacteria, including *P. aeruginosa* [205]. CW3 isolates also have well-defined margins and smooth colonies like the *pel* mutant so they might lack this glucose-rich component of the extracellular matrix [205]. The majority (65%) of isolates from patient X (all CW4 tissue and CW5 bone isolates plus 24 CW5 tissue isolates) are orange and are not as smooth as isolates from CW2/3 (see Table 8 and Figure 25). The other 35% (all CW5 blood isolates and 16 CW5 tissue isolates – that were white on LB agar plates (Figure 24), and are identified as profile 2) are red, small, and wrinkly on CRA plates (Figure 25).

A wrinkled colony phenotype (in a similar medium containing Congo red and Coomassie brilliant blue) is generally associated with increased biofilm formation due to increased cellular levels of c-diGMP (bis-(3'-5')-cyclic-dimeric guanosine monophosphate), as in the case of the *wspF* mutant used [206]. However, patient Z profile 2 isolates grew more and were not as wrinkly as Δ*wspF*, so it is unlikely that this gene is the only one involved in the development of a wrinkled phenotype. Identifying these genes is nevertheless relevant, since isolates with this distinct morphotype were responsible for the development of septicaemia in patient X. CW6 isolates were all smooth and spread on CRA plates, however T25 had a red centre and whiter edge, the opposite of the other 39 isolates from patient Y. Interestingly,

the morphotype of CW6 T25 closely resembles the morphotype of PAO1; nevertheless, this is unlikely to be a case of contamination since the remaining CW6 T25 and PAO1 phenotypes analysed in this work were very different.

Together with colony morphology, this trend towards low diversity was found when analysing several *P. aeruginosa* phenotypes that can also be classified as social traits, such as QS signal molecules, pyocyanin and exoprotease production. In general, isolates from different patients behave differently, while within the same patient no differences between the isolates was apparent, independent of the sample origin (bone or tissue). The exception is the septicaemia-causing isolates (from here on referred to as patient X profile 2 isolates) that are phenotypically different from other CW4/CW5 isolates (patient X profile 1 isolates), and the CW6 T25 isolate that is also very different from the rest of the CW6 population. These differences could be explained either by the presence of two distinct *P. aeruginosa* strains in the ulcers of patients X and Y, rather than true *P. aeruginosa* phenotypic diversity as has been observed in other chronic infections such as cystic fibrosis (CF), or by single nucleotide polymorphisms (SNPs) in genes related to the phenotypes tested.

In DFUs there seems to be a tendency for the loss of social traits in *P. aeruginosa* populations with the increased duration of infection. Isolates from patient X who had an infected ulcer for 26 months (CW4 and CW5) were negative for pyocyanin, exoproteases, 3-oxo-C12-HSL, and AQs including PQS and HHQ, while isolates from patients V (CW2) and W (CW3) that had infected ulcers for less than 6 months were positive for the same phenotypes (see summary Table 16). However,

P. aeruginosa taken from patient Y who also had a long-term ulcer (infected for about 48 months) still produced high levels of pyocyanin, but no exoproteases. Considering this information, it is likely that the loss of pyocyanin production in samples from patient X is a consequence of either mutations in the phenazine (*phz*) biosynthesis operons or, more likely, a defective QS regulatory system given that the CW5 and CW4 isolates do not produce 3-oxo-C12-HSL or PQS (Table 16, Figure 32). In *P.aeruginosa*, pyocyanin regulation is complex (see [207]) and depends on *las*, *rhl* and *pqs* regulatory systems although pyocyanin can still be produced in the absence of the *las* system [208]. Indeed, the QS hierarchy shown in Figure 21 is not a strict hierarchy with the *las* system at the top, but an interdependent network such that to a certain extent *P. aeruginosa* can overcome a deficiency in one of its QS systems by allowing another to take over for example, during late stationary phase [208, 209].

Others have reported that social traits are lost in CF infections over time [210-212], and the appearance of *las* mutants is also common [213, 214], even though some *lasR* point mutants are still functional [210]. However, samples from more patients are required to unequivocally establish that this occurs in diabetic chronic wounds, even though all *P. aeruginosa* isolates from patient X had a large deletion in the *las* region. Nonetheless, with these data it can be postulated that at least the reduction in exoprotease production may be an adaptation to the chronic environment – as it was also observed in the context of CF [215]. As such, the suggestion that extracellular bacterial proteases are potential therapeutic targets [216], does not seem relevant, even though for example the inhibition of LasB, a well-known *P. aeruginosa* exoprotease, has been reported to disrupt biofilms [217].

The results also show that there is a similar trend with respect to an increase in antibiotic resistance over time, which is indeed expected since it is well established that the longer an infection persists, the higher the probability of bacteria evolving resistance to the antibiotics used [218]. In this case, at the time of sampling, *P. aeruginosa* isolated from patient X was already fully ciprofloxacin-resistant, as the patient had been given this antibiotic when *P. aeruginosa* was first detected (2 years prior to CW4 sampling). Interestingly, the profile 2 isolates were also resistant to piperacillin-tazobactam, however this resistance pattern was detected and prompt intervention guaranteed that the patient was given a combination of daptomycin, gentamicin, and metronidazole instead of piperacillin-tazobactam to treat the *P. aeruginosa* septicaemia.

For patient Y, the majority of *P. aeruginosa* isolates were fully resistant, or at least showed an intermediate resistance to all antibiotics tested. This was probably also caused by long-term exposure to antibiotics since this patient had previously had osteomyelitis that required lengthy antibiotic treatment. At the time of sampling, patient Y was being given meropenem and vancomycin – antibiotics with little efficacy against *P. aeruginosa*, either because the population had evolved resistance (meropenem), or because it preferentially targets Gram-positives (vancomycin).

Pyoverdine (PVD) and pyochelin (PCH) production appears not to change over time, i.e., there were no differences between short-term ulcers and long-term ulcers. *P. aeruginosa* populations from patients V and W (short-term ulcers – identified as triangles in Figure 29) produced moderate levels of both siderophores, as well as the population taken from patient Y (who had a long-term ulcer – identified as circles in

Figure 29). Interestingly, even though it produced similar levels of PVD, CW6 T25 produced high levels of PCH and as an "outlier" was easy to identify in the ++ category of the PCH plot (Figure 29).

As for *P. aeruginosa* populations taken from the long-term ulcer of patient X, the Table 16 summary indicates that all isolates had low levels of PCH, and profile 1 isolates had moderate levels of PVD, whereas profile 2 isolates produced negligible amounts of PVD. Although PCH production was correctly classed as low because all isolates are in the ± category, closer observation (compare CW5 B and CW5 S in the PCH plot in Figure 29) revealed a significant difference between the levels of PCH: while profile 1 isolates produced on average 12.8k RFU/OD_{600}, profile 2 isolates produced almost double of that amount, in average 26.6k RFU/OD_{600} (see also Figure 42 in Chapter 4).

P. aeruginosa strains that colonise chronic wounds originate from endogenous sources such as the gastrointestinal tract and the surrounding skin, or from exogenous sources such as the environment including local healthcare facilities [91]. Thus, being able to switch between siderophores may benefit bacteria in changeable environments, as PVD is a highly efficient but costly siderophore, while PCH is metabolically cheaper but a less effective iron chelator due to its lower affinity for iron [139, 219]. It has been shown that the relative prevalence of strains producing both siderophores may decrease when the environment is less prone to change and/or is biased towards specific conditions [139]. In chronic ulcers there is increased iron availability in wound fluids [220], so a reduction in iron scavenging molecules may be expected, in particular of PVD since this siderophore has been

shown to be strongly downregulated in response to increasing iron supplementation [139]. However, siderophores can have other roles, such as signalling and free radical generation, not related with iron uptake.

Iron-loaded PVD acts as a signal molecule that can trigger the production of two extracellular virulence factors, the protease PrpL/Protease IV and exotoxin A, a potent *P. aeruginosa* toxin [221-224]. PCH has also been shown to cause oxidative damage and inflammation in endothelial cells, and its toxicity has been directly linked to its action as a catalyst in the production of reactive oxygen species (ROS) [225, 226]. PCH also has antibacterial activity against bacteria that do not produce siderophores of the catecholate class (such as PVD) [227]. On the whole, PCH plays an important role in the prolonged inflammatory response typical of chronic infections, such as CF [228] and diabetic ulcers, and its levels are increased in a synthetic CF sputum medium [229]. As such, the levels PCH observed in the majority of the *P. aeruginosa* populations could relate to these activities.

3.3.2 High phenotypic diversity in a population taken from a DLU

With respect to colony morphology on Congo red agar (CRA) plates, five different morphotypes were found among the 40 *P. aeruginosa* isolates taken from a diabetic leg ulcer (DLU) population (Table 8, Figure 25). This high diversity could be explained by the fact that this patient's sample was taken only two months after *P. aeruginosa* infection was detected for the first time; hence, the population may not yet have adapted fully to the wound environment, as observed for DFUs.

The only phenotype analysed where there was low phenotypic diversity for *P. aeruginosa* isolates taken from a DLU, was the production of quorum-sensing signals. Chiefly, most isolates were positive for both molecules tested. Only three isolates (T17, T22, and T36) produced low levels of 3-oxo-C12-HSL, while only one isolate (T17) produced low levels of C4-HSL (Table 9).

Regarding exoprotease production, *P. aeruginosa* isolates from this diabetic leg ulcer were almost equitably distributed between normal, low, or no production (see Table 10). This is similar to the wide range of protease levels quantified in culture supernatants taken from a single CF patient, which ranged from 0.008 µg/ml to 26.5 µg/ml between colonies [230], and with results reported for other *P. aeruginosa* chronic leg ulcers isolates, where varying levels of exoproteases, particularly AprA, were identified [231]. An interesting study found that two short fluorescently-labelled peptide substrates specific for *P. aeruginosa* exoproteases had diagnostic potential for the identification of *P. aeruginosa* in chronic leg ulcers [232].

With respect to pyocyanin (PYO), the DLU isolates showed wide variation (see Table 12), especially when compared to isolates taken from diabetic foot ulcers (and described in the previous section). Korganonkar et al. found that production of pyocyanin by *P. aeruginosa* was intensified after exposure to peptidoglycan fragments from the cell wall of Gram-positive bacteria [233]. According to the hospital records, *S. aureus* was also identified in the ulcer of patient Z, which may explain the high pyocyanin production observed by 11 isolates. Of these, T17 produced as much as 3 times more PYO than the majority of the leg ulcer isolates tested (Table 12). It is possible that the wide range of PYO produced could be the

result of differing abilities of these isolates to detect peptidoglycan [233]. However, note that pyocyanin production has been shown to markedly vary depending on *P. aeruginosa* growth environment [234], so these differences may not be relevant *in vivo*. Note that PYO results together with the decreased production of both C4-HSL and 3-oxo-C12-HSL (Figure 26) in T17, makes this isolate phenotypically very similar to isolates from the Liverpool Epidemic Strain (LES) collection, where the QS system is dysregulated and there is increased pyocyanin production [235]. Furthermore, isolates T11, T17, and T30 that were among the five highest producers of pyocyanin found, all formed red and small colonies with a smooth edge on CRA plates. This specific colony morphotype might be directly linked to high pyocyanin production, since a study using Congo red and Coomassie blue agar found that a *P. aeruginosa* pyocyanin overproducer (DKN370) also formed smooth and compact colonies in contrast to the wrinkled colonies formed by *P. aeruginosa* PA14 strain [236].

Several studies highlight that variation in antibiotic susceptibility can be accounted for by the proximity of inhibition zones to breakpoint values. This was confirmed here as among the 40 isolates taken from this patient, five isolates which had intermediate susceptibility to ciprofloxacin (T10, T16, T17, T20, and T35) had zones of inhibition with average diameters ranging from 21 mm to 22.5 mm (breakpoint for susceptibility: ≥23 mm). The same was observed for meropenem, were T1, T2, and T3 had a zone of inhibition with an average diameter of 19 mm (breakpoint for susceptibility: ≥20 mm) [237].

Finally, from the siderophore production results of patient Z, PVD levels were generally low, with 55% of the isolates having negligible PVD production (Table 11).

This is consistent with research done by [212] in which isolates from CF patients were compared at two time points, 6 months vs 96 months post-infection, and after 96 months the loss of PVD production was observed. This was associated with a reduction in virulence, indicating that while PVD is important in acute infections, this may not be the case in chronic settings [212] including chronic ulcers. Consistent with that found for diabetic foot ulcers, pyochelin (PCH) levels were predominantly average (Table 11 and Figure 29). As mentioned before, *P. aeruginosa* strains that produced both PVD and PCH were less prevalent in an environment akin to chronic infections [139]. Although our results showed that 45% of the isolates still produced both siderophores, this could be because the patient sample was taken only two months after *P. aeruginosa* infection was detected. Hence, the wound environment may not yet have settled into a steady state, as observed for chronic diabetic foot ulcers in the previous section. Nevertheless, our results are in agreement with the observation that PCH becomes the predominant siderophore due to repression sensitivities caused by different iron availabilities in PVD [139], as is the case in chronic wounds where there is a high concentration of iron in comparison to acute ulcers [220]. Moreover, the high concentration of iron also leads to the generation of more free radicals by PCH, which directly contributes to increase tissue inflammation [225]. This might potentiate the appearance of PVD negative strains in chronic ulcers – in common with the results obtained for DFU blood isolates and more generally in DLUs.

It is relevant to point out that only one isolate (CW6 T25) out of the total of 320 *P. aeruginosa* isolates tested from DFUs produced high levels of PCH. In the

population of the DLU patient, 7 isolates were found to produce high levels of PCH, and surprisingly 4 produced very high levels of this siderophore – almost double the amount noted for the remaining isolates from this population. This over production of PCH is isolate specific and independent of PVD production, as observed from the broad variability: T30 had negligible PVD production, T11 and T17 had moderate PVD production, whereas T36 produced very high levels of PVD. Also noteworthy is the fact that isolate T36, which overproduces both PVD and PCH, produced colonies with a distinct spiky edge in CRA plates. Although there hasn't been any mention of this in the literature, the spiky edges may relate to mutations in global regulators that impact on both surface components and iron uptake mechanisms.

3.3.3 Genomic analysis of *P. aeruginosa* chronic wound isolates

By comparing the whole genome sequences (Figures 33 and 34), it is apparent that, in general, the genomes of isolates from different chronic wounds appear to be related. However, they appear to be more closely related if they are grouped by patient comparing the different colours (N.B. patient X has two colours, purple and blue representing isolates from CW4 and CW5 respectively, since this ulcer was sampled twice).

With respect to the virulence-related regions highlighted in Figures 33 and 34 variations between PAO1 and the chronic wound isolates are apparent. For the Hcp secretion islands encoded by T6SS, the genomic region in each isolate is similar to that of PAO1 with only some minor differences in H1, while in the T3SS region no differences between PAO1 and the chronic wound isolates were apparent. For the genes involved with the formation of extracellular matrix polysaccharides, there were

no changes in *alg*, *psl*, and *pel* operons (even though a gene adjacent to *pel* is altered in patients X and Z), while the alginate regulon 2 appears to have differences in isolates from patients X and V. The LPS O-antigen region has very low similarity with PAO1 in all isolates from diabetic foot ulcers (patients V to Y) but is similar when PAO1 and all DLU isolates from patient Z are compared.

This is interesting since lipopolysaccharides (LPS) which are characteristic outer membrane components of Gram-negative bacteria, are potent activators of monocytes and macrophages [238], and of many factors involved in the innate immune response. Specific variations in the LPS structure (O-antigen--core oligosaccharide--lipid A), mainly at the level of the O-antigen but also lipid A, have been shown to vary in response to different host environments, as in pathogenic or symbiotic interactions (reviewed in [239]). The differences in the LPS O-antigen regions that were found between DFU and DLU suggest that *P. aeruginosa* colonisation success in different types of ulcer may be dependent in part on the type of LPS produced by the infecting strain or the amount produced and/or shed. In a study comparing wound fluids from non-healing chronic wounds with an acute wound showing normal healing, low LPS levels (~ 8.7 ng/mL) were found in the diabetic foot ulcers but very high LPS levels (~ 121 ng/mL) in the venous leg ulcers [240].

Analysing the regions associated with motility genes, the only difference between the chronic wound isolates and PAO1 is in the flagella 1 region. This region, particularly between PA1088 and PA1092, has very low similarity to PAO1 in all DFU isolates, while in all those from the leg ulcer, these genes are the same as in PAO1.

PA1088 through PA1091 are not associated with virulence, and are classed as hypothetical proteins on Pseudomonas.com, with the exception of PA1091 which codes FgtA, a flagellar glycosyl transferase. Even though not fully characterised yet, genes PA1088 to PA1090 were associated with post-translational glycosylation of the type-b flagellin of PAO1 [241].

P. aeruginosa can be classified into flagellin a- and b-types depending on the protein encoded by the *fliC* gene (PA1092). The primary structure of a-type and b-type flagellins differs by 35% (predominantly in the central domain), although they fold into similar structures during polymerization of the flagellum (reviewed in [242]). The fact that PAO1 produces type-b flagellin raises the question of whether the difference between foot and leg isolates in this region could be explained by a difference in the flagellin type. To answer this, all chronic wound genomes, PAO1, and PAK, a *P. aeruginosa* strain identified as producing type-a flagellin, were blasted against the PAO1 *fliC* nucleotide sequence taken from Pseudomonas.com database. As a result, all isolates from diabetic foot ulcers could be identified as type-a flagellin (like PAK), and all isolates from the diabetic leg ulcer as type-b flagellin (like PAO1). Genes PA1088 to PA1090 were also identical between the diabetic foot ulcer isolates and PAK, which is expected as they were associated with specific glycosylation of the type-a flagellin [243, 244]. Since flagellin was also identified as a potent stimulator of the inflammatory response via Toll-like receptor 5 [245, 246], the differences between flagellin types may be relevant in a chronic wound scenario.

Regarding pf1 phage region there is high variability between all chronic wound isolates, and in pyocin-related regions, S2 is also very variable. However,

pyocins S4 and S5 appear not to be present in any chronic wound isolate, while the region associated with R and F type pyocins is variable to different extents only in isolates from diabetic foot ulcers. PAO1 R- and F-pyocins are similar to the lambda and P2 phage families [247], but do not appear to have been associated with differences between foot and leg ulcers. The only mention of *P. aeruginosa* pyocins and ulcers in the literature is related to the typing of *P. aeruginosa* strains via their pyocin sensitivities (for example in [248]).

With respect to the regions R1 to R8 (Figures 33 and 34) that highlight zones with less than 75% identity (that appear as blank spaces in each ring), these mostly contain hypothetical proteins, and the majority are likely to be involved with mobile elements such as bacteriophages, transposons and insertion sequences. In particular, R1 is only present in patients V and W, and R3 in patients V and Y, while R2 and R7 are not present in all genomes studied, even though not all of R7 genes (only described as hypothetical proteins) are absent from CW2 isolates. R4, R5, R6 and R8 have in general low similarity between all chronic wound isolates and PAO1, however there is a region at the end of R5 that is present in isolates from DLU patient Z, but absent in all isolates from diabetic foot ulcers. This specific region from genes PA2224 to PA2228 encodes mostly hypothetical proteins with the exception of *qsrO* (PA2226) and *vqsM* (PA2227) that are part of an operon starting with PA2228. VqsM was identified as a virulence and QS modulator [249] that acts upon VqsR, a major virulence regulator within the quorum-sensing network [250]. However, the authors that subsequently identified *qsrO* (QS repressor open reading frame) suggest that VqsM is unlikely to be involved in QS-regulation, since that role is specific for QsrO,

and that this protein alone is capable of down-regulating all three QS-systems in *P. aeruginosa* [251]. Either way, this entire operon (or one of the genes in the operon) appears to influence QS negatively, but the relevance of the lack of these genes in diabetic foot ulcers remains to be explained.

As for the remaining regions, which are related to phenotypes studied in section 2.3, the *phz1* and *phz2* operons that code for genes required for pyocyanin biosynthesis show only slight differences across all genomes as does the *pch* operon responsible for the production of pyochelin (PCH). The region involved with pyoverdine (PVD) production however, shows very low similarities across all genomes. In fact, the PVD locus has been described as the most divergent region in the *P. aeruginosa* core genome [252]. In particular, the pyoverdine outer membrane receptor *fvpA* showed substantial intra-type variation, was found to be under positive selection, and the most divergent alignable gene in the region [253].

PVD consists of three different moieties (reviewed in detail by [254]): the dihydroxyquinoline chromophore (conserved among all pseudomonads) that binds Fe^{3+} and is responsible for the fluorescence of this molecule, the peptide chain (linked to the chromophore and composed of 6 to 14 aa in linear or cyclic conformation) that interacts with Fe^{3+} and allows receptor recognition, and the dicarboxylic (acyl) side-chain (whose residue is dependent on the strain and / or growth conditions) that does not contribute to iron chelation nor iron transport. *P. aeruginosa* can be divided into three siderovars each characterised by the production of a specific PVD peptidic chain (type I, II, III), and strains show the same *fpvA* receptor type as the corresponding PVD type [255-258]. There is however high variability in *fpvA* II, with at least two

subgroups (*fpvA* IIb and *fpvA* IIa) named so far [259]. Moreover, a second receptor specific for type I PVD, FpvB has been identified, which is also present in type II and III strains [260].

Since the PVD locus shows such variability, the siderovars of the sequenced chronic wound isolates were identified *in silico* using the PVD receptor genes. All chronic wound genomes were blasted against representative *fpvA* strains (nucleotide sequences were taken from the NCBI submissions associated with [259]). As a result, CW6 and CW2 isolates could be assigned to PVD type I in common with PAO1 and PA14, while CW4, CW5, and CW3 isolates could assigned to PVD type IIa in common with PACS2. On the other hand, CW7 isolates were PVD type III in common with LES strains, and all isolates had *fpvB*. These results are in agreement with a siderotyping study that found the same proportion of each PVD type in clinical strains, while type I was over-represented in environmental strains [259]. However, from our results we can conclude that PVD type does not associate with PVD production since, for instance, all CW7 isolates were type III, but their PVD production in SWF varied between negligible (–) for T1 and T13, low (±) for T3, moderate (+) for T11 and T17, and very high (+++) for T36 (Table 11). However, PVD production is likely to vary with the growth conditions used and this requires further investigation.

With respect to QS-related genomic regions, significant differences between PAO1 and the chronic wound isolates were only found in the *las* operon, where patient X isolates share a substantial deletion that includes *lasR, lasI* and *rsaL*, represented by a white line common in purple and blue isolates in Figure 33. From the phenotypic results, all patient X isolates were suspected of being *las* mutants due

to lack of 3-oxo-C12-HSL. After the genomic analysis of the operons for the three quorum-sensing systems, isolates from patient X were confirmed as *las* mutants since they do not have *lasR*, *rsaI* or *lasI* (Table 18, Figure 35). Concerning the other mutations identified in these regions, it can be said that non-synonymous substitutions had in general lower frequencies (Tables 18 to 21). Since the mutations identified in the anthranilate synthase *phnA*/*B* genes for CW4/CW5 isolates cannot alone explain the lack of AQ production in these isolates, further investigation will be described in Chapter 4 given that multiple biochemical pathways are able to generate the AQ precursor anthranilate. However, the mutations identified in PqsA and PqsR (Table 20) were probably enough to stop the production of AQ in *P. aeruginosa* isolated from patient X (CW4/CW5).

With respect to the phylogeny results, there is no strain type (such as environmental or CF-like) that infects diabetic ulcers preferentially. However, isolates found in the leg ulcer (CW7) are markedly distinct from all of the other isolates found in diabetic foot ulcers. Moreover, strain type does not correlate with the duration of the ulcer. Within DFUs, CW6 isolates were closer to a hyper virulent CF strain, while CW2 isolates resembled a *P. aeruginosa* that caused an ear infection (Figure 37). CW3 isolates were closer to an environmental *P. aeruginosa* isolated from the rhizosphere, whereas all patient X isolates were closer to another adult CF isolate. Note that being phylogenetically close does not mean that the *P. aeruginosa* infecting a given ulcer originated from that particular *P. aeruginosa* strain – in fact, even BWH035 and both CW2 isolates, that were very close phylogenetically, have more than 3000 SNPs between them.

Isolates from patient X can be grouped into 2 lineages that match the profile 1/ profile 2 phenotypes reported in section 3.2.1 In Figure 37, isolates that display profile 1 (CW4 T1, CW4 T40, CW5 T1, CW5 T40, and CW5 B1) are highlighted in purple, while isolates that display profile 2 (CW5 T2, CW5 T34, and CW5 S1) are highlighted in blue. However, these isolates do not have any differentiating mutations in the QS genes analysed. Their genetic differences will be explored in greater detail in Chapter 4, but these data suggest that both CW5 profiles belong to the same strain.

In the previous sections it was suggested that the phenotypic differences found in patients X and Y could be explained either by the presence of two distinct *P. aeruginosa* strains in their ulcers (as the result of a *de novo* infection with a nosocomial or environmental drug-resistant strain) or by the infection of a single *P. aeruginosa* strain that shows phenotypic diversity, with a low number of SNPs shared between isolates. From the genomic results presented in Figure 37, it is clear that there is only one *P. aeruginosa* strain per patient. Moreover, the GC content and genome size (Table 17) also support this claim, since they vary only slightly in isolates from the same CW, and so are specific for each patient: patient V isolates have GC content of 66.1 % and a genome size of about 6.9 Mbp, patient W isolates 66.2 % and 6.65 Mbp, patient X isolates 66.4 % and 6.45 Mbp, patient Y 66.0 % and 6.84 Mbp, and patient Z 66.4 % and 6.3 Mbp.

3.4 Conclusions

Globally, the marked phenotypic variation found within *P. aeruginosa* isolates in a single population taken from the diabetic leg ulcer, sharply contrasts with the very low levels of phenotypic diversity found in diabetic foot ulcers. This high variability may translate into a higher pathogenic level, in the sense that the most virulent isolates may possibly become dominant as time goes by. In this scenario, an early anti-pseudomonal treatment could undoubtedly help in managing the infection; however, it could also drive the evolution of the population, and shape it to allow better adaptation to the chronic wound environment over time.

The genomic analysis presented supports the hypothesis that isolates from diabetic foot ulcers as a group are genetically different from diabetic leg ulcer isolates (even though only one DLU population was analysed). Thus, it is reasonable to expect less phenotypic diversity within them, and that a type-specific adaptation to different chronic ulcers might depend on specific pathophysiological factors of the ulcer environment that give a competitive advantage only to specific types of *P. aeruginosa*. Where possible, we associated the phenotypic data of the different populations with specific mutations (Table 22).

Moreover, it is apparent that *P. aeruginosa* colonisation in a diabetic chronic wound is via a single strain per ulcer, and potentially per patient, even though some sample-specific phenotypic profiles can arise from a homogenous population, as happened in the case of patient X.

Table 22: Summary table associating phenotypic with genotypic data

Phenotypes	Description
Colony morphology in Congo red agar	No changes in *alg*, *psl*, and *pel* operons Alginate regulon 2 shows differences in patient V (CW2) and patient X (CW4/5) but this should not affect phenotype No mutations found in *wspF*
Siderophore production	**PCH**: region with small differences only in patient W (CW6) **PVD**: CW have different PVD types (I, IIa, and III) but these do not correlate with PVD production; all have *fpvB*
Pyocyanin production	*phz1* and *phz2* show small differences not analysed in detail
Total exoproteases	No mutations identified that can explain why CW6 T25 produces exoproteases while all other CW6 isolates do not
Quorum-sensing signals	CW4/5 isolates from patient X lost the entire *las* region which explains why they are 3-oxo-C12-HSL negative, and SNPs present in *pqsA* and *pqsR* may explain lack of AQ production
Motility	DFU isolates (CW2-CW6) have type-a flagellin DLU isolates (CW7) have type-b flagellin (like PAO1)

Chapter 4: Rise of a Blood-invasive *P. aeruginosa* Isolate in a Patient with a Chronic Diabetic Foot Ulcer

4.1 Introduction & Objectives

In Chapter 3 questions were raised with respect to the impact of the phenotypic differences identified in *P. aeruginosa* chronic foot ulcer isolates from patient X on wound healing and infection. Since the differences observed may be associated with the deterioration in the patient's health, it was important to determine whether they impact on antibiotic resistance and virulence in order to understand why antibiotic treatment failed and the patient's foot required amputation.

Much research has been devoted to understanding the specific contributions of virulence determinants produced by pathogenic bacteria to different diseases. As discussed in Chapter 3, *P. aeruginosa* is undoubtedly one of the key organisms to consider due to its ability to thrive in a wide range of external environments and hosts, but also because of its relevance for nosocomial infections, and its intrinsic antibiotic resistance [261, 262].

P. aeruginosa adaptive responses have been linked to the deployment of a large number of two-component systems reviewed in detail by [263], comprising of a sensor kinase, and a response regulator, that allow this bacterium to sense and adapt to its environment [181, 264]. Sophisticated global regulatory networks, such as QS, are essential for this process in order to coordinate production of a plethora

of virulence factors and antibiotic resistance determinants essential for adaptation to different host compartments, including chronic wounds [265-267].

Motility in *P. aeruginosa* has been associated with increased invasiveness in several infection models [268-271] and is divided into three main modes: swimming, swarming, and twitching. When in planktonic culture, *P. aeruginosa* locomotion is mostly governed by a single polar flagellum, whose structure and relevance for adhesion and virulence has been reviewed by [272]. The complex protein export through the bacterial flagellar type III export pathway has been reviewed by several authors [273, 274]. However, once the bacteria have attached themselves to a surface, they move mainly via twitching motility, which is dependent on type-IV pili [275], or via swarming motility that involves flagella, pili and surfactant rhamnolipids [276], and is dependent on a functioning cell-to-cell communication system, since this is mostly the result of a collective behaviour [277, 278].

Iron is an essential microbial nutrient and the ability to acquire iron *in vivo* is required for the establishment of bacterial and fungal infections [279, 280] and the development of infection [281]. In iron-restricted environments, *P. aeruginosa* produces two iron-chelating siderophores, pyoverdine (PVD) and pyochelin (PCH) [282] that are metabolically costly to produce, such that their biosynthesis and export are tightly regulated to avoid imposing a heavy burden on the producer bacteria [223]. PVD and PCH iron acquisition systems function slightly differently, as reviewed by [283, 284], and *P. aeruginosa* uses additional pathways to acquire iron depending on the nature of the infection site [282, 285] (Figure 38). Furthermore, different iron sources can affect the expression of *P. aeruginosa* virulence traits in different ways

(reviewed in detail in [286]), and multiple pathways of iron acquisition have been suggested to be relevant during *P. aeruginosa* chronic infection in the CF lungs [287, 288].

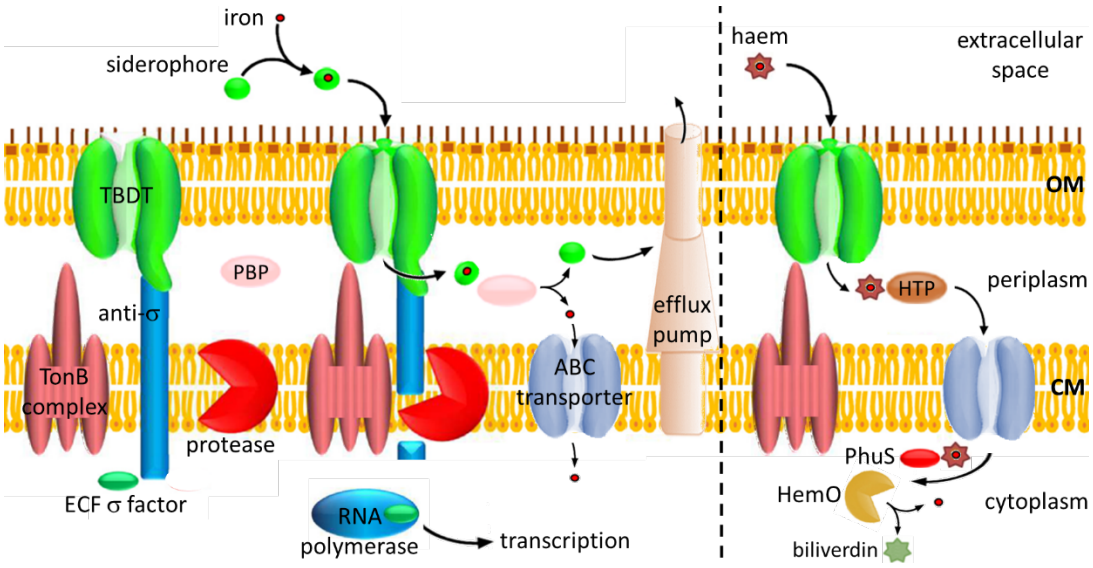


Figure 38: Siderophore and haem iron uptake systems in *P. aeruginosa*. TBDT – TonB-dependent transporter (includes receptors and transducers); anti-σ – sigma factor regulator; TonB complex – energy-transducing complex formed by TonB1, ExbB and ExbD; ECF σ factor – extra cytoplasmic function sigma factor; PBP – periplasm binding protein; ABC transporter – ATP-binding cassette transporter; HTP – haem transport protein; PhuS and HemO – haem oxygenase proteins; OM – outer membrane; CM – cytoplasmic membrane. Left of dashes: siderophore-mediated iron acquisition involves cell-surface signalling systems that directly regulate transcription through the activation of alternative sigma factors. Right of dashes: general view of the haem uptake systems.

In the PVD-mediated iron acquisition system (left side Figure 38), previously exported apo-PVD chelates extracellular ferric ions forming the ferripyoverdine complex. This is then recognised and transported by the TonB-dependent transporter (TBDT) FpvA. A conformational change in FpvA triggers a proteolytic cascade that degrades the anti-σ regulator FpvR, releasing the extra cytoplasmic sigma factors (ECF σ factors) FpvI and PvdS. In the periplasm, iron is released from PVD by a recently described mechanism that involves a reduction step where FpvG, an inner membrane

protein, acts as a reductase, and the periplasmic binding protein (PBP) FpvC acts as an iron acceptor [289]. The free iron is guided by FpvF, another PBP, and transported into the cytoplasm by the ATP-binding cassette (ABC) transporter FpvDE, while apo-pyoverdine is recycled and exported via the efflux pump PvdRT-OpmQ. In the cytoplasm, the released FpvI and PvdS, readily associate with RNA polymerase to drive transcription of the receptor (*fpvA*), and PVD biosynthesis genes, respectively, activating an auto-induction pathway [224, 290-292]. A recent study has suggested that for PvdS to be fully active, it needs to be transcribed *de novo* after FpvR degradation [293]. PvdS also controls the transcription of virulence genes such as exotoxin A and the extracellular protease PrpL/Protease IV [223, 294].

Iron is not, however, readily available *in vivo*, since host iron transport proteins such as transferrin and lactoferrin contribute to host defences by withholding iron from invading pathogens so preventing their growth *in vivo* [295]. To counteract/circumvent this, as well as acquiring iron from transferrin via PVD, *P. aeruginosa* can also utilize iron from haem proteins such as haemoglobin in two well characterized systems: the *P*seudomonas haem uptake (Phu) and the haem assimilation system (Has) [296]. In the *phu* system (right side Figure 38) haem binds directly to the TBDT PhuR and is then transported to the periplasm. There haem is bound to PhuT, a soluble haem-transport protein (HTP), which interacts with an ABC transporter (PhuUV) that translocates it to the cytoplasm. Alternatively, in the *has* system, haem is extracted by the haemophore HasA and transported into the cell by the TBDT HasR. Once in the cytoplasm, the combined action of PhuS (which was previously considered only a chaperone protein that specifically transfers haem) and

HemO, a haem oxygenase, leads to efficient haem breakdown with the release of biliverdin, CO and Fe^{2+} [297]. Note that the main role of the *has* system has been suggested to be the sensing of extracellular haem via an anti-σ factor (HasS)/ ECF σ factor (HasI) pair that interacts with HasR in a similar manner to that presented for PVD (FpvA-FpvR-FpvI) [298]. Furthermore, there is another TBDT, HxuC (PA1302) that participates in a putative haem uptake/sensing system, together with the ECF σ factor (PA1300) and putative anti-σ factor (PA1301) [299].

The involvement of these tree types of molecules (TBDT, anti-σ, and ECF σ factors) is also a requirement in the majority of cell-surface signalling (CSS) systems used by Gram-negative bacteria. *P. aeruginosa* can use these sophisticated regulatory systems to sense signals (such as lack of iron availability or presence of an antibiotics) from outside the cell, and transmit them into the cytoplasm, activating a myriad of processes facilitating stress responses, iron transport and pathogenicity (reviewed in detail by [300]).

P. aeruginosa employs almost all mechanisms of antimicrobial resistance known [301], and these can be specific for a drug class or affect many different classes of antibiotics [302-304]. Specific mechanisms include the direct alteration of the target proteins, which can either be enzymes essential for bacterial DNA replication (such as topoisomerase IV and gyrase), outer membrane uptake channels by which the antibiotics enter the cells (such as OprD, which mediates influx of carbapenems), and efflux pumps that prevent accumulation of antibiotics inside the cell [305]. Also important are the regulatory systems responsible for key biochemical pathways, such

as those that regulate the production of the chromosomally encoded and inducible β-lactamase (Figure 39). Mutations in repressors like *ampD* or *ampR* allow the bacterium to overproduce β-lactamase, an enzyme coded by *ampC* that degrades β-lactam rings, effectively inactivating penicillin-like antibiotics [306, 307].

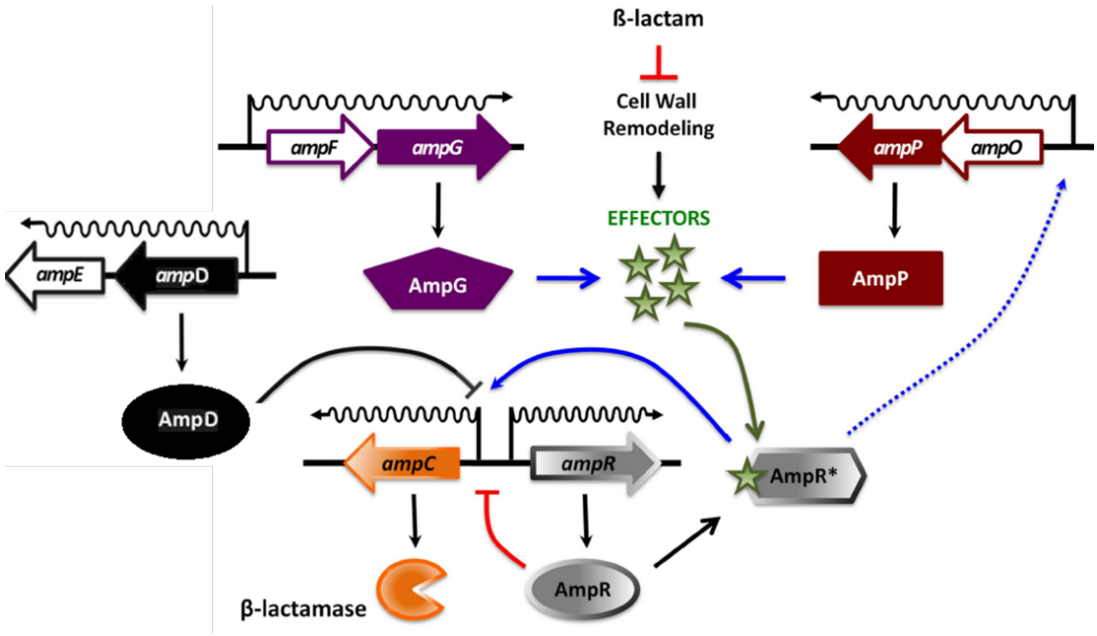


Figure 39: Model for regulation of AmpC β-lactamase induction in *P. aeruginosa*. *In vitro* studies suggest that the transcriptional regulator AmpR can act as either a repressor or an activator for β-lactamase expression, depending upon the presence of different peptidoglycan remodelling intermediates (adapted from [308]). Note that AmpR is a major pathogenesis regulator, and is involved with the acute to chronic infections switch in *P. aeruginosa* (reviewed in detail by [306]).

General resistance mechanisms include efflux pumps than can export either exogenous toxic compounds such as antimicrobials [303], or endogenous metabolites such as anthranilate [309], siderophores, pyocyanin, and QS signal molecules. There are five major families of efflux transporters: the resistance-nodulation-division (RND) family, the small multidrug resistance (SMR) family, the major facilitator superfamily (MFS), the multidrug and toxic compound extrusion (MATE) family and the adenosine triphosphate (ATP)-binding cassette – reviewed in detail in [305].

The members of the RND family are unique to Gram-negative bacteria, and the most significant contributors to antimicrobial resistance (AMR) in *P. aeruginosa*. MexAB-OprM and MexXY-OprM are the most studied since they have a major role in *P. aeruginosa* intrinsic AMR [310]. Other relevant RND pumps include MexCD-OprJ, MexEF-OprN which is involved in the transport of AQs [311], and MexGHI-OpmD that impacts on virulence in *P. aeruginosa* and is QS regulated [309].

Moreover, MexAB-OprM is constitutively expressed and rapid emergence of mutants in these genes has been observed even with no antibiotic challenge [312], which denotes its importance for other factors, such has in the efflux of 3-oxo-C12-HSL [313, 314]. Its expression profile is different from MexXY-OprM since MexXY is produced in response to antimicrobial agents that target the ribosome [315, 316], and regulates aminoglycoside resistance [317]. The genes in these operons are tightly regulated by repressors that do not allow transcription in the absence of antibiotics, but when antibiotics are present, are deactivated by anti-repressors (see details for MexAB-OprM repressor (MexR)/anti-repressor (ArmR) in [318], and for MexXY repressor (MexZ)/ anti-repressor (ArmZ) in [319]).

This chapter will describe experiments designed to determine how the septicaemia-causing isolates evolved from the *P. aeruginosa* clones already present in patient X's DFU by investigating genotypic and phenotypic diversity at two time points. In particular, the differences between profiles 1 and 2 observed for the *P. aeruginosa* isolates obtained from patient X (Chapter 3) will be explored as a function of their ability to enter the blood stream and cause septicaemia. Following presentation of the patient case study, a comparison between the phenotypes of the

first (CW4) and the later time points (CW5) will be highlighted, and a detailed genomic analysis between isolates displaying phenotypic profiles 1 and 2 will be described, including a full characterisation of the single nucleotide polymorphisms (SNPs) alongside a comparison of their transcriptomes using RNAseq.

4.2 Results

4.2.1 Patient medical history

Presentation for patient X: a 58 year-old male with a medical history of type-II diabetes, reduced sensation in the lower limbs and poor blood supply due to peripheral neuropathy and ischaemia, and impaired immune response, with a chronic heel ulcer which had steadily deteriorated despite treatment. Initially the wound was non-healing but stable (i.e. there were no clinical signs of infection) and eventually resulted in a local infection where the *P. aeruginosa* species present developed antibiotic resistance over time. The patient was allergic to penicillins so he was first treated with ciprofloxacin.

As shown in Figure 40, *P. aeruginosa* was first sampled two years after the appearance of the ulcer. As described in Chapter 1, an ulcer does not become immediately infected (see Figure 13), so in this case contamination with *P. aeruginosa* probably occurred very early, and only after the bacteria had colonised the surface of the ulcer, did deeper penetration into the tissue develop, provoking a localised infection that was diagnosed. One of the challenges in the treatment of chronic non-healing ulcers is to avoid this change from contamination to colonisation as well as

preventing colonising bacteria from triggering the formation of biofilms that lead to infection.

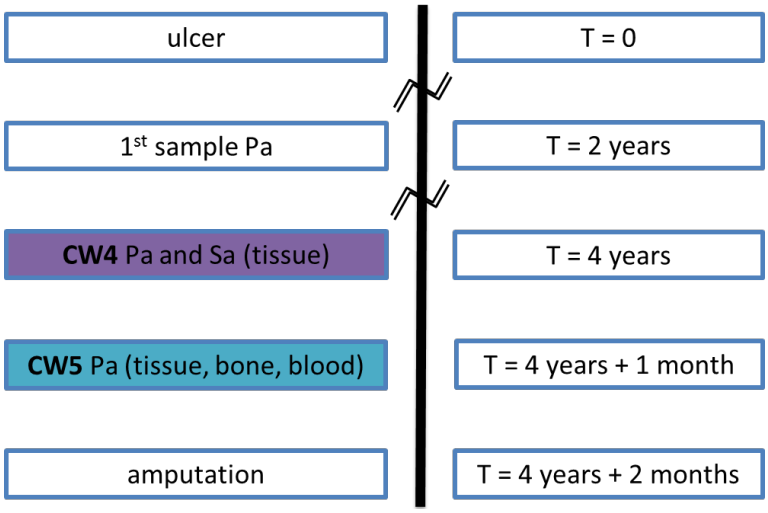


Figure 40: Timeline of hospital visits for patient X. Filled boxes indicate sampling times of each chronic wound (CW) biopsy with description of the type of sample collected; Pa – *P. aeruginosa*; Sa – *S. aureus*.

After *P. aeruginosa* was first detected in the ulcer (T = 2 years), anti-pseudomonal treatment was administered. As no samples from this time point were available, the antibiotics administered in the patient may have exerted a strong negative selective pressure that affected the bacterial population. What is clear is that the *P. aeruginosa* community adopted a state where a single phenotype that is highly adapted to the chronic wound environment was present (see Chapter 2).

At T= 4 years (time point CW4) the patient presented to the hospital. The ulcer was noted to be sloughing and deep, but not exposing bone. The wound was debrided as much as possible to remove necrotic and infected tissue. A tissue biopsy was taken and sent for microbiological analysis. By culturing in different selective media, *P. aeruginosa*, methicillin-resistant *S. aureus* (MRSA), group B *Streptococcus, Enterococcus*, diphtheroids, and *E. coli* with different antibiotic susceptibilities were

identified. Notably, both *P. aeruginosa* and MRSA strains were resistant to ciprofloxacin.

The patient remained unwell despite the initial debridement and antibiotic therapy. Osteomyelitis was diagnosed with X-rays and soon after blood cultures revealed *P. aeruginosa* bacteraemia (i.e., presence of bacteria in the bloodstream). Consequently, the patient received surgery at T = 4 years + 1 month (time point CW5) to remove infected bone. Bacteraemia is uncommon in patients with diabetic foot osteomyelitis and indicates an established, deep infection. During surgery biopsies from bone and tissue were taken. Post-operatively, the patient's antibiotic regimen was adjusted to daptomycin, gentamicin and metronidazole following confirmation that *S. aureus* was absent from the new cultures.

After the surgery, the patient's health condition deteriorated further despite additional wound debridement and the change in antibiotic therapy. The patient suffered sepsis (an inflammatory response to bacteraemia) and the infection failed to resolve. Further rapid deterioration resulted in a decision to amputate the affected leg below the knee (T= 4 years + 2 months). After surgery, intravenous antibiotics were administered, the sepsis and bacteraemia resolved and the patient slowly recovered.

4.2.2 Overview of the phenotypic analysis

The results of the phenotypic analysis (colony morphology on CRA, siderophore and pyocyanin production, total exoproteases quantification, and AHL

detection) and of the antibiotic resistance profiles for all 160 *P. aeruginosa* isolates from patient X (as detailed in Chapter 3) are summarised in Table 23.

Table 23: Summary of the phenotypic assays of *P. aeruginosa* CW4 and CW5 isolates sampled from the diabetic foot ulcer of patient X at two different time points.

Sample	Morphology CRA		Siderophores		PYO	TP	QS signals		BSAC
	Colour	Shape	PVD	PCH			C4	C12	
CW4 T	orange	smooth	±	±	–	–	+	–	CIP
CW5 (1)	orange	smooth	±	±	–	–	+	–	CIP
CW5 (2)	red	wrinkly	–	±	–	–	+	–	CIP, TZP

CW5 (1): phenotypic profile 1 (bone isolates), CW5 (2): phenotypic profile 2 (blood isolates), CRA: Congo Red Agar, PVD: pyoverdine, PCH: pyochelin, PYO: pyocyanin, TP: total exoproteases, QS: quorum-sensing, C4: C4-HSL, C12: 3-oxo-C12-HSL, BSAC: antibiotic resistance assay through BSAC method. For siderophores and pyocyanin: – negligible, ± low. For proteases and QS signals: + production, – no production. For antibiotic resistance, acronyms represent the antibiotics to which bacteria showed resistance: CIP, Ciprofloxacin and TZP, Piperacillin-tazobactam.

As described in Chapter 3, it was possible to divide the chronic wound isolates into two distinct phenotypic profiles either by their morphology on CRA or by siderophore quantification (Figures 41 and 42). Profile 1 includes all 40 isolates from tissue CW4, all 40 isolates from bone CW5, and 24 isolates from tissue CW5 (isolates 1, 5, 10-12, 18, 20-30, 32, and 35-40). Isolates are orange and smooth on CRA and produce low levels of PVD and PCH (between 20k and 30k RFU/OD_{600}). Profile 2 includes all 40 isolates from blood CW5 and 16 isolates from tissue CW5 (isolates 2-4, 6-9, 13-17, 19, 31, 33, and 34). Isolates are bright red and wrinkly on CRA and produce negligible amounts of PVD and low levels of PCH.

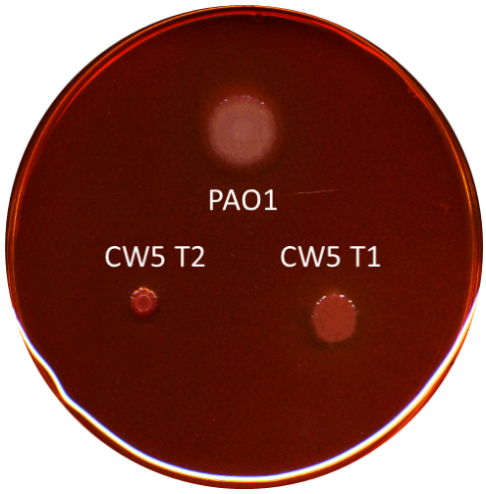


Figure 41: Colony morphology of patient X *P. aeruginosa* morphotypes on Congo Red Agar plate. Top: PAO1 used as control, bottom: CW5 T1 corresponds to phenotypic profile 1 isolates while CW5 T2 corresponds to profile 2 isolates.

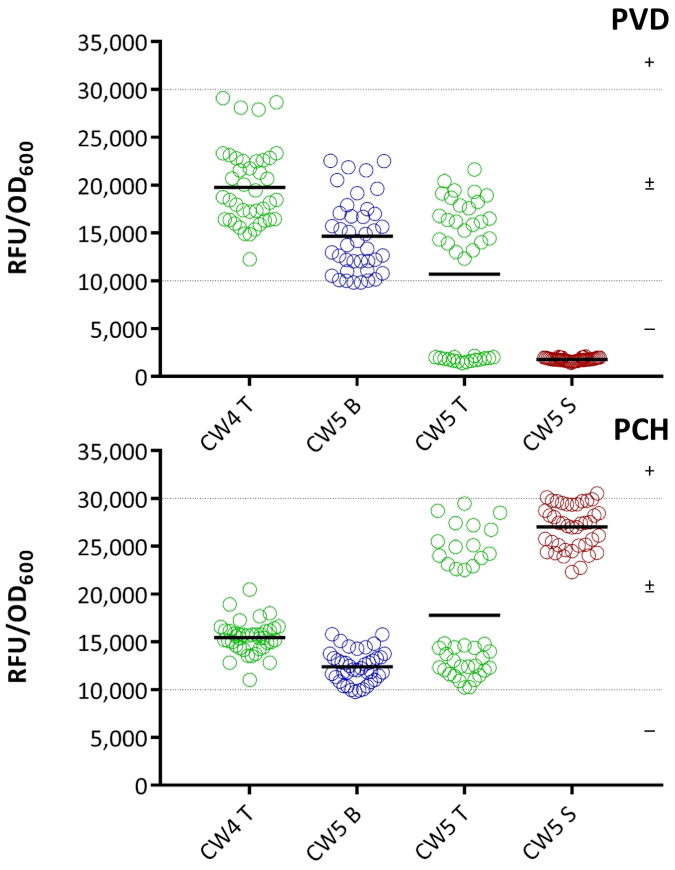


Figure 42: Pyoverdine (PVD) and pyochelin (PCH) production by all *P. aeruginosa* isolates from patient X. Type of sample: T - tissue (green), B - bone (blue), and S - blood (red). Faint lines and signs on the right represent RFU/OD_{600} categories of Figure 28, namely: -, 0 to 10k; ±, 10k to 30k; and +, 30k to 50k. CW5 T has two distinct groups that correspond to profile 1 isolates (like CW5 B), and profile 2 isolates (like CW5 S).

In Figure 43 an example of the BSAC antibiotic susceptibility assay is shown for two representative isolates of patient X (in this chapter either CW5 T1 or CW5 B1 are used as representatives of phenotypic profile 1, while CW5 T2 or CW5 S are used as representatives of phenotypic profile 2). Profile 2 isolates, which mainly consist of *P. aeruginosa* isolated from the bloodstream, show a higher degree of antibiotic susceptibility than isolates with profile 1 from tissue and bone. Also, as with CW4 isolates, both CW5 isolates are fully resistant to ciprofloxacin since the area around the CIP disk shows normal bacterial growth.

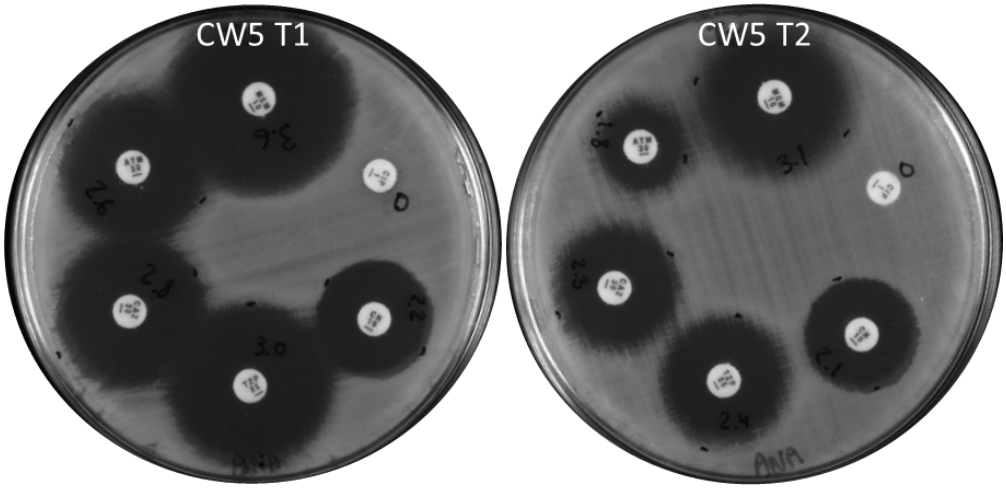


Figure 43: Antibiotic susceptibility assay in 2 chronic wound isolates from patient X. Clockwise from the top: MEM, Meropenem; CIP, Ciprofloxacin; CN, Gentamicin; TZP, Piperacillin-tazobactam; CAZ, Ceftazidime; and ATM, Aztreonam. CW5 T1 (left) corresponds to phenotypic profile 1 isolates while CW5 T2 (right) corresponds to phenotypic profile 2 isolates (CW5 T1). Both isolate are 100% resistant to CIP, and comparative to CW5 T1, CW5 T2 shows increased resistance to all antibiotics tested, as revealed by the smaller inhibition zones.

As the genomic analysis presented in Chapter 3 for patient X isolates did not reveal mutations in the *pqs* operon specific to either the bone or the blood isolates, production of AQs was expected to be the same for CW4/CW5 isolates (Figure 44).

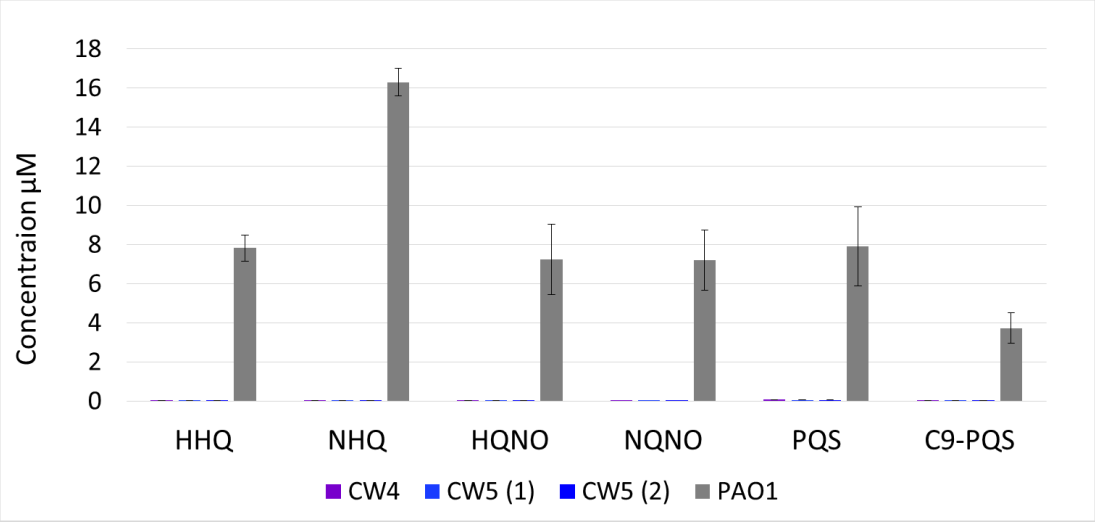


Figure 44: Quantification of AQs produced by clinical strains of *P. aeruginosa* from patient X, and the lab strain PAO1. Note that AQ concentrations below 0.1 µM are unlikely to have biological activity, and consequently AQ production by CW4 and CW5 is deemed negligible**.**

4.2.3 Genome analysis

8 samples were sequenced from patient X: A (CW4T1) and B (CW4T40) considered to be of the ancestral phenotype because they were sampled a month earlier than the other isolates, profile 1: C (CW5B1), D (CW5T1), and G (CW5T40), and profile 2: E (CW5T2), F (CW5T34), and H (CW5S1) – see Table 6 in methods section 2.9 for full description. Genome assemblies were used to construct a whole genome sequence diagram comparing the patient X isolates with PAO1 using BRIG (Figure 45).

Variations in the virulence-regions highlighted have already been discussed in detail in section 3.3.3. From this new analysis, it is clear that there are no specific regions of low identity present in phenotype 2 isolates (light blue) as noted by the lack of a white line only covering the 3 genomes in the middle. This could mean that there are no mutations between phenotypes 1 and 2. However, that seemed very

unlikely and so a more detailed analysis was done since BRIG does not have sufficient resolution to identify SNPs.

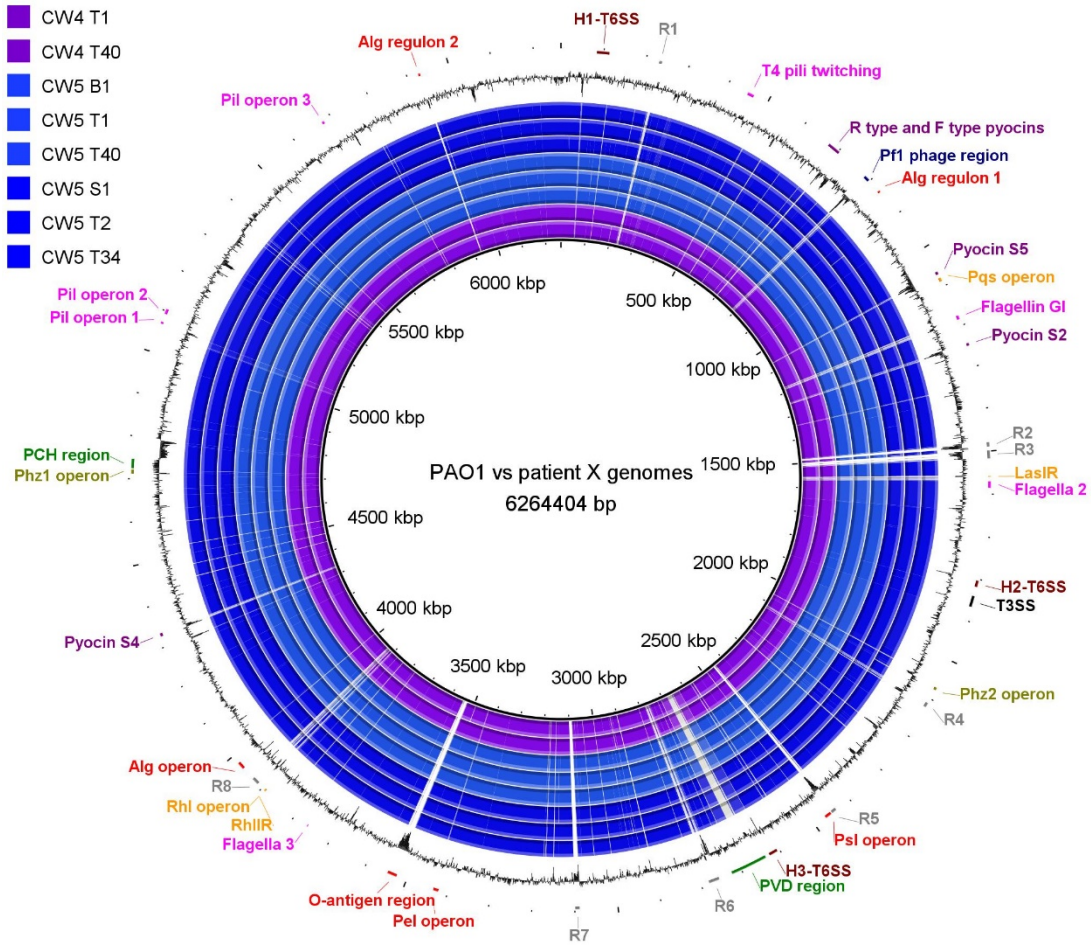


Figure 45: Whole genome sequence comparison of *P. aeruginosa* chronic wound isolates from patient X with PAO1. From inside out, this circular map shows the PAO1 reference (thin black line), two CW4 isolates (purple), CW5 profile 1 (light blue; 3 isolates), CW5 profile 2 (dark blue; 3 isolates), and the outer ring shows PAO1 G+C content. Ring shades denote different levels of nucleotide identity from PAO1 according to BLASTn, ranging from 75% (lightest) to 100% (darkest). Matches with less than 75% identity, or regions with no BLAST matches, appear as blank spaces in each ring. Low-identity regions common to most genomes are identified by grey arcs (R1 to R8) and mostly contain hypothetical proteins – see Appendix B. Virulence-associated regions are identified by colour-coded arcs: brown (Hcp secretion islands 1, 2 and 3 encoded by T6SS), pink (motility genes – type IV pili, flagellin genomic island, and flagellar operons), dark blue (phage regions), red (extracellular matrix polysaccharides – alginate, Pel, Psl operons and LPS O-antigen region), purple (pyocin regions), orange (quorum-sensing genes – *las*, *rhl,* and *pqs* operons), and black (genes involved with T3SS). Diagram generated using BRIG [153].

4.2.3.1 Mutations common to all patient X genomes

Gene sequences were compared as described in the methods section 2.9 to identify mutations in some genes associated with ciprofloxacin resistance (*gyr*) and anthranilate synthesis (*trp* and *kyn*) (Table 24) since this metabolite is an essential AQ precursor, and as seen in Figure 44, patient X isolates do not produce AQs.

Table 24: List of amino acid substitutions in genes of the *gyr*, *trp* and *kyn* pathways.

Gene	Mutation	PAO1 aa	CW4/CW5 aa	Impact
gyrA	p.T83I	Threonine	Isoleucine	**-3.720**
gyrB	-	-	-	n.a.
trpE	p.V83M	Valine	Methionine	0.367
trpG	p.D111N p.V143I	Aspartate Valine	Asparagine Isoleucine	0.530 -0.029
kynA	-	-	-	n.a.
kynB	p.N16S p.P67S	Asparagine Proline	Serine Serine	1.242 -1.384
kynU	-	-	-	n.a.

Data obtained through PATRIC BLAST service using BLASTn against the patient X genomes (Table 6). Mutations identified were present in all CW4/CW5 genomes; p.X*n*Z indicates a substitution on protein position *n* where amino acid (aa) X was replaced by amino acid Z; Impact was calculated with PROVEAN and values in bold correspond to a predicted deleterious impact on the biological function of each protein; **-** indicates no mutations, i.e. gene has the same sequence as PAO1; n.a. indicates not applicable.

Both CW4 and CW5 isolates were fully resistant to ciprofloxacin and this is likely to have been caused by the p.T83I substitution in GyrB. Anthranilate synthesis (and therefore AQ production) may have been affected by the mutations identified in the *trp* and *kyn* pathways, even tough the function of the proteins is not predicted to be affected.

4.2.3.2 Mutations that differentiate phenotypic profile 1 (bone) and 2 (blood)

PATRIC variation analysis service was used to identify SNPs between the phenotype 1 genomes (C, D, and G) and the phenotype 2 genomes (E, F, and H). This was done using either CW4 genomes (A and B) as the reference, since these strains were sampled at a previous time point, or the PAO1 reference genome. Only SNPs identified by the combination of the SNP caller Free-Bayes with all of the four aligners available in PATRIC at the time were used. Also, only SNPs present simultaneously in all three genomes of strains with a given phenotype were considered (Table 25).

Table 25: SNPs identified through PATRIC variation analysis service in CW5 phenotypic profile 2 genomes (C, D, and G) that are not present in phenotypic profile 1 genomes (E, F, and H).

Gene name	Reference codon (CW4)	Variant codon (CW5 2)	Ref aa	Name	Var aa	Name	Mutation Type
fliJ	**C**AG	**T**AG	Q	Glutamine	STOP	Stop codon	Nonsyn
pvdS	G**T**G	G**C**G	V	Valine	A	Alanine	Nonsyn
amn	CC**C**	CC**T**	P	Proline	P	Proline	Syn
mexZ	CGC**GGT**GCG	CGC**---**GCG	RGA	Glycine	RA	-	Del

Gene name	Locus tag	Gene function	PanX	Impact
fliJ	PA1105	Flagellar protein required for flagellum assembly	0/123	**-239.910**
pvdS	PA2426	σ factor controlling pyoverdine biosynthesis	1/121	-2.197
amn	PA3970	AMP nucleosidase (purine metabolism)	123/123	0
mexZ	PA2020	Transcriptional regulator, AcrR family	0/99	**-15.733**

Ref aa: amino acid present in the reference genome, Var aa: amino acid present in the variant (phenotypic profile 2) genomes. Nonsyn: nonsynonymous mutation, Syn: synonymous mutation, Del: deletion. Pan X: frequency of the variant amino acids in other *P. aeruginosa* genomes available on the PanX database; Impact was calculated with PROVEAN and values in bold correspond to a predicted deleterious impact on the biological function of each protein.

Through this detailed variation analysis it was possible to show that isolates with the phenotypic profile 2 (phenotype of the bacteria present in the blood (CW5 S) and 16 isolates of CW5 tissue) have three SNPs and one deletion that are not present in isolates with the phenotypic profile 1 (phenotype of the bacteria present in the bone (CW5 B) and also all isolates from CW4 and 24 isolates of CW5 tissue).

The SNP identified in *fliJ* reflects a change from C to T in a codon that is conserved across all 123 *P. aeruginosa* strains present in PanX database. This non-synonymous substitution changes the aa at position 31 from a glutamine to a stop codon (Figure 46). Due to the introduction of the stop codon (TAG), a new open reading frame was detected by the automatic annotation in the three genomes of strains with phenotype 2, with TTG coding for a methionine in position 33 (blue box in Figure 46).



Figure 46: Multiple sequence alignment analysis of *fliJ* via PATRIC platform. PAO1 *fliJ* sequence (Pseudomonas.com) was used as a query for BLASTn against the genome group that included 8 *P. aeruginosa* chronic wound isolates from patient X (Table 6). Results were observed through the MSA amino acid option that generates an alignment where each amino acid is represented by a different colour and logos at the top represent the amino acid conserved for each position. The red box in position 11 highlights a mutation not considered because it was only present in CW5 T40. The black box in position 31 highlights the *fliJ* mutation described in Table 25. The blue

box highlights a possible open reading frame that might be used by phenotype 2 isolates to restore *fliJ* production.

The 3D structure of the FliJ protein has been elucidated for *Salmonella typhimurium*, but not for the *P. aeruginosa* orthologue [320]. As the flagella system protein secretion and assembly mechanisms are very similar in *P. aeruginosa* and *S. typhimuirum*, FliJ is highly likely to share the same function in both bacteria. FliJ is part of the $FliH_2$-$FliI_6$ ATPase ring complex that directly interacts with the soluble cytoplasmic domain of FlhAB flagellar export gate apparatus (Figure 47) – see [321] for a more detailed explanation. For a full diagram of the genes involved in *P. aeruginosa* flagellar assembly please see Appendix C.

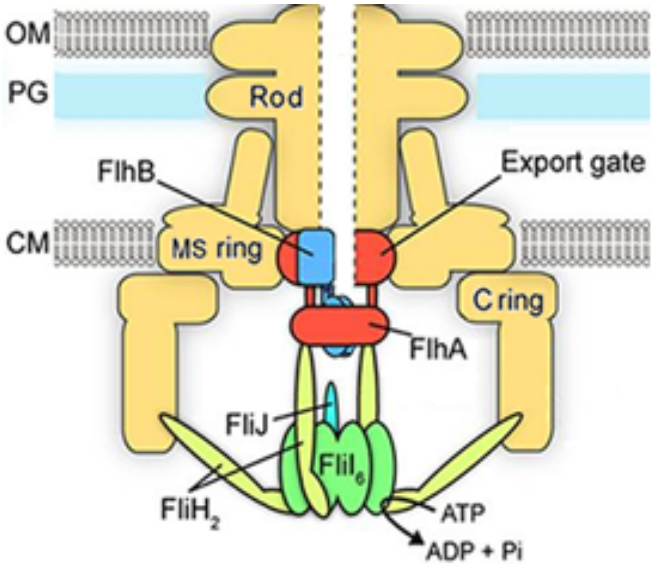


Figure 47: Partial structure of the flagellar type III export apparatus in Gram-negative bacteria (adapted from [322]). FlhA and FlhB are part of the export gate located within a central pore of the MS ring. FliI and FliJ form a ring complex with ATP-synthase activity, and FliH stably anchors the $FliI_6$-FliJ complex to the FlhAB platform of the export gate and to the C ring. OM: outer membrane, PG: peptidoglycan layer, CM: cytoplasmic membrane. For full flagellum structure see diagram in Appendix C.

The non-synonymous substitution identified will influence the size of FliJ, leading to a reduction from 148 to 93 amino acids which will affect the overall

structure, and/or compromise its formation (Figure 48). In recent work with the plant pathogen *Pseudomonas cichorri,* a ΔfliJ mutant that did not produce flagella was used and characterised, and found not to swim [323].

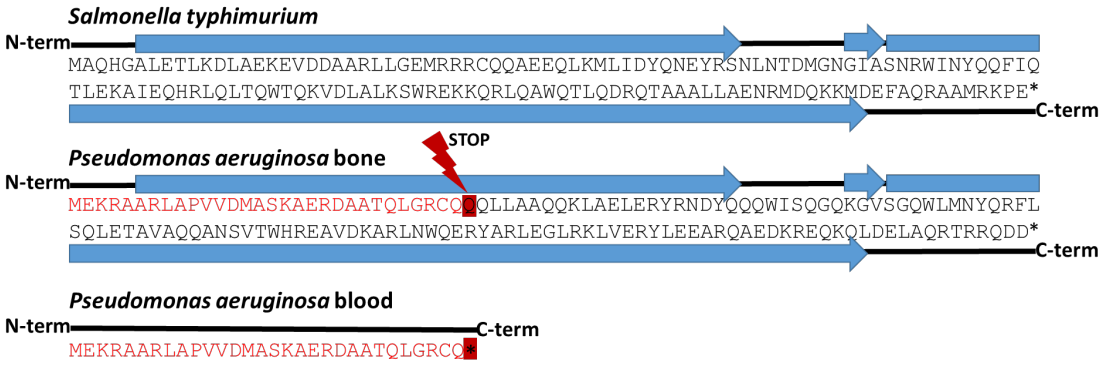


Figure 48: Primary amino acid sequence of the FliJ proteins in *S. typhimurium* and *P. aeruginosa*. The mutation at position 31 (highlighted in red) inserts a stop codon, which prevents the formation of an α-helix (blue arrows) essential for FliJ function.

The SNP identified in *pvdS* reflects a change from T to C in a codon that is conserved in 120 *P. aeruginosa* strains present in PanX database. The same SNP was identified in PA_D22 strain (SAMN04914475, [324]), a *P. aeruginosa* taken from a late isolate of an 82-year old patient with ventilator associated pneumonia in China. This non-synonymous substitution changes the aa in position 26 from a valine to an alanine (Figure 49).

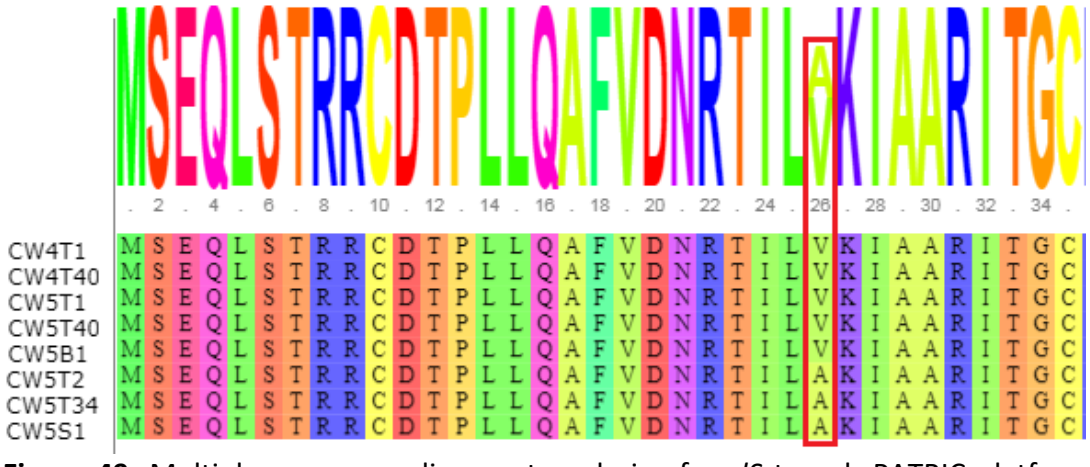


Figure 49: Multiple sequence alignment analysis of *pvdS* trough PATRIC platform.

PAO1 *pvdS* sequence (Pseudomonas.com) was used as a query for BLASTn against the genome group that included 8 *P. aeruginosa* chronic wound isolates from patient X (Table 6). Results were observed through the MSA amino acid option that generates an alignment where each amino acid is represented by a different colour and logos at the top represent the amino acid conserved for each position. The red box in position 26 highlights the *pvdS* mutation described in Table 25.

Alanine and valine are both hydrophobic and are chemically very similar; therefore, theoretically, it is not clear whether this will have an impact on PvdS function. However, this aa is in a region that has been shown to have significant similarities with other polymerases [325]. In particular, the RNA polymerase σ^{70} region 2, constituted by three α-helices with high similarity to PvdS (purple region in Figure 50), has the highest level of similarity with other sigma factors. As such, mutations in this region have a higher probability of altering the function of the protein, principally its binding to core RNA polymerase.

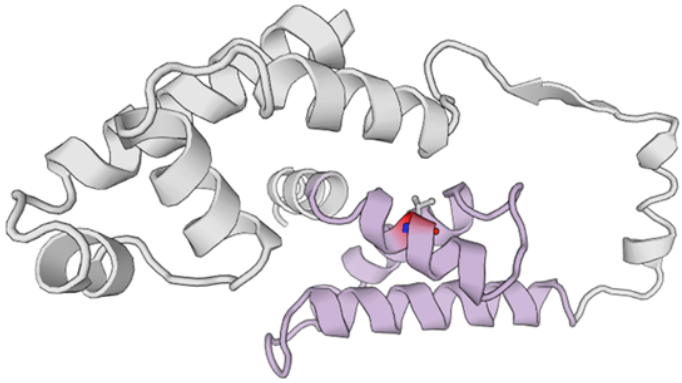


Figure 50: Predicted structure of the PvdS protein with valine 26 highlighted by the red shaded stick and ball amino acid in the middle of the purple α-helix that shows very high similarity with the RNA polymerase σ^{70} region 2.

The SNP identified in *amn* (adenosine monophosphate nucleosidase) reflects a change from C to T in the third position of a codon. This synonymous substitution changes the nucleotide at position 375 (Figure 51), but does not change the

corresponding amino acid. Actually, the corresponding proline in position 125 is conserved in all 123 *P. aeruginosa* strains present in PanX database.

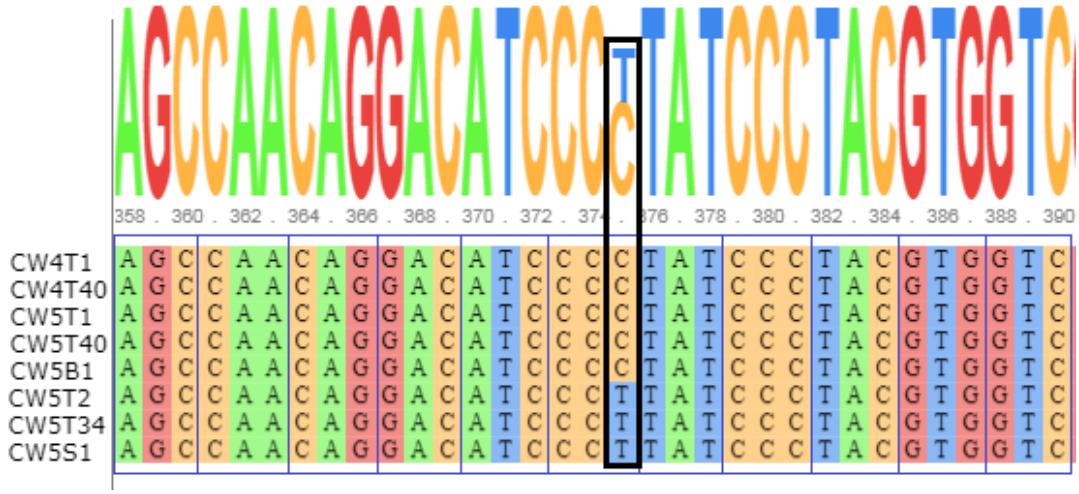


Figure 51: Multiple sequence alignment analysis of *amn* trough PATRIC platform. PAO1 *amn* sequence (Pseudomonas.com) was used as a query for BLASTn against the genome group that included 8 *P. aeruginosa* chronic wound isolates from patient X (Table 6). Results were observed through the MSA nucleotide option that generates an alignment where each nucleotide is represented by a different colour and logos at the top represent the nucleotide conserved for each position. The black box in position 375 highlights the *amn* mutation described in Table 25. Thin blue boxes mark the codons for the stretch of the sequence visible.

The last difference between profile 1 and profile 2 isolates is an in-frame deletion of a codon in *mexZ*. This deletion removed a glycine from position 46 (Figure 52), which is conserved across all 123 *P. aeruginosa* strains present in PanX database. After confirming the results of the alignment, a deletion of 9 amino acids, p.I161_G169del, was found in all profile 1 strains (blue box in Figure 52). This in-frame deletion is unique to these isolates, and is not present in any other strain sequenced here, nor in the *P. aeruginosa* strains in PanX.



Figure 52: Multiple sequence alignment analysis of *mexZ* trough PATRIC platform. PAO1 *mexZ* sequence (Pseudomonas.com) was used as a query for BLASTn against the genome group that included 8 *P. aeruginosa* chronic wound isolates from patient X (Table 6). Results were observed through the MSA nucleotide option that generates an alignment where each nucleotide is represented by a different colour and logos at the top represent the nucleotide conserved for each position. The black box in position 46 highlights the *mexZ* mutation described in Table 25. The black line in the middle indicates an interruption in the figure. The blue box from position 161 to position 169 indicates a deletion in profile 1 strains.

Even though p.G46del only removes one aa, it is likely to affect the activity of the protein because it is located in the DNA-binding region of MexZ, as can be seen in Figure 53, where Gly46 is highlighted. Likewise, p.I161_G169del may have an impact on the formation of the functional homodimer, since the deletion occurred in the dimerization region (around Gly172 in Figure 53).



Figure 53: Three-dimensional illustration of MexZ mutations, localized on the MexZ/DNA model (adapted from [326]). The two MexZ molecules of the dimer are

coloured green and brown, respectively. Residues are represented by spheres in yellow for those located at the dimer interface, in blue for those located at the protein-DNA interface, and in red for all the other. Note that glycine 46, the amino acid deleted in profile 2 strains is blue as it is in the DNA-binding region.

4.2.4 Motility assays

One of the mutations with predicted protein function impact identified by the genomic analysis was the flagellum assembly gene *fliJ*. Consequently, the three most common motility strategies used by *P. aeruginosa* – swarming, swimming, and twitching – were investigated (Figure 54). Note that in this section we used PAO1 (Nottingham sub strain) as a comparator for *P. aeruginosa* motility behaviour.

Figure 54 below clearly shows that, in contrast to CW5 bone isolates (phenotypic profile 1), CW5 blood isolates (phenotypic profile 2) do not swarm or swim while neither group exhibited twitching. The pattern of swarming for the CW5 bone isolate was different from that of PAO1, while swimming motility was comparable.

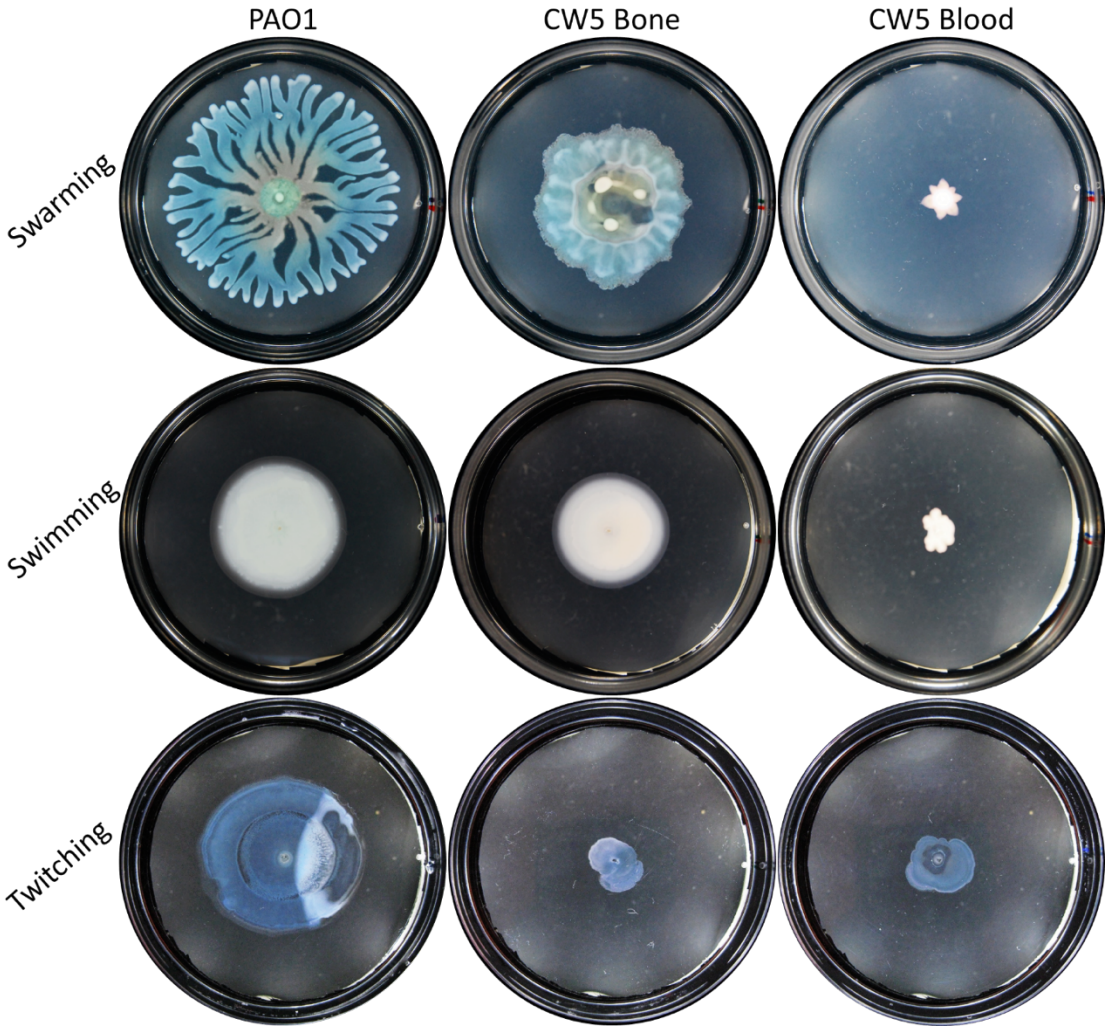


Figure 54: *P. aeruginosa* PAO1 and representative CW5 isolate motility. Each row from the top: swarming assay, swimming assay and twitching assay; each column from the left: PAO1, CW5 bone isolate (phenotypic profile 1), and CW5 blood isolate (phenotypic profile 2). Each assay was repeated in triplicate for each strain (representative data shown).

4.2.5 Microscopy

In order to demonstrate that the *fliJ* mutation impacted on flagellum assembly, we examined patient X's profile 1 (bone) and profile 2 (blood) isolates using transmission electron and TIRF microscopy. The results obtained show that bone isolates (CW5 B1) have flagella and can move (Figure 55), while blood isolates (CW5 S1) do not produce flagella and appear to be longer and thinner than bone isolates

(CW5 B1) on average – even though this difference was not statistically significant (n= 20 cells) (Figures 56 and 57).

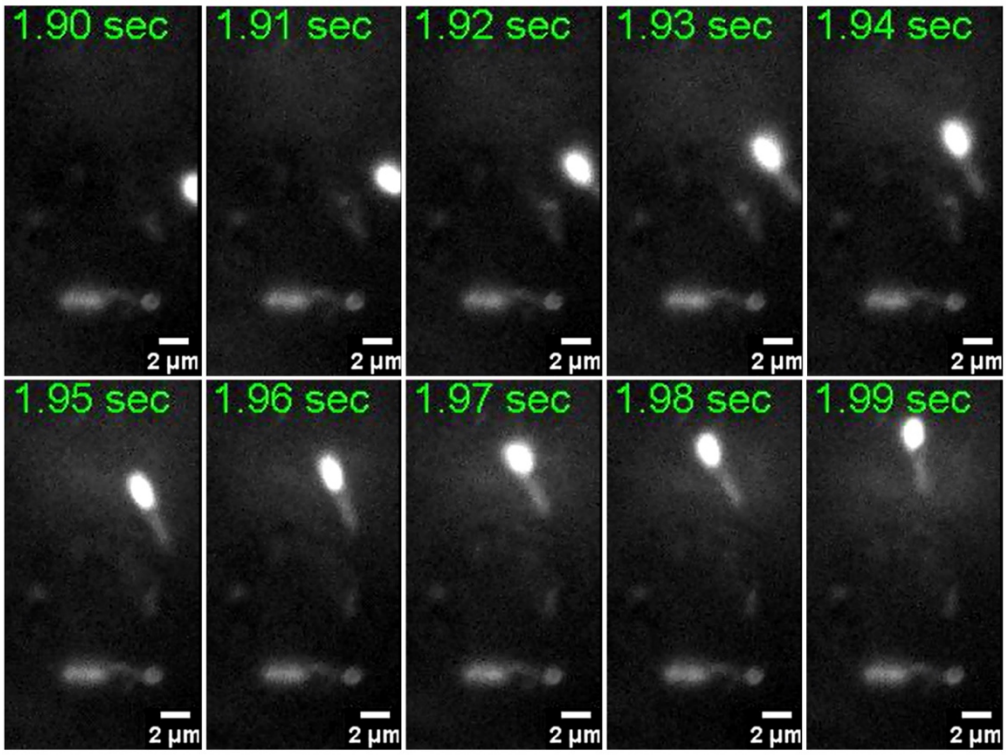


Figure 55: Frames of a video of a clinical *P. aeruginosa* strain isolated from bone of patient X (CW5 bone) stained with Alexa Fluor 488. TIRF microscopy images amplified 60x, numerical aperture 1.4; scale bar indicates 2 µm. CW5 blood isolates from the same patient did not stain with this dye (data not shown).

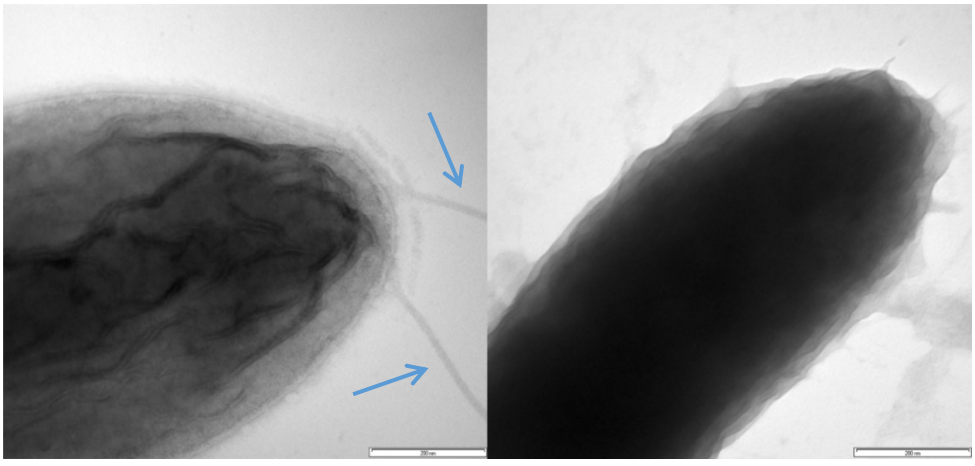


Figure 56: Transmission electron microscopy images of two clinical *P. aeruginosa* strains isolated from bone (left) and blood (right) of patient X (chronic wound ulcer). Images amplified ~87,000 x; scale bar indicates 200 nm. Exterior of the cell appears to be different in both strains but this was not conserved across the cells imaged; flagellum indicated with blue arrows.

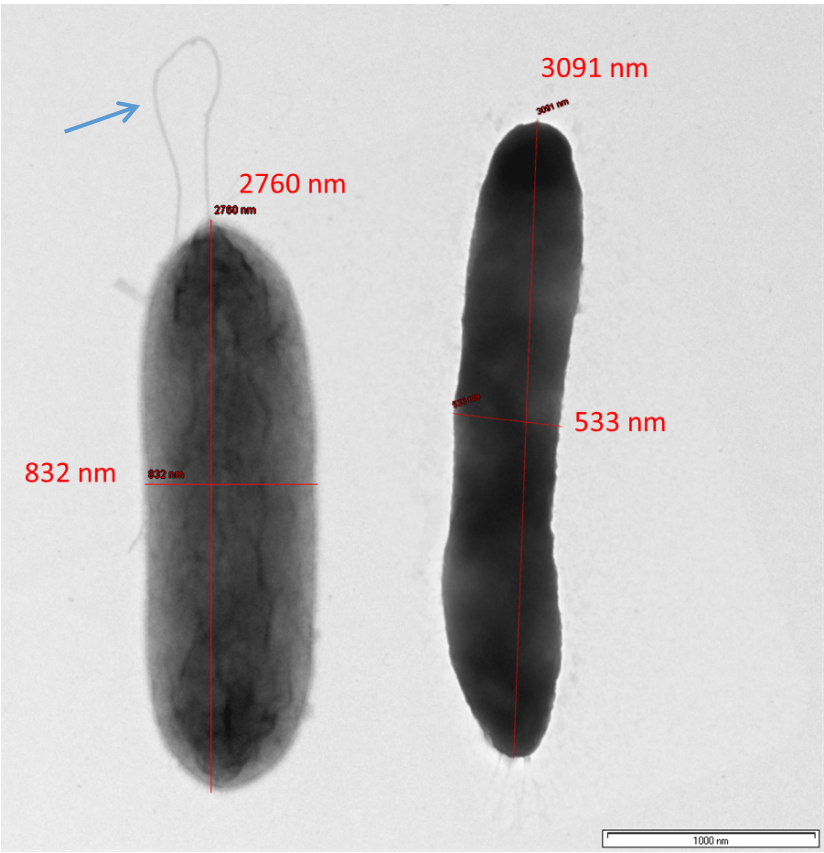


Figure 57: Transmission electron microscopy images of two clinical *P. aeruginosa* strains isolated from bone (left) and blood (right) of patient X (chronic wound ulcer). Composite of two images amplified ~20,000 x; scale bar indicates 1 µm (1000 nm); total surface area of bacteria estimated from measurements in red (nm) from bone: 832 nm x 2760 nm, and blood 533 nm x 3091 nm; flagellum indicated with blue arrow.

4.2.6 Pilot infection assays

To evaluate the effects of the mutations identified in Table 25 in *P. aeruginosa* virulence, two pilot infection assays were carried out in representative CW5 bone and blood isolates. First, the survival of *G. mellonella* larvae was assessed for one week after infection (Figure 58) with bacterial cells (top) or cell-free supernatant (bottom).

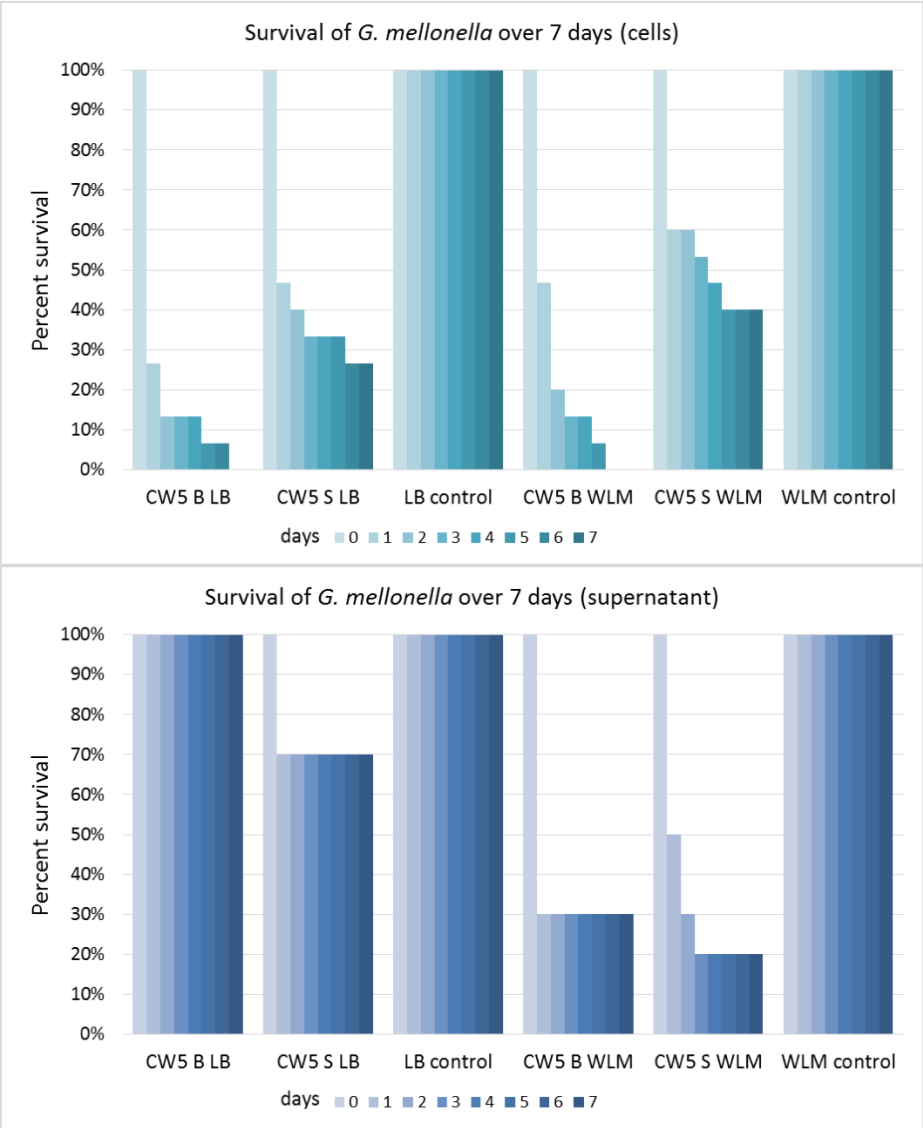


Figure 58: Pilot infection experiment in a *G. mellonella* larval infection model using patient X's bone and blood isolates. Blue gradient (lighter – darker) corresponds to earlier to later days; 3 larvae were analysed per condition and strain; bacteria were grown in either LB or WLM (wound like medium).

With respect to the ability of the bacterial cells to cause infection (Figure 58, top), the survival of larvae was reduced in bone isolates when compared with blood isolates for both media (LB and WLM). For the cell-free supernatants (Figure 58, bottom), larval survival was markedly reduced for both isolates when WLM but not LB was used as the growth medium.

The relative ability of bone and blood isolates to invade the tissues was evaluated using a murine chronic wound model, which generally does not lead to a fatal infection. Four days post-infection, the bacterial loads at the wound site, liver, and spleen were compared, as well as possible differences in wound closure rate and spleen size (Figure 59).

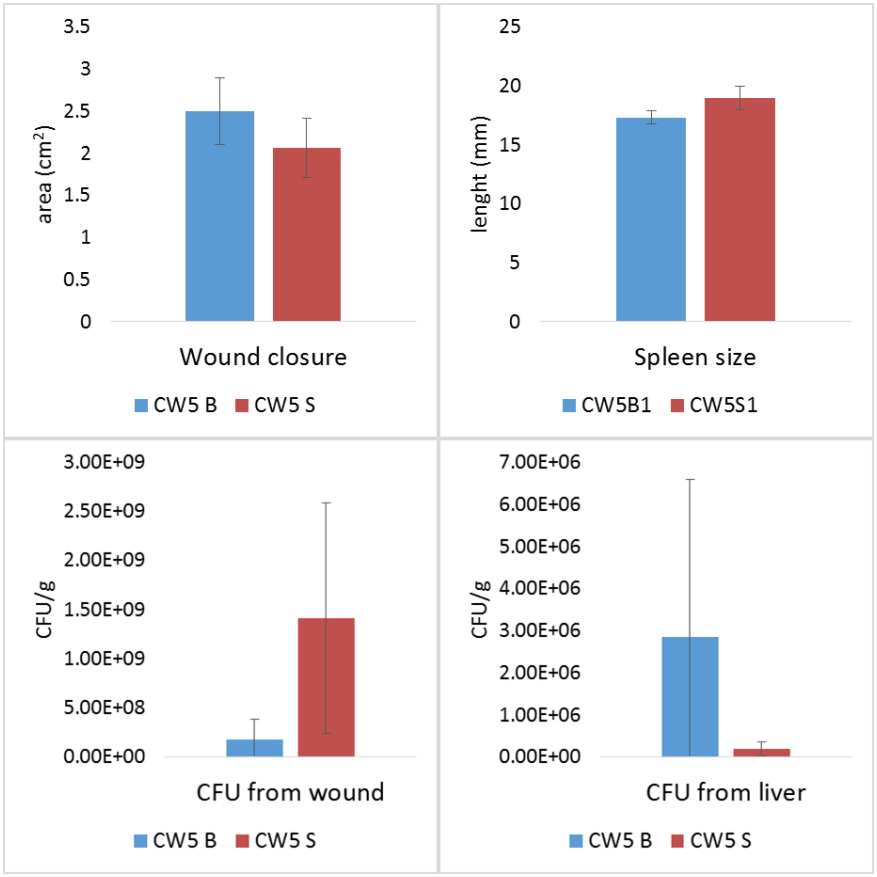


Figure 59: Pilot infection experiments in a murine chronic wound model using patient X's bone and blood isolates. A total of 6 mice (3 per strain) were kept until day 4 post-infection. Top left: area of wound, top right: length of spleen, bottom left: CFU per gram of wound tissue, bottom right: CFU per gram of liver. No bacteria were recovered from the spleen (data not shown).

4.2.7 Transcriptome analysis

Since the phenotypic diversity between CW5 profile 1 (bone) and profile 2 (blood) isolates could not be fully explained by comparative genome analysis, the

transcriptomes of the two strains were determined using RNAseq. Briefly, three biological replicates of *P. aeruginosa* chronic wound isolates from blood (CW5 S1) and bone (CW5 B1) were grown for 8 h and 18 h, the cells harvested, and the RNA extracted and sequenced. The differences in gene expression between bone and blood isolates were deemed significant for P values < 0.05. Results were deemed as biologically significant if |log2 fold-change| ≥ 0.95, which corresponds to an absolute fold change equal or higher than 1.93. The first point (8 h) was selected as 1 h before the production of both pyoverdine and pyochelin had peaked (Figure 60).

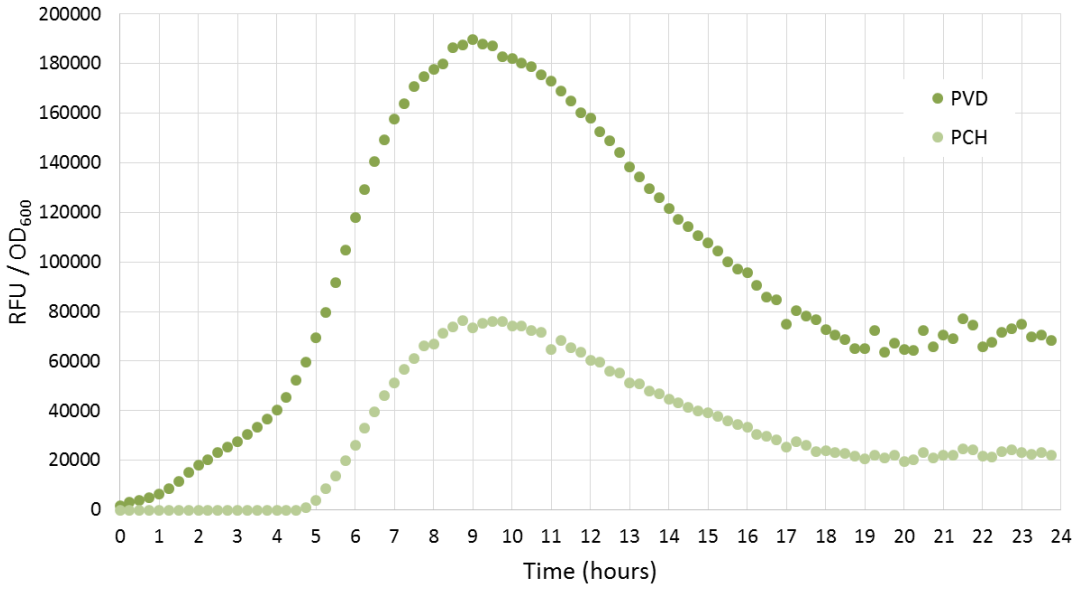


Figure 60: Siderophore production measured over time in the lab strain PAO1. Excitation / emission wavelengths for pyoverdine (PVD dark green) and pyochelin (PCH light green) are described in section 2.3.4.

The second point (18 h) was selected to provide a comparable time point with that used for the overnight culture for all 360 *P. aeruginosa* chronic diabetic wound isolates that were phenotyped (Chapter 3).

For the two conditions analysed (bone vs blood at 8 h and 18 h), no batch effects apart from the differences in sample type (bone vs blood) were observed (Figure 61).

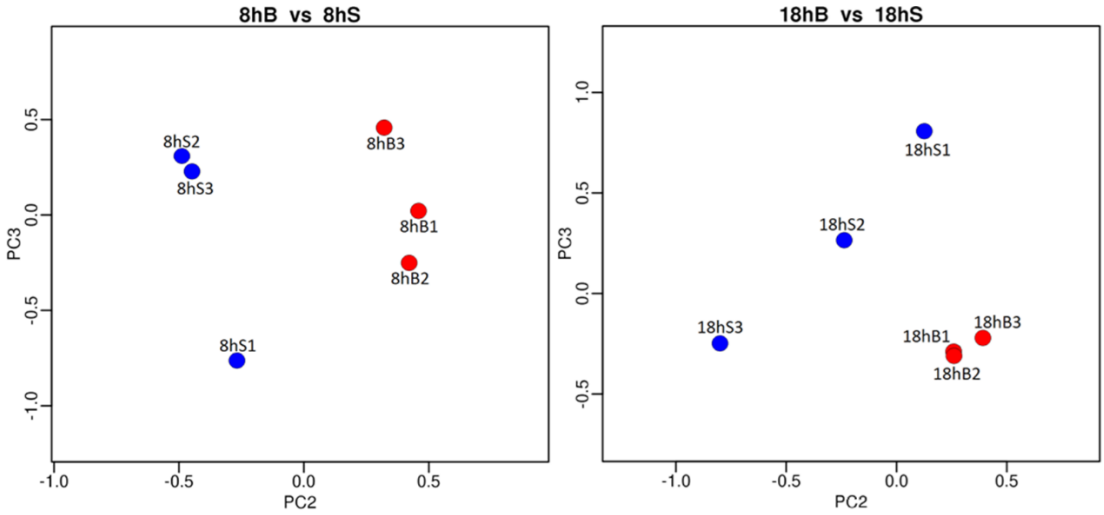


Figure 61: Principal component analysis of the distribution of gene-level expression. Data for six chronic wound samples analysed at 8h (left) and 18h (right) was used. Blue represents CW5 blood replicates, while red represents CW5 bone replicates. Note that there is no variation between the samples other than the CW type (bone or blood).

A preliminary global analysis of the RNAseq data indicates that the majority of the *P. aeruginosa* genes can be found within the |fold change| = 2. This means that the majority of differential gene expression between bone and blood isolates is not biologically significant, as expected since these isolates came from a homogeneous chronic wound ulcer (Figure 62).

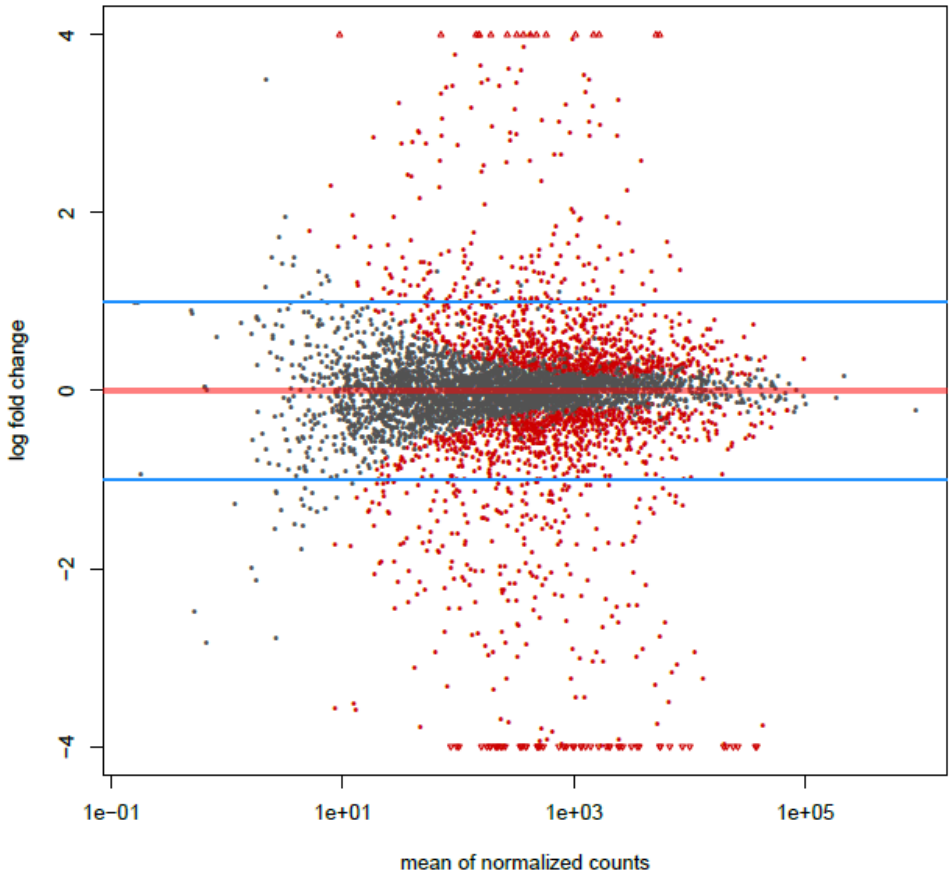
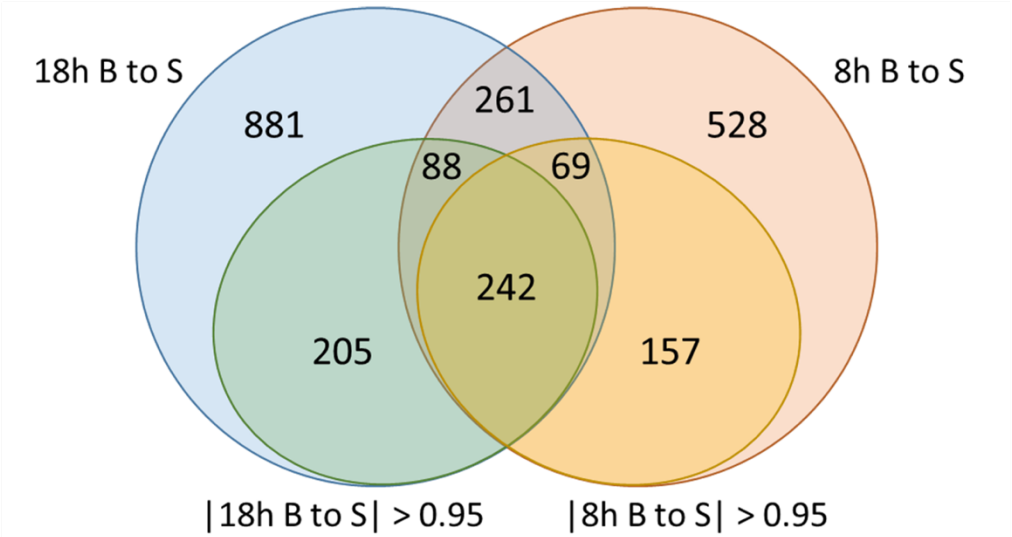


Figure 62: MA-plot providing a global view of the differential genes with the log2 fold change over the mean of normalized counts. Log2 fold change corresponds to the log of the ratio of level counts for each gene between two samples, while the mean of normalized counts is the average level of counts for each gene across the two samples. Blue lines mark the region within which fold-change is approximately 2. Red dots denote significant differentially expressed genes, while black dots denote non-differentially expressed genes. Closed circles with a positive log2 fold change indicate genes which were upregulated in the bone compared with the blood isolates and closed circles with a negative log2 fold change indicate genes which were downregulated.

An initial statistical analysis filtered genes whose expression significantly changed (P value < 0.05) between bone (B) and blood (S) at both time points. This preliminary analysis retained a total of 1746 differentially expressed genes at 18h (18 h B to S, in blue), and a total of 1345 differentially expressed genes at 8 h (8 h B to S, in red) (Figure 63).



		Down	Up	total
green	|18h B to S| > 0.95	75	130	205
green + red	|18h B to S| > 0.95 ∩ 8h B to S	35	53	88
green + red + yellow	|18h B to S| > 0.95 ∩ |8h B to S| > 0.95	109	133	242
	total	219	316	535

Figure 63: Venn diagram showing the genes whose expression significantly changes between CW5 bone (B) and CW5 blood (S) at 18h and at 8h. |B to S| > 0.95 represents the genes that have more than ~2 fold change difference at 18h in green, and at 8h in yellow. For the subsequent analysis only information from |18h B to S| > 0.95 (in green – 535 genes) is going to be used, and the table clarifies how many of the genes are up- or downregulated in CW5 blood when compared to CW5 bone using that cut-off.

From here, the cut-off |B to S| > 0.95 was used to eliminate all differences that do not have a likely biological significance, i.e., all genes whose differential expression was less than |fold change|=2. This left a total of 535 differentially expressed genes at 18h (|18 h B to S| > 0.95, in green), and a total of 468 differentially expressed genes at 8 h (|8h B to S| > 0.95, in red). This section will focus on the analysis of biologically significant differentially expressed genes in bone and blood isolates at 18 h. The proportion of up- and down- regulated genes at 18 h was calculated and summarised in Table 26.

Table 26: Summary of differentially expressed genes in the CW5 blood isolate when compared with the CW5 bone isolate after 18 h growth.

|log2 Fold Change|	|Fold Change|	Downregulated	Upregulated
0.95 to 2	1.93 to 4	141	158
2 to 4	4 to 16	60	102
4 to 5	16 to 32	12	35
5 to 6	32 to 64	5	17
≥ 6	≥ 64	1	4
	Total of genes:	219	316

From the 1746 differentially expressed genes between CW5 bone and CW5 blood isolates at 18h, only 535 have an expression higher than 0.95 log2 fold change (cut-off used for potential biological significance).

Gene ontology (GO) analysis was used to identify the biological processes common to the genes that were differently expressed. The results for significantly downregulated genes are summarised in Table 27, while results for significantly upregulated genes are summarised in Table 28. Biological processes involving genes both up- and downregulated are summarised in Table 29.

A total of 15 biological processes were associated with genes downregulated in the CW5 blood isolate when compared to the CW5 bone isolate (Table 27). Globally, more than half of the genes associated with the GO term were significantly altered. In detail, all genes involved with hydroxyproline transport and regulation of protein secretion, and 75% of all genes involved with chromosome condensation and response to amino acids were significantly downregulated. Note that for the GO terms “protein secretion via the T3SS”, “negative regulation of protein secretion” and “extracellular polysaccharide biosynthetic processes”, there were 3 genes – *fliI*, *mexR*,

and *pelA* respectively – that were significantly upregulated while 72.22 %, 66.67%, and 42.86% of all other genes were significantly downregulated.

Table 27: Biological processes associated with genes that are significantly downregulated in CW5 blood when compared to CW5 bone after 18 h growth.

GO term	Biological process	Genes involved
GO:0034589	hydroxyproline transport	100%
GO:0050708	regulation of protein secretion	100%
GO:0030261	chromosome condensation	75%
GO:0043200	response to amino acid	75%
GO:0030254	**protein secretion by the T3SS**	**72.22%**
GO:0035999	tetrahydrofolate interconversion	66.67%
GO:0050709	**negative regulation of protein secretion**	**66.67%**
GO:0042710	biofilm formation	56.25%
GO:0045226	**extracellular polysaccharide biosynthetic process**	**42.86%**
GO:0015947	methane metabolic process	33.33%
GO:0019441	tryptophan catabolic process to kynurenine	33.33%
GO:1902201	negative regulation of flagellum-dependent cell motility	20%
GO:0006554	lysine catabolic process	16.67%
GO:0006119	oxidative phosphorylation	10.00%
GO:0009117	nucleotide metabolic process	2.17%

The % of genes involved was calculated as the number of genes with more than 2 fold-change divided by the total number of genes associated with that biological process. T3SS: type III secretion system; GO terms in bold include an upregulated gene: *fliI* in 30254, *mexR* in 50709, and *pelA* in 45226. For a more detailed table see Appendix D.

Fourteen biological processes were associated with genes upregulated in the CW5 blood isolate when compared to the CW5 bone isolate (Table 28). Globally, more than half of the genes associated with each GO term was significantly altered. In detail, all genes involved with ferric-enterobactin transport and pyochelin biosynthetic process, and ~90% of all genes involved with regulation of iron (III) transport were significantly upregulated. Note that for the GO terms “siderophore

transport", "cell surface receptor signalling pathways", and "DNA-templated transcription and initiation", *femI* (which is an ECF σ factor) was downregulated significantly while 72.73 %, 61.54 %, and 48% of all other genes respectively were significantly upregulated.

Table 28: Biological processes associated with genes that are significantly upregulated in CW5 blood when compared with CW5 bone after 18 h growth.

GO term	Biological process	Genes involved
GO:0015685	ferric-enterobactin transport	100%
GO:0042864	pyochelin biosynthetic process	100%
GO:0034756	regulation of iron ion transport	90.91%
GO:0044780	bacterial-type flagellum assembly	76.47%
GO:0015891	**siderophore transport**	**72.73%**
GO:0007166	**cell surface receptor signalling pathway**	**61.54%**
GO:0071973	bacterial-type flagellum-dependent cell motility	60.87%
GO:0071475	cellular hyperosmotic salinity response	50%
GO:0006352	**DNA-templated transcription, initiation**	**48%**
GO:0015838	amino-acid betaine transport	42.86%
GO:0006741	NADP biosynthetic process	33.33%
GO:0031460	glycine betaine transport	30%
GO:0006559	L-phenylalanine catabolic process	16.67%
GO:0032885	regulation of polysaccharide biosynthetic process	14.29%

% of genes involved was calculated as the number of genes with more than 2 fold-change difference divided by the total number of genes associated with that biological process. *femI* is associated to the GO terms in bold, but is downregulated in blood. For a more detailed table see Appendix D.

At least another 8 biological processes were associated with differentially expressed genes in the CW5 blood isolate when compared to the CW5 bone isolate (Table 29). However, these changes could be for either direction, depending on the genes and on the processes. Here, only chemotaxis had more than 50% of its associated genes significantly expressed. In particular, 13 out of 45 genes associated

with chemotaxis were downregulated in blood when compared to bone, and 10 out of 45 genes were upregulated. A full list of each gene associated with different GO terms can be found in the Appendix D.

Table 29: Biological processes associated with genes that significantly change in CW5 blood when compared with CW5 bone after 18 h growth.

GO term	Biological process	Down -regulated	Up	Genes involved
GO:0006935	chemotaxis	13	10	51.11%
GO:0009405	pathogenesis	13	3	24.62%
GO:0007165	signal transduction	15	7	21.15%
GO:0006598	polyamine catabolic process	1	1	15.38%
GO:0006950	response to stress	1	1	13.33%
GO:0006099	tricarboxylic acid cycle	1	1	11.11%
GO:0006091	generation of precursor metabolites and energy	6	2	9.09%
GO:0006520	cellular amino acid metabolic process	4	3	5.22%

The number of genes that significantly change (down or up) are indicated for each GO term. % of genes involved was calculated as the number of genes with more than 2 fold-change difference divided by the total number of genes associated with that biological process. For a more detailed table see Appendix D.

Around half of the genes that significantly varied in expression in the CW5 blood isolate when compared to the CW5 bone isolate at 18 h code for proteins that have not yet been identified/characterized, i.e. hypotheticals. From the list of downregulated genes, this means a total of 111/229 (50.7%), and in the list of upregulated genes a total of 159/316 (50.6%). Table 30 summarises genes that have a fold change > 25.

Table 30: Genes that have > 25 fold difference in expression in the CW5 blood when compared with the CW5 bone isolate after 18 h growth, using PAO1 genome as mapping reference.

Gene ID	Name	Protein Function	Fold Change
PA0672	*hemO*	haem oxygenase	100.99
PA4229	*pchC*	pyochelin biosynthetic protein	88.57
PA3530	*bfd*	bacterioferritin-associated ferredoxin	80.12
PA4228	*pchD*	pyochelin biosynthesis protein	64.02
PA4230	*pchB*	salicylate biosynthesis protein	63.15
PA2426	*pvdS*	ECF sigma factor	62.16
PA4221	*fptA*	Fe(III)-pyochelin outer membrane receptor	58.54
PA0424	*mexR*	multidrug resistance operon repressor	54.71
PA1695	***pscP***	**translocation protein in type III secretion**	**-52.41**
PA4226	*pchE*	dihydroaeruginoic acid synthetase	50.43
PA2686	*pfeR*	two-component response regulator (PfeS/PfeR)	49.90
PA4843	***gcbA***	**diguanylate cyclase**	**-49.75**
PA4709	*phuS*	cytoplasmic haem-binding protein	47.70
PA4704.3	*prrH*	non-coding RNA regulated by haem	46.48
PA4710	*phuR*	Haem uptake outer membrane receptor	45.62
PA2687	*pfeS*	two-component sensor (PfeR/PfeS)	42.21
PA4231	*pchA*	salicylate biosynthesis isochorismate synthase	40.95
PA0471	*fiuR*	ferric transmembrane sensor	40.67
PA3526	***motY***	**component of the sodium-type flagellar motor**	**-39.08**
PA0472	*fiuI*	ECF sigma factor	34.55
PA4470	*fumC1*	fumarate hydratase	34.32
PA1696	***pscO***	**translocation protein in type III secretion**	**-32.19**
PA1694	***pscQ***	**translocation protein in type III secretion**	**-32.16**
PA4224	*pchG*	pyochelin biosynthetic protein	31.37
PA4219	*ampO*	involved with β-lactamase resistance	30.86
PA3531	***bfrB***	**Bacterioferritin**	**-30.69**
PA3407	*hasAp*	heme acquisition protein	30.23
PA4227	*pchR*	pyochelin transcriptional regulator	29.37
PA1697	***pscN***	**ATP synthase in type III secretion system**	**-28.84**
PA1452	*flhA*	flagellar biosynthesis protein	28.82
PA2467	*foxR*	Anti-sigma factor	28.24
PA0425	*mexA*	RND multidrug efflux protein	25.58

Genes in bold highlights those downregulated in CW5 blood when compared with CW5 bone. All others are genes upregulated in CW5 blood when compared to CW5 bone. Note that 7 genes that code for hypothetical proteins (5 upregulated/ 2 downregulated) were not included.

Genes that are downregulated in the CW5 blood isolate compared with the CW5 bone isolate (bold values, Table 30) represent only 21.9% of the genes whose FC > 25, and are mostly related to T3SS, with the exception of: *bfrB*, that codes for a bacterioferritin iron storage protein; *motY*, which is involved in the flagellar assembly; and *gcbA*, a c-di-GMP cyclase which promotes initial attachment to surfaces through regulation of motility. It is interesting however, that genes from a 30 kbp region involved with T3SS (GO:0030254), including both positive (GO:0050708) and negative (GO:0050709) regulators of T3SS, and pathogenesis (GO:0009405), are all downregulated (Figure 64).

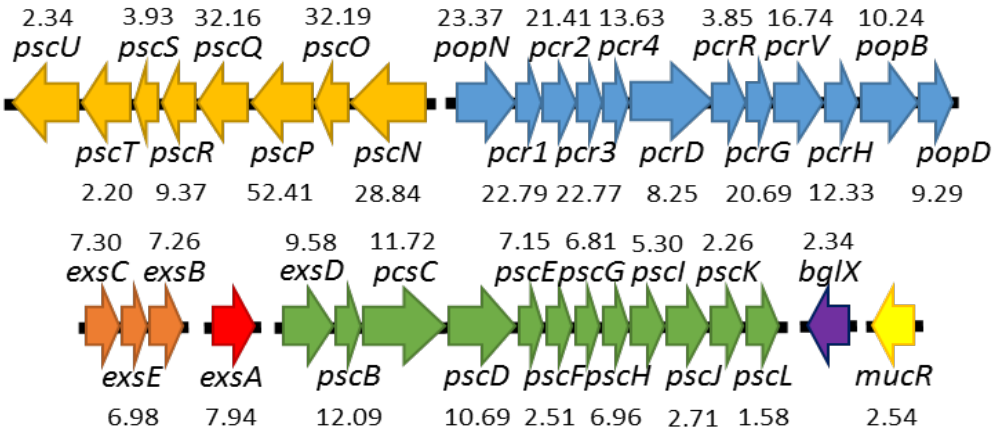


Figure 64: A 30 kbp region consisting of type III secretion systems (T3SS) genes that are downregulated in the CW5 blood when compared to the CW5 bone isolates. Each colour represents an operon, arrows represent individual (named) genes, and numbers indicate gene expression (fold-change). This region codes for proteins required for the assembly of the T3SS injectisome and effector proteins.

By comparison, the upregulated genes are more abundant (78.1%) and mostly involve mainly iron metabolism genes, including *hemO*/*phuS* that code for haem oxygenase proteins (FC of 100.99 and 47.70 respectively). In addition, several genes related to a region involved with pyochelin biosynthesis (Figure 65) are overexpressed in the CW5 blood isolates when compared with the bone isolates.

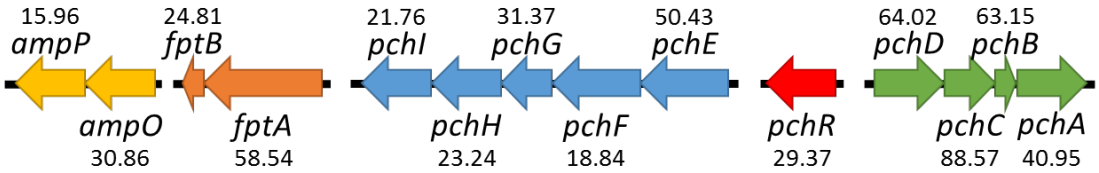


Figure 65: A 25 kbp region consisting of PCH-related genes that are upregulated in the CW5 blood when compared with the CW5 bone isolates. Each colour represents an operon, arrows represent individual (named) genes, and numbers indicate gene expression (fold-change). Operons in orange and red are under the control of the ferric uptake regulation (Fur) protein.

Figure 65 depicts 36% of all genes upregulated in Table 30, i.e., whose fold-change is higher than 25. However, expression of the Fur repressor gene does not differ between the CW5 blood and bone isolates. Moreover, other 5 genes upregulated in blood when compared to bone are associated with cell-surface signalling systems – each involving an ECF σ factor, an anti-σ factor, and a TBDT – so a separate list was compiled incorporating all of the CSS systems described for *P. aeruginosa* (Table 31).

Table 31: Genes involved with cell-surface signalling (CSS) systems in *P. aeruginosa* that are differentially expressed in CW5 blood when compared to CW5 bone isolates after 18 h growth (list adapted from [300]).

ECF σ factor	FC	anti-σ	FC	TBDT	FC	Function - regulation of:
FpvI	**5.13**	FpvR	**2.41**	FpvA/B	**26.2**/12.9	Pyoverdine uptake
PvdS	62.16	FpvR	**2.41**	FpvA/B	**26.2**/12.9	Pyoverdine synthesis [#]
FiuI	34.55	FiuR	40.67	FiuA	23.48	Ferrichrome uptake
PA4896	24.24	PA4895	32.53	PA4897	10.22	Siderophore uptake
FoxI	21.07	FoxR	28.24	FoxA	19.52	Ferrioxamine uptake
FecI	7.66	FecR	6.53	FecA	7.88	Ferric citrate uptake
PA1300	4.98	PA1301	9.44	PA1302	13.22	Haem uptake
PA0149	4.81	PA0150	1.76	PA0151	2.18	Metal uptake
HasI	3.97	HasS	1.76	HasR	19.32	Haem uptake
VreI	3.31	VreR	1.35	VreA	4.70	Virulence
PA1363	2.57	PA1364	2.56	PA1365	1.75	Alcaligin uptake
FemI	-2.63	FemR	1.86	FemA	5.49	Mycobactin uptake
PA2050	n.s.	PA2051	n.s.	PA2059/70	n.s.	Metal uptake
PA2093	n.s.	PA2094	n.s.	PA2089/90	n.s.	Siderophore uptake

ECF - extracytoplasmic function; FC - fold change; TBDT - TonB-dependent transporter. Note that in FC column positive values correspond to genes upregulated in the CW5 blood when compared with the CW5 bone isolates; n.s. – expression not significant (p>0.05); values in bold indicate that genome C (CW5 B1) was used as reference (all others were obtained using PAO1 as reference); values underlined indicate expression not biologically significant ($log_2FC<|0.95|$); superscript # denotes that PvdS also directly regulates production of exotoxin A and the endoprotease Piv/PrpL.

Since the majority (76.47%) of genes involved with flagellum assembly were upregulated in the CW5 blood when compared to the CW5 bone isolates, a separate analysis was carried out for the genes involved in flagella assembly (Table 32). Note that the only two genes downregulated are *fliC,* which codes for flagellin - the main protein structural component of the *P. aeruginosa* flagellum filament, and *motY*, which codes for a protein involved with the generation of the flagellar torque.

For a full list of all genes whose expression differs between the CW5 blood isolates compared with the CW5 bone isolates after 18 h growth, see Appendix E (219 downregulated genes, and 316 upregulated genes).

Table 32: *P. aeruginosa* flagellar assembly genes that are differentially expressed in the CW5 blood when compared with the CW5 bone isolates after 18 h growth

Gene ID	Gene	Function in flagellar apparatus:	Fold Change
PA1454	*fleN*	Flagellar biosynthesis regulator	9.38
PA1099	*fleR*	Two component system that regulates motility	17.69
PA1098	*fleS*	and adhesion	20.33
PA1077	*flgB*	Proximal rod	2.60
PA1078	*flgC*		2.68
PA1079	*flgD*	Hook cap	2.41
PA1080	*flgE*	Hook protein	<u>1.30</u>
PA1081	*flgF*	Proximal rod	7.52
PA1082	*flgG*	Distal rod	19.25
PA1083	*flgH*	L ring	16.18
PA1084	*flgI*	P ring	13.43
PA1085	*flgJ*	Peptidoglycan hydrolase / rod capping protein	7.49
PA1086	*flgK*	Hook-filament junction	6.27
PA1087	***flgL***	**Hook-filament junction**	**3.35**

Gene ID	Gene	Function in flagellar apparatus:	Fold Change
PA3351	*flgM*	Negative regulator of flagellin synthesis	1.93
PA1455	*fliA*	σ factor for flagellar operon	6.13
PA1092	***fliC***	**Filament protein (flagellin)**	**-32.97**
PA1094	***fliD***	**Filament cap**	**9.57**
PA1100	*fliE*	Proximal rod	1.30
PA1101	*fliF*	MS ring	7.52
PA1102	*fliG*	C ring	7.65
PA1103	*fliH*	ATPase ring complex	4.11
PA1104	*fliI*		3.12
PA1105	*fliJ*		2.24
PA1441	*fliK*	Flagellar hook-length control	3.46
PA1443	*fliM*	C ring	9.04
PA1444	*fliN*		7.99
PA1445	*fliO*	Export gate	6.30
PA1446	*fliP*		5.05
PA1447	*fliQ*		3.33
PA1448	*fliR*		2.78
PA1449	*flhB*		2.21
PA1452	*flhA*	Export gate	28.82
PA1453	*flhF*	Flagellar biosynthesis regulator	15.68
PA3526	*motY*	Sodium-type flagellar protein	-39.08

Shaded areas represent different operons; values underlined indicate expression unlikely to be biologically significant (log2FC<|0.95|); values in bold indicate that genome C (CW5 B1) was used as a reference; negative fold-change values indicate downregulation in the CW5 blood when compared with CW5 bone isolates. For a diagram of flagellar assembly in PAO1, please see Appendix C.

4.3 Discussion

The medical history of patient X described in this chapter provides a context for the CW4 and CW5 phenotypic assays and genomic analysis of the *P. aeruginosa* isolates taken from this patient. Since *P. aeruginosa* isolates with phenotypic profile 1 were obtained from the first time point (CW4 – tissue biopsy), they were considered to harbour the ancestral genotype and phenotype from which the profile 2 isolates emerged. That these two phenotypic profiles correspond to the same strain and not

to a *de novo* infection with a nosocomial or environmental drug-resistant strain was established from the data presented in Chapter 3.

The *P. aeruginosa* isolates from the tissue biopsy carried out at the second time point (CW5) had both phenotypic profiles in a 2:3 ratio (profile 2 – 16/40 isolates, while profile 1 – 24/40 isolates) and, since only isolates with phenotypic profile 2 were found in the blood cultures (CW5 S), the differences between phenotypic profile 1 and 2 were hypothesised to have allowed *P. aeruginosa* to invade the blood stream. From 6 biological parameters assessed (Table 23), three were different: colony morphology on CRA, siderophore production, and antibiotic susceptibility. Even though colony morphology on CRA is a useful high-throughput method for rapidly screening large numbers of isolates for gross differences, there is not enough information in the literature to facilitate correlation of morphotype with a specific mutation, especially given that the isolates are highly pleiotropic since they carry multiple mutations. In the next sections, the differences in the phenotypic profiles 1 and 2 are linked with specific mutations identified in the genomic analysis.

4.3.1 Antibiotic susceptibility

The ability to resist antibiotics is of paramount importance for the survival of bacteria in the context of human disease. During infection, several bacterial traits, such as the formation of biofilms or the overexpression of efflux pumps or antibiotic inactivating enzymes, act collectively to increase the tolerance or resistance of the population to antimicrobials. All *P. aeruginosa* isolates from patient X's first biopsy were already fully resistant to ciprofloxacin, and this resistance could be directly linked to a mutation in a DNA gyrase gene, a well-known ciprofloxacin target [327].

The pT83I substitution detected in the GyrA protein (Table 24) has previously been identified as responsible for *P. aeruginosa* fluoroquinolone resistance [328, 329].

The SNP variation carried out for bone and blood isolates identified a *mexZ* mutation (p.G46del) that is predicted to have a major effect on MexZ activity due to its location within the DNA-binding region (Figure 53). A study of *P. aeruginosa* aminoglycoside resistance identified several mutations (including the one reported here) associated with a decrease in MexZ repressor activity [326]. In *mexZ* mutants, frequently found in CF patients, the lack of this repressor allows the overproduction of the MexXY-OprM pump, contributing to the development of multidrug antibiotic resistance [212]. However, blood isolates were not classed as resistant to gentamicin since the zone diameter (21 mm in average – Figure 43) identified in the BSAC assay is higher than the breakpoint limit for *P. aeruginosa* gentamicin resistance (R ≤ 17 mm). Resistance to other aminoglycosides could be affected, but was not investigated.

Surprisingly, the GO term associated with response to antibiotics (GO:0046677) is not identified in the biological processes associated with genes that significantly change in the CW5 blood when compared to the CW5 bone isolate after 18 h growth (Tables 27 to 29). The reason for this is that only 4 out of the 32 genes associated with this category were overexpressed, namely *mexA*, *ampP*, *dnpA*, and PA5159. However, the majority of the genes involved with AMR in *P. aeruginosa* are not assigned to GO:0046677, and are instead associated with GO terms for specific resistance mechanisms, such as "β-lactam antibiotic catabolic process" (GO:0030655).

The piperacillin-tazobactam resistance shown by blood isolates against penicillins could be related to the significant increase in *ampP*/*ampO* expression (15.95/30.86 FC increased in blood when compared to bone), which are involved in the regulation of an inducible β-lactamase [308] even though the mechanism is not fully understood yet (Figure 39). However, despite the >15 fold increase in expression, this did not affect *ampC* expression, and therefore it is not likely to have an impact on β-lactam susceptibility. Two other genes (PA1540/PA1541) are also upregulated albeit to a lesser extent (3.26/3.54 FC respectively), and even though the proteins are still uncharacterised, they are identified as integral membrane components with PA15141 classed as a probable drug efflux transporter (Pseudomonas.com). Moreover, the increased expression of genes involved with *P. aeruginosa* RND efflux pumps, in particular MexRAB-OprM (54.71/25.58/16.63/8.5 FC increased in blood when compared to bone), will most likely result in a generalised increased in resistance [330], and not to a specific adaptive response, which potentiates the development of multidrug resistance bacteria.

4.3.2 Lack of AQ production

The inability of the CW4 and CW5 isolates to produce AQs is clearly a consequence of multiple mutations in genes involved in both AQ biosynthesis and AQ signal transduction. For example, PqsR, the dedicated LysR-type regulator for the *pqs* biosynthesis operon (described in detail in [331]) carries a predicted inactivating mutation (see Chapter 3 Table 20). In addition, genes (*trpE* and *kynB*) in two of the main pathways for anthranilate biosynthesis, a key precursor for all the AQs, carry other substitutions, even tough these are not predicted to affect the function of the

respective proteins (Table 24). The inability of CW4 and CW5 isolates to produce AQs is also likely to have implications for iron-acquisition given that PQS is an iron chelator involved in regulating the iron starvation response [332]. Nevertheless, the causality of these mutations can only be confirmed after individual complementation with plasmids containing a wild-type copy of these genes rescues AQ production in patient X isolates.

4.3.3 Siderophore production, iron metabolism and CSS systems

Siderophore production is directly relevant to *P. aeruginosa* virulence, (see sections 3.3.1 and 4.1). Although differences in siderophore production between profile 1 and profile 2 isolates initially appeared to be limited to PVD production (Table 23), PCH production also varies (see Figure 42). Profile 1 isolates (bone) produce on average 14,643 ± 3,854 RFU/OD_{600} of PVD and 12,370 ± 1,636 RFU/OD_{600} of PCH, while profile 2 isolates (blood) produce negligible amounts of PVD (1,778 ± 156 RFU/OD_{600}) and on average 27,011 ± 2,282 RFU/OD_{600} of PCH. This suggests the occurrence of a siderophore switch in blood isolates, with the production of PVD being lost and the production of PCH increasing when compared to bone isolates.

With respect to this, the SNP variation analysis carried out between CW5 bone and blood isolates identified a mutation in *pvdS* – that encodes PvdS, an ECF sigma factor responsible for the coordinated expression of the PVD-related genes. The *pvdS* substitution p.V26A is predicted to have a mild effect on the PvdS protein since alanine is chemically similar to valine [333]; however, it is likely that this caused the switch of PVD by PCH production in blood isolates (Figure 42). In fact, this same mutation was identified in *P. aeruginosa* PA_D22, a strain taken from a patient with

ventilator associated pneumonia, and in this recent study the authors associated the p.V26A mutation to a reduced PvdS functionality [324]. Previous work also states that, among other aa, the leucine adjacent to that position (L25) is conserved throughout sigma proteins, and residues at these positions were implicated in the binding of core RNA polymerase by σ^{70} [325].

As discussed in the introduction of this chapter, a recent study suggested that PvdS released from FpvR is non-functional, and is transcribed *de novo* in the absence of FpvR [293]. However, the transcriptome analysis identified a 62.16-fold increase in *pvdS* transcription in blood isolates when compared to bone isolates while there was only a 2.41-fold increase in *fpvR* transcription (Table 31), so it is unlikely that FpvR is inhibiting PvdS activity. In a recent review, Chevalier and collaborators describe the PvdS regulon as containing about 80 genes, that are involved with pyoverdine biosynthesis and uptake, but also with T3SS [334]. A binding-motif TAAAT-N16/17-CGT was identified upstream of PvdS-dependent genes in a first transcriptome analysis of *P. aeruginosa* response to iron-limitation [335], and the full regulon, as well as other σ factor-associated networks, was identified for PA14 [336]. Apart from the PVD-related genes (whose function and mode of action is reviewed in detail by [337], other genes were identified as part of the PvdS regulon, namely *piv*/*prpL*, *toxA*, *sspA*/*B*, *exsA*, and *exoT*/*S*. ExsA had been already linked to PvdS in other pseudomonads [338], and codes for a major T3SS regulator, that is also controlled by SigX, an ECF σ factor involved with the control of osmolarity in *P. aeruginosa* [339].

From the results of the transcriptome analysis, *exsA* was downregulated 7.94-fold in CW5 blood when compared to the bone isolate – as were other genes involved

with T3SS (Figure 64). Apart from *exsAB*, mainly other housekeeping σ factors like RpoN, RpoS, and SigX regulate the expression of proteins involved with T3SS. In blood isolates, the downregulation of genes involved with protein transport and secretion, as well as biofilm formation and biosynthesis of extracellular polysaccharides (Table 27) are indicative of a free-living lifestyle, which is an expected adaptation to bloodstream colonisation. Moreover, a 2mM (8mg/dL) concentration of Ca^{2+} is sufficient to repress the expression of *P. aeruginosa* T3SS genes in vitro [340, 341], and the normal reference range of calcium in human blood is between 8.8 and 10.5 mg/ dL, so enough to induce such downregulation.

Although the expression of the genes involved with PVD biosynthesis did not change significantly (not shown), those involved with PVD uptake were upregulated. These included the *fpvGHJK* and *fpvCDEF* operons that can also be linked to the regulation by other σ factors, specifically FpvI. The σ/anti-σ pair FpvI/FpvR was upregulated 5.13/ 2.4-fold respectively, which is enough to upregulate the TBDTs FpvA and FpvB, the *fpv* operons mentioned above, and other genes such as *hasR* and *prrH* (see Tables 30 and 31). In summary, it is reasonable to assume that the low PVD production is indeed caused by the low functionality of the PvdS protein due to the p.V26A mutation, even though further confirmation has to be done by complementing the CW5 blood isolate with a copy of the CW5 bone *pvdS* gene.

Interestingly, there are three *P. aeruginosa* sigma factors whose motifs are AT-rich: FpvI, FecI, and FecI2 (see Figure 2 in [336]), and this is a particular characteristic of iron-starvation target promoters which harbor an “iron box” [342]. FecI is involved with the uptake of ferric citrate and was identified as the only iron-

starvation sigma factor in *E. coli* [343].It is also upregulated 7.66-fold in *P. aeruginosa* CW5 blood isolates when compared to bone isolates (Table 31). On the other hand, FecI2, identified as PA14_27690 in PA14, is commonly present in *P. aeruginosa* but is missing in the PAO1 reference strain [344]. The FecI2 regulon encompasses 19 iron-starvation and virulence-related genes, and the majority of these are upregulated in CW5 blood isolates when compared to bone isolates, including: *pchR* (29.37), *hasR* (19.32), *hasAp* (30.23), *phuR* (45.62), *hxuC* (13.22), *fecA* (7.88), and *pvdS* (62.16) (Appendix E).

Importantly, FecI2 also regulates itself, however since *fecI2* is absent from laboratory PAO1 strains, our initial transcriptome analysis using the PAO1 genome as a reference did not map this gene. When using CW5B1 as reference, there were less than 5 reads mapped to *fecI2* in all conditions (either bone or blood isolates at both time points), so a more detailed analysis using RT-qPCR will be needed to evaluate the conservation and expression of this gene. Nonetheless, the overexpression of PCH-related genes (Figure 65) and the subsequent increased production of PCH in blood compared to bone isolates (bottom plot, Figure 42) can be related to the increase in *pchR* expression. Note that the only σ factor associated with *pchR* is FecI2, by both RNA and motif analysis [336]. In conclusion, the data obtained supports the hypothesis that the p.V26A mutation identified in *pvdS* affects the protein's function since (i) the expression of all genes specific to the PvdS regulon is not changed, even though expression of PvdS is increase 62-fold in CW5 blood when compared to CW5 bone isolates, and (ii) the overexpression of other iron uptake systems can be explained by the action of alternative ECF sigma factors.

Since PCH has a much lower affinity for iron (K_f= 10^5 M^{-1}) [345] than PVD (K_f=10^{24} M^{-1}) [223], it is possible that its main role might be associated with regulatory systems through cell-surface signalling instead of iron chelation. Other authors have suggested that the role of siderophores during infection is beyond simple iron chelation, and that targeting siderophore-mediated virulence regulation might have therapeutic potential [346]. In the CW5 blood isolates iron acquisition most likely involves haem uptake, and is probably mainly accomplished through the *phu* system (right side Figure 38) since *hemO* and *phuS* that code for haem oxygenase proteins are hugely upregulated when compared to bone isolates (FC of 100.99 and 47.70 respectively).

Moreover, other genes involved with haem acquisition are upregulated, as well as CSS systems for heterologous siderophores such as enterobactin produced by enteric bacteria such as *E. coli* (Table 31). It is possible that some siderophores produced by bacteria in the gut [347] might leak into the bloodstream and through CSS systems and two component systems (e.g., the PfeR/S two component system for enterobactin transport that is overexpressed in CW5 blood compared to bone isolates) (check Table 30, FC of 49.90 and 42.21 respectively), *P. aeruginosa* is able to sense and upregulate the production of diverse heterologous iron chelator receptors, effectively hijacking iron (a process known as siderophore piracy – see [282]).

4.3.4 *fliJ* mutation – effect on motility

The CW5 blood vs bone isolate genome analysis further identified several SNPs specific to each isolate, but only 4 mutations were common to the three CW5 blood isolates analysed (profile 2: E, F, and H genomes) and not present in any of the

three CW5 bone isolates (profile1: C, D, and G genomes). From these mutations (Table 25), the *mexZ* deletion and *pvdS* substitution have already been discussed. The *in silico* analysis further revealed a synonymous substitution in *amn* that does not affect the protein, and a *fliJ* non-synonymous substitution that has a drastic effect on the FliJ protein (Figure 48).

As the predicted effect of the *fliJ* substitution was a loss of the FliJ protein, it was hypothesised that this mutation would negatively influence motility. Note that the *fliJ* mutation is not present in earlier time point isolates sampled from the same patient (CW4 T1 and CW4 T40 – genomes A and B), but the genetic background of all the isolates analysed is identical. As such, this result becomes even more interesting since isolates with both phenotypic profiles were present in the tissue (CW5 T). To test the extent to which motility was affected, three motility strategies commonly used by *P. aeruginosa* were evaluated.

Swarming is regulated by a plethora of genes and is one of the most complex forms of motility. The QS RhlR/C4-HSL system controls the production of rhamnolipid surfactants, which are required to reduce the surface friction and allow the swarm colony to move across surfaces, through the regulation of *rhlAB* [348]. Since CW5 profile 2 isolates from patient X produce C4-HSL, their inability to swarm is more likely a consequence of the lack of a flagellum rather than a QS defect. This is supported by the microscopy data (Figures 55 to 57) that shows that phenotypic profile 2 isolates are incapable of producing flagella, while phenotypic profile 1 isolates have normal, functioning flagella. Moreover, CW5 bone isolates, which have both *las* and *pqs*

systems affected but the *rhl* system intact, can swarm, even though they do not develop the dendritic fractal-like pattern typical of PAO1 (Figure 54).

Twitching motility requires type IV pili and although analysis of CW5 profile 1 and profile 2 isolate genomes did not reveal any mutations in *pil* operons, both isolates show similar but reduced twitching (Figure 54) compared with PAO1 probably as a consequence of the pleiotropic mutations to global regulatory genes. In contrast to the CW5 profile 2 isolate which could not swim consistent with the *fliJ* mutation and loss of flagella, the CW5 profile 1 isolate exhibited the same swimming phenotype on agar plates as PAO1 (Figure 54).

In addition, flagella are important during infection and for biofilm formation because of their role in bacterial adhesion to surfaces and invasion of host cells (reviewed in [272]). Flagellin can be recognised and targeted by the immune system as discussed in Chapter 3, and several publications have shown that *P. aeruginosa* strains with functional flagella are cleared swiftly in acute infection modes [349, 350]. As such, the loss or lack of flagella was hypothesised to offer an advantage for *P. aeruginosa* during an infection, and indeed strains with mutations in flagella-related genes have been found to be positively selected during acute lung infections [351], and during colonization of the gastrointestinal tract in mice [352]. However, a study using a PA14 Δ*lasR* mutant with Tn insertions in several genes encoding flagella components found that the loss of flagella in this virulence attenuated strain did not confer a selective advantage in an acute murine infection model, and suggested that the infective process of *P. aeruginosa* in a chronic biofilm model only required instead expression of flagellin [353].

The *P. aeruginosa* CW5 blood isolates exhibited strong upregulation of the majority of the genes involved with flagellum assembly (~76%) and cell motility (~61%) (Table 28 and 32) even though they do not produce flagella and are non-motile. The lack of FliJ because of the *fliJ* mutation renders the bacteria incapable of exporting the initial hook subunits since this depends on the FlhA-FliJ protein-protein interaction [321]. Consequently, there appears to be a feedback mechanism since the production of FliC, the flagellin filament protein, and MotY, a protein involved with the generation of the proton flow, are strongly downregulated (32.97, and 39.08 FC respectively) in CW5 blood isolates when compared to CW5 bone isolates, although such mechanism has not been previously described. From these observations, we can hypothesise that initially, in the localised tissue infection, the *fliJ* mutation may have reduced bacterial fitness, but it facilitated a successful colonisation of a new niche since it facilitated evasion of host innate immunity. This is consistent with the suggestion that the main driver for *P. aeruginosa* pathogenicity is the host response rather than the actual use of specific virulence factors [353, 354].

4.3.5 Infection pilot assays

From the data discussed so far, it can also be hypothesized that the loss of the flagellum, and / or the *pvdS* mutation increased the ability of *P. aeruginosa* to spread systemically in patient X despite the loss of swarming and swimming motilities, and the PVD to PCH switch. To test this hypothesis, two sets of pilot experiments were conducted: one using a mouse model that has been extensively used to investigate chronic wound infections [147, 355], and the other using *G. mellonella* larvae, identified as a good predictor for *P. aeruginosa* virulence [146]. Both experiments

tested the ability of CW5 bone vs blood isolates to cause infection using either bacterial cells or cell-free supernatants.

Overall, the results from the mice pilot (Figure 59) did not reveal any reproducible major differences between CW5 bone (profile 1) and blood isolates (profile 2), and suggests that both isolates are able to spread systemically. In addition, results from the larvae pilot (Figure 58) did not reveal consistent differences between the ability of CW5 bone or blood isolates to kill the larvae. In detail, results were heavily dependent on the growth medium used, as when bacterial cells were used the CW5 bone isolates were deadlier than CW5 blood isolates in both media, but when supernatants were used the reverse happened (even though the difference in larvae survival is only significant for LB, and not for WLM).

Taken together these observations seem to indicate that the CW5 blood isolates have not become more virulent due to the phenotypic differences observed, particularly the absence of the flagellum and the siderophore switch that might be expected to reduce virulence. However, there seems to be a direct link with the media in which bacteria are grown and their virulence effect, in both larvae and mice. As discussed before, the wound environment could be influencing the behaviour of *P. aeruginosa* and, as such, these experiments will probably be more informative if done in a model that can closer mimic the conditions of the host, including the damage diabetes does in the immune system [64].

4.4 Conclusion

Opportunistic pathogens such as *P. aeruginosa* that can infect a multitude of different hosts and subsist in heterogeneous environments such as hospital settings [356], excel at being highly adaptable. It has however it been suggested that *P. aeruginosa* virulence determinants are host specific [357]. As such, the relevance and context of virulence factors for infections and particularly the great importance of host context must be taken into consideration when selecting disease models to test for specific characteristics relevant to different infection stages [358].

With the insight provided by the pilot host-pathogen interaction experiments, one possible scenario is that the *fliJ, pvdS* and *mexZ* mutations appeared in the *P. aeruginosa* population through clonal expansion after the restriction of *P. aeruginosa* growth was removed due to the loss of selective pressure exerted by other microorganisms in the wound. It can be speculated that isolates with both profiles 1 and 2 entered the blood vessels – since the biopsy from CW5 tissue had both in a 2:3 ratio (profile 2/profile1) – and activated the patient's innate immune response. However, blood isolates have an advantage since the loss of flagella facilitates evasion of immune system detection via toll receptor 5 [245, 246]. This may have allowed profile 2 bacteria to spread systemically, successfully colonising the blood and triggering sepsis. At this point, the antibiotics administered may not have been effective as the bacteria were actively upregulating genes involved in regulating efflux pumps associated with increased antibiotic resistance. Foot amputation removed the source of *P. aeruginosa* infection and saved this patient's life probably as the high dose intravenous antibiotics were only able to clear the

bloodstream infection, but were not able to clear the *P. aeruginosa* deep tissue/bone infection that persisted in the diabetic foot ulcer.

While bacteraemia is uncommon in diabetic patients, without proper care osteomyelitis will develop and this deep-seated infection will most likely reach the circulatory system and cause major systemic infection. Even when diabetic patients recover from sepsis, recent studies suggest that there is an increased long-term mortality due to sepsis-associated persistent alterations in innate and adaptive immune responses, that will lead to chronic inflammation, immune suppression, and bacterial persistence (reviewed in detail in a recent work by [359]).

Therefore, there is an urgent need to deepen our knowledge of bacterial transition from a well-adapted and stable infection site where there is a homogenous population to become blood-stream invasive. The fine-tuned balance between polymicrobial communities, which also promotes increased selective pressures for antibiotic resistance to emerge, plays a significant role in this. Hence studies of the interactions between *P. aeruginosa* and *S. aureus* that co-existed within diabetic wound ulcers will be presented in Chapter 5.

Chapter 5: *P. aeruginosa* and *S. aureus*: Ecologic Interactions and Evolution in Chronic Diabetic Foot Ulcers

5.1 Introduction

In Chapter 4 it was hypothesised that the development of phenotypic heterogeneity in a stable *P. aeruginosa* population isolated from a long-term diabetic ulcer could be due to differences in wound bacterial diversity. In Chapter 1 section 1.6.1 the evolution of bacterial diversity was discussed and the polymicrobial context of infections in diabetic chronic ulcers was highlighted. In this chapter experiments exploring interactions between the previously characterised *P. aeruginosa* wound isolates and *S. aureus* sampled from the same patients will be described.

S. aureus is a Gram-positive bacterium that can either be a human commensal, transiently colonising the skin and upper respiratory system, or a highly virulent pathogen that causes a wide range of diseases such as skin infections or pneumonia that can evolve into life-threatening septicaemia [360, 361]. *S. aureus* is associated with hospital-acquired infections, and has the ability to form biofilms, particularly on implanted medical devices, leading to for instance to endocarditis and osteomyelitis [362].

S. aureus and *P. aeruginosa* co-infections are common in chronic diabetic [131] and non-diabetic wounds [363], and in the lungs of CF patients [364], but also in acute burn wounds [365] or catheter-related infections [366]. The presence of both pathogens is a sign of poor prognosis [367, 368], especially if one or both are multi-antibiotic resistant organisms [131, 369]. The abundance of each species varies from

location to location since bacterial diversity has been linked to factors such as geographical and climate conditions, hygiene habits, over-the-counter availability of antibiotics, and poor control over self-medication (see Chapter 1 section 1.6).

A retrospective anonymised data mining study was done in collaboration with three clinical institutions (Ethics reference no: 253-182, approved by the Faculty of Medicine & Health Sciences Research Ethics Committee). Over a one-year period, three cases of *P. aeruginosa*/*S. aureus* co-infections were detected in non-diabetic wounds, while 22 cases were detected in diabetic foot ulcers in the Nottingham City Hospital diabetic ward and diabetic foot clinic. At the same institution, but over a four-year period, *P. aeruginosa* was found in 16.5% to 22.3% of wounds, while *S. aureus* was found in 20.2% to 26.6% of wounds, and co-infection with both species varied between 0.9% and 1.7% (data from 1344 ulcers). Data of 60 ulcers from the High Risk Foot Service at Liverpool Hospital in Australia revealed that *P. aeruginosa* was present in 8.3% while *S. aureus* was present in 20%, and co-infection was present in 3.3% of the infected ulcers. On the other hand, data of 83 ulcers from the Southwest Regional Wound Care Center in Texas revealed a similar proportion of individual colonisation of *P. aeruginosa* (7.2%) and *S. aureus* (24.1%), but no ulcer was infected with both simultaneously.

One of the biggest problems when comparing bacterial diversity data from different countries is the different sampling techniques used. Swab cultures have been shown to underestimate the presence of, for instance, *P. aeruginosa* in chronic wounds when compared to tissue biopsy [114], and this may be explained by a different spatial structure of *P. aeruginosa* and *S. aureus* in chronic wounds: while

S. aureus has a tendency to colonize the surface of the wound, *P. aeruginosa* is mainly found in the deepest part of the tissue as seen in Figure 66 [115]. Recent publications on other chronic infection scenarios have highlighted the relevance of spatial structure for bacterial community dynamics and ecological interactions [370].

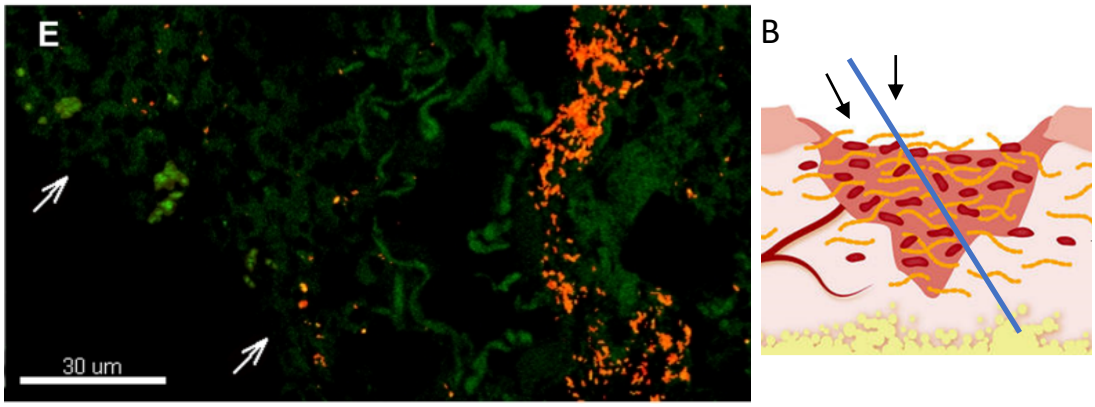


Figure 66: Confocal laser scanning microscopy images of *S. aureus* and *P. aeruginosa* in chronic wounds. The bacteria were detected by PNA-FISH with a mixture of FITC-labelled *S. aureus*-specific probe (green) and TxR-labelled *P. aeruginosa*-specific probe (red). The section of the wound was made according to the diagram (B) and arrows point to the wound surface. Scale bars: 30 µm (adapted from [115]).

Individual virulence factors of *P. aeruginosa* and *S. aureus* have been widely studied [184, 371-373]. Briefly, well-known *S. aureus* virulence factors include fibronectin-binding proteins, clumping factors and collagen-binding proteins involved with cell adhesion – reviewed in [374], and cell wall-anchored proteins involved with tissue colonisation and invasion [375]. Protein A (SpA) [376], staphyloxanthin [377], and capsular polysaccharides are also involved with evasion from host defences [378], while the small pore-forming toxin α-hemolysin (Hla), Panton-Valentine leukocidin (PVL), the phenol soluble modulins (including δ toxin), and numerous other exotoxins and exoproteases cause tissue damage, reviewed by [379]. Furthermore,

S. aureus is able to induce blood coagulation [380], and has diverse iron scavenging mechanisms fine-tuned to acquire iron from the host [381].

Similar to the *P. aeruginosa* quorum-sensing system described in Chapter 3 introduction, *S. aureus* is able to upregulate virulence pathways through QS via, for instance, the accessory gene regulator (agr) system [382, 383]. In *S. aureus* QS differentially regulates the production of both cell surface (negatively regulated) and secreted (positively regulated) virulence factors [384].

In recent years there has been an increased awareness towards the impact of interspecies interactions in treatment failure due to antibiotic resistance, and several researchers have focused on elucidating the mechanisms of *P. aeruginosa – S. aureus* interactions. For example, *P. aeruginosa* has been shown to inhibit *S. aureus* respiration through the production of HQNO [385], and induce resistance toward antibiotic killing [386]. *P. aeruginosa* has also been shown to stimulate *S. aureus* virulence, pigment production, and biofilm formation [377, 385, 387]. Besides, *P. aeruginosa* can use rhamnolipids to disperse *S. aureus* biofilms [388], and even kill and use *S. aureus* as an iron source through the action of the LasA protease [389].

S. aureus has evolved different ways of dealing with these stressors such as increasing its resistance to molecules that inhibit respiration by the formation of small colony variants [386], or shift from aerobic respiration to lactic acid fermentation, producing lactate [390]. Moreover, *S. aureus* can stimulate production of *P. aeruginosa* virulence factors through peptidoglycan sensing [233], the *S. aureus* adhesin SpA was found to inhibit *P. aeruginosa* biofilm formation [391], and co-evolution with *S. aureus* was associated with alterations in *P. aeruginosa* LPS

biosynthesis [392]. However, the majority of these interspecies studies mentioned above used well characterized laboratory strains.

Laboratory adapted strains of *P. aeruginosa* effectively kill co-cultured *S. aureus*, but when clinical strains are used these bacteria exhibit an almost commensal interaction. For example, a dominant CF lineage of *P. aeruginosa* has been shown to develop a commensal-like interaction with *S. aureus* [172]; *P. aeruginosa* was shown to protect *S. aureus* from *Dictyostelium discoideum* phagocytosis in biofilms [393], and increase its tolerance to several antibiotics [394]. Another recent study using *P. aeruginosa* and *S. aureus* strains associated with skin infections found that *S. aureus* mediates a significant increase in *P. aeruginosa* attachment to human keratinocytes [395].

The dynamic long-term infection environment of diabetic chronic wound ulcers will most likely allow bacteria to establish a community that potentiates microbial interactions, either by niche competition or cooperation. However, the interaction between bacterial pathogens occurring *in vivo* is likely to be different from the interaction between laboratory adapted strains, so in this chapter clinical isolates of *S. aureus* and *P. aeruginosa* isolated from the same or different diabetic chronic ulcers and their interactions will be investigated.

5.2 Results

The growth of *P. aeruginosa* and *S. aureus* isolated from CW2 Bone and CW4 Tissue in SWF was monitored over 20 h. The number of colonies in each dilution plate

was used to calculate the number of colony forming units (CFU) per mL at each time point for each sample (in triplicate) (Figure 67).

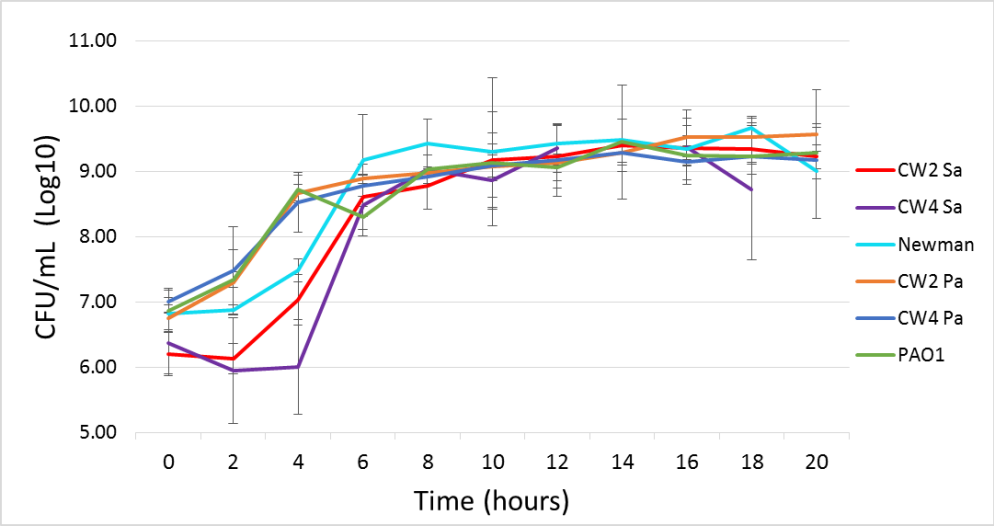


Figure 67: Growth curves for *P. aeruginosa* and *S. aureus* chronic wound isolates and lab adapted strains (PAO1 and *S. aureus* Newman). Error bars represent the standard deviation between triplicates. CW2, isolates from bone sample of patient; CW4, isolates from tissue sample of patient X; Sa, *S. aureus*; Pa, *P. aeruginosa*.

Under the conditions used, the *S. aureus* strains exhibit a longer lag phase than *P. aeruginosa* during the first 5 h, but both two species reach similar stationary phase cell numbers. This effect is more pronounced in both *S. aureus* chronic wound isolates (CW2 *S. aureus* / CW4 Sa) than in the lab strain Newman. To account for this and avoid giving *P. aeruginosa* an advantage in co-culture, all other experiments used a 1:2 (*P. aeruginosa*/ *S. aureus*) inoculation rate when growing the bacteria overnight in a liquid mixed culture.

5.2.1 P. aeruginosa vs S. aureus colony drop assays

Cultures of *S. aureus* and *P. aeruginosa* were added as spots onto dry LB agar plates. Three isolates of *S. aureus* (the lab strain Newman, the MSSA from CW2, and the MRSA from CW4) were spotted in triplicate with five isolates of *P. aeruginosa*

from each representative DFU sample type. After incubation, the interacting colonies were photographed (Figure 68).

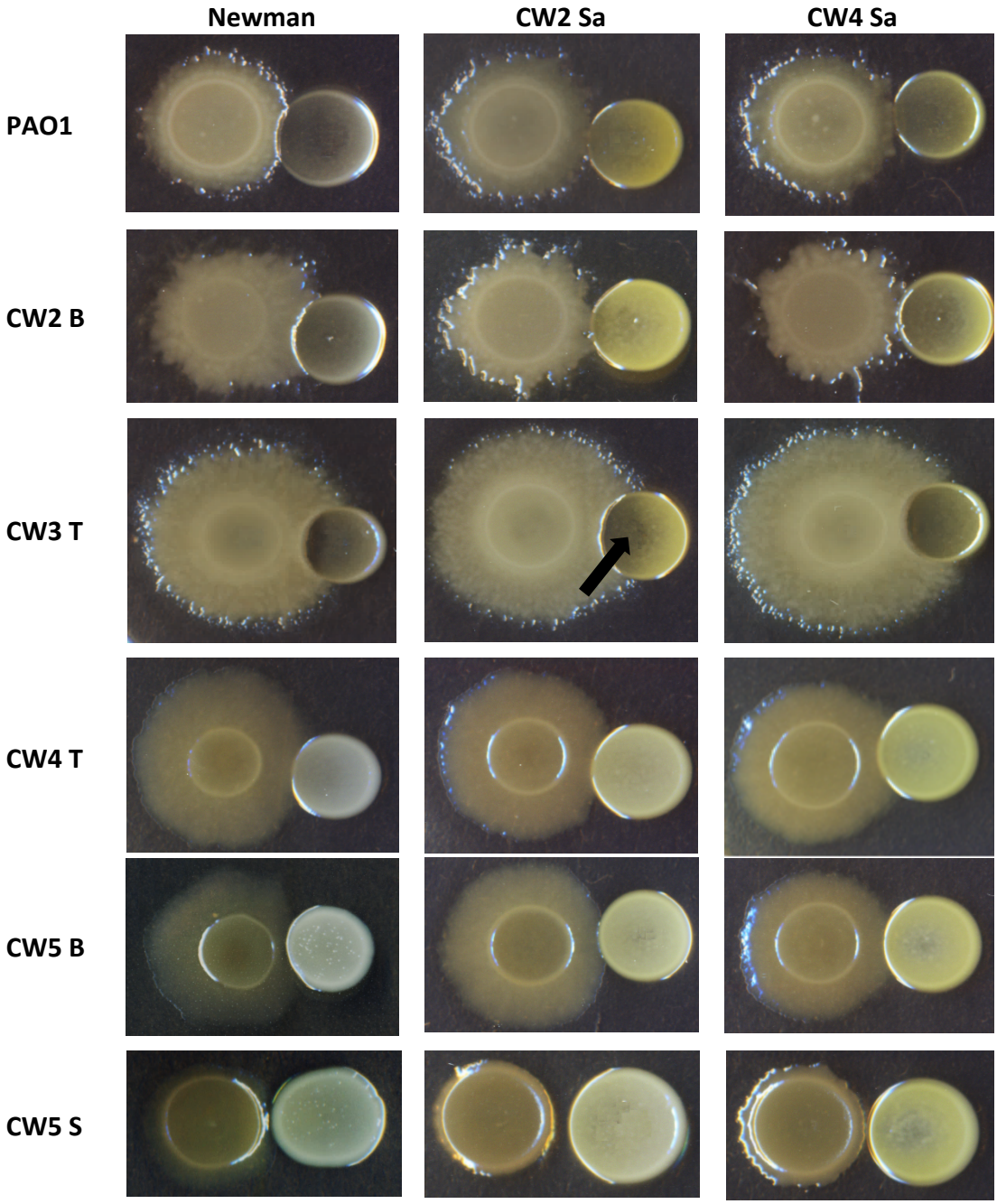


Figure 68: *P. aeruginosa* and *S. aureus* colony drop interaction assays. Spots were plated 5 mm apart from overnight bacterial cultures diluted to OD_{600}~0.2. Each column (right spot) represents a different *S. aureus* (Sa) strain: Newman, *S. aureus* isolated from CW2, and *S. aureus* isolated from CW4; and each row (left spot) represents a different *P. aeruginosa* strain; CW - chronic wound, B - bone, T - tissue, S – blood; black arrow indicates an example of a zone of *S. aureus* clearing; each assay was repeated in triplicate (representative data shown).

P. aeruginosa strains PAO1 and CW3 induced a zone of clearing in all three *S. aureus* strains, while *P. aeruginosa* and *S. aureus* isolated from the same wound did not influence each other (CW2 B vs SA CW2, and CW4 T vs SA CW4). Additionally, all *S. aureus* strains appeared not to be negatively influenced by isolates from patient X (CW4/CW5), and showed a whiter colour than when plated alone or with other CW.

5.2.2 *P. aeruginosa* vs *S. aureus* cell-free interaction assays

Cell-free interactions between *P. aeruginosa* and *S. aureus* isolates were investigated over time using a transwell membrane set-up (see Figure 16) that allowed the incubation of each species in the same well but on either side of a membrane, with *S. aureus* always in the top compartment and *P. aeruginosa* always in the bottom compartment, to mimic their distribution in a chronic wound setting.

As expected, *S. aureus* grew slower than *P. aeruginosa* during the first 5 h in both co-culture and monoculture conditions, and this effect was more pronounced for CW4 isolates than for CW2 isolates (Figure 69). For both CW2 and CW4 isolates *S. aureus* grew more than *P. aeruginosa* in both conditions between 10 and 12 h. For 24 and 48h time points, in CW2 isolates (top plot Figure 69) *P. aeruginosa* and *S. aureus* growth was comparable, while in CW4 isolates (bottom plot Figure 69) there was a decrease in *S. aureus* grown in co-culture, when compared to *S. aureus* grown in monoculture, and vice-versa for *P. aeruginosa*.

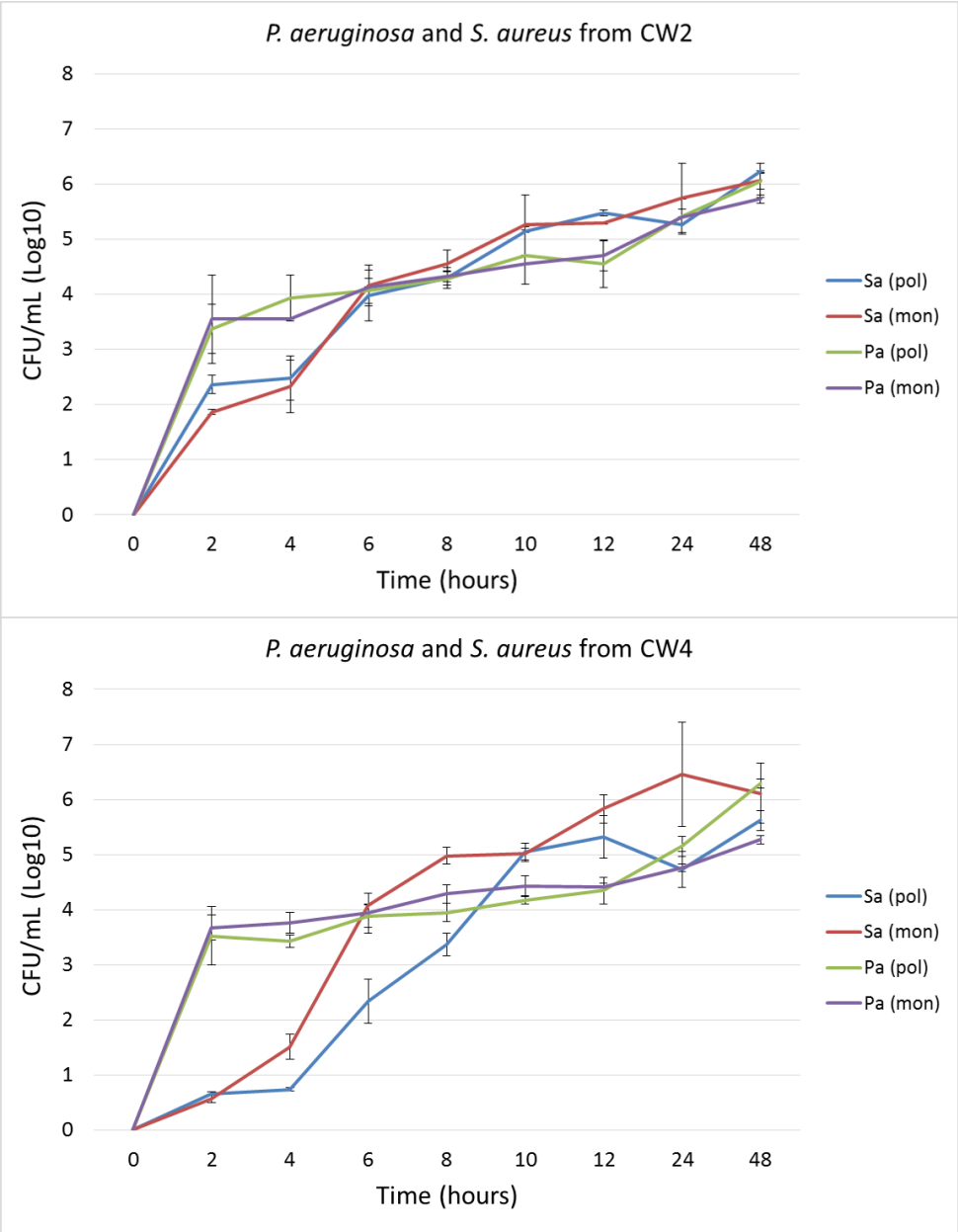


Figure 69: Cell-free interactions between *P. aeruginosa* and *S. aureus* grown in SWF. Bacteria were either grown in co-culture (pol) or in monocultures (mon) – see Figure 16 (section 2.12) for diagram of transwell assay set-up. Top: bacteria isolated from CW2 Bone (patient V), bottom: bacteria isolated from CW4 Tissue (patient X).

In this first experiment each compartment was sampled every 2 h after initial seeding, however in the co-culture settings, *P. aeruginosa* colonies were found in plates from Sa-only compartments (and vice-versa). This cross-contamination likely happened due to difficulty in taking 100 µL from the bottom compartment without removing the transwell from the plate, and without the tip touching the medium in

the top compartment (Figure 70). Thus, the cell-free interaction assay was repeated, and this time sampling was done only once, at 24 h (Figure 71).

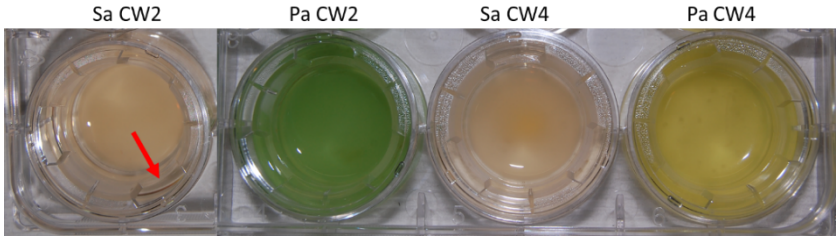


Figure 70: Monocultures of *S. aureus* and *P. aeruginosa* in the cell-free interaction assay after 24 h incubation. Red arrow points to one of the slits that enables a sample to be taken from the bottom compartment. *S. aureus* (Sa) was incubated in the top compartment, while *P. aeruginosa* (Pa) was incubated in the bottom compartment.

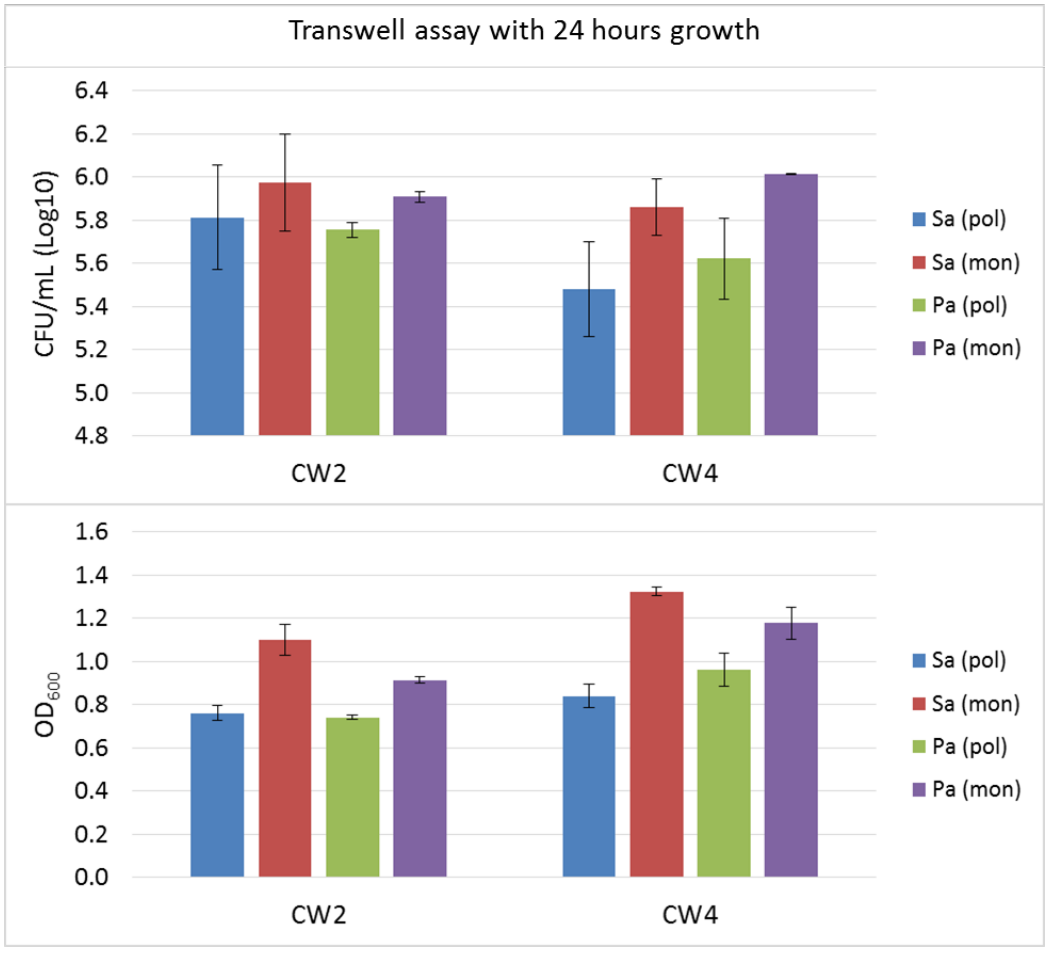


Figure 71: Cell-free interactions between *P. aeruginosa* and *S. aureus* grown in SWF for 24h. Bacteria from CW2 Bone (left) and CW4 Tissue (right) were either grown in a co-culture (pol) or in monocultures (mon) – see Figure 16 (section 2.12) for diagram of transwell assay set-up. Top: CFU/mL calculated from 10^{-6} dilution plates, bottom: OD_{600} (read using 100 µL).

In this second assay bacteria were sampled after 24 h of incubation. Results were mostly consistent with what was observed in the first assay (Figure 69). In CW2 isolates (left side of both plots in Figure 71), both *P. aeruginosa* and *S. aureus* growth was slightly inferior in co-culture when compared to monoculture. In CW4 isolates (right side of both plots in Figure 71), there was also a decrease in *P. aeruginosa* and *S. aureus* grown together (co-culture), when compared to each species grown alone (monoculture). These differences were more evident in the CFU/mL plot (top) than on the OD_{600} plot (bottom).

This inconsistency was probably caused by the formation of biofilms on the bottom of the wells. Compared to growth in 50 mL tubes with 200 rpm shaking, the slower shaking speed used for this set-up (60 rpm) allowed bacteria to aggregate more. However, in chronic wounds bacteria grow in tissue, which presents a solid matrix where spatial structure is important, as discussed in the introduction. Therefore, a semi-solid biofilm model was adapted and used to quantify *P. aeruginosa* and *S. aureus* interactions.

5.2.3 *P. aeruginosa* and *S. aureus* interactions in a semi-solid biofilm model

An adaptation of the semi-solid *in vitro* wound biofilm model described by [173] was used to investigate the interactions between clinical isolates of *P. aeruginosa* and *S. aureus* sampled from two distinct diabetic foot ulcers. This *in vitro* biofilm model mimics the non-surface attached spatial distribution of mature biofilms found in chronic ulcers, as discussed in the introduction, and involves growing bacteria between two agar layers (Figure 72).

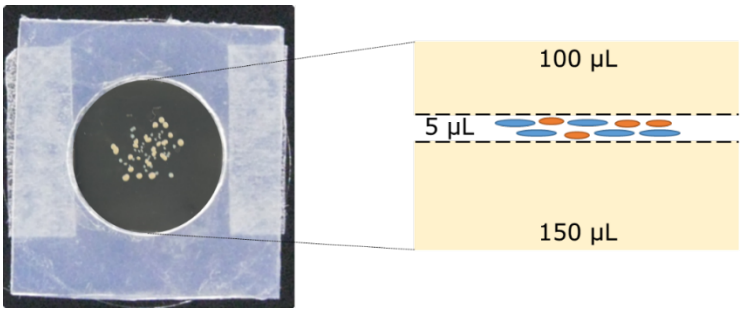


Figure 72: Semi-solid *in vitro* biofilm model of *P. aeruginosa* and *S. aureus* polymicrobial infection. Here, bacteria from CW2 Bone were grown between two agar layers in Bolton broth agar (0.5%) cast in a 2 x 2 cm silicone mould.

Bacteria were inoculated into the semi-solid biofilm model either from mixed overnight cultures, where 2 colonies of *S. aureus* + 1 colony *P. aeruginosa* were grown in the same tube (red arrow in Figure 18, section 2.13.1), or from monoculture overnights mixed at the time the gel was cast (blue arrow in Figure 18, section 2.13.1). These two methods yielded comparable results (not shown), and for all other experiments, bacteria were grown O/N independently and then mixed in a dilution 10^{-3} before further diluting to 10^{-4} cells in the medium used to make the gel (either Bolton broth or SCW), and then inoculated, as described in methods section 2.13.1. This option was used to avoid the disadvantage of the initial slow growth rate of the clinical *S. aureus* isolates, as previously discussed (see Figure 67).

When bacteria were incubated between two Bolton broth agar layers, and the gels were incubated for 24 h at 37 °C, CFU/mL viable counts revealed that for CW2 isolates *S. aureus* did not show any differences when grown alone or in co-culture, while *P. aeruginosa* shows a higher fitness when grown in co-culture (left side, Figure 73). For CW4 isolates the inverse happened, and *P. aeruginosa* grew the same alone or in co-culture, while *S. aureus* had an advantage in co-culture (right side, Figure 73).

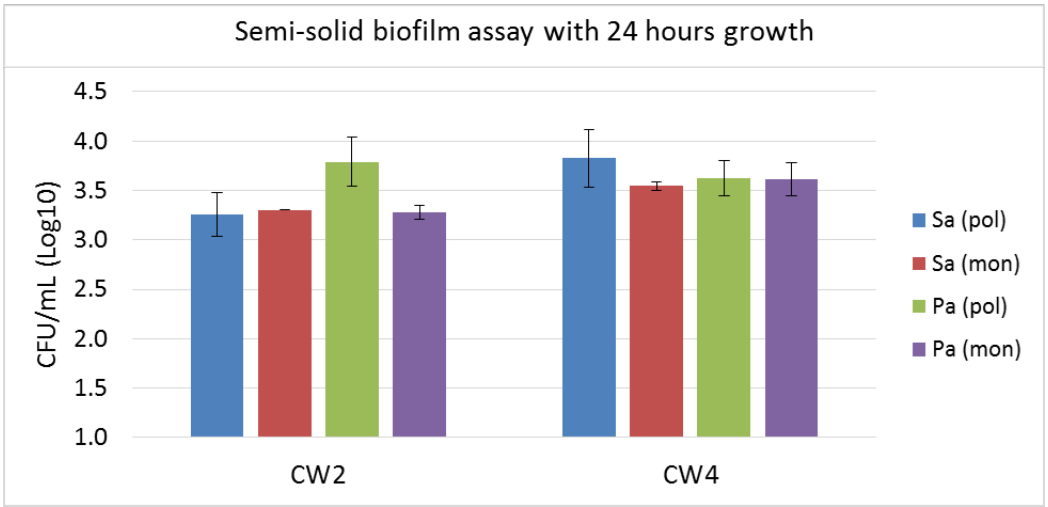


Figure 73: *P. aeruginosa* and *S. aureus* interactions in a semi-solid biofilm model. Bacteria from CW2 Bone (left) and CW4 Tissue (right) were either grown in co-culture (pol) or in monocultures (mon).

These results are different from the data obtain from the cell-free interaction assay, which is expected since the spatial structure has been shown to be very relevant for polymicrobial interactions of these two species [396, 397]. In order to understand in more detail whether *P. aeruginosa* and *S. aureus* are capable of forming polymicrobial biofilms, bacteria grown in the semi-solid biofilm model were examined using confocal microscopy.

Since the clinical strains from both species were not tagged, a fluorescent Gram stain method, developed by [174], was used. This method involves the use of two fluorescent dyes, Syto 13 (a non-discriminatory nucleic acid stain that exhibits bright, green fluorescence upon binding to nucleic acids) and hexidium iodide (a nucleic acid stain that selectively stains almost all Gram-positive bacteria). With this it is then possible to distinguish between the Gram-negative *P. aeruginosa* labelled in green, and the Gram-positive *S. aureus* labelled in orange due to a combination of green and red fluorescence (Figure 74).

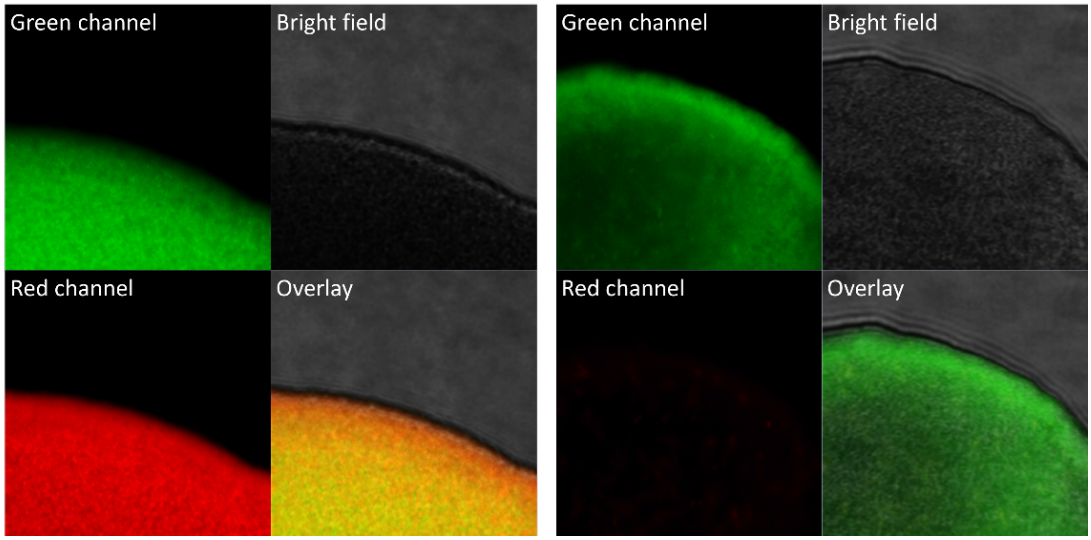


Figure 74: Example of fluorescent Gram stain in chronic wound isolates of *S. aureus* and *P. aeruginosa*. *S. aureus* (left) and *P. aeruginosa* (right) isolated from CW2 grown in monoculture were inoculated in semi-solid biofilm model. All cells were rendered green by Syto13, while hexidium iodide rendered only Gram positive red, resulting in orange overlay.

CW2 and CW4 *S. aureus* and *P. aeruginosa* isolates were incubated using Bolton broth agar in the silicone moulds or in 8-well chamber slides with the layered set-up described above. It was possible to observe that both *S. aureus* and *P. aeruginosa* grew in large non-surface attached aggregates, of roughly 0.1 to 0.2 mm (see Figure 72) however each individual aggregate appeared to be composed by only one species (Figure 75). Biofilms for CW2 and CW4 isolates were indistinguishable, and aggregates of both species were usually clustered. An interesting observation was the inability of the stains to penetrate deeply into the aggregates, as Z-stack crossed sections showed that these aggregates were usually round, but the interior did not fluoresce (not shown). Note that with the conditions used it was only possible to capture images at 10x magnification.

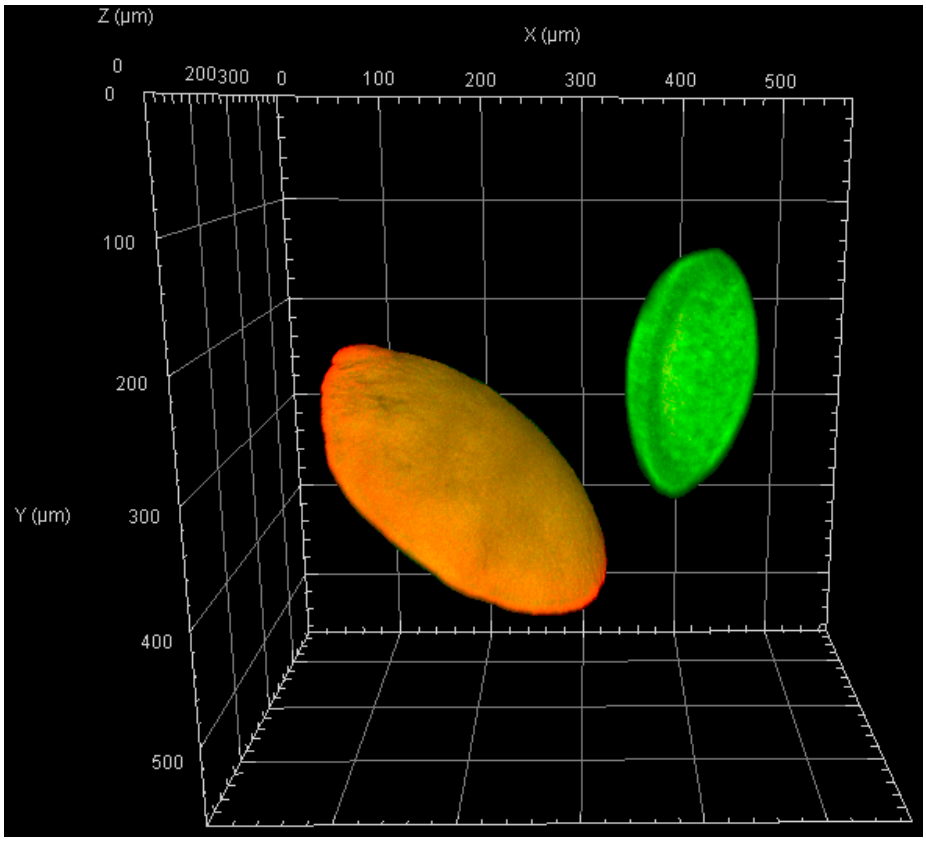


Figure 75: *P. aeruginosa* and *S. aureus* suspended aggregates in a semi-solid *in vitro* biofilm model. Bacteria isolated from CW4 grown in monoculture were mixed and inoculated in Bolton broth agar. *P. aeruginosa* was rendered green by Syto13, while *S. aureus* was rendered orange by Syto13 and hexidium iodide.

To better mimic the conditions of a non-healing ulcer, synthetic wound fluid was solidified with rat tail collagen, as previously described [133], and then applied to the silicone moulds or to 8-well slides with the layered set-up described above. However, collagen solidified rapidly after polymerisation, and it was not easy to properly mix the bacteria with this medium. As such, it took several attempts to obtain good images. Results were similar to those obtained using Bolton broth agar, even though aggregates seemed less homogenous and less round (not shown).

Instead of using the layered set-up described above, an alternative method was adopted and SCW (SWF solidified with rat tail collagen) was mixed with bacteria in the 10^{-4} dilution tube and 200 µL were immediately transferred to 8-well chamber

slides (see section 2.13.1). Results obtained this way showed however marked differences when compared with the layered set-up described before. This time, *P. aeruginosa* created a more fluid biofilm throughout the entire gel, and smaller aggregates of *S. aureus* were observed closer to the surface of the well (Figure 76). These results were very similar for pairs of isolates from CW2 or CW4, and even with this method, *S. aureus* and *P. aeruginosa* did not form mixed polymicrobial biofilms.

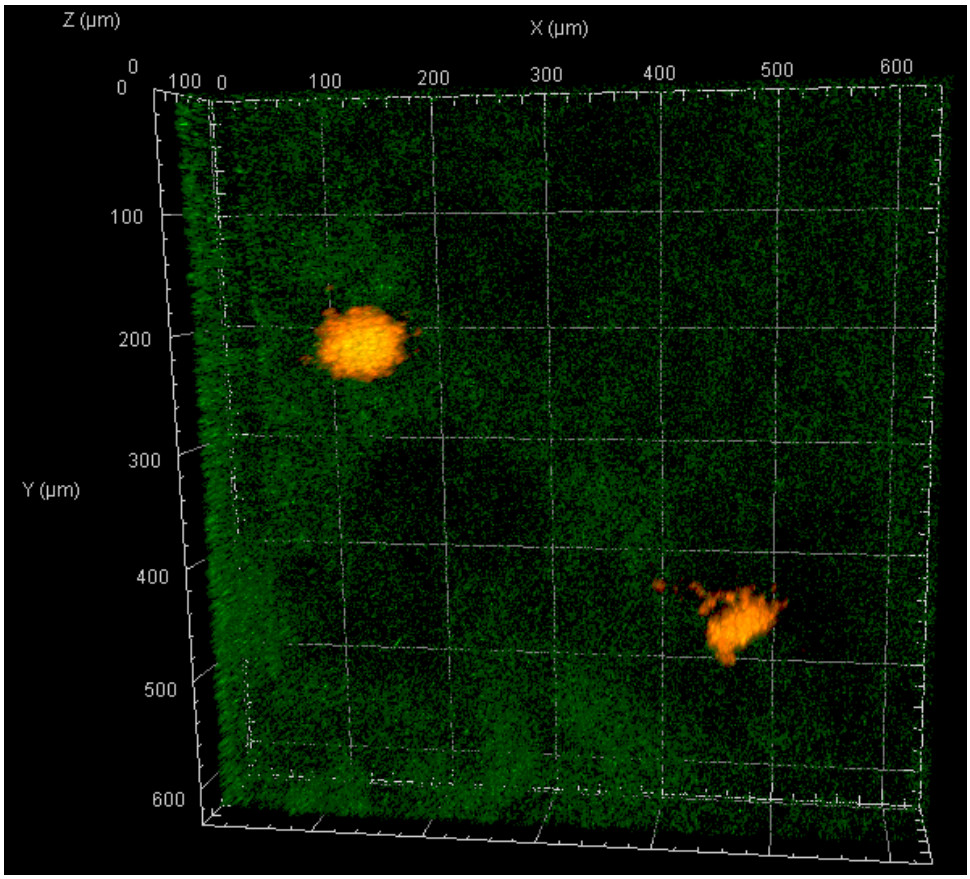


Figure 76: *P. aeruginosa* and *S. aureus* interaction in SCW semi-solid biofilm model. Bacteria isolated from CW4 grown in monoculture were mixed and inoculated in 200 µL of synthetic chronic wound (SCW). *P. aeruginosa* was rendered green by Syto13, while *S. aureus* was rendered orange by Syto13 and hexidium iodide.

These results are probably closer to the *P. aeruginosa*/ *S. aureus* distribution observed in tissue sections taken from diabetic non-healing ulcers [115], and as such

this new adapted protocol better reflects the nature of polymicrobial infections in chronic wounds.

5.2.4 Identification of *P. aeruginosa* and *S. aureus* metabolites by LC-MS/MS

P. aeruginosa and *S. aureus* strains isolated from the same CW can co-exist when grown together in synthetic wound fluid (Figure 69), and when plated on LB plates (Figure 68). In contrast, when *P. aeruginosa* and *S. aureus* strains were isolated from different wounds, *P. aeruginosa* appear to outcompete and/or inhibit *S. aureus*, except when *P. aeruginosa* from patient X (that does not produce AQs) was used (Figure 68). Additionally, *P. aeruginosa* and *S. aureus* isolated from either CW2 or CW4 can successfully grow together in a semi-solid biofilm model (Figures 75 and 76) from two starter monocultures or after grown together overnight in SWF at a 1:2 ratio (*P. aeruginosa*/ *S. aureus*).

In an effort to identify the *P. aeruginosa* and/or *S. aureus* metabolites produced by these clinical strains which may explain some of these interactions, an untargeted metabolite profiling approach using high-resolution tandem mass spectrometry (MS/MS) coupled with hydrophilic interaction liquid chromatography (HILIC) was used. Initially we wanted to analyse the molecules produced when this set of bacteria interact in both liquid (SWF) vs solid (SCW) media. However, the MS suite at the School of Pharmacy is not a “containment level 2” space so it was not possible to work with live bacteria in solid media. Nonetheless, the experiment was carried using SWF and a combination of different *P. aeruginosa*/*S. aureus* conditions (Table 7) described in detail in the methods (section 2.14.1).

Cell-free supernatants of *P. aeruginosa* and *S. aureus* grown on monoculture or co-culture were analysed. After LC-MS/MS analysis the raw data was analysed with Compound Discoverer software (Thermo Fisher Scientific). From here lists of hits, each corresponding to individual molecular ions, were obtained for each condition (1 to 10 – see Table 7, section 2.14.1), and these were further analysed using scripts written specifically for this experiment. Briefly, all hits identified in conditions 9 and 10 (that contained only SWF and no bacteria) were removed from conditions 1 to 8. Then hits identified in monoculture conditions (5 to 8) were removed from each specific co-culture: for instance, for condition 1 that analysed the interaction of *P. aeruginosa* and *S. aureus* isolated from CW2, the hits from the condition 5 (monoculture of *P. aeruginosa* from CW2) and condition 6 (monoculture of *S. aureus* from CW2) were subtracted. Furthermore, the common hits specific to conditions where bacteria were from the same ulcer (conditions 1 and 4), or from different ulcers (conditions 2 and 4) were identified.

When analysing metabolites produced by bacteria isolated from the same ulcer, a total of 140 hits were specific for condition 1 (Pa2 vs Sa2), while a total of 151 hits were specific for condition 4 (Pa4 vs Sa4). When these two lists were compared, 3 hits were common, but they corresponded to only two metabolites (Table 33).

Table 33: Metabolites identified in interactions with *P. aeruginosa* and *S. aureus* isolated from the same ulcer.

Molecular Weight	Replicates in Pa2 vs Sa2	Replicates in Pa4 vs Sa4	Chemical Formula	Possible Name
297.267	1/6	1/6	C_{18} H_{35} N O_2	UNII:OUT5YHB7BO
368.365	1/6	2/6	C_{24} H_{48} O_2	3,15-Dimethyldocosanoic acid

Possible name column indicates one option corresponding molecules identified in databases – see Appendix F for list of database IDs.

When analysing metabolites specifically produced when *P. aeruginosa* and *S. aureus* that evolved in different ulcers interacted, a total of 473 hits were specific for condition 2 (Pa2 vs Sa4), while a total of 32 hits were specific for condition 3 (Pa4 vs Sa2). When these two lists were compared, 9 hits were common, but they corresponded to only six metabolites (Table 34).

Table 34: Metabolites identified in interactions with *P. aeruginosa* and *S. aureus* isolated from different ulcers.

Molecular weight	Replicates in Pa2 vs Sa4	Replicates in Pa4 vs Sa2	Chemical Formula	Possible Name
137.048	4/6	6/6	$C_7 H_7 N O_2$	Aminobenzoic acid / Anthranilic acid
187.096	1/6	3/6	$C_7 H_{13} N_3 O_3$	5-guanidino-3-methyl-2-oxopentanoic acid
225.097	1/6	1/6	n/a	n/a
261.111	2/6	1/6	$C_{13} H_{15} N_3 O_3$	Trp-Gly / Gly-Trp
519.181	1/6	1/6	n/a	n/a
657.502	1/6	1/6	n/a	n/a

Possible name column indicates one option corresponding molecules identified in databases – see Appendix F for list of database IDs; n/a - not found in databases.

Further identification of these metabolites will require an additional in depth analyses, which could not be completed in time for the results to be included in this thesis.

5.3 Discussion and Conclusion

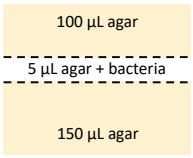
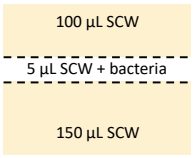
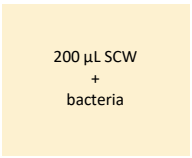
The results presented in this chapter show that when *P. aeruginosa* and *S. aureus* are isolated from the same CW they can co-exist, while *P. aeruginosa* can kill *S. aureus* isolated from a different CW (Figure 68). This makes sense because co-infections with these species have been suggested to be more virulent and result in worse patient outcomes than for single species infections [131]. For example, in CF, clinical *P. aeruginosa* strains were shown to evolve metabolic divergence from wild type strains, which promoted a commensal-like interaction where a CF evolved *P. aeruginosa* benefits from interacting with *S. aureus* [172].

In this study, all *S. aureus* strains were not influenced by *P. aeruginosa* isolates from CW5, and showed a whiter pigmentation than when plated alone or with other CW *P. aeruginosa* strains. Interestingly, this is the opposite of what was reported previously with *S. aureus* and *P. aeruginosa* isolated from the same clinical sample obtained from a patient with a soft tissue wound [377]. These authors reported that *P. aeruginosa* induced a yellow pigment production (staphyloxanthin) in a white variant of *S. aureus*, but it is not clear whether the wound was chronic or acute as this can influence the type of interaction occurring between these bacteria as previously discussed.

The cell-free interaction assays using a transwell membrane set-up were technically complicated to execute, since sampling more than once invariably led to cross-contamination between wells. Others have reported similar problems (personal communication, 2017 Microbiology Society Annual Conference). Similarly, the semi-solid *in vitro* biofilm model as developed by Crone et al. [173] was also found

not to be optimal and required further refinement to better mimic the conditions of a non-healing wound. A range of adaptations (see methods section 2.13.1) were included in this model, and a summary of the limitations and advantages found for the different combinations of structure (multi-layered or more realistic) and media (Bolton broth agar or SCW) is presented in the table below (Table 35).

Table 35: Adaptations made in the semi-solid *in vitro* wound biofilm model.

structure + medium	Limitations	Advantages
	Agar is not a natural component of the wound environment	Includes spatial structure relevant for polymicrobial interactions in diabetic ulcers
	Technically challenging to make as collagen in SCW solidifies very rapidly	Easy to image as bacteria are confined to a specific position in the matrix
	Bacteria in the top portion are not imaged due to the limited depth of field of the confocal microscope	Easy to make, and results are closer to the bacterial distribution observed in diabetic non-healing ulcers

For a detailed description of each structure and medium see Figure 19 and methods section 2.13.1. First row: multilayer structure + Bolton broth agar; second row: multilayer structure + synthetic chronic wound (SCW); third row: more realistic structure + SCW.

The findings presented in Figures 75 and 76 collectively suggest that in chronic wounds *P. aeruginosa* and *S. aureus* cause polymicrobial infections but not polymicrobial biofilms, which is in agreement with recent literature reports [173, 398, 399]. Further assays using the adapted *in vitro* biofilm model will help to quantify the interactions observed in the colony drop assays (Figure 68), clarifying whether

P. aeruginosa wound isolates outcompete *S. aureus*, or if there is a dynamic interaction that depends on external factors.

P. aeruginosa and *S. aureus* have been suggested to interact both competitively and reciprocally during the process of host colonisation, in order to increase the chances of establishing a biofilm and developing a successful infection while later separating into distinct niches [395]. In a scenario where these species have been evolving together, but also interacting with other organisms, as it is the case of long-term non-healing wounds, it would be interesting to determine the balance between competition and cooperation, and how this can be altered to benefit the bacteria when for instance antibiotics are present.

This was attempted in this thesis through the identification of *P. aeruginosa* and *S. aureus* metabolites by LC-MS/MS. Even though our analysis is far from complete, other small molecules have already been described to be relevant for these species interactions [385]. Of particular relevance are the AQs including PQS and the AQNOs due to the high variability and quantity found to be produced by *P. aeruginosa*, and their diverse roles. A recent publication showed that an unsaturated N-oxide AQ produced by *P. aeruginosa* exhibited 20-fold higher bacteriostatic activity against *S. aureus* strains than the most potent saturated AQNO [400]. New techniques such as 3D-printing of bacterial aggregates [401] or time of flight-secondary-ion mass spectrometry (TOF-SIMS) will be a good way forward, as they can combine an in depth profiling analysis with relatively high spatial resolution and sensitivity. TOF-SIMS in particular has already been shown to be useful in measuring the distribution of antimicrobials in samples [402] and could be further

adapted to detect both exogenous and endogenous compounds in polymicrobial settings.

The context and spatial positioning of bacteria has been shown to be very relevant for the study of polymicrobial infections, even as a potential therapeutic target [370]. This idea is discussed in [403], where the authors highlight that even though traditionally *P. aeruginosa* and *S. aureus* have been seen as competitors, in chronic infection settings co-operation between them can be relevant for the microbial community assembly and function. They cite as an example the work of [396] that showed that a mucoid *P. aeruginosa* phenotype frequently found in individuals with long-term chronic CF infection has a diminished ability to kill *S. aureus*, which promotes co-existence between these two species. Another example is an investigation that suggested that HQNO, a *P. aeruginosa* metabolite which inhibits *S. aureus* respiration, can paradoxically protect *S. aureus* from the antimicrobial activity of vancomycin [394]. These and other interactions, such as those described in the introduction of this chapter, are a good attempt in understanding the complex *P. aeruginosa* – *S. aureus* communication. However, the preferential use of laboratory adapted strains can skew the findings, since there is no guarantee that these interactions occur in an *in vivo* situation. As such, a combination of a robust polymicrobial infection model and the use of clinical strains will be essential for future work in this field.

Chapter 6: Conclusions and Future Work

A major goal of this project was to determine whether *P. aeruginosa* phenotypic diversity arises universally as a response to a prolonged and non-healing infection, or to specific environments. This was addressed in Chapter 3, where the data supports the concept that, contrary to what happens in *P. aeruginosa* from chronic CF lung infections, only low levels of phenotypic diversity are found in diabetic foot ulcers. However, marked phenotypic heterogeneity in *P. aeruginosa* isolates from a single population taken from a diabetic leg ulcer was observed. As such, it can be concluded that *P. aeruginosa* phenotypic diversity is not a universal consequence of chronic infections, and is likely to be specific for each infection type and anatomical location. Moreover, *P. aeruginosa* colonisation of a diabetic chronic wound is via a single strain per ulcer, and potentially per patient, although a common origin, from either environmental or nosocomial sources, could not be established.

Whether *P. aeruginosa* phenotypic diversity correlates with the clinical status of a patient was also explored. This analysis was possible due to the combination of longitudinal samples from patient X, the observation of the deterioration in the patient's health between each time point, and the intriguing phenotypic differences identified between *P. aeruginosa* isolates from bone and blood. The simplest explanation for the observations presented in Chapter 4 is that *P. aeruginosa* isolates displaying both phenotypes entered the blood vessels and activated the patient's innate immune response differently. As the loss of flagellum facilitated evasion of the innate immune system, blood isolates were able to go undetected and were able to spread systemically causing a subsequent rapid decline in the patient's health. It was

also speculated that the specific *P. aeruginosa* phenotypic population present in the blood evolved through clonal expansion after the restriction of *P. aeruginosa* growth was removed due to the loss of selective pressure exerted by other microorganisms, such as *S. aureus*, a relevant player in the wound polymicrobial community.

This lead to the third and broader aim, which was to understand how ecology influences the evolution of polymicrobial communities within wound infections and how this contributes to antibiotic resistant polymicrobial infections. In Chapter 5 this issue was addressed by exploring interactions between the previously characterised *P. aeruginosa* and *S. aureus* isolates from the same patients. By growing these clinical strains in an adapted chronic wound polymicrobial infection model it was shown that *P. aeruginosa* and *S. aureus* isolated from the same CW can co-exist, while *P. aeruginosa* can kill *S. aureus* isolated from a different CWs. These findings are an important first step in understanding how ecology influences the evolution of different species within actual wound infections, but further work is needed in order to elucidate the mechanisms that could be essential to this scenario, and to increase our understanding of polymicrobial interactions in order to reduce the occurrence of chronic wound infections.

One of the points that requires further investigation is with respect to *P. aeruginosa* phenotypic diversity in diabetic leg ulcers. Whether this is indeed high or if it is specific for the only DLU ulcer analysed needs additional patients' DLU isolates to be investigated. Fortunately, it will be possible to follow the progression of patient Z's *P. aeruginosa* phenotypic diversity since the clinical microbiology lab has sampled this patient at a later time point. This analysis will be useful in

determining whether *P. aeruginosa* phenotypic variation remains high over time, or if a single *P. aeruginosa* isolate (of the ones described in Chapter 3) dominates, such that the population becomes phenotypically homogenous, as observed for the five diabetic foot ulcers analysed. If the population has not shifted towards a single isolate, it will further support our conclusions that universal adaptation of *P. aeruginosa* to chronicity does not happen. Otherwise, the link between bacterial wound populations, type and physiological circumstances behind each chronic wound type and infection will need to be independently investigated.

In recent years, with the increased availability and lower cost of high-throughput sequencing technologies such as Illumina or Oxford Nanopore, there has been a tendency to move from culture based microbiological analyses to the use of molecular approaches. Although these methods have been demonstrated to give a good insight of bacterial wound diversity (see Chapter 1, section 1.6.1) [404], the relevance of these studies for wound care is not well-stablished, as in most, the reads cannot be reliably identified at the lowest taxonomic levels, and family-level groupings can contain a wide range of organisms with greatly differing virulence potential. As such, these will not give direct information about which key pathogens are responsible for the worsening of a patient's health, and how these interact within the polymicrobial community.

Nonetheless, several of these studies revealed interesting findings, for example, that a polymicrobial mixture of Gram-positive and Gram-negative aerobes and anaerobes is associated with delayed healing when compared to wounds colonised with only a single organism [405]; and that non-healing DFUs have a stable

microbiome with less variation over time in comparison to healing DFUs [406]. They also have been shown to be relevant as a tool to test antimicrobial resistance in a way that could overcome the lengthy plate-based conventional approach of screening for antimicrobial resistance, reviewed in [407], whose validity has been challenged due to the presence of phenotypic variability in chronic infection scenarios.

However, detailed studies of the interactions between major pathogens identified in polymicrobial wound infections are fundamental, and very important for understanding disease progression, as supported by studies that have shown that these types of interactions result in differential immune responses and enhanced virulence (see Chapter 5 sections 5.1 and 5.3). Moreover, recent research is consistent with most of the current guidelines on the prevention and treatment of biofilms being of limited utility for chronic wounds, as bacteria are present in biofilms as aggregated communities as reported here (e.g. Figures 75 and 76). Then, further analysis focusing, for instance, on the antibiotic response of chronic wound isolates in good *in vitro* wound-like models or *in vivo* models, will be invaluable.

Additionally, a study investigating *P. aeruginosa* transcriptome during human vs laboratory infections suggested that antibiotic resistance assays in the clinical laboratory, such as the BSAC method, frequently underestimate resistance in patients [408]. This is because multiple genes known to confer antibiotic resistance had substantially higher expression in human infections than under laboratory conditions, highlighting the necessity of using model systems (and strains) that more accurately represent the biology and characteristics of infection. An interesting and relevant line of investigation could involve the use of the modified *in vitro* biofilm

model described in Chapter 5, or even *in vivo* models like those used in the infection assays presented in Chapter 4, to analyse the *P. aeruginosa* transcriptome differences between bone and blood isolates as compared with the transcriptome results obtained under normal laboratory conditions. However, it is relevant to point out that information from RNA transcriptomes have to be properly validated either by phenotypic studies and/or by qPCR.

References

1. Mustoe, T.A., K. O'Shaughnessy, and O. Kloeters, *Chronic wound pathogenesis and current treatment strategies: a unifying hypothesis.* Plast Reconstr Surg, 2006. **117**(7 Suppl): p. 35S-41S.

2. Mediligence, *Worldwide Wound Management, Forecast to 2026: Established and Emerging Products, Technologies and Markets in the Americas, Europe, Asia/Pacific and Rest of World.* 2018. **S254**.

3. Augustin, M., *Cumulative life course impairment in chronic wounds.* Curr Probl Dermatol, 2013. **44**: p. 125-9.

4. Phillips, C.J., et al., *Estimating the costs associated with the management of patients with chronic wounds using linked routine data.* Int Wound J, 2015.

5. Reinke, J.M. and H. Sorg, *Wound repair and regeneration.* Eur Surg Res, 2012. **49**(1): p. 35-43.

6. Baltzis, D., I. Eleftheriadou, and A. Veves, *Pathogenesis and treatment of impaired wound healing in diabetes mellitus: new insights.* Adv Ther, 2014. **31**(8): p. 817-36.

7. Ennis, W.J. and P. Meneses, *Wound healing at the local level: the stunned wound.* Ostomy Wound Manage, 2000. **46**(1A Suppl): p. 39S-48S; quiz 49S-50S.

8. Falanga, V., *Classifications for wound bed preparation and stimulation of chronic wounds.* Wound Repair Regen, 2000. **8**(5): p. 347-52.

9. Edwards, R. and K.G. Harding, *Bacteria and wound healing.* Curr Opin Infect Dis, 2004. **17**(2): p. 91-6.

10. Eming, S.A., T. Krieg, and J.M. Davidson, *Inflammation in wound repair: molecular and cellular mechanisms.* J Invest Dermatol, 2007. **127**(3): p. 514-25.

11. Schultz, G.S., et al., *Wound bed preparation: a systematic approach to wound management.* Wound Repair Regen, 2003. **11 Suppl 1**: p. S1-28.

12. Demidova-Rice, T.N., M.R. Hamblin, and I.M. Herman, *Acute and impaired wound healing: pathophysiology and current methods for drug delivery, part 1: normal and chronic wounds: biology, causes, and approaches to care.* Adv Skin Wound Care, 2012. **25**(7): p. 304-14.

13. Boyko, T.V.L., M. T.; Yang, G. P., *Review of the Current Management of Pressure Ulcers.* Adv Wound Care (New Rochelle), 2018. **7**(2): p. 57-67.

14. Etufugh, C.N. and T.J. Phillips, *Venous ulcers.* Clin Dermatol, 2007. **25**(1): p. 121-30.

15. (EWMA), E.W.M.A., *Position Document: Identifying criteria for wound infection.* London: MEP Ltd,, 2005.

16. Mustoe, T., *Understanding chronic wounds: a unifying hypothesis on their pathogenesis and implications for therapy.* Am J Surg, 2004. **187**(5A): p. 65S-70S.

17. Wu, L., et al., *Transforming growth factor-beta1 fails to stimulate wound healing and impairs its signal transduction in an aged ischemic ulcer model: importance of oxygen and age.* Am J Pathol, 1999. **154**(1): p. 301-9.

18. Zhao, R., et al., *Inflammation in Chronic Wounds.* Int J Mol Sci, 2016. **17**(12).

19. Peirce, S.M., T.C. Skalak, and G.T. Rodeheaver, *Ischemia-reperfusion injury in chronic pressure ulcer formation: a skin model in the rat.* Wound Repair Regen, 2000. **8**(1): p. 68-76.

20. Schreml, S., et al., *Oxygen in acute and chronic wound healing.* Br J Dermatol, 2010. **163**(2): p. 257-68.

21. WHO, W.H.O., *Global report on Diabetes*. 2016.

22. American Diabetes, A., *Diagnosis and classification of diabetes mellitus.* Diabetes care, 2009. **32 Suppl 1**(Suppl 1): p. S62-S67.

23. Pendsey, S.P., *Understanding diabetic foot.* International journal of diabetes in developing countries, 2010. **30**(2): p. 75-79.

24. Armstrong, D.G., A.J.M. Boulton, and S.A. Bus, *Diabetic Foot Ulcers and Their Recurrence.* N Engl J Med, 2017. **376**(24): p. 2367-2375.

25. Rathur, H.M. and A.J. Boulton, *Recent advances in the diagnosis and management of diabetic neuropathy.* J Bone Joint Surg Br, 2005. **87**(12): p. 1605-10.

26. Dinh, T. and A. Veves, *Microcirculation of the diabetic foot.* Curr Pharm Des, 2005. **11**(18): p. 2301-9.

27. Muller, M.D., et al., *Physiology in medicine: peripheral arterial disease.* Journal of applied physiology (Bethesda, Md. : 1985), 2013. **115**(9): p. 1219-1226.

28. Brownlee, M., *The pathobiology of diabetic complications: a unifying mechanism.* Diabetes, 2005. **54**(6): p. 1615-25.

29. Geraldes, P. and G.L. King, *Activation of protein kinase C isoforms and its impact on diabetic complications.* Circ Res, 2010. **106**(8): p. 1319-31.

30. Reiber, G.E., B.A. Lipsky, and G.W. Gibbons, *The burden of diabetic foot ulcers.* Am J Surg, 1998. **176**(2A Suppl): p. 5S-10S.

31. Zhang, P., et al., *Global epidemiology of diabetic foot ulceration: a systematic review and meta-analysis (dagger).* Ann Med, 2017. **49**(2): p. 106-116.

32. Leung, P.C., *Diabetic foot ulcers--a comprehensive review.* Surgeon, 2007. **5**(4): p. 219-31.

33. Cuzzell, J., *Wound assessment and evaluation: diabetic ulcer protocol.* Dermatol Nurs, 2003. **15**(2): p. 153.

34. Oyibo, S.O., et al., *A comparison of two diabetic foot ulcer classification systems: the Wagner and the University of Texas wound classification systems.* Diabetes Care, 2001. **24**(1): p. 84-8.

35. Santema, T.B., et al., *Comparing the Meggitt-Wagner and the University of Texas wound classification systems for diabetic foot ulcers: inter-observer analyses.* Int Wound J, 2015.

36. Game, F., *Classification of diabetic foot ulcers.* Diabetes Metab Res Rev, 2016. **32 Suppl 1**: p. 186-94.

37. Wolcott, R.D., D.D. Rhoads, and S.E. Dowd, *Biofilms and chronic wound inflammation.* J Wound Care, 2008. **17**(8): p. 333-41.

38. Watters, C., et al., *Pseudomonas aeruginosa biofilms perturb wound resolution and antibiotic tolerance in diabetic mice.* Med Microbiol Immunol, 2013. **202**(2): p. 131-41.

39. Crane, M.J., et al., *The monocyte to macrophage transition in the murine sterile wound.* PLoS One, 2014. **9**(1): p. e86660.

40. Greenlee-Wacker, M.C., *Clearance of apoptotic neutrophils and resolution of inflammation.* Immunol Rev, 2016. **273**(1): p. 357-70.

41. Hesketh, M., et al., *Macrophage Phenotypes Regulate Scar Formation and Chronic Wound Healing.* Int J Mol Sci, 2017. **18**(7).

42. Das, A., et al., *Monocyte and macrophage plasticity in tissue repair and regeneration.* Am J Pathol, 2015. **185**(10): p. 2596-606.

43. Miao, M., et al., *Diabetes-impaired wound healing and altered macrophage activation: a possible pathophysiologic correlation.* Wound Repair Regen, 2012. **20**(2): p. 203-13.

44. Okizaki, S., et al., *Suppressed recruitment of alternatively activated macrophages reduces TGF-beta1 and impairs wound healing in streptozotocin-induced diabetic mice.* Biomed Pharmacother, 2015. **70**: p. 317-25.

45. Goren, I., et al., *A transgenic mouse model of inducible macrophage depletion: effects of diphtheria toxin-driven lysozyme M-specific cell lineage ablation on wound inflammatory, angiogenic, and contractive processes.* Am J Pathol, 2009. **175**(1): p. 132-47.

46. Shook, B., et al., *CD301b+ Macrophages Are Essential for Effective Skin Wound Healing.* J Invest Dermatol, 2016. **136**(9): p. 1885-91.

47. Jetten, N., et al., *Wound administration of M2-polarized macrophages does not improve murine cutaneous healing responses.* PLoS One, 2014. **9**(7): p. e102994.

48. Dionne, S., et al., *Quantitative PCR analysis of TNF-alpha and IL-1 beta mRNA levels in pediatric IBD mucosal biopsies.* Dig Dis Sci, 1997. **42**(7): p. 1557-66.

49. Kube, D., et al., *Proinflammatory cytokine responses to P. aeruginosa infection in human airway epithelial cell lines.* Am J Physiol Lung Cell Mol Physiol, 2001. **280**(3): p. L493-502.

50. Llewelyn, M. and J. Cohen, *Superantigens: microbial agents that corrupt immunity.* Lancet Infect Dis, 2002. **2**(3): p. 156-62.

51. Toth, B., et al., *The role of gammadelta T cells in the regulation of neutrophil-mediated tissue damage after thermal injury.* J Leukoc Biol, 2004. **76**(3): p. 545-52.

52. Aujla, S.J., P.J. Dubin, and J.K. Kolls, *Interleukin-17 in pulmonary host defense.* Exp Lung Res, 2007. **33**(10): p. 507-18.

53. Doring, G., *Cystic fibrosis respiratory infections: interactions between bacteria and host defence.* Monaldi Arch Chest Dis, 1997. **52**(4): p. 363-6.

54. Johansson, C., M. Ingman, and M. Jo Wick, *Elevated neutrophil, macrophage and dendritic cell numbers characterize immune cell populations in mice chronically infected with Salmonella.* Microb Pathog, 2006. **41**(2-3): p. 49-58.

55. Montemurro, P., et al., *The neutrophil-activating protein (HP-NAP) of Helicobacter pylori is a potent stimulant of mast cells.* Eur J Immunol, 2002. **32**(3): p. 671-6.

56. Sindrilaru, A., et al., *An unrestrained proinflammatory M1 macrophage population induced by iron impairs wound healing in humans and mice.* J Clin Invest, 2011. **121**(3): p. 985-97.

57. Wallace, H.J. and M.C. Stacey, *Levels of tumor necrosis factor-alpha (TNF-alpha) and soluble TNF receptors in chronic venous leg ulcers--correlations to healing status.* J Invest Dermatol, 1998. **110**(3): p. 292-6.

58. Patel, S., A. Maheshwari, and A. Chandra, *Biomarkers for wound healing and their evaluation.* J Wound Care, 2016. **25**(1): p. 46-55.

59. Diegelmann, R.F. and M.C. Evans, *Wound healing: an overview of acute, fibrotic and delayed healing.* Front Biosci, 2004. **9**: p. 283-9.

60. Lebeaux, D., et al., *From in vitro to in vivo Models of Bacterial Biofilm-Related Infections.* Pathogens, 2013. **2**(2): p. 288-356.

61. Lebeaux, D. and J.M. Ghigo, *[Management of biofilm-associated infections: what can we expect from recent research on biofilm lifestyles?].* Med Sci (Paris), 2012. **28**(8-9): p. 727-39.

62. Lipsky, B.A., et al., *2012 Infectious Diseases Society of America clinical practice guideline for the diagnosis and treatment of diabetic foot infections.* Clin Infect Dis, 2012. **54**(12): p. e132-73.

63. Hobizal, K.B. and D.K. Wukich, *Diabetic foot infections: current concept review.* Diabet Foot Ankle, 2012. **3**.

64. Nunan, R., K.G. Harding, and P. Martin, *Clinical challenges of chronic wounds: searching for an optimal animal model to recapitulate their complexity.* Disease Models & Mechanisms, 2014. **7**(11): p. 1205.

65. Wagner, F.W., Jr., *The dysvascular foot: a system for diagnosis and treatment.* Foot Ankle, 1981. **2**(2): p. 64-122.

66. van Battum, P., et al., *Differences in minor amputation rate in diabetic foot disease throughout Europe are in part explained by differences in disease severity at presentation.* Diabet Med, 2011. **28**(2): p. 199-205.

67. Mutluoglu, M., et al., *The implications of the presence of osteomyelitis on outcomes of infected diabetic foot wounds.* Scand J Infect Dis, 2013. **45**(7): p. 497-503.

68. Moxey, P.W., et al., *Lower extremity amputations--a review of global variability in incidence.* Diabet Med, 2011. **28**(10): p. 1144-53.

69. Trautner, C., et al., *Incidence of lower limb amputations and diabetes.* Diabetes Care, 1996. **19**(9): p. 1006-9.

70. Fosse, S., et al., *Incidence and characteristics of lower limb amputations in people with diabetes.* Diabet Med, 2009. **26**(4): p. 391-6.

71. Jensen, P.S., et al., *Progression of disease preceding lower extremity amputation in Denmark: a longitudinal registry study of diagnoses, use of medication and healthcare services 14 years prior to amputation.* BMJ Open, 2017. **7**(11): p. e016030.

72. Hoffmann, M., et al., *Survival of diabetes patients with major amputation is comparable to malignant disease.* Diab Vasc Dis Res, 2015. **12**(4): p. 265-71.

73. Tentolouris, N., et al., *Mortality in diabetic and nondiabetic patients after amputations performed from 1990 to 1995: a 5-year follow-up study.* Diabetes Care, 2004. **27**(7): p. 1598-604.

74. Ramsey, S.D., et al., *Incidence, outcomes, and cost of foot ulcers in patients with diabetes.* Diabetes Care, 1999. **22**(3): p. 382-7.

75. Margolis, D.J., J. Kantor, and J.A. Berlin, *Healing of diabetic neuropathic foot ulcers receiving standard treatment. A meta-analysis.* Diabetes Care, 1999. **22**(5): p. 692-5.

76. Treece, K.A., et al., *Validation of a system of foot ulcer classification in diabetes mellitus.* Diabet Med, 2004. **21**(9): p. 987-91.

77. Singh, N., D.G. Armstrong, and B.A. Lipsky, *Preventing foot ulcers in patients with diabetes.* JAMA, 2005. **293**(2): p. 217-28.

78. Jeffcoate, W.J. and K.G. Harding, *Diabetic foot ulcers.* Lancet, 2003. **361**(9368): p. 1545-51.

79. Bennett, G., C. Dealey, and J. Posnett, *The cost of pressure ulcers in the UK.* Age Ageing, 2004. **33**(3): p. 230-5.

80. Gohel, M.S., et al., *Long term results of compression therapy alone versus compression plus surgery in chronic venous ulceration (ESCHAR): randomised controlled trial.* BMJ, 2007. **335**(7610): p. 83.

81. Alexiadou, K. and J. Doupis, *Management of diabetic foot ulcers.* Diabetes therapy : research, treatment and education of diabetes and related disorders, 2012. **3**(1): p. 4-4.

82. Gottrup, F., *Education in Wound Management in Europe with a Special Focus on the Danish Model.* Adv Wound Care (New Rochelle), 2012. **1**(3): p. 133-137.

83. Jarbrink, K., et al., *The humanistic and economic burden of chronic wounds: a protocol for a systematic review.* Syst Rev, 2017. **6**(1): p. 15.

84. Dowsett, C., *Using the TIME framework in wound bed preparation.* Br J Community Nurs, 2008. **13**(6): p. S15-6, S18, S20 passim.

85. Dowsett, C.a.N., H., *Wound bed preparation: Time in practice.* Wounds UK, 2005. **1**(3): p. 58-70.

86. Harris, P.L., *Critical limb ischaemia: management and outcome. Report of a national survey. The Vascular Surgical Society of Great Britain and Ireland.* Eur J Vasc Endovasc Surg, 1995. **10**(1): p. 108-13.

87. Cavanagh, P.R. and S.A. Bus, *Off-loading the diabetic foot for ulcer prevention and healing.* J Vasc Surg, 2010. **52**(3 Suppl): p. 37S-43S.

88. Han, G. and R. Ceilley, *Chronic Wound Healing: A Review of Current Management and Treatments.* Adv Ther, 2017. **34**(3): p. 599-610.

89. Kranke, P., et al., *Hyperbaric oxygen therapy for chronic wounds.* Cochrane Database Syst Rev, 2004(2): p. CD004123.

90. Barrientos, S., et al., *Clinical application of growth factors and cytokines in wound healing.* Wound repair and regeneration : official publication of the Wound Healing Society [and] the European Tissue Repair Society, 2014. **22**(5): p. 569-578.

91. Bowler, P.G., B.I. Duerden, and D.G. Armstrong, *Wound Microbiology and Associated Approaches to Wound Management.* Clinical Microbiology Reviews, 2001. **14**(2): p. 244-269.

92. Schommer, N.N. and R.L. Gallo, *Structure and function of the human skin microbiome.* Trends Microbiol, 2013. **21**(12): p. 660-8.

93. Dow, G., A. Browne, and R.G. Sibbald, *Infection in chronic wounds: controversies in diagnosis and treatment.* Ostomy Wound Manage, 1999. **45**(8): p. 23-7, 29-40; quiz 41-2.

94. Gardner, S.E., R.A. Frantz, and B.N. Doebbeling, *The validity of the clinical signs and symptoms used to identify localized chronic wound infection.* Wound Repair Regen, 2001. **9**(3): p. 178-86.

95. Trengove, N.J., et al., *Qualitative bacteriology and leg ulcer healing.* J Wound Care, 1996. **5**(6): p. 277-80.

96. Bowler, P.G. and B.J. Davies, *The microbiology of infected and noninfected leg ulcers.* Int J Dermatol, 1999. **38**(8): p. 573-8.

97. Stephens, P., et al., *Anaerobic cocci populating the deep tissues of chronic wounds impair cellular wound healing responses in vitro.* Br J Dermatol, 2003. **148**(3): p. 456-66.

98. Lipsky, B.A., et al., *Skin and soft tissue infections in hospitalised patients with diabetes: culture isolates and risk factors associated with mortality, length of stay and cost.* Diabetologia, 2010. **53**(5): p. 914-23.

99. Danielsen, L., et al., *Ulcer bed infection. Report of a case of enlarging venous leg ulcer colonized by Pseudomonas aeruginosa.* APMIS, 1998. **106**(7): p. 721-6.

100. Madsen, S.M., et al., *Bacterial colonization and healing of venous leg ulcers.* APMIS, 1996. **104**(12): p. 895-9.

101. Karchmer, A.W. and G.W. Gibbons, *Foot infections in diabetes: evaluation and management.* Curr Clin Top Infect Dis, 1994. **14**: p. 1-22.

102. Kingston, D. and D.V. Seal, *Current hypotheses on synergistic microbial gangrene.* Br J Surg, 1990. **77**(3): p. 260-4.

103. Eckman, M.H., et al., *Foot infections in diabetic patients. Decision and cost-effectiveness analyses.* JAMA, 1995. **273**(9): p. 712-20.

104. Sloan, T.J., et al., *Examining diabetic heel ulcers through an ecological lens: microbial community dynamics associated with healing and infection.* J Med Microbiol, 2019. **68**(2): p. 230-240.

105. Kalan, L.R., et al., *Strain- and Species-Level Variation in the Microbiome of Diabetic Wounds Is Associated with Clinical Outcomes and Therapeutic Efficacy.* Cell Host Microbe, 2019. **25**(5): p. 641-655 e5.

106. Armstrong, D.G., P.J. Liswood, and W.F. Todd, *1995 William J. Stickel Bronze Award. Prevalence of mixed infections in the diabetic pedal wound. A retrospective review of 112 infections.* J Am Podiatr Med Assoc, 1995. **85**(10): p. 533-7.

107. Clokie, M., et al., *New horizons in the understanding of the causes and management of diabetic foot disease: report from the 2017 Diabetes UK Annual Professional Conference Symposium.* Diabet Med, 2017. **34**(3): p. 305-315.

108. Howell-Jones, R.S., et al., *A review of the microbiology, antibiotic usage and resistance in chronic skin wounds.* J Antimicrob Chemother, 2005. **55**(2): p. 143-9.

109. Hatipoglu, M., et al., *Causative pathogens and antibiotic resistance in diabetic foot infections: A prospective multi-center study.* J Diabetes Complications, 2016. **30**(5): p. 910-6.

110. Uckay, I., et al., *Diabetic foot infections: what have we learned in the last 30 years?* Int J Infect Dis, 2015. **40**: p. 81-91.

111. Uckay, I., et al., *Diabetic foot infections: state-of-the-art.* Diabetes Obes Metab, 2014. **16**(4): p. 305-16.

112. Cooper, R.A., et al., *A clinical investigation into the microbiological status of 'locally infected' leg ulcers.* Int Wound J, 2009. **6**(6): p. 453-62.

113. Davies, C.E., et al., *A prospective study of the microbiology of chronic venous leg ulcers to reevaluate the clinical predictive value of tissue biopsies and swabs.* Wound Repair Regen, 2007. **15**(1): p. 17-22.

114. Bjarnsholt, T., et al., *Why chronic wounds will not heal: a novel hypothesis.* Wound Repair Regen, 2008. **16**(1): p. 2-10.

115. Fazli, M., et al., *Nonrandom distribution of Pseudomonas aeruginosa and Staphylococcus aureus in chronic wounds.* J Clin Microbiol, 2009. **47**(12): p. 4084-9.

116. Blackshaw, E.L. and S.L.A. Jeffery, *Efficacy of an imaging device at identifying the presence of bacteria in wounds at a plastic surgery outpatients clinic.* J Wound Care, 2018. **27**(1): p. 20-26.

117. Sapico, F.L., et al., *The infected foot of the diabetic patient: quantitative microbiology and analysis of clinical features.* Rev Infect Dis, 1984. **6 Suppl 1**: p. S171-6.

118. Jeffcoate, W., J. Lima, and L. Nobrega, *The Charcot foot.* Diabet Med, 2000. **17**(4): p. 253-8.

119. Bessa, L.J., et al., *Bacterial isolates from infected wounds and their antibiotic susceptibility pattern: some remarks about wound infection.* Int Wound J, 2015. **12**(1): p. 47-52.

120. Lipsky, B.A., et al., *IWGDF guidance on the diagnosis and management of foot infections in persons with diabetes.* Diabetes/Metabolism Research and Reviews, 2016. **32**(S1): p. 45-74.

121. Ahman, J., E. Matuschek, and G. Kahlmeter, *The quality of antimicrobial discs from nine manufacturers-EUCAST evaluations in 2014 and 2017.* Clin Microbiol Infect, 2018.

122. Edmonds, M. and A. Foster, *The use of antibiotics in the diabetic foot.* Am J Surg, 2004. **187**(5A): p. 25S-28S.

123. Workentine, M.L., et al., *Phenotypic Heterogeneity of Pseudomonas aeruginosa Populations in a Cystic Fibrosis Patient.* PLoS ONE, 2013. **8**(4): p. e60225.

124. Darch, S.E., et al., *Recombination is a key driver of genomic and phenotypic diversity in a Pseudomonas aeruginosa population during cystic fibrosis infection.* Sci Rep, 2015. **5**: p. 7649.

125. Clark, S.T., et al., *Phenotypic diversity within a Pseudomonas aeruginosa population infecting an adult with cystic fibrosis.* Sci Rep, 2015. **5**: p. 10932.

126. Kwon, K.T. and D.G. Armstrong, *Microbiology and Antimicrobial Therapy for Diabetic Foot Infections.* Infect Chemother, 2018. **50**(1): p. 11-20.

127. Winstanley, C., S. O'Brien, and M.A. Brockhurst, *Pseudomonas aeruginosa Evolutionary Adaptation and Diversification in Cystic Fibrosis Chronic Lung Infections.* Trends in microbiology, 2016. **24**(5): p. 327-337.

128. Foweraker, J.E., et al., *Phenotypic variability of Pseudomonas aeruginosa in sputa from patients with acute infective exacerbation of cystic fibrosis and its*

impact on the validity of antimicrobial susceptibility testing. J Antimicrob Chemother, 2005. **55**(6): p. 921-7.

129. Boulton, A.J., et al., *The global burden of diabetic foot disease.* Lancet, 2005. **366**(9498): p. 1719-24.

130. Trivedi, U., et al., *Prevalence of Multiple Antibiotic Resistant Infections in Diabetic versus Nondiabetic Wounds.* J Pathog, 2014. **2014**: p. 173053.

131. DeLeon, S., et al., *Synergistic interactions of Pseudomonas aeruginosa and Staphylococcus aureus in an in vitro wound model.* Infect Immun, 2014. **82**(11): p. 4718-28.

132. Boratyn, G.M., et al., *BLAST: a more efficient report with usability improvements.* Nucleic Acids Research, 2013. **41**(W1): p. W29-W33.

133. Werthen, M., et al., *An in vitro model of bacterial infections in wounds and other soft tissues.* APMIS, 2010. **118**(2): p. 156-64.

134. Romero, M., et al., *Genome-wide mapping of the RNA targets of the Pseudomonas aeruginosa riboregulatory protein RsmN.* Nucleic acids research, 2018. **46**(13): p. 6823-6840.

135. Baba, T., et al., *Genome sequence of Staphylococcus aureus strain Newman and comparative analysis of staphylococcal genomes: polymorphism and evolution of two major pathogenicity islands.* Journal of bacteriology, 2008. **190**(1): p. 300-310.

136. Mayer-Hamblett, N., et al., *Pseudomonas aeruginosa in vitro phenotypes distinguish cystic fibrosis infection stages and outcomes.* Am J Respir Crit Care Med, 2014. **190**(3): p. 289-97.

137. Swift, S., et al., *Quorum sensing in Aeromonas hydrophila and Aeromonas salmonicida: identification of the LuxRI homologs AhyRI and AsaRI and their cognate N-acylhomoserine lactone signal molecules.* J Bacteriol, 1997. **179**(17): p. 5271-81.

138. Winson, M.K., et al., *Construction and analysis of luxCDABE-based plasmid sensors for investigating N-acyl homoserine lactone-mediated quorum sensing.* FEMS Microbiol Lett, 1998. **163**(2): p. 185-92.

139. Dumas, Z., A. Ross-Gillespie, and R. Kummerli, *Switching between apparently redundant iron-uptake mechanisms benefits bacteria in changeable environments.* Proc Biol Sci, 2013. **280**(1764): p. 20131055.

140. Dietrich, L.E., et al., *The phenazine pyocyanin is a terminal signalling factor in the quorum sensing network of Pseudomonas aeruginosa.* Mol Microbiol, 2006. **61**(5): p. 1308-21.

141. Reszka, K.J., et al., *Oxidation of pyocyanin, a cytotoxic product from Pseudomonas aeruginosa, by microperoxidase 11 and hydrogen peroxide.* Free Radic Biol Med, 2004. **36**(11): p. 1448-59.

142. Ortori, C.A., et al., *Simultaneous quantitative profiling of N-acyl-L-homoserine lactone and 2-alkyl-4(1H)-quinolone families of quorum-sensing signaling molecules using LC-MS/MS.* Anal Bioanal Chem, 2011. **399**(2): p. 839-50.

143. Rashid, M.H. and A. Kornberg, *Inorganic polyphosphate is needed for swimming, swarming, and twitching motilities of Pseudomonas aeruginosa.* Proc Natl Acad Sci U S A, 2000. **97**(9): p. 4885-90.

144. Friedlander, R.S., et al., *Bacterial flagella explore microscale hummocks and hollows to increase adhesion.* Proc Natl Acad Sci U S A, 2013. **110**(14): p. 5624-9.

145. Turner, L., W.S. Ryu, and H.C. Berg, *Real-time imaging of fluorescent flagellar filaments.* J Bacteriol, 2000. **182**(10): p. 2793-801.

146. Jander, G., L.G. Rahme, and F.M. Ausubel, *Positive correlation between virulence of Pseudomonas aeruginosa mutants in mice and insects.* J Bacteriol, 2000. **182**(13): p. 3843-5.

147. Rumbaugh, K.P., J.A. Griswold, and A.N. Hamood, *The role of quorum sensing in the in vivo virulence of Pseudomonas aeruginosa.* Microbes Infect, 2000. **2**(14): p. 1721-31.

148. Bolger, A.M., M. Lohse, and B. Usadel, *Trimmomatic: a flexible trimmer for Illumina sequence data.* Bioinformatics, 2014. **30**(15): p. 2114-20.

149. Wattam, A.R., et al., *Improvements to PATRIC, the all-bacterial Bioinformatics Database and Analysis Resource Center.* Nucleic Acids Res, 2017. **45**(D1): p. D535-D542.

150. Bankevich, A., et al., *SPAdes: a new genome assembly algorithm and its applications to single-cell sequencing.* Journal of computational biology : a journal of computational molecular cell biology, 2012. **19**(5): p. 455-477.

151. Seemann, T., *Prokka: rapid prokaryotic genome annotation.* Bioinformatics, 2014. **30**(14): p. 2068-9.

152. Brettin, T., et al., *RASTtk: a modular and extensible implementation of the RAST algorithm for building custom annotation pipelines and annotating batches of genomes.* Sci Rep, 2015. **5**: p. 8365.

153. Alikhan, N.F., et al., *BLAST Ring Image Generator (BRIG): simple prokaryote genome comparisons.* BMC Genomics, 2011. **12**: p. 402.

154. Ding, W.B., Franz; Neher, Richard A., *panX: pan-genome analysis and exploration.* Nucleic Acids Research, 2018. **46**(1): p. e5-e5.

155. Kumar, S., G. Stecher, and K. Tamura, *MEGA7: Molecular Evolutionary Genetics Analysis Version 7.0 for Bigger Datasets.* Mol Biol Evol, 2016. **33**(7): p. 1870-4.

156. Winsor, G.L., et al., *Enhanced annotations and features for comparing thousands of Pseudomonas genomes in the Pseudomonas genome database.* Nucleic Acids Res, 2016. **44**(D1): p. D646-53.

157. Van Dongen, S., *Graph Clustering by Flow Simulation*, in *Centre for Mathematics and Computer*

Science. 2000, University of Utrecht.

158. Edgar, R.C., *MUSCLE: multiple sequence alignment with high accuracy and high throughput.* Nucleic Acids Res, 2004. **32**(5): p. 1792-7.

159. Eddy, S.R., *Profile hidden Markov models.* Bioinformatics, 1998. **14**(9): p. 755-63.

160. Talavera, G. and J. Castresana, *Improvement of phylogenies after removing divergent and ambiguously aligned blocks from protein sequence alignments.* Syst Biol, 2007. **56**(4): p. 564-77.

161. Price, M.N., P.S. Dehal, and A.P. Arkin, *FastTree 2--approximately maximum-likelihood trees for large alignments.* PLoS One, 2010. **5**(3): p. e9490.

162. Stamatakis, A., *RAxML version 8: a tool for phylogenetic analysis and post-analysis of large phylogenies.* Bioinformatics, 2014. **30**(9): p. 1312-3.

163. Rambaut, A. *FigTree*. 2006; Available from: http://tree.bio.ed.ac.uk/software/figtree/.

164. Li, H., *Toward better understanding of artifacts in variant calling from high-coverage samples.* Bioinformatics, 2014. **30**(20): p. 2843-51.

165. Langmead, B. and S.L. Salzberg, *Fast gapped-read alignment with Bowtie 2.* Nat Methods, 2012. **9**(4): p. 357-9.

166. Frith, M.C., M. Hamada, and P. Horton, *Parameters for accurate genome alignment.* BMC Bioinformatics, 2010. **11**: p. 80.

167. Marth, G.T., et al., *A general approach to single-nucleotide polymorphism discovery.* Nat Genet, 1999. **23**(4): p. 452-6.

168. Jiang, H., et al., *Skewer: a fast and accurate adapter trimmer for next-generation sequencing paired-end reads.* BMC Bioinformatics, 2014. **15**: p. 182.

169. Kim, D., B. Langmead, and S.L. Salzberg, *HISAT: a fast spliced aligner with low memory requirements.* Nat Methods, 2015. **12**(4): p. 357-60.

170. Anders, S., P.T. Pyl, and W. Huber, *HTSeq--a Python framework to work with high-throughput sequencing data.* Bioinformatics (Oxford, England), 2015. **31**(2): p. 166-169.

171. Love, M.I., W. Huber, and S. Anders, *Moderated estimation of fold change and dispersion for RNA-seq data with DESeq2.* Genome biology, 2014. **15**(12): p. 550-550.

172. Michelsen, C.F., et al., *Staphylococcus aureus alters growth activity, autolysis, and antibiotic tolerance in a human host-adapted Pseudomonas aeruginosa lineage.* J Bacteriol, 2014. **196**(22): p. 3903-11.

173. Crone, S., et al., *A novel in vitro wound biofilm model used to evaluate low-frequency ultrasonic-assisted wound debridement.* J Wound Care, 2015. **24**(2): p. 64, 66-9, 72.

174. Mason, D.J., et al., *A fluorescent Gram stain for flow cytometry and epifluorescence microscopy.* Applied and environmental microbiology, 1998. **64**(7): p. 2681-2685.

175. Schatschneider, S., et al., *Quantitative Isotope-Dilution High-Resolution-Mass-Spectrometry Analysis of Multiple Intracellular Metabolites in Clostridium autoethanogenum with Uniformly (13)C-Labeled Standards Derived from Spirulina.* Anal Chem, 2018. **90**(7): p. 4470-4477.

176. Surrati, A., et al., *Non-destructive characterisation of mesenchymal stem cell differentiation using LC-MS-based metabolite footprinting.* Analyst, 2016. **141**(12): p. 3776-87.

177. Huang, W., et al., *PAMDB: a comprehensive Pseudomonas aeruginosa metabolome database.* Nucleic Acids Res, 2018. **46**(D1): p. D575-D580.

178. Thomsen, T.R., et al., *The bacteriology of chronic venous leg ulcer examined by culture-independent molecular methods.* Wound Repair Regen, 2010. **18**(1): p. 38-49.

179. Wu, W., et al., *Chapter 41 - Pseudomonas aeruginosa*, in *Molecular Medical Microbiology (Second Edition)*, Y.-W. Tang, et al., Editors. 2015, Academic Press: Boston. p. 753-767.

180. Williams, P., *Quorum sensing, communication and cross-kingdom signalling in the bacterial world.* Microbiology, 2007. **153**(Pt 12): p. 3923-38.

181. Stover, C.K., et al., *Complete genome sequence of Pseudomonas aeruginosa PAO1, an opportunistic pathogen.* Nature, 2000. **406**(6799): p. 959-64.

182. Trunk, K., et al., *Anaerobic adaptation in Pseudomonas aeruginosa: definition of the Anr and Dnr regulons.* Environ Microbiol, 2010. **12**(6): p. 1719-33.

183. Bleves, S., et al., *Protein secretion systems in Pseudomonas aeruginosa: A wealth of pathogenic weapons.* Int J Med Microbiol, 2010. **300**(8): p. 534-43.

184. Strateva, T.M., I., *Contribution of an arsenal of virulence factors to pathogenesis of Pseudomonas aeruginosa infections.* Annals of Microbiology, 2011. **61**(4): p. 717-732.

185. Lyczak, J.B., C.L. Cannon, and G.B. Pier, *Establishment of Pseudomonas aeruginosa infection: lessons from a versatile opportunist.* Microbes Infect, 2000. **2**(9): p. 1051-60.

186. Heck, L.W., et al., *Specific cleavage of human type III and IV collagens by Pseudomonas aeruginosa elastase.* Infect Immun, 1986. **51**(1): p. 115-8.

187. Schmidtchen, A., et al., *Elastase-producing Pseudomonas aeruginosa degrade plasma proteins and extracellular products of human skin and fibroblasts, and inhibit fibroblast growth.* Microb Pathog, 2003. **34**(1): p. 47-55.

188. Colvin, K.M., et al., *The Pel and Psl polysaccharides provide Pseudomonas aeruginosa structural redundancy within the biofilm matrix.* Environmental microbiology, 2012. **14**(8): p. 1913-1928.

189. Ryder, C., M. Byrd, and D.J. Wozniak, *Role of polysaccharides in Pseudomonas aeruginosa biofilm development.* Curr Opin Microbiol, 2007. **10**(6): p. 644-8.

190. Franklin, M.J., et al., *Biosynthesis of the Pseudomonas aeruginosa Extracellular Polysaccharides, Alginate, Pel, and Psl.* Frontiers in microbiology, 2011. **2**: p. 167-167.

191. Winstanley, C. and J.L. Fothergill, *The role of quorum sensing in chronic cystic fibrosis Pseudomonas aeruginosa infections.* FEMS Microbiol Lett, 2009. **290**(1): p. 1-9.

192. Ho Sui, S.J., et al., *Raloxifene attenuates Pseudomonas aeruginosa pyocyanin production and virulence.* Int J Antimicrob Agents, 2012. **40**(3): p. 246-51.

193. Banin, E., M.L. Vasil, and E.P. Greenberg, *Iron and Pseudomonas aeruginosa biofilm formation.* Proc Natl Acad Sci U S A, 2005. **102**(31): p. 11076-81.

194. Hauser, A.R. and E.A. Ozer, *Pseudomonas aeruginosa.* Nature Reviews Microbiology, 2011. **9**(3).

195. Williams, P. and M. Camara, *Quorum sensing and environmental adaptation in Pseudomonas aeruginosa: a tale of regulatory networks and multifunctional signal molecules.* Curr Opin Microbiol, 2009. **12**(2): p. 182-91.

196. Moradali, M.F., S. Ghods, and B.H.A. Rehm, *Pseudomonas aeruginosa Lifestyle: A Paradigm for Adaptation, Survival, and Persistence.* Frontiers in Cellular and Infection Microbiology, 2017. **7**(39).

197. Venturi, V., *Regulation of quorum sensing in Pseudomonas.* FEMS Microbiol Rev, 2006. **30**(2): p. 274-91.

198. Erickson, D.L., et al., *Pseudomonas aeruginosa Quorum-Sensing Systems May Control Virulence Factor Expression in the Lungs of Patients with Cystic Fibrosis.* Infection and Immunity, 2002. **70**(4): p. 1783-1790.

199. Barr, H.L., et al., *Pseudomonas aeruginosa quorum sensing molecules correlate with clinical status in cystic fibrosis.* Eur Respir J, 2015. **46**(4): p. 1046-54.

200. Balasubramanian, D., et al., *A dynamic and intricate regulatory network determines Pseudomonas aeruginosa virulence.* Nucleic Acids Research, 2013. **41**(1): p. 1-20.

201. Lee, J. and L. Zhang, *The hierarchy quorum sensing network in Pseudomonas aeruginosa.* Protein Cell, 2015. **6**(1): p. 26-41.

202. D'Argenio, D.A., et al., *Growth phenotypes of Pseudomonas aeruginosa lasR mutants adapted to the airways of cystic fibrosis patients.* Mol Microbiol, 2007. **64**(2): p. 512-33.

203. Damkiaer, S., et al., *Evolutionary remodeling of global regulatory networks during long-term bacterial adaptation to human hosts.* Proc Natl Acad Sci U S A, 2013. **110**(19): p. 7766-71.

204. Marvig, R.L., et al., *Convergent evolution and adaptation of Pseudomonas aeruginosa within patients with cystic fibrosis.* Nat Genet, 2015. **47**(1): p. 57-64.

205. Friedman, L. and R. Kolter, *Genes involved in matrix formation in Pseudomonas aeruginosa PA14 biofilms.* Mol Microbiol, 2004. **51**(3): p. 675-90.

206. Hickman, J.W., D.F. Tifrea, and C.S. Harwood, *A chemosensory system that regulates biofilm formation through modulation of cyclic diguanylate levels.* Proc Natl Acad Sci U S A, 2005. **102**(40): p. 14422-7.

207. Higgins, S., et al., *Differential Regulation of the Phenazine Biosynthetic Operons by Quorum Sensing in Pseudomonas aeruginosa PAO1-N.* Front Cell Infect Microbiol, 2018. **8**: p. 252.

208. Diggle, S.P., et al., *The Pseudomonas aeruginosa quinolone signal molecule overcomes the cell density-dependency of the quorum sensing hierarchy, regulates rhl-dependent genes at the onset of stationary phase and can be produced in the absence of LasR.* Molecular Microbiology, 2003. **50**(1): p. 29-43.

209. Dekimpe, V. and E. Deziel, *Revisiting the quorum-sensing hierarchy in Pseudomonas aeruginosa: the transcriptional regulator RhlR regulates LasR-specific factors.* Microbiology, 2009. **155**(Pt 3): p. 712-23.

210. Feltner, J.B., et al., *LasR Variant Cystic Fibrosis Isolates Reveal an Adaptable Quorum-Sensing Hierarchy in Pseudomonas aeruginosa.* mBio, 2016. **7**(5): p. e01513-16.

211. Jiricny, N., et al., *Loss of social behaviours in populations of Pseudomonas aeruginosa infecting lungs of patients with cystic fibrosis.* PLoS One, 2014. **9**(1): p. e83124.

212. Smith, E.E., et al., *Genetic adaptation by Pseudomonas aeruginosa to the airways of cystic fibrosis patients.* Proc Natl Acad Sci U S A, 2006. **103**(22): p. 8487-92.

213. Schaber, J.A., et al., *Analysis of quorum sensing-deficient clinical isolates of Pseudomonas aeruginosa.* J Med Microbiol, 2004. **53**(Pt 9): p. 841-53.

214. Hoffman, L.R., et al., *Pseudomonas aeruginosa lasR mutants are associated with cystic fibrosis lung disease progression.* J Cyst Fibros, 2009. **8**(1): p. 66-70.

215. Hamood, A.N., J. Griswold, and J. Colmer, *Characterization of elastase-deficient clinical isolates of Pseudomonas aeruginosa.* Infect Immun, 1996. **64**(8): p. 3154-60.

216. Suleman, L., *Extracellular Bacterial Proteases in Chronic Wounds: A Potential Therapeutic Target?* Adv Wound Care (New Rochelle), 2016. **5**(10): p. 455-463.

217. Cathcart, G.R., et al., *Novel inhibitors of the Pseudomonas aeruginosa virulence factor LasB: a potential therapeutic approach for the attenuation of virulence mechanisms in pseudomonal infection.* Antimicrob Agents Chemother, 2011. **55**(6): p. 2670-8.

218. Friedman, N.D., E. Temkin, and Y. Carmeli, *The negative impact of antibiotic resistance.* Clin Microbiol Infect, 2016. **22**(5): p. 416-22.

219. Brandel, J., et al., *Pyochelin, a siderophore of Pseudomonas aeruginosa: physicochemical characterization of the iron(III), copper(II) and zinc(II) complexes.* Dalton Trans, 2012. **41**(9): p. 2820-34.

220. Wenk, J., et al., *Selective pick-up of increased iron by deferoxamine-coupled cellulose abrogates the iron-driven induction of matrix-degrading metalloproteinase 1 and lipid peroxidation in human dermal fibroblasts in vitro: a new dressing concept.* J Invest Dermatol, 2001. **116**(6): p. 833-9.

221. Lamont, I.L., et al., *Siderophore-mediated signaling regulates virulence factor production in Pseudomonasaeruginosa.* Proc Natl Acad Sci U S A, 2002. **99**(10): p. 7072-7.

222. Redly, G.A. and K. Poole, *FpvIR control of fpvA ferric pyoverdine receptor gene expression in Pseudomonas aeruginosa: demonstration of an interaction between FpvI and FpvR and identification of mutations in each compromising this interaction.* J Bacteriol, 2005. **187**(16): p. 5648-57.

223. Visca, P., F. Imperi, and I.L. Lamont, *Pyoverdine siderophores: from biogenesis to biosignificance.* Trends Microbiol, 2007. **15**(1): p. 22-30.

224. Cornelis, P., *Iron uptake and metabolism in pseudomonads.* Appl Microbiol Biotechnol, 2010. **86**(6): p. 1637-45.

225. Britigan, B.E., et al., *Interaction of the Pseudomonas aeruginosa secretory products pyocyanin and pyochelin generates hydroxyl radical and causes synergistic damage to endothelial cells. Implications for Pseudomonas-associated tissue injury.* J Clin Invest, 1992. **90**(6): p. 2187-96.

226. Vinckx, T., et al., *A proteome analysis of the response of a Pseudomonas aeruginosa oxyR mutant to iron limitation.* Biometals, 2011. **24**(3): p. 523-32.

227. Adler, C., et al., *Catecholate siderophores protect bacteria from pyochelin toxicity.* PLoS One, 2012. **7**(10): p. e46754.

228. Lyczak, J.B., C.L. Cannon, and G.B. Pier, *Lung infections associated with cystic fibrosis.* Clin Microbiol Rev, 2002. **15**(2): p. 194-222.

229. Hare, N.J., et al., *Proteomic profiling of Pseudomonas aeruginosa AES-1R, PAO1 and PA14 reveals potential virulence determinants associated with a transmissible cystic fibrosis-associated strain.* BMC Microbiol, 2012. **12**: p. 16.

230. Jaffar-Bandjee, M.C., et al., *Production of elastase, exotoxin A, and alkaline protease in sputa during pulmonary exacerbation of cystic fibrosis in patients chronically infected by Pseudomonas aeruginosa.* J Clin Microbiol, 1995. **33**(4): p. 924-9.

231. Schmidtchen, A., H. Wolff, and C. Hansson, *Differential proteinase expression by Pseudomonas aeruginosa derived from chronic leg ulcers.* Acta Derm Venereol, 2001. **81**(6): p. 406-9.

232. Wildeboer, D., et al., *Specific protease activity indicates the degree of Pseudomonas aeruginosa infection in chronic infected wounds.* Eur J Clin Microbiol Infect Dis, 2012. **31**(9): p. 2183-9.

233. Korgaonkar, A., et al., *Community surveillance enhances Pseudomonas aeruginosa virulence during polymicrobial infection.* Proceedings of the

National Academy of Sciences of the United States of America, 2013. **110**(3): p. 1059-1064.

234. Sellers, W., E.S. Wynne, and C.D. Graber, *An improved medium for pyocyanin production by Pseudomonas aeruginosa.* Tech Doc Rep SAMTDR USAF Sch Aerosp Med, 1962. **62-36**: p. 2p.

235. Fothergill, J.L., et al., *Widespread pyocyanin over-production among isolates of a cystic fibrosis epidemic strain.* BMC Microbiol, 2007. **7**: p. 45.

236. Dietrich, L.E., et al., *Redox-active antibiotics control gene expression and community behavior in divergent bacteria.* Science, 2008. **321**(5893): p. 1203-6.

237. Andrews, J.M. and R.A. Howe, *BSAC standardized disc susceptibility testing method (version 10).* J Antimicrob Chemother, 2011. **66**(12): p. 2726-57.

238. Hambleton, J., et al., *Activation of c-Jun N-terminal kinase in bacterial lipopolysaccharide-stimulated macrophages.* Proc Natl Acad Sci U S A, 1996. **93**(7): p. 2774-8.

239. Lerouge, I. and J. Vanderleyden, *O-antigen structural variation: mechanisms and possible roles in animal/plant-microbe interactions.* FEMS Microbiol Rev, 2002. **26**(1): p. 17-47.

240. Trostrup, H., et al., *S100A8/A9 is an important host defence mediator in neuropathic foot ulcers in patients with type 2 diabetes mellitus.* Arch Dermatol Res, 2016. **308**(5): p. 347-55.

241. Verma, A., et al., *Glycosylation of b-Type flagellin of Pseudomonas aeruginosa: structural and genetic basis.* Journal of bacteriology, 2006. **188**(12): p. 4395-4403.

242. Spangenberg, C., et al., *Genetic diversity of flagellins of Pseudomonas aeruginosa.* FEBS Letters, 1996. **396**(2-3): p. 213-217.

243. Schirm, M., et al., *Structural and genetic characterization of glycosylation of type a flagellin in Pseudomonas aeruginosa.* Journal of bacteriology, 2004. **186**(9): p. 2523-2531.

244. Arora, S.K., et al., *A genomic island in Pseudomonas aeruginosa carries the determinants of flagellin glycosylation.* Proc Natl Acad Sci U S A, 2001. **98**(16): p. 9342-7.

245. Miao, E.A., et al., *TLR5 and Ipaf: dual sensors of bacterial flagellin in the innate immune system.* Semin Immunopathol, 2007. **29**(3): p. 275-88.

246. Hayashi, F., et al., *The innate immune response to bacterial flagellin is mediated by Toll-like receptor 5.* Nature, 2001. **410**(6832): p. 1099-103.

247. Michel-Briand, Y. and C. Baysse, *The pyocins of Pseudomonas aeruginosa.* Biochimie, 2002. **84**(5-6): p. 499-510.

248. Urbano, P., et al., *Epidemiological studies of Pseudomonas aeruginosa infections in leg ulcers.* Med Microbiol Immunol, 1983. **172**(1): p. 41-5.

249. Dong, Y.H., et al., *VqsM, a novel AraC-type global regulator of quorum-sensing signalling and virulence in Pseudomonas aeruginosa.* Mol Microbiol, 2005. **58**(2): p. 552-64.

250. Juhas, M., et al., *Global regulation of quorum sensing and virulence by VqsR in Pseudomonas aeruginosa.* Microbiology, 2004. **150**(Pt 4): p. 831-41.

251. Köhler, T., et al., *QsrO a novel regulator of quorum-sensing and virulence in Pseudomonas aeruginosa.* PloS one, 2014. **9**(2): p. e87814-e87814.

252. Spencer, D.H., et al., *Whole-genome sequence variation among multiple isolates of Pseudomonas aeruginosa.* J Bacteriol, 2003. **185**(4): p. 1316-25.

253. Smith, E.E., et al., *Evidence for diversifying selection at the pyoverdine locus of Pseudomonas aeruginosa.* J Bacteriol, 2005. **187**(6): p. 2138-47.

254. Cezard, C., N. Farvacques, and P. Sonnet, *Chemistry and biology of pyoverdines, Pseudomonas primary siderophores.* Curr Med Chem, 2015. **22**(2): p. 165-86.

255. Ernst, R.K., et al., *Genome mosaicism is conserved but not unique in Pseudomonas aeruginosa isolates from the airways of young children with cystic fibrosis.* Environ Microbiol, 2003. **5**(12): p. 1341-9.

256. de Chial, M., et al., *Identification of type II and type III pyoverdine receptors from Pseudomonas aeruginosa.* Microbiology, 2003. **149**(Pt 4): p. 821-31.

257. De Vos, D., et al., *Study of pyoverdine type and production by Pseudomonas aeruginosa isolated from cystic fibrosis patients: prevalence of type II pyoverdine isolates and accumulation of pyoverdine-negative mutations.* Arch Microbiol, 2001. **175**(5): p. 384-8.

258. Cornelis, P., D. Hohnadel, and J.M. Meyer, *Evidence for different pyoverdine-mediated iron uptake systems among Pseudomonas aeruginosa strains.* Infect Immun, 1989. **57**(11): p. 3491-7.

259. Bodilis, J., et al., *Distribution and evolution of ferripyoverdine receptors in Pseudomonas aeruginosa.* Environ Microbiol, 2009. **11**(8): p. 2123-35.

260. Ghysels, B., et al., *FpvB, an alternative type I ferripyoverdine receptor of Pseudomonas aeruginosa.* Microbiology, 2004. **150**(Pt 6): p. 1671-80.

261. Murray, J.L., et al., *Intrinsic Antimicrobial Resistance Determinants in the Superbug Pseudomonas aeruginosa.* MBio, 2015. **6**(6): p. e01603-15.

262. Mesaros, N., et al., *Pseudomonas aeruginosa: resistance and therapeutic options at the turn of the new millennium.* Clin Microbiol Infect, 2007. **13**(6): p. 560-78.

263. Francis, V.I., E.C. Stevenson, and S.L. Porter, *Two-component systems required for virulence in Pseudomonas aeruginosa.* FEMS Microbiol Lett, 2017. **364**(11).

264. Rodrigue, A., et al., *Two-component systems in Pseudomonas aeruginosa: why so many?* Trends Microbiol, 2000. **8**(11): p. 498-504.

265. Driscoll, J.A., S.L. Brody, and M.H. Kollef, *The epidemiology, pathogenesis and treatment of Pseudomonas aeruginosa infections.* Drugs, 2007. **67**(3): p. 351-68.

266. Coggan, K.A. and M.C. Wolfgang, *Global regulatory pathways and cross-talk control pseudomonas aeruginosa environmental lifestyle and virulence phenotype.* Curr Issues Mol Biol, 2012. **14**(2): p. 47-70.

267. Gooderham, W.J. and R.E. Hancock, *Regulation of virulence and antibiotic resistance by two-component regulatory systems in Pseudomonas aeruginosa.* FEMS Microbiol Rev, 2009. **33**(2): p. 279-94.

268. Pletzer, D., et al., *New Mouse Model for Chronic Infections by Gram-Negative Bacteria Enabling the Study of Anti-Infective Efficacy and Host-Microbe Interactions.* MBio, 2017. **8**(1).

269. Zolfaghar, I., D.J. Evans, and S.M. Fleiszig, *Twitching motility contributes to the role of pili in corneal infection caused by Pseudomonas aeruginosa.* Infect Immun, 2003. **71**(9): p. 5389-93.

270. Feldman, M., et al., *Role of flagella in pathogenesis of Pseudomonas aeruginosa pulmonary infection.* Infect Immun, 1998. **66**(1): p. 43-51.

271. Drake, D. and T.C. Montie, *Flagella, motility and invasive virulence of Pseudomonas aeruginosa.* J Gen Microbiol, 1988. **134**(1): p. 43-52.

272. Haiko, J. and B. Westerlund-Wikström, *The role of the bacterial flagellum in adhesion and virulence.* Biology, 2013. **2**(4): p. 1242-1267.

273. Ince, D., F.S. Sutterwala, and T.L. Yahr, *Secretion of Flagellar Proteins by the Pseudomonas aeruginosa Type III Secretion-Injectisome System.* Journal of Bacteriology, 2015. **197**(12): p. 2003-2011.

274. Minamino, T., *Protein export through the bacterial flagellar type III export pathway.* Biochim Biophys Acta, 2014. **1843**(8): p. 1642-8.

275. Mattick, J.S., *Type IV pili and twitching motility.* Annu Rev Microbiol, 2002. **56**: p. 289-314.

276. Kohler, T., et al., *Swarming of Pseudomonas aeruginosa is dependent on cell-to-cell signaling and requires flagella and pili.* J Bacteriol, 2000. **182**(21): p. 5990-6.

277. Yeung, A.T., et al., *Swarming of Pseudomonas aeruginosa is controlled by a broad spectrum of transcriptional regulators, including MetR.* J Bacteriol, 2009. **191**(18): p. 5592-602.

278. Shrout, J.D., et al., *The impact of quorum sensing and swarming motility on Pseudomonas aeruginosa biofilm formation is nutritionally conditional.* Mol Microbiol, 2006. **62**(5): p. 1264-77.

279. Cassat, J.E. and E.P. Skaar, *Iron in infection and immunity.* Cell host & microbe, 2013. **13**(5): p. 509-519.

280. Howard, D.H., *Acquisition, transport, and storage of iron by pathogenic fungi.* Clinical microbiology reviews, 1999. **12**(3): p. 394-404.

281. Wright, J.A., T. Richards, and S.K.S. Srai, *The role of iron in the skin and cutaneous wound healing.* Frontiers in pharmacology, 2014. **5**: p. 156-156.

282. Cornelis, P. and J. Dingemans, *Pseudomonas aeruginosa adapts its iron uptake strategies in function of the type of infections.* Frontiers in cellular and infection microbiology, 2013. **3**: p. 75-75.

283. Schalk, I.J. and L. Guillon, *Pyoverdine biosynthesis and secretion in Pseudomonas aeruginosa: implications for metal homeostasis.* Environ Microbiol, 2013. **15**(6): p. 1661-73.

284. Braud, A., et al., *The Pseudomonas aeruginosa pyochelin-iron uptake pathway and its metal specificity.* J Bacteriol, 2009. **191**(11): p. 3517-25.

285. Poole, K. and G.A. McKay, *Iron acquisition and its control in Pseudomonas aeruginosa: many roads lead to Rome.* Front Biosci, 2003. **8**: p. d661-86.

286. Reinhart, A.A. and A.G. Oglesby-Sherrouse, *Regulation of Pseudomonas aeruginosa Virulence by Distinct Iron Sources.* Genes (Basel), 2016. **7**(12).

287. Minandri, F., et al., *Role of Iron Uptake Systems in Pseudomonas aeruginosa Virulence and Airway Infection.* Infection and Immunity, 2016. **84**(8): p. 2324-2335.

288. Konings, A.F., et al., *Pseudomonas aeruginosa uses multiple pathways to acquire iron during chronic infection in cystic fibrosis lungs.* Infection and immunity, 2013. **81**(8): p. 2697-2704.

289. Ganne, G., et al., *Iron Release from the Siderophore Pyoverdine in Pseudomonas aeruginosa Involves Three New Actors: FpvC, FpvG, and FpvH.* ACS Chem Biol, 2017. **12**(4): p. 1056-1065.

290. Cornelis, P., S. Matthijs, and L. Van Oeffelen, *Iron uptake regulation in Pseudomonas aeruginosa.* Biometals, 2009. **22**(1): p. 15-22.

291. Mettrick, K.A. and I.L. Lamont, *Different roles for anti-sigma factors in siderophore signalling pathways of Pseudomonas aeruginosa.* Mol Microbiol, 2009. **74**(5): p. 1257-71.

292. Hartney, S.L., et al., *TonB-dependent outer-membrane proteins and siderophore utilization in Pseudomonas fluorescens Pf-5.* Biometals, 2011. **24**(2): p. 193-213.

293. Bishop, T.F., L.W. Martin, and I.L. Lamont, *Activation of a Cell Surface Signaling Pathway in Pseudomonas aeruginosa Requires ClpP Protease and New Sigma Factor Synthesis.* Frontiers in microbiology, 2017. **8**: p. 2442-2442.

294. Malloy, J.L., et al., *Pseudomonas aeruginosa protease IV degrades surfactant proteins and inhibits surfactant host defense and biophysical functions.* Am J Physiol Lung Cell Mol Physiol, 2005. **288**(2): p. L409-18.

295. Nairz, M., et al., *The struggle for iron - a metal at the host-pathogen interface.* Cell Microbiol, 2010. **12**(12): p. 1691-702.

296. Ochsner, U.A., Z. Johnson, and M.L. Vasil, *Genetics and regulation of two distinct haem-uptake systems, phu and has, in Pseudomonas aeruginosa.* Microbiology, 2000. **146 (Pt 1)**: p. 185-98.

297. Lee, M.J.Y., et al., *Function Coupling Mechanism of PhuS and HemO in Heme Degradation.* Scientific Reports, 2017. **7**(1): p. 11273.

298. Smith, A.D. and A. Wilks, *Differential contributions of the outer membrane receptors PhuR and HasR to heme acquisition in Pseudomonas aeruginosa.* The Journal of biological chemistry, 2015. **290**(12): p. 7756-7766.

299. Cope, L.D., et al., *Involvement of HxuC outer membrane protein in utilization of hemoglobin by Haemophilus influenzae.* Infect Immun, 2001. **69**(4): p. 2353-63.

300. Llamas, M.A., et al., *Cell-surface signaling in Pseudomonas: stress responses, iron transport, and pathogenicity.* FEMS Microbiol Rev, 2014. **38**(4): p. 569-97.

301. Strateva, T. and D. Yordanov, *Pseudomonas aeruginosa - a phenomenon of bacterial resistance.* J Med Microbiol, 2009. **58**(Pt 9): p. 1133-48.

302. McDermott, P.F., R.D. Walker, and D.G. White, *Antimicrobials: modes of action and mechanisms of resistance.* Int J Toxicol, 2003. **22**(2): p. 135-43.

303. Poole, K., *Mechanisms of bacterial biocide and antibiotic resistance.* J Appl Microbiol, 2002. **92 Suppl**: p. 55S-64S.

304. Wright, G.D., *Mechanisms of resistance to antibiotics.* Curr Opin Chem Biol, 2003. **7**(5): p. 563-9.

305. Blanco, P., et al., *Bacterial Multidrug Efflux Pumps: Much More Than Antibiotic Resistance Determinants.* Microorganisms, 2016. **4**(1).

306. Balasubramanian, D.K., H. Mathee, K., *Pseudomonas aeruginosa AmpR: an acute-chronic switch regulator.* Pathog Dis, 2015. **73**(2): p. 1-14.

307. Kong, K.F., et al., *Pseudomonas aeruginosa AmpR is a global transcriptional factor that regulates expression of AmpC and PoxB beta-lactamases, proteases, quorum sensing, and other virulence factors.* Antimicrob Agents Chemother, 2005. **49**(11): p. 4567-75.

308. Kong, K.-F.A., Alian; Schneper, Lisa; Mathee, Kalai, *Pseudomonas aeruginosa β-lactamase induction requires two permeases, AmpG and AmpP.* BMC microbiology, 2010. **10**: p. 328-328.

309. Aendekerk, S., et al., *The MexGHI-OpmD multidrug efflux pump controls growth, antibiotic susceptibility and virulence in Pseudomonas aeruginosa via 4-quinolone-dependent cell-to-cell communication.* Microbiology, 2005. **151**(Pt 4): p. 1113-25.

310. Poole, K., *Multidrug efflux pumps and antimicrobial resistance in Pseudomonas aeruginosa and related organisms.* J Mol Microbiol Biotechnol, 2001. **3**(2): p. 255-64.

311. Lamarche, M.G. and E. Deziel, *MexEF-OprN efflux pump exports the Pseudomonas quinolone signal (PQS) precursor HHQ (4-hydroxy-2-heptylquinoline).* PLoS One, 2011. **6**(9): p. e24310.

312. Join-Lambert, O.F., et al., *Differential selection of multidrug efflux mutants by trovafloxacin and ciprofloxacin in an experimental model of Pseudomonas aeruginosa acute pneumonia in rats.* Antimicrob Agents Chemother, 2001. **45**(2): p. 571-6.

313. Pearson, J.P., C. Van Delden, and B.H. Iglewski, *Active efflux and diffusion are involved in transport of Pseudomonas aeruginosa cell-to-cell signals.* J Bacteriol, 1999. **181**(4): p. 1203-10.

314. Evans, K., et al., *Influence of the MexAB-OprM multidrug efflux system on quorum sensing in Pseudomonas aeruginosa.* J Bacteriol, 1998. **180**(20): p. 5443-7.

315. Jeannot, K., et al., *Induction of the MexXY efflux pump in Pseudomonas aeruginosa is dependent on drug-ribosome interaction.* J Bacteriol, 2005. **187**(15): p. 5341-6.

316. Masuda, N., et al., *Contribution of the MexX-MexY-oprM efflux system to intrinsic resistance in Pseudomonas aeruginosa.* Antimicrob Agents Chemother, 2000. **44**(9): p. 2242-6.

317. Hocquet, D., et al., *Involvement of the MexXY-OprM efflux system in emergence of cefepime resistance in clinical strains of Pseudomonas aeruginosa.* Antimicrob Agents Chemother, 2006. **50**(4): p. 1347-51.

318. Wilke, M.S., et al., *The crystal structure of MexR from Pseudomonas aeruginosa in complex with its antirepressor ArmR.* Proc Natl Acad Sci U S A, 2008. **105**(39): p. 14832-7.

319. Yamamoto, M., et al., *Role of MexZ and PA5471 in transcriptional regulation of mexXY in Pseudomonas aeruginosa.* Microbiology, 2009. **155**(10): p. 3312-3321.

320. Ibuki, T., et al., *Common architecture of the flagellar type III protein export apparatus and F- and V-type ATPases.* Nat Struct Mol Biol, 2011. **18**(3): p. 277-82.

321. Ibuki, T., et al., *Interaction between FliJ and FlhA, components of the bacterial flagellar type III export apparatus.* J Bacteriol, 2013. **195**(3): p. 466-73.

322. Inoue, Y.M., Y. V.; Namba, K.; Minamino, T., *Novel insights into the mechanism of well-ordered assembly of bacterial flagellar proteins in Salmonella.* Sci Rep, 2018. **8**(1): p. 1787.

323. Hung, N.B., et al., *Elucidation of the functional role of flagella in virulence and ecological traits of Pseudomonas cichorii using flagella absence (DeltafliJ) and deficiency (DeltafliI) mutants.* Res Microbiol, 2016. **167**(4): p. 262-271.

324. Wang, K., et al., *The rapid in vivo evolution of Pseudomonas aeruginosa in ventilator-associated pneumonia patients leads to attenuated virulence.* Open biology, 2017. **7**(9): p. 170029.

325. Wilson, M.J. and I.L. Lamont, *Mutational analysis of an extracytoplasmic-function sigma factor to investigate its interactions with RNA polymerase and DNA.* J Bacteriol, 2006. **188**(5): p. 1935-42.

326. Guenard, S., et al., *Multiple mutations lead to MexXY-OprM-dependent aminoglycoside resistance in clinical strains of Pseudomonas aeruginosa.* Antimicrob Agents Chemother, 2014. **58**(1): p. 221-8.

327. Feng, Y., et al., *Dynamics of Mutations during Development of Resistance by Pseudomonas aeruginosa against Five Antibiotics.* Antimicrobial agents and chemotherapy, 2016. **60**(7): p. 4229-4236.

328. Handel, N., et al., *Interaction between mutations and regulation of gene expression during development of de novo antibiotic resistance.* Antimicrob Agents Chemother, 2014. **58**(8): p. 4371-9.

329. Takenouchi, T., E. Sakagawa, and M. Sugawara, *Detection of gyrA mutations among 335 Pseudomonas aeruginosa strains isolated in Japan and their susceptibilities to fluoroquinolones.* Antimicrobial agents and chemotherapy, 1999. **43**(2): p. 406-409.

330. Jorth, P., et al., *Evolved Aztreonam Resistance Is Multifactorial and Can Produce Hypervirulence in Pseudomonas aeruginosa.* mBio, 2017. **8**(5).

331. Farrow, J.M., 3rd and E.C. Pesci, *Two distinct pathways supply anthranilate as a precursor of the Pseudomonas quinolone signal.* J Bacteriol, 2007. **189**(9): p. 3425-33.

332. Rampioni, G., et al., *Unravelling the Genome-Wide Contributions of Specific 2-Alkyl-4-Quinolones and PqsE to Quorum Sensing in Pseudomonas aeruginosa.* PLOS Pathogens, 2016. **12**(11): p. e1006029.

333. Barnes, M.R., *Bioinformatics for geneticists : a bioinformatics primer for the analysis of genetic data*. 2nd ed ed, ed. M.R. Barnes. 2007, England: Chichester, England ; Hoboken, NJ : John Wiley & Sons, c2007.

334. Chevalier, S.B., E.;Bazire, A.;Tahrioui, A.;Duchesne, R.;Tortuel, D.;Maillot, O.;Clamens, T.;Orange, N.;Feuilloley, M. G. J.;Lesouhaitier, O.;Dufour, A.;Cornelis, P., *Extracytoplasmic function sigma factors in Pseudomonas aeruginosa.* Biochim Biophys Acta Gene Regul Mech, 2018.

335. Ochsner, U.A., et al., *GeneChip® expression analysis of the iron starvation response in Pseudomonas aeruginosa: identification of novel pyoverdine biosynthesis genes.* Molecular Microbiology, 2002. **45**(5): p. 1277-1287.

336. Schulz, S., et al., *Elucidation of Sigma Factor-Associated Networks in Pseudomonas aeruginosa Reveals a Modular Architecture with Limited and Function-Specific Crosstalk.* PLOS Pathogens, 2015. **11**(3): p. e1004744.

337. Ringel, M.T. and T. Brüser, *The biosynthesis of pyoverdines.* Microbial cell (Graz, Austria), 2018. **5**(10): p. 424-437.

338. Swingle, B., et al., *Characterization of the PvdS-regulated promoter motif in Pseudomonas syringae pv. tomato DC3000 reveals regulon members and insights regarding PvdS function in other pseudomonads.* Mol Microbiol, 2008. **68**(4): p. 871-89.

339. Brinkman, F.S., et al., *Influence of a putative ECF sigma factor on expression of the major outer membrane protein, OprF, in Pseudomonas aeruginosa and*

Pseudomonas fluorescens. Journal of bacteriology, 1999. **181**(16): p. 4746-4754.

340. Kim, J., et al., *Factors triggering type III secretion in Pseudomonas aeruginosa.* Microbiology, 2005. **151**(Pt 11): p. 3575-87.

341. Horsman, S.R., R.A. Moore, and S. Lewenza, *Calcium chelation by alginate activates the type III secretion system in mucoid Pseudomonas aeruginosa biofilms.* PLoS One, 2012. **7**(10): p. e46826.

342. de Lorenzo, V., et al., *Operator sequences of the aerobactin operon of plasmid ColV-K30 binding the ferric uptake regulation (fur) repressor.* J Bacteriol, 1987. **169**(6): p. 2624-30.

343. Ochs, M., et al., *Surface signaling in transcriptional regulation of the ferric citrate transport system of Escherichia coli: mutational analysis of the alternative sigma factor FecI supports its essential role in fec transport gene transcription.* Mol Gen Genet, 1996. **250**(4): p. 455-65.

344. Potvin, E., F. Sanschagrin, and R.C. Levesque, *Sigma factors in Pseudomonas aeruginosa.* FEMS Microbiol Rev, 2008. **32**(1): p. 38-55.

345. Youard, Z.A., N. Wenner, and C. Reimmann, *Iron acquisition with the natural siderophore enantiomers pyochelin and enantio-pyochelin in Pseudomonas species.* Biometals, 2011. **24**(3): p. 513-22.

346. Wilson, B.R., et al., *Siderophores in Iron Metabolism: From Mechanism to Therapy Potential.* Trends Mol Med, 2016. **22**(12): p. 1077-1090.

347. Kortman, G.A., et al., *Nutritional iron turned inside out: intestinal stress from a gut microbial perspective.* FEMS Microbiol Rev, 2014. **38**(6): p. 1202-34.

348. Wittgens, A., et al., *Novel insights into biosynthesis and uptake of rhamnolipids and their precursors.* Appl Microbiol Biotechnol, 2017. **101**(7): p. 2865-2878.

349. Patankar, Y.R., et al., *Flagellar motility is a key determinant of the magnitude of the inflammasome response to Pseudomonas aeruginosa.* Infect Immun, 2013. **81**(6): p. 2043-52.

350. Lovewell, R.R., et al., *Step-wise loss of bacterial flagellar torsion confers progressive phagocytic evasion.* PLoS Pathog, 2011. **7**(9): p. e1002253.

351. Ramphal, R., et al., *Control of Pseudomonas aeruginosa in the lung requires the recognition of either lipopolysaccharide or flagellin.* J Immunol, 2008. **181**(1): p. 586-92.

352. Skurnik, D., et al., *A comprehensive analysis of in vitro and in vivo genetic fitness of Pseudomonas aeruginosa using high-throughput sequencing of transposon libraries.* PLoS Pathog, 2013. **9**(9): p. e1003582.

353. Lorenz, A., et al., *Importance of flagella in acute and chronic Pseudomonas aeruginosa infections.* Environ Microbiol, 2018.

354. Turner, K.H., et al., *Requirements for Pseudomonas aeruginosa acute burn and chronic surgical wound infection.* PLoS Genet, 2014. **10**(7): p. e1004518.

355. Gabrilska, R.A. and K.P. Rumbaugh, *Biofilm models of polymicrobial infection.* Future microbiology, 2015. **10**(12): p. 1997-2015.

356. Obritsch, M.D., et al., *Nosocomial infections due to multidrug-resistant Pseudomonas aeruginosa: epidemiology and treatment options.* Pharmacotherapy, 2005. **25**(10): p. 1353-64.

357. Dubern, J.-F., et al., *Integrated whole-genome screening for Pseudomonas aeruginosa virulence genes using multiple disease models reveals that pathogenicity is host specific.* Environmental microbiology, 2015. **17**(11): p. 4379-4393.

358. Granato, E.T., et al., *Do Bacterial "Virulence Factors" Always Increase Virulence? A Meta-Analysis of Pyoverdine Production in Pseudomonas aeruginosa As a Test Case.* Frontiers in microbiology, 2016. **7**: p. 1952-1952.

359. Frydrych, L.M., et al., *Diabetes and Sepsis: Risk, Recurrence, and Ruination.* Front Endocrinol (Lausanne), 2017. **8**: p. 271.

360. Tong, S.Y., et al., *Staphylococcus aureus infections: epidemiology, pathophysiology, clinical manifestations, and management.* Clin Microbiol Rev, 2015. **28**(3): p. 603-61.

361. Krismer, B., et al., *The commensal lifestyle of Staphylococcus aureus and its interactions with the nasal microbiota.* Nat Rev Microbiol, 2017. **15**(11): p. 675-687.

362. Archer, N.K., et al., *Staphylococcus aureus biofilms: properties, regulation, and roles in human disease.* Virulence, 2011. **2**(5): p. 445-459.

363. Serra, R., et al., *Chronic wound infections: the role of Pseudomonas aeruginosa and Staphylococcus aureus.* Expert Rev Anti Infect Ther, 2015. **13**(5): p. 605-13.

364. Ahlgren, H.G., et al., *Clinical outcomes associated with Staphylococcus aureus and Pseudomonas aeruginosa airway infections in adult cystic fibrosis patients.* BMC Pulm Med, 2015. **15**: p. 67.

365. Park, H.S., et al., *Early pathogenic colonisers of acute burn wounds: A retrospective review.* Burns, 2017. **43**(8): p. 1757-1765.

366. Rodriguez-Bano, J., *Selection of empiric therapy in patients with catheter-related infections.* Clin Microbiol Infect, 2002. **8**(5): p. 275-81.

367. Maliniak, M.L., A.A. Stecenko, and N.A. McCarty, *A longitudinal analysis of chronic MRSA and Pseudomonas aeruginosa co-infection in cystic fibrosis: A single-center study.* J Cyst Fibros, 2016. **15**(3): p. 350-6.

368. Barnabie, P.M. and M. Whiteley, *Iron-Mediated Control of Pseudomonas aeruginosa-Staphylococcus aureus Interactions in the Cystic Fibrosis Lung.* J Bacteriol, 2015. **197**(14): p. 2250-1.

369. Kumar, A. and Y.P. Ting, *Presence of Pseudomonas aeruginosa influences biofilm formation and surface protein expression of Staphylococcus aureus.* Environmental Microbiology, 2015. **17**(11): p. 4459-4468.

370. Stacy, A., et al., *The biogeography of polymicrobial infection.* Nat Rev Microbiol, 2016. **14**(2): p. 93-105.

371. Bronner, S., H. Monteil, and G. Prevost, *Regulation of virulence determinants in Staphylococcus aureus: complexity and applications.* FEMS Microbiol Rev, 2004. **28**(2): p. 183-200.

372. Novick, R.P., *Autoinduction and signal transduction in the regulation of staphylococcal virulence.* Mol Microbiol, 2003. **48**(6): p. 1429-49.

373. Nadal Jimenez, P., et al., *The Multiple Signaling Systems Regulating Virulence in Pseudomonas aeruginosa.* Microbiology and Molecular Biology Reviews : MMBR, 2012. **76**(1): p. 46-65.

374. DeLeo, F.R., B.A. Diep, and M. Otto, *Host defense and pathogenesis in Staphylococcus aureus infections.* Infectious disease clinics of North America, 2009. **23**(1): p. 17-34.

375. Foster, T.J., et al., *Adhesion, invasion and evasion: the many functions of the surface proteins of Staphylococcus aureus.* Nat Rev Microbiol, 2014. **12**(1): p. 49-62.

376. Goldmann, O. and E. Medina, *Staphylococcus aureus strategies to evade the host acquired immune response.* Int J Med Microbiol, 2018. **308**(6): p. 625-630.

377. Antonic, V., et al., *Pseudomonas aeruginosa induces pigment production and enhances virulence in a white phenotypic variant of Staphylococcus aureus.* Infect Drug Resist, 2013. **6**: p. 175-86.

378. Kuipers, A., et al., *The Staphylococcus aureus polysaccharide capsule and Efb-dependent fibrinogen shield act in concert to protect against phagocytosis.* Microbiology (Reading, England), 2016. **162**(7): p. 1185-1194.

379. Powers, M.E. and J. Bubeck Wardenburg, *Igniting the fire: Staphylococcus aureus virulence factors in the pathogenesis of sepsis.* PLoS pathogens, 2014. **10**(2): p. e1003871-e1003871.

380. Crosby, H.A., J. Kwiecinski, and A.R. Horswill, *Staphylococcus aureus Aggregation and Coagulation Mechanisms, and Their Function in Host-Pathogen Interactions.* Advances in applied microbiology, 2016. **96**: p. 1-41.

381. Hammer, N.D. and E.P. Skaar, *Molecular mechanisms of Staphylococcus aureus iron acquisition.* Annual review of microbiology, 2011. **65**: p. 129-147.

382. Murray, E.J., et al., *Targeting Staphylococcus aureus quorum sensing with nonpeptidic small molecule inhibitors.* Journal of medicinal chemistry, 2014. **57**(6): p. 2813-2819.

383. Yarwood, J.M. and P.M. Schlievert, *Quorum sensing in Staphylococcus infections.* J Clin Invest, 2003. **112**(11): p. 1620-5.

384. Wang, B. and T.W. Muir, *Regulation of Virulence in Staphylococcus aureus: Molecular Mechanisms and Remaining Puzzles.* Cell Chem Biol, 2016. **23**(2): p. 214-224.

385. Fugere, A., et al., *Interspecific small molecule interactions between clinical isolates of Pseudomonas aeruginosa and Staphylococcus aureus from adult cystic fibrosis patients.* PLoS One, 2014. **9**(1): p. e86705.

386. Hoffman, L.R., et al., *Selection for Staphylococcus aureus small-colony variants due to growth in the presence of Pseudomonas aeruginosa.* Proc Natl Acad Sci U S A, 2006. **103**(52): p. 19890-5.

387. Baldan, R., et al., *Adaptation of Pseudomonas aeruginosa in Cystic Fibrosis airways influences virulence of Staphylococcus aureus in vitro and murine models of co-infection.* PLoS One, 2014. **9**(3): p. e89614.

388. Davies, D.G. and C.N.H. Marques, *A fatty acid messenger is responsible for inducing dispersion in microbial biofilms.* Journal of bacteriology, 2009. **191**(5): p. 1393-1403.

389. Mashburn, L.M., et al., *Staphylococcus aureus serves as an iron source for Pseudomonas aeruginosa during in vivo coculture.* J Bacteriol, 2005. **187**(2): p. 554-66.

390. Filkins, L.M., et al., *Coculture of Staphylococcus aureus with Pseudomonas aeruginosa Drives S. aureus towards Fermentative Metabolism and Reduced Viability in a Cystic Fibrosis Model.* Journal of Bacteriology, 2015. **197**(14): p. 2252-2264.

391. Armbruster, C.R., et al., *Staphylococcus aureus Protein A Mediates Interspecies Interactions at the Cell Surface of Pseudomonas aeruginosa.* MBio, 2016. **7**(3).

392. Tognon, M., et al., *Co-evolution with Staphylococcus aureus leads to lipopolysaccharide alterations in Pseudomonas aeruginosa.* ISME J, 2017. **11**(10): p. 2233-2243.

393. Yang, L., et al., *Pattern differentiation in co-culture biofilms formed by Staphylococcus aureus and Pseudomonas aeruginosa.* FEMS Immunol Med Microbiol, 2011. **62**(3): p. 339-47.

394. Orazi, G. and G.A. O'Toole, *Pseudomonas aeruginosa Alters Staphylococcus aureus Sensitivity to Vancomycin in a Biofilm Model of Cystic Fibrosis Infection.* mBio, 2017. **8**(4).

395. Alves, P.M., et al., *Interaction between Staphylococcus aureus and Pseudomonas aeruginosa is beneficial for colonisation and pathogenicity in a mixed biofilm.* Pathog Dis, 2018. **76**(1).

396. Limoli, D.H., et al., *Pseudomonas aeruginosa Alginate Overproduction Promotes Coexistence with Staphylococcus aureus in a Model of Cystic Fibrosis Respiratory Infection.* MBio, 2017. **8**(2).

397. Hotterbeekx, A., et al., *In vivo and In vitro Interactions between Pseudomonas aeruginosa and Staphylococcus spp.* Front Cell Infect Microbiol, 2017. **7**: p. 106.

398. Woods, J., et al., *Development and application of a polymicrobial, in vitro, wound biofilm model.* J Appl Microbiol, 2012. **112**(5): p. 998-1006.

399. Phalak, P., et al., *Metabolic modeling of a chronic wound biofilm consortium predicts spatial partitioning of bacterial species.* BMC Syst Biol, 2016. **10**(1): p. 90.

400. Szamosvari, D. and T. Bottcher, *An Unsaturated Quinolone N-Oxide of Pseudomonas aeruginosa Modulates Growth and Virulence of Staphylococcus aureus.* Angew Chem Int Ed Engl, 2017. **56**(25): p. 7271-7275.

401. Connell, J.L., et al., *Real-time monitoring of quorum sensing in 3D-printed bacterial aggregates using scanning electrochemical microscopy.* Proceedings of the National Academy of Sciences of the United States of America, 2014. **111**(51): p. 18255-18260.

402. Davies, S.K., et al., *Visualizing Antimicrobials in Bacterial Biofilms: Three-Dimensional Biochemical Imaging Using TOF-SIMS.* mSphere, 2017. **2**(4).

403. Darch, S.E., C.B. Ibberson, and M. Whiteley, *Evolution of Bacterial "Frenemies".* MBio, 2017. **8**(3).

404. Dowd, S.E., et al., *Survey of bacterial diversity in chronic wounds using pyrosequencing, DGGE, and full ribosome shotgun sequencing.* BMC Microbiol, 2008. **8**: p. 43.

405. Dalton, T., et al., *An in vivo polymicrobial biofilm wound infection model to study interspecies interactions.* PloS one, 2011. **6**(11): p. e27317-e27317.

406. Loesche, M., et al., *Temporal Stability in Chronic Wound Microbiota Is Associated With Poor Healing.* J Invest Dermatol, 2017. **137**(1): p. 237-244.

407. Anjum, M.F., *Screening methods for the detection of antimicrobial resistance genes present in bacterial isolates and the microbiota.* Future Microbiol, 2015. **10**(3): p. 317-20.

408. Cornforth, D.M., et al., *Pseudomonas aeruginosa transcriptome during human infection.* Proc Natl Acad Sci U S A, 2018. **115**(22): p. E5125-E5134.

List of Appendices

Appendix A: Standard calibration curves for the alkyl quinolones quantification by LC-MS/MS

Appendix B: Regions with less than 75% identity in BRIG diagrams

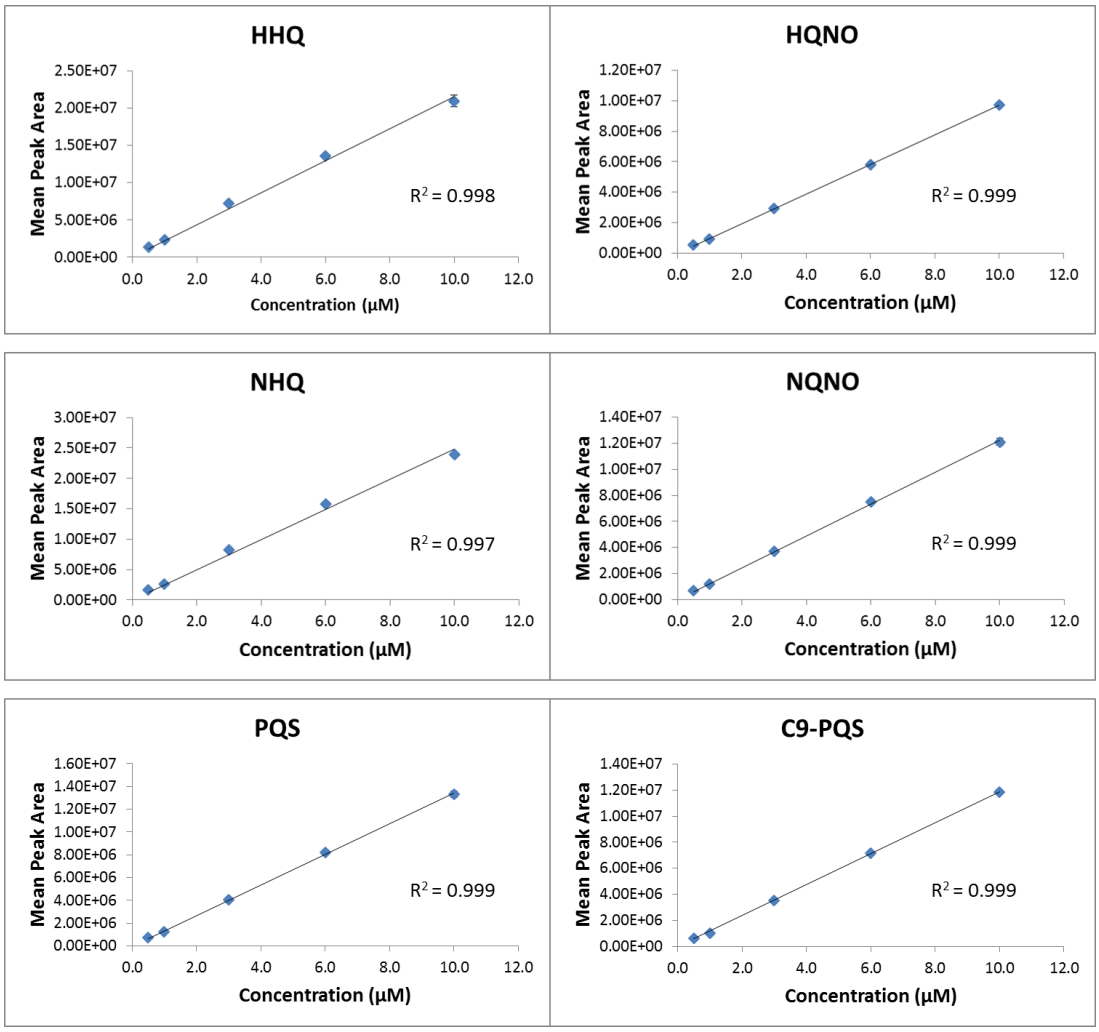
Appendix C: Genes involved with the flagellar assembly pathway in *P. aeruginosa* PAO1

Appendix D: Biological processes associated with genes significantly expressed in CW5 blood when compared to CW5 bone after 18 h growth

Appendix E: List of all genes whose expression differs between the CW5 blood isolates compared with the CW5 bone isolates after 18 h growth

Appendix F: Metabolites identified in interactions with *P. aeruginosa* and *S. aureus*

Appendix A: Standard calibration curves for the alkyl quinolones quantification by LC-MS/MS



Six AQs were tested, and all standard calibration curves had $R^2 > 0.995$. For each AQ five standard concentrations were used: 0.5 µM, 1 µM, 3 µM, 6 µM, and 10 µM.

Appendix B: Regions with less than 75% identity in BRIG diagrams

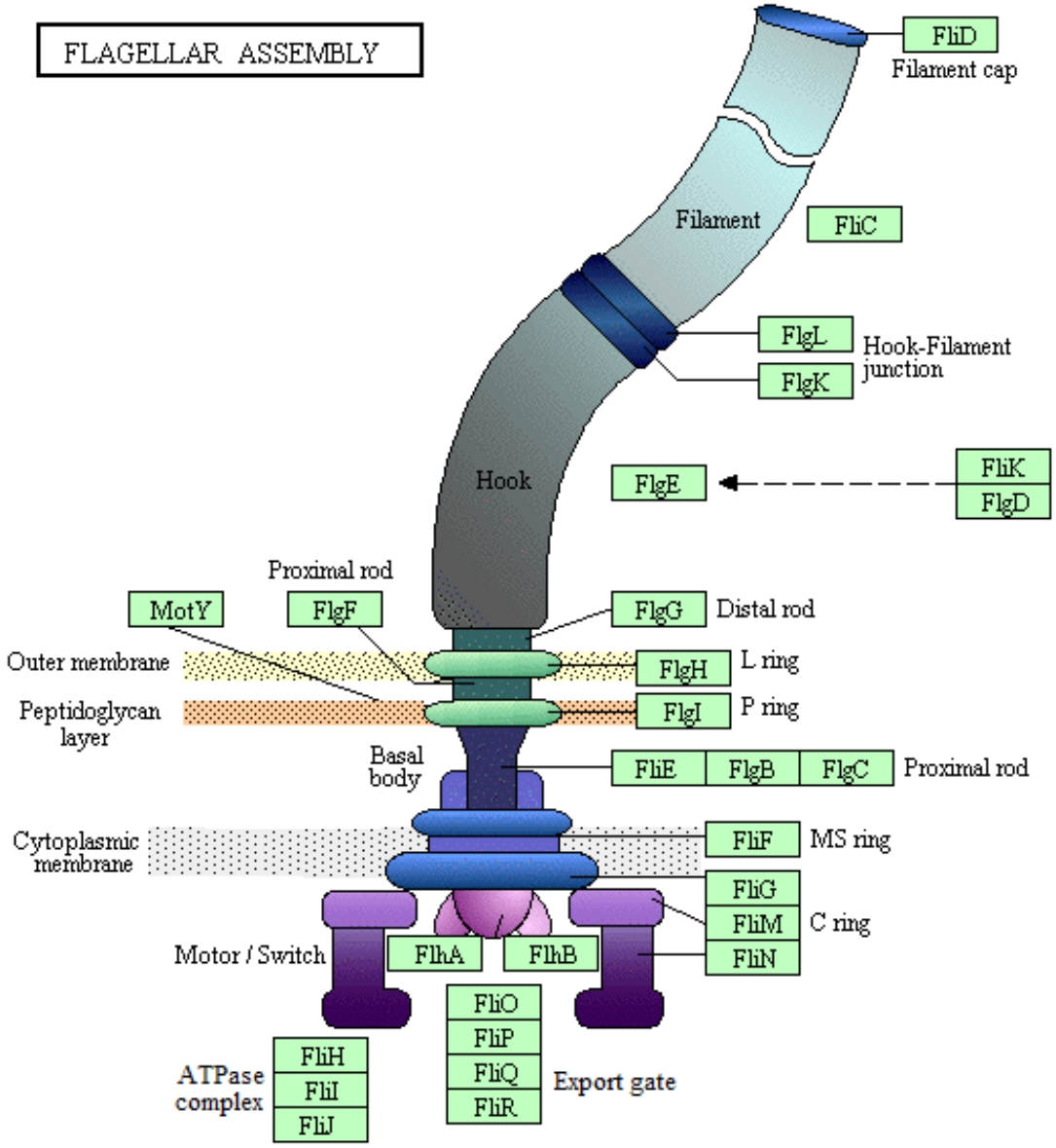
Regions that appear as blank spaces in each ring (zones with less than 75% identity) and that are common to the majority of the chronic wound isolates analysed in this work, were manually identified, checked and numbered R1 to R8. They mostly contain hypothetical proteins, but a description of the start and end positions, the total size of each region, and a detailed list of the corresponding genes and the predicted protein function can be found in the table below.

Region name	Start position	End position	Region size (bp)	Genes and predicted function	Virulence factor list or Pathogen associated list
R1	230543	237111	6568	PA0202: aromatic aa metabolism PA0203–PA0206: ABC transporter for polyamines PA0207: transcriptional regulator	-
R2	1479021	1489095	10074	PA1366–PA1367: toxin/antitoxin system PA1368: potential transposase PA1369–PA1372: hypothetical proteins of unknown function	PA1369
R3	1498338	1516927	18589	PA1381: hypothetical protein of unknown function PA1382: type II/III protein secretion system PA1383: hypothetical protein of unknown function PA1384: GalE UDP-glucose 4-epimerase PA1385: glycosyl transferase PA1386: ABC transporter PA1387: nucleotide-diphospho-sugar transferase PA1388–PA1391: glycosyl transferases PA1392: hypothetical protein with nucleoside triphosphate hydrolase domain PA1393: adenosine 5'-phosphosulfate (APS) kinase	PA1385
R4	2111691	2122222	10531	PA1931: probable ferredoxin PA1932: probable hydroxylase molybdopterin-containing subunit PA1933: probable hydroxylase large subunit; PA1934–PA1936: hypothetical proteins of unknown function PA1937: hypothetical protein with DNA binding and transposase domains PA1938: hypothetical protein with nucleic acid binding and DNA integration domains PA1939: hypothetical protein with ATPase domain	PA1936

Region name	Start position	End position	Region size (bp)	Genes and predicted function	Virulence factor list or Pathogen associated list
R5	2439150	2450765	11615	PA2218: TAT protein with dipeptidyl-peptidase-like domain PA2219: membrane protein OpdE with major facilitator superfamily (MFS) domain PA2220: probable transcriptional regulator OprR PA2221: DNA integration protein PA2222: hypothetical protein with lysozyme-like domain PA2223: hypothetical protein with toxin homologue of phage lysozyme domain PA2224: hypothetical protein of unknown function PA2225: hypothetical protein with lipoprotein lipid attachment site PA2226: QsrO quorum-sensing regulator PA2227: AraC-type transcriptional regulator VqsM PA2228: unknown with lipoprotein lipid attachment site, beta-lactamase-related	-
R6	2755725	2780614	24889	PA2455: hypothetical protein with N-acetyltransferase activity PA2456–PA2457: hypothetical protein of unknown function PA2458: hypothetical protein involved with protein binding PA2459–PA2461: hypothetical proteins of unknown function PA2462: hypothetical protein involved in arginine metabolism PA2463: hypothetical protein involved with protein transport	PA2456 PA2462
R7	3088660	3098979	10319	PA2730–PA2731: hypothetical proteins of unknown function PA2732: hypothetical protein involved with DNA modification PA2733: conserved hypothetical protein PA2734: hypothetical protein of unknown function PA2735: probable restriction-modification system protein PA2736: hypothetical protein involved with regulation of transcription	-

Region name	Start position	End position	Region size (bp)	Genes and predicted function	Virulence factor list or Pathogen associated list
R8	3914117	3930230	16113	PA3497: hypothetical protein of unknown function PA3498:probable oxidoreductase PA3499: hypothetical protein identified as a structural homologue of YjgF family PA3500: conserved hypothetical protein involved with oxireductase activity PA3501–PA3503: hypothetical proteinPA3504: probable aldehydrogenase PA3505: hypothetical protein possibly with aspartate dehydrogenase activity PA3506: probable decarboxylase PA3507: probable short-chan dehydrogenase PA3508: probable transcriptional regulator PA3509: probable hydrolase PA3510: hypothetical protein of unknown function PA3511: probable short-chan dehydrogenase PA3512: probable permease of ABC transporter PA3513: hypothetical protein of unknown function PA3514: probable ATP-binding component of ABC transporter	PA3498

Appendix C: Genes involved with the flagellar assembly pathway in *P. aeruginosa* PAO1 (adapted from KEGG pathway pae02040*)*



Gram-negative flagella are divided into three parts: the basal body (with MS, C, P, and L rings and the rod which is embedded in the cell envelope), the hook (FlgE) and hook-filament junction zone (FlgK, FlgL), and finally the filament (FliC) plus the filament cap (FliD). The Mot complex is responsible for the generation of proton flow that energises the motor components of the basal body, while the hook zone is essential to transmit the torque produced by the motor to the filament, and the filament itself acts like a helical screw to produce thrust essential for motility.

Appendix D: Biological processes associated with genes significantly expressed in CW5 blood when compared to CW5 bone at 18 h

GO term for biological process		% bio	Total in category	Genes in blood that change expression	
Code	Full term description			Downregulated	Upregulated
GO:0034589	hydroxyproline transport	100.0%	4	4 (lhpO, lhpN, lhpM, lhpP)	-
GO:0050708	regulation of protein secretion	100.0%	4	4 (pcr2, exsC, pscB, spcS)	-
GO:0030261	chromosome condensation	75.0%	4	3 (pctC, pctB, ctpL)	-
GO:0043200	response to amino acid	75.0%	4	3 (pctC, pctB, pctA)	-
GO:0030254	protein secretion by the type III secretion system	72.2%	36	25 (pscU, pscR, pscQ, pscP, pscO, PA1697, popN, pcr1, pcr2, pcr3, pcr4, pcrV, pcrH, exsC, exsE, pscB, pscC, pscD, pscE, pscF, pscG, pscH, pscI, pscJ, pscK)	1 (fliI = 3.12 FC)
GO:0035999	tetrahydrofolate interconversion	66.7%	3	2 (glyA1, glyA2)	-
GO:0050709	negative regulation of protein secretion	66.7%	12	7 (popN, pcr1, pcrD, pcrG, exsE, exsA, exsD)	1 (mexR = 54.71 FC)
GO:0042710	biofilm formation	56.3%	16	9 (pslB, pslC, pslD, pslE, pslF, pslG, pslH, pslI, lecB)	-
GO:0045226	extracellular polysaccharide biosynthetic process	42.9%	21	8 (pslB, pslC, pslD, pslE, pslF, pslG, pslH, pslI)	1 (pelA = 1.94 FC)
GO:0015947	methane metabolic process	33.3%	3	1 (glyA2)	-
GO:0019441	tryptophan catabolic process to kynurenine	33.3%	3	1 (kynU)	-
GO:1902201	negative regulation of bacterial-type flagellum-dependent cell motility	20.0%	5	1 (gcbA)	-
GO:0006554	lysine catabolic process	16.7%	6	1 (glyA2)	-
GO:0006119	oxidative phosphorylation	10.0%	10	1 (nouE)	-
GO:0009117	nucleotide metabolic process	2.2%	46	1 (purD)	-

GO term for biological process		% bio	Total in category	Genes in blood that change expression	
Code	Full term description			Downregulated	Upregulated
GO:0015685	ferric-enterobactin transport	100.0%	4	-	4 (fepC, fepB, fepD, fepG)
GO:0042864	pyochelin biosynthetic process	100.0%	4	-	4 (pchF/pchE/pchC/pchA)
GO:0034756	regulation of iron ion transport	90.9%	11	-	10 (fiuR, fiuI, PA1300, PA1363, femA, foxR, foxI, hasI, fecI, PA4896)
GO:0044780	bacterial-type flagellum assembly	76.5%	17	-	13 (flgB, flgC, flgF, flgG, flgI, flgJ, flgK, fliI, fliQ, fliR, flhB, flhA, PA3352)
GO:0015891	siderophore transport	72.7%	22	1 (femI = 2.63 FC)	15 (PA0151, PA0434, fiuA, pirA, femA, foxA, pfeA, PA3268, fecA, fvbA, fpvB, fptA, PA4514, chtA, tonB1)
GO:0007166	cell surface receptor signaling pathway	61.5%	13	1 (femI = 2.63 FC)	7 (PA0151, fiuA, PA1302, foxA, hasR, fecA, PA4897)
GO:0071973	bacterial-type flagellum-dependent cell motility	60.9%	23	-	14 (flgB, flgC, flgF, flgG, flgH, flgI, fliE, fliF, fliG, fliI, fliJ, PA1442, fliM, fliN)
GO:0071475	cellular hyperosmotic salinity response	50.0%	2	-	3 (opuCD, opuCC, opuCB)
GO:0006352	DNA-templated transcription, initiation	48.0%	25	1 (femI = 2.63 FC)	11 (PA0149, fiuI, vreI, PA1300, PA1363, fliA, pvdS, foxI, hasI, fecI, PA4896)
GO:0015838	amino-acid betaine transport	42.9%	7	-	3 (opuCD, opuCC, opuCB)
GO:0006741	NADP biosynthetic process	33.3%	3	-	1 (PA4149)
GO:0031460	glycine betaine transport	30.0%	10	-	3 (opuCD, opuCC, opuCB)
GO:0006559	L-phenylalanine catabolic process	16.7%	6	-	1 (phhB)
GO:0032885	regulation of polysaccharide biosynthetic process	14.3%	7	-	1 (glmR)

GO term for biological process		% bio	Total in category	Genes in blood that change expression	
Code	Full term description			Downregulated	Upregulated
GO:0006935	chemotaxis	51.1%	45	13 (PA0173, PA0174, aer2, PA0177, PA1608, ctpH, PA2652, PA3349, pctC, pctA, pctB, ctpL, PA5072)	10 (fliG, fliJ, PA1442, fliN, fliO, fliP, cheZ, PA1463, PA1464, PA2654)
GO:0009405	pathogenesis	24.6%	65	13 (exoT, pscP, popN, pcrV, popB, pscE, pscF, pscG, pscH, pscK, exoY, exoS, spcS)	3 (tonB1, mexA, vreI)
GO:0007165	signal transduction	21.2%	104	15 (siaA, aer2, PA0177, PA1608, ctpH, PA2652, PA2788, PA2867, PA3349, pctC, pctA, pctB, PA4633, ctpL, PA5072)	7 (PA0930, fleS, PA1243, PA1463, PA1464, PA2654, pfeS)
GO:0006598	polyamine catabolic process	15.4%	13	1 (pauA7)	1 (pauA3)
GO:0006950	response to stress	13.3%	15	1 (pcrH)	1 (PA5027)
GO:0006099	tricarboxylic acid cycle	11.1%	18	1 (prpC)	1 (fumC1)
GO:0006091	generation of precursor metabolites and energy	9.1%	88	6 (nuoE, nuoF, fhp, nosR, nosZ, PA4133)	2 (zwf, glgB)
GO:0006520	cellular amino acid metabolic process	5.2%	134	4 (glyA2,mmsA,hutH,glyA1)	3 (bkdA1,bkdA2,betB)

"% bio" was calculated as the number of genes with more than 2 fold-change divided by the total number of genes associated with that biological process.

Appendix E: List of all genes whose expression differs between the CW5 blood isolates compared with the CW5 bone isolates after 18 h growth. From a total of 1746 differentially expressed genes at 18 h, 219 were downregulated genes (618 genes deleted because they were below log2FC 0.95) and 316 were upregulated genes (593 genes deleted because they were below log2FC 0.95). List ordered by decreasing fold change values.

GeneID	Gene Name	log2FoldChange	Fold Change
PA0672	hemO,heme oxygenase	-6.66	100.99
PA4229	pchC,pyochelin biosynthetic protein PchC	-6.47	88.57
PA3530	bfd,bacterioferritin-associated ferredoxin Bfd	-6.32	80.12
PA1913	hypothetical protein	6.29	78.24
PA4228	pchD,pyochelin biosynthesis protein PchD	-6.00	64.02
PA5373	betB,betaine aldehyde dehydrogenase	-6.00	64.00
PA4230	pchB,salicylate biosynthesis protein PchB	-5.98	63.15
PA2426	pvdS,sigma factor PvdS	-5.96	62.16
PA4221	fptA,Fe(III)-pyochelin outer membrane receptor precursor	-5.87	58.54
PA0424	mexR,multidrug resistance operon repressor MexR	-5.77	54.71
PA1695	pscP,translocation protein in type III secretion	5.71	52.41
PA4226	pchE,dihydroaeruginoic acid synthetase	-5.66	50.43
PA2686	pfeR,two-component response regulator PfeR	-5.64	49.90
PA4843	gcbA,GcbA	5.64	49.75
PA4709	phuS,PhuS	-5.58	47.70
PA4704.3	prrH,PrrH	-5.54	46.48
PA4710	phuR,Heme/Hemoglobin uptake outer membrane receptor PhuR precursor	-5.51	45.62
PA2687	pfeS,two-component sensor PfeS	-5.40	42.21
PA4469	hypothetical protein	-5.39	41.82
PA4231	pchA,salicylate biosynthesis isochorismate synthase	-5.36	40.95
PA0471	fiuR,FiuR	-5.35	40.67
PA3526	motY,MotY	5.29	39.08
PA0800	hypothetical protein	-5.28	38.83
PA0472	fiuI,FiuI	-5.11	34.55
PA4470	fumC1,fumarate hydratase	-5.10	34.32

PA4895	probable transmembrane sensor	-5.02	32.53
PA1696	pscO,translocation protein in type III secretion	5.01	32.19
PA1694	pscQ,translocation protein in type III secretion	5.01	32.16
PA4224	pchG,pyochelin biosynthetic protein PchG	-4.97	31.37
PA4219	ampO,AmpO	-4.95	30.86
PA3531	bfrB,bacterioferritin	4.94	30.69
PA3407	hasAp,heme acquisition protein HasAp	-4.92	30.23
PA4227	pchR,transcriptional regulator PchR	-4.88	29.37
PA1697	ATP synthase in type III secretion system	4.85	28.84
PA1452	flhA,flagellar biosynthesis protein FlhA	-4.85	28.82
PA2467	foxR,Anti-sigma factor FoxR	-4.82	28.24
PA4357	conserved hypothetical protein	-4.80	27.92
PA0982	hypothetical protein	4.79	27.65
PA4471	hypothetical protein	-4.75	26.84
PA0425	mexA,Resistance-Nodulation-Cell Division multidrug efflux membrane fusion protein MexA precursor	-4.68	25.58
PA4220	fptB	-4.63	24.81
PA3406	hasD,transport protein HasD	-4.63	24.73
PA1100	fliE,flagellar hook-basal body complex protein FliE	-4.60	24.33
PA4896	probable sigma-70 factor, ECF subfamily	-4.60	24.24
PA4844	ctpL,CtpL	4.56	23.57
PA0470	fiuA,Ferrichrome receptor FiuA	-4.55	23.48
PA1698	popN,Type III secretion outer membrane protein PopN precursor	4.55	23.37
PA4358	feoB,FeoB	-4.54	23.26
PA4223	pchH, probable ATP-binding component of ABC transporter	-4.54	23.24
PA1699	pcr1,Pcr1	4.51	22.79
PA1701	pcr3,Pcr3	4.51	22.77
PA3350	hypothetical protein	-4.48	22.27
PA3405	hasE,metalloprotease secretion protein	-4.46	22.04
PA4222	pchI, probable ATP-binding component of ABC transporter	-4.44	21.76
PA0802	hypothetical protein	-4.42	21.45

PA1700	pcr2,Pcr2	4.42	21.41
PA4468	sodM,superoxide dismutase	-4.42	21.41
PA2468	foxI,ECF sigma factor FoxI	-4.40	21.07
PA1101	fliF,Flagella M-ring outer membrane protein precursor	-4.38	20.89
PA4310	pctB,chemotactic transducer PctB	4.38	20.79
PA5217	probable binding protein component of ABC iron transporter	-4.38	20.76
PA1705	pcrG,regulator in type III secretion	4.37	20.69
PA1098	fleS,two-component sensor	-4.35	20.33
PA4467	hypothetical protein	-4.33	20.06
PA2466	foxA,Ferrioxamine receptor FoxA	-4.29	19.52
PA3408	hasR,Heme uptake outer membrane receptor HasR precursor	-4.27	19.32
PA1082	flgG,flagellar basal-body rod protein FlgG	-4.27	19.25
PA2688	pfeA,Ferric enterobactin receptor, outer membrane protein PfeA precursor	-4.24	18.96
PA4225	pchF,pyochelin synthetase	-4.24	18.84
PA1099	fleR,two-component response regulator	-4.15	17.69
PA1706	pcrV,type III secretion protein PcrV	4.07	16.74
PA1083	flgH,flagellar L-ring protein precursor FlgH	-4.02	16.18
PA4218	ampP,AmpP	-4.00	15.96
PA4371	hypothetical protein	-4.00	15.96
PA2664	fhp,flavohemoprotein	4.00	15.95
PA1453	flhF,flagellar biosynthesis protein FlhF	-3.97	15.68
PA3404	probable outer membrane protein precursor	-3.97	15.66
PA2197	conserved hypothetical protein	3.94	15.37
PA4515	conserved hypothetical protein	-3.94	15.32
PA5531	tonB1,TonB1	-3.93	15.25
PA0801	hypothetical protein	-3.93	15.20
PA2788	probable chemotaxis transducer	3.86	14.53
PA4708	phuT,Heme-transport protein, PhuT	-3.84	14.34
PA4516	hypothetical protein	-3.80	13.97
PA4160	fepD,ferric enterobactin transport protein FepD	-3.77	13.69

PA0426	mexB,Resistance-Nodulation-Cell Division multidrug efflux transporter MexB	-3.77	13.63
PA1702	pcr4,Pcr4	3.77	13.63
PA1084	flgI,flagellar P-ring protein precursor FlgI	-3.75	13.43
PA1302	probable heme utilization protein precursor, HxuC	-3.72	13.22
PA4168	fpvB,second ferric pyoverdine receptor FpvB	-3.69	12.87
PA3842	spcS,specific Pseudomonas chaperone for ExoS, SpcS	3.65	12.58
PA1707	pcrH,regulatory protein PcrH	3.62	12.33
PA1715	pscB,type III export apparatus protein	3.60	12.09
PA2149	hypothetical protein	-3.59	12.02
PA0263	hcpC,secreted protein Hcp	-3.58	11.92
PA1716	pscC,Type III secretion outer membrane protein PscC precursor	3.55	11.72
PA2140	probable metallothionein	-3.52	11.47
PA4370	icmP,Insulin-cleaving metalloproteinase outer membrane protein precursor	-3.50	11.33
PA3722	hypothetical protein	3.49	11.24
PA2198	hypothetical protein	3.49	11.22
PA1255	lhpK,D-hydroxyproline epimerase, LhpK	3.46	10.97
PA3283	conserved hypothetical protein	3.45	10.94
PA4675	chtA,ChtA	-3.45	10.94
PA2403	fpvG,FpvG	-3.45	10.90
PA1717	pscD,type III export protein PscD	3.42	10.69
PA5386	cdhA,CdhA, Carnitine dehydrogenase	3.42	10.68
PA3843	hypothetical protein	3.41	10.66
PA1708	popB,translocator protein PopB	3.36	10.24
PA4897	TonB-dependent receptor	-3.35	10.22
PA5384	hocS,HocS	3.34	10.14
PA4359	conserved hypothetical protein, feoA	-3.32	10.00
PA1442	conserved hypotetical protein	-3.31	9.91
PA1714	exsD,ExsD	3.26	9.58
PA1301	probable transmembrane sensor	-3.24	9.44
PA0931	pirA,ferric enterobactin receptor PirA	-3.23	9.41

PA1454	fleN,flagellar synthesis regulator FleN	-3.23	9.38
PA1693	pscR,translocation protein in type III secretion	3.23	9.37
PA1709	popD,Translocator outer membrane protein PopD precursor	3.22	9.29
PA4929	hypothetical protein	3.20	9.21
PA1256	lhpO,ABC transporter ATP-binding protein, LhpO	3.18	9.07
PA1443	fliM,flagellar motor switch protein FliM	-3.18	9.04
PA3284	hypothetical protein	3.16	8.95
PA4161	fepG,ferric enterobactin transport protein FepG	-3.12	8.69
PA0427	oprM,Major intrinsic multiple antibiotic resistance efflux outer membrane protein OprM precursor	-3.09	8.50
PA5387	cdhC,CdhC, Carnitine dehydrogenase-related gene C	3.06	8.36
PA2405	fpvJ,FpvJ	-3.05	8.27
PA1703	pcrD,type III secretory apparatus protein PcrD	3.04	8.25
PA2406	fpvK,FpvK	-3.04	8.22
PA0044	exoT,exoenzyme T	3.02	8.11
PA3177	hypothetical protein	-3.02	8.10
PA4133	cytochrome c oxidase subunit (cbb3-type)	3.02	8.08
PA0930	two-component sensor	-3.00	8.01
PA1444	fliN,flagellar motor switch protein FliN	-3.00	7.99
PA1713	exsA,transcriptional regulator ExsA	2.99	7.94
PA3901	fecA,Fe(III) dicitrate transport protein FecA	-2.98	7.88
PA4309	pctA,chemotactic transducer PctA	2.97	7.82
PA4159	fepB,ferrienterobactin-binding periplasmic protein precursor FepB	-2.94	7.69
PA3899	fecI,FecI	-2.94	7.66
PA1102	fliG,flagellar motor switch protein FliG	-2.94	7.65
PA2404	fpvH,FpvH	-2.93	7.64
PA1081	flgF,flagellar basal-body rod protein FlgF	-2.91	7.52
PA1719	pscF,type III export protein PscF	2.91	7.51
PA1085	flgJ,flagellar protein FlgJ	-2.91	7.49
PA2199	probable dehydrogenase	2.90	7.47
PA4633	probable chemotaxis transducer	2.90	7.45

PA5385	cdhB,CdhB, Carnitine dehydrogenase-related gene B	2.89	7.43
PA2191	exoY,adenylate cyclase ExoY	2.88	7.34
PA0433	hypothetical protein	-2.87	7.33
PA1710	exsC,ExsC, exoenzyme S synthesis protein C precursor.	2.87	7.30
PA1257	lhpN,amino acid ABC transporter membrane protein, LhpN	2.87	7.29
PA1712	exsB,exoenzyme S synthesis protein B	2.86	7.26
PA4570	hypothetical protein	-2.85	7.19
PA0929	two-component response regulator	-2.84	7.16
PA1718	pscE,type III export protein PscE	2.84	7.15
PA1711	exsE,ExsE	2.80	6.98
PA1721	pscH,type III export protein PscH	2.80	6.96
PA1720	pscG,type III export protein PscG	2.77	6.81
PA1260	lhpP,ABC transporter periplasmic-binding protein, LhpP	2.77	6.81
PA1462	probable plasmid partitioning protein	-2.76	6.79
PA3282	hypothetical protein	2.75	6.75
PA0434	hypothetical protein - possible siderophore related	-2.75	6.70
PA3601	conserved hypothetical protein	-2.73	6.64
PA3600	conserved hypothetical protein	-2.71	6.53
PA3900	fecR,FecR	-2.71	6.53
PA1445	fliO,flagellar protein FliO	-2.66	6.30
PA3662	hypothetical protein	2.65	6.29
PA3570	mmsA,methylmalonate-semialdehyde dehydrogenase	2.65	6.27
PA1086	flgK,flagellar hook-associated protein 1 FlgK	-2.65	6.27
PA2146	conserved hypothetical protein	-2.62	6.16
PA1455	fliA,sigma factor FliA (rpoF)	-2.62	6.13
PA2954	hypothetical protein	-2.60	6.07
PA3767	conserved hypothetical protein	-2.60	6.05
PA3281	hypothetical protein	2.59	6.01
PA3740	hypothetical protein	2.59	6.00
PA4307	pctC,chemotactic transducer PctC	2.59	6.00

PA5072	probable chemotaxis transducer	2.56	5.91
PA2166	hypothetical protein	-2.56	5.90
PA2407	fpvC,FpvC	-2.54	5.81
PA4134	hypothetical protein	2.53	5.78
PA2134	hypothetical protein	-2.47	5.55
PA3569	mmsB,3-hydroxyisobutyrate dehydrogenase	2.46	5.52
PA1910	femA,ferric-mycobactin receptor, FemA	-2.46	5.49
PA2161	hypothetical protein	-2.46	5.49
PA0435	hypothetical protein	-2.45	5.45
PA3768	probable metallo-oxidoreductase	-2.43	5.38
PA1259	lhpH,LhpH	2.43	5.38
PA2955	hypothetical protein	-2.41	5.32
PA2654	probable chemotaxis transducer	-2.41	5.31
PA1722	pscI,type III export protein PscI	2.41	5.30
PA4158	fepC,ferric enterobactin transport protein FepC	-2.38	5.22
PA2181	hypothetical protein	-2.37	5.17
PA2143	hypothetical protein	-2.36	5.15
PA2034	hypothetical protein	-2.36	5.14
PA2196	TetR family transcriptional regulator	2.35	5.09
PA1446	fliP,flagellar biosynthetic protein FliP	-2.34	5.05
PA2033	hypothetical protein	-2.32	4.99
PA4372	hypothetical protein	-2.32	4.98
PA1300	ECF sigma factor	-2.31	4.98
PA0977	hypothetical protein	2.30	4.92
PA1096	hypothetical protein	-2.29	4.91
PA4688	hitB,iron (III)-transport system permease HitB	-2.29	4.89
PA4208	opmD,probable outer membrane protein precursor	2.28	4.87
PA0149	probable sigma-70 factor, ECF subfamily	-2.27	4.81
PA2159	conserved hypothetical protein	-2.25	4.74
PA4514	probable outer membrane receptor for iron transport	-2.25	4.74

PA2567	hypothetical protein	2.24	4.74
PA0674	vreA,VreA - virulence regulator involving ECF sigma factor	-2.23	4.70
PA2148	conserved hypothetical protein	-2.22	4.67
PA4513	probable oxidoreductase	-2.19	4.58
PA2142	probable short-chain dehydrogenase	-2.19	4.57
PA1463	hypothetical protein	-2.18	4.53
PA4171	probable protease	-2.18	4.52
PA4090	hypothetical protein	-2.18	4.52
PA5388	caiX,CaiX	2.16	4.47
PA2178	hypothetical protein	-2.16	4.47
PA2154	conserved hypothetical protein	-2.14	4.42
PA3274	hypothetical protein	-2.14	4.41
PA5216	probable permease of ABC iron transporter	-2.13	4.38
PA2165	probable glycogen synthase	-2.12	4.35
PA2179	hypothetical protein	-2.11	4.33
PA1845	tsi1,Tsi1	-2.10	4.30
PA2164	probable glycosyl hydrolase	-2.09	4.27
PA3897	hypothetical protein	2.09	4.26
PA2169	hypothetical protein	-2.07	4.21
PA2144	glgP,glycogen phosphorylase	-2.07	4.20
PA1783	nasA,nitrate transporter	-2.06	4.16
PA2184	conserved hypothetical protein	-2.06	4.16
PA4707	phuU,PhuU	-2.05	4.14
PA2867	probable chemotaxis transducer	2.04	4.13
PA1103	probable flagellar assembly protein	-2.04	4.11
PA2151	conserved hypotetical protein	-2.04	4.11
PA2135	probable transporter	-2.03	4.09
PA4167	probable oxidoreductase	-2.03	4.08
PA2160	probable glycosyl hydrolase	-2.03	4.07
PA4172	probable nuclease	-2.02	4.06

PA2180	hypothetical protein	-2.02	4.05
PA3841	exoS,exoenzyme S	2.00	4.00
PA3410	hasI,HasI	-1.99	3.97
PA2158	probable alcohol dehydrogenase (Zn-dependent)	-1.98	3.94
PA2163	hypothetical protein	-1.98	3.94
PA1692	probable translocation protein in type III secretion	1.97	3.93
PA2542	conserved hypothetical protein	-1.97	3.92
PA2157	hypothetical protein	-1.95	3.87
PA4687	hitA,ferric iron-binding periplasmic protein HitA	-1.95	3.87
PA4324	hypothetical protein	1.95	3.87
PA2162	probable glycosyl hydrolase	-1.95	3.86
PA1704	pcrR,transcriptional regulator protein PcrR	1.95	3.85
PA3931	conserved hypothetical protein	-1.94	3.83
PA0793	hypothetical protein	1.94	3.83
PA2150	conserved hypothetical protein	-1.93	3.80
PA2137	hypothetical protein	-1.92	3.79
PA2107	hypothetical protein	-1.92	3.79
PA0496	conserved hypothetical protein	1.92	3.78
PA0794	probable aconitate hydratase	1.88	3.68
PA2200	Cyclic-guanylate-specific phosphodiesterase	1.85	3.61
PA1541	probable drug efflux transporter	-1.82	3.54
PA2156	conserved hypothetical protein	-1.82	3.52
PA2183	hypothetical protein	-1.80	3.49
PA1844	tse1,Tse1	-1.79	3.46
PA1441	putative flagellar hook-length control protein FliK	-1.79	3.46
PA3307	hypothetical protein	1.78	3.44
PA1545	hypothetical protein	1.76	3.38
PA2357	msuE,NADH-dependent FMN reductase MsuE	-1.75	3.36
PA4091	hpaA,4-hydroxyphenylacetate 3-monooxygenase large chain	-1.74	3.35
PA1132	hypothetical protein	1.74	3.34

PA1447	fliQ,flagellar biosynthetic protein FliQ	-1.74	3.33
PA2381	hypothetical protein	-1.73	3.32
PA2761	hypothetical protein	-1.73	3.32
PA2190	conserved hypothetical protein	-1.73	3.32
PA2514	antC,anthranilate dioxygenase reductase	1.73	3.31
PA0675	vreI,ECF sigma factor, VreI	-1.72	3.31
PA2186	hypothetical protein	-1.72	3.30
PA2408	fpvD,FpvD	-1.72	3.30
PA4148	probable short-chain dehydrogenase	-1.72	3.29
PA2141	hypothetical protein	-1.72	3.28
PA1456	cheY,two-component response regulator CheY	-1.71	3.26
PA1540	conserved hypotetical protein	-1.70	3.26
PA3352	hypothetical protein	-1.69	3.23
PA3268	probable TonB-dependent receptor	-1.69	3.23
PA2120	hypothetical protein	-1.69	3.23
PA2138	ligD,Multifunctional non-homologous end joining protein LigD	-1.69	3.23
PA2016	liuR,regulator of liu genes	1.69	3.23
PA1882	probable transporter	-1.67	3.18
PA1909	hypothetical protein	-1.67	3.17
PA4601	morA,motility regulator	1.67	3.17
PA4770	lldP,L-lactate permease	1.65	3.14
PA3189	probable permease of ABC sugar transporter	1.65	3.14
PA1474	hypothetical protein	1.64	3.12
PA1104	fliI,flagellum-specific ATP synthase FliI	-1.64	3.12
PA5106	conserved hypothetical protein	1.63	3.09
PA0796	prpB,carboxyphosphonoenolpyruvate phosphonomutase	1.62	3.07
PA1258	lhpM,Permease of ABC transporter, LhpM	1.61	3.06
PA0803	hypothetical protein	-1.61	3.04
PA2155	probable phospholipase	-1.60	3.03
PA4373	hypothetical protein	-1.59	3.01

PA1316	probable major facilitator superfamily (MFS) transporter	-1.59	3.00
PA4771	lldD,L-lactate dehydrogenase	1.58	2.99
PA5157	probable transcriptional regulator	1.58	2.99
PA2153	glgB,1,4-alpha-glucan branching enzyme	-1.57	2.97
PA3720	hypothetical protein	1.57	2.96
PA3349	probable chemotaxis protein	1.56	2.95
PA2685	vgrG4,VgrG4	-1.55	2.93
PA2433	hypothetical protein	-1.55	2.93
PA2187	hypothetical protein	-1.54	2.91
PA3729	conserved hypothetical protein	1.53	2.89
PA2152	probable trehalose synthase	-1.53	2.89
PA3188	probable permease of ABC sugar transporter	1.53	2.89
PA3865	probable amino acid binding protein	1.52	2.87
PA2245	pslO,hypotetical protein	-1.52	2.87
PA0176	aer2,aerotaxis transducer Aer2	1.52	2.86
PA5158	probable outer membrane protein precursor	1.52	2.86
PA2173	hypothetical protein	-1.52	2.86
PA2233	pslC,PslC	1.51	2.84
PA0173	probable methylesterase	1.51	2.84
PA2172	hypothetical protein	-1.51	2.84
PA0175	cheR2, probable chemotaxis protein methyltransferase	1.50	2.83
PA3392	nosZ,nitrous-oxide reductase precursor	1.50	2.82
PA1870	hypothetical protein	-1.49	2.82
PA0174	conserved hypothetical protein	1.49	2.81
PA1967	hypothetical protein	-1.49	2.81
PA4141	hypothetical protein	1.49	2.80
PA1464	probable purine-binding chemotaxis protein, cheW	-1.49	2.80
PA2409	fpvE,FpvE	-1.48	2.79
PA1448	fliR,flagellar biosynthetic protein FliR	-1.47	2.78
PA3728	hypothetical protein	1.47	2.77

PA2170	hypothetical protein	-1.46	2.76
PA1679	hypothetical protein	1.45	2.73
PA2171	hypothetical protein	-1.45	2.72
PA4877	hypothetical protein	-1.44	2.72
PA1254	lhpC,delta1-pyrroline-4-hydroxy-2-carboxylate deaminase, LphC	1.44	2.72
PA1731	conserved hypothetical protein	-1.44	2.71
PA1723	pscJ,type III export protein PscJ	1.44	2.71
PA2868	hypothetical protein	1.43	2.70
PA2147	katE,catalase HPII	-1.43	2.70
PA2069	probable carbamoyl transferase	1.43	2.70
PA5098	hutH,histidine ammonia-lyase	1.43	2.70
PA2652	methyl-accepting chemotaxis protein	1.43	2.69
PA2078	(7S,10S)-hydroperoxide diol synthase	1.43	2.69
PA1078	flgC,flagellar basal-body rod protein FlgC	-1.42	2.68
PA2322	gluconate permease, gntP (also gntU/T)	-1.42	2.68
PA0744	probable enoyl-CoA hydratase/isomerase	1.42	2.68
PA3731	conserved hypothetical protein	1.42	2.68
PA1730	conserved hypothetical protein	-1.41	2.66
PA0059	osmC,osmotically inducible protein OsmC	-1.41	2.66
PA2244	pslN,hypotetical protein	-1.40	2.64
PA3092	fadH1,2,4-dienoyl-CoA reductase FadH1	-1.40	2.64
PA3732	Uncharacterized protein	1.40	2.64
PA1912	femI,ECF sigma factor, FemI	1.40	2.63
PA1242	sprP,SprP	-1.40	2.63
PA3691	hypothetical protein	-1.39	2.61
PA1077	flgB,flagellar basal-body rod protein FlgB	-1.38	2.60
PA2462	hypothetical protein	1.38	2.60
PA5181.1	P34, non-coding RNA gene	-1.38	2.59
PA2444	glyA2,serine hydroxymethyltransferase	1.37	2.59
PA4364	hypothetical protein	1.37	2.59

PA2136	hypothetical protein	-1.37	2.58
PA5510	probable transporter	1.37	2.58
PA4859	probable permease of ABC transporter	1.37	2.58
PA2182	hypothetical protein	-1.37	2.58
PA0795	prpC,citrate synthase 2	1.36	2.57
PA1363	ECF sigma factor	-1.36	2.57
PA4149	conserved hypothetical protein	-1.36	2.57
PA1364	probable transmembrane sensor	-1.36	2.56
PA0546	metK,methionine adenosyltransferase	1.35	2.56
PA3766	probable aromatic amino acid transporter	-1.35	2.56
PA1404	hypothetical protein	-1.35	2.55
PA5097	probable amino acid permease	1.35	2.54
PA1727	mucR,MucR	1.34	2.54
PA1907	hypothetical protein	-1.34	2.53
PA2192	conserved hypothetical protein	-1.34	2.53
PA0840	probable oxidoreductase	1.34	2.53
PA0547	probable transcriptional regulator	1.34	2.53
PA2755	eco,ecotin precursor	-1.33	2.52
PA3659	probable aminotransferase	1.32	2.50
PA5509	hypothetical protein	1.32	2.49
PA5482	hypothetical protein	-1.31	2.48
PA1041	probable outer membrane protein precursor	-1.31	2.47
PA1253	lhpG,alpha-ketoglutaric semialdehyde dehydrogenase, LhpG	1.30	2.46
PA5374	betI,transcriptional regulator BetI	-1.30	2.46
PA2167	hypothetical protein	-1.29	2.44
PA3888	opuCD,OpuC ABC transporter, permease protein, OpuCD	-1.29	2.44
PA4092	hpaC,4-hydroxyphenylacetate 3-monooxygenase small chain	-1.28	2.43
PA1608	probable chemotaxis transducer	1.28	2.42
PA2176	hypothetical protein	-1.27	2.42
PA3719	armR,antirepressor for MexR, ArmR	1.27	2.41

PA1473	hypothetical protein	1.27	2.41
PA1079	flgD,flagellar basal-body rod modification protein FlgD	-1.27	2.41
PA3692	lptF,Lipotoxon F, LptF	-1.27	2.40
PA2465	hypothetical protein	-1.26	2.40
PA3222	hypothetical protein	-1.25	2.38
PA2728	hypothetical protein	1.25	2.37
PA4706	phuV,PhuV	-1.24	2.37
PA0417	chpE,probable chemotaxis protein	1.24	2.37
PA3485	tsi3,Tsi3	1.24	2.37
PA0817	probable ring-cleaving dioxygenase	-1.24	2.36
PA5375	betT1,BetT1	-1.24	2.36
PA3119	conserved hypothetical protein	-1.24	2.36
PA0046	hypothetical protein	1.24	2.36
PA2168	hypothetical protein	-1.23	2.35
PA2236	pslF,PslF	1.23	2.35
PA5550	glmR,GlmR transcriptional regulator	-1.23	2.34
PA1690	pscU,translocation protein in type III secretion	1.23	2.34
PA1726	bglX,periplasmic beta-glucosidase	1.22	2.34
PA3898	probable transcriptional regulator	1.22	2.33
PA1323	hypothetical protein	-1.22	2.33
PA0047	hypothetical protein	1.22	2.33
PA5508	pauA7,Glutamylpolyamine synthetase homologue	1.21	2.32
PA2234	pslD,PslD	1.21	2.31
PA1457	cheZ,chemotaxis protein CheZ	-1.20	2.30
PA4489	magD,MagD	1.20	2.30
PA2329	probable ATP-binding component of ABC transporter	1.20	2.30
PA2641	nuoF,NADH dehydrogenase I chain F	1.20	2.29
PA0441	dht,dihydropyrimidinase	1.19	2.28
PA5492.1	ersA, non-coding RNA gene	-1.19	2.28
PA4341	probable transcriptional regulator	-1.18	2.27

PA0747	probable aldehyde dehydrogenase	1.18	2.27
PA0146	conserved hypothetical protein	-1.18	2.27
PA1724	pscK,type III export protein PscK	1.17	2.26
PA2328	hypothetical protein	1.17	2.26
PA2247	bkdA1,2-oxoisovalerate dehydrogenase (alpha subunit)	-1.17	2.25
PA2604	conserved hypothetical protein	-1.17	2.25
PA1324	hypothetical protein	-1.17	2.25
PA0866	aroP2,aromatic amino acid transport protein AroP2	-1.17	2.25
PA3484	tse3,Tse3	1.16	2.24
PA1105	fliJ,flagellar protein FliJ	-1.16	2.24
PA4587	ccpR,cytochrome c551 peroxidase precursor	1.16	2.23
PA4156	fvbA,FvbA	-1.16	2.23
PA4023	probable transport protein	-1.15	2.22
PA2543	conserved hypothetical protein	-1.15	2.21
PA3689	probable transcriptional regulator	-1.14	2.21
PA1449	flhB,flagellar biosynthetic protein FlhB	-1.14	2.21
PA2185	katN,non-heme catalase KatN	-1.14	2.21
PA1691	pscT,translocation protein in type III secretion	1.14	2.20
PA3889	opuCC,OpuC ABC transporter, periplasmic substrate-binding protein, OpuCC	-1.14	2.20
PA5433	conserved hypothetical protein	-1.14	2.20
PA3727	hypothetical protein	1.13	2.19
PA3190	probable binding protein component of ABC sugar transporter	1.13	2.19
PA4635	conserved hypothetical protein	-1.13	2.19
PA4326	hypothetical protein	1.13	2.19
PA2235	pslE,PslE	1.12	2.18
PA0151	probable TonB-dependent receptor	-1.12	2.18
PA1243	probable sensor/response regulator hybrid	-1.12	2.17
PA2330	hypothetical protein	1.12	2.17
PA2566.1	Uncharacterized protein	1.11	2.16
PA4322	conserved hypothetical protein	1.11	2.16

PA4487	magF,MagF	1.11	2.16
PA5529	probable sodium/proton antiporter	-1.11	2.16
PA1871	lasA,LasA protease precursor	-1.11	2.15
PA5528	hypothetical protein	-1.10	2.15
PA2238	pslH,PslH	1.10	2.14
PA3391	nosR,regulatory protein NosR	1.10	2.14
PA1177	napE,periplasmic nitrate reductase protein NapE	-1.10	2.14
PA5160	drug efflux transporter	1.09	2.13
PA3610	potD,polyamine transport protein PotD	1.09	2.13
PA2640	nuoE,NADH dehydrogenase I chain E	1.08	2.12
PA0871	phhB,pterin-4-alpha-carbinolamine dehydratase	-1.08	2.12
PA1229	probable transcriptional regulator	1.08	2.11
PA2175	hypothetical protein	-1.07	2.10
PA2389	pvdR,PvdR	-1.07	2.10
PA0776	hypothetical protein	-1.07	2.10
PA0124	hypothetical protein	1.07	2.10
PA0355	pfpI,protease PfpI	-1.07	2.10
PA4876	osmE,osmotically inducible lipoprotein OsmE	-1.07	2.09
PA2729	hypothetical protein	1.06	2.09
PA0172	siaA,SiaA	1.06	2.09
PA4714	conserved hypothetical protein	-1.06	2.09
PA4738	conserved hypothetical protein	-1.06	2.08
PA3862	dauB,NAD(P)H-dependent anabolic L-arginine dehydrogenase, DauB	1.06	2.08
PA2555	probable AMP-binding enzyme	1.06	2.08
PA3863	dauA,FAD-dependent catabolic D-arginine dehydrogenase, DauA	1.06	2.08
PA3221	csaA,CsaA protein	-1.05	2.07
PA2561	ctpH,CtpH	1.05	2.07
PA1152	hypothetical protein	-1.05	2.07
PA5415	glyA1,serine hydroxymethyltransferase	1.04	2.06
PA5027	hypothetical protein	-1.04	2.06

PA0819	hypothetical protein	-1.04	2.05
PA4772	probable ferredoxin	1.04	2.05
PA3361	lecB,fucose-binding lectin PA-IIL	1.04	2.05
PA4151	acoB,acetoin catabolism protein AcoB	-1.04	2.05
PA0797	probable transcriptional regulator	1.04	2.05
PA4663	moeB,molybdopterin biosynthesis MoeB protein	1.03	2.05
PA0777	hypothetical protein	-1.03	2.04
PA0369	Uncharacterized protein	1.03	2.04
PA3106	probable short-chain dehydrogenase	1.03	2.04
PA5366	pstB,ATP-binding component of ABC phosphate transporter	1.03	2.04
PA4311	conserved hypothetical protein	-1.02	2.03
PA4855	purD,phosphoribosylamine--glycine ligase	1.02	2.03
PA4207	mexI,probable Resistance-Nodulation-Cell Division (RND) efflux transporter	1.02	2.03
PA3492	conserved hypothetical protein	1.02	2.03
PA2174	hypothetical protein	-1.02	2.03
PA2331	hypothetical protein	1.02	2.02
PA4680	hypothetical protein	1.02	2.02
PA2237	pslG,PslG	1.01	2.02
PA0045	hypothetical protein	1.01	2.02
PA2262	probable 2-ketogluconate transporter, kguT	-1.01	2.01
PA4205	mexG,hypotetical protein	1.00	2.01
PA1566	pauA3,Glutamylpolyamine synthetase	-1.00	2.00
PA2248	bkdA2,2-oxoisovalerate dehydrogenase (beta subunit)	-1.00	2.00
PA1786	nasS,NasS (nasF)	-1.00	1.99
PA0805	hypothetical protein	-0.99	1.99
PA0505	hypothetical protein	0.99	1.99
PA0089	tssG1,TssG1	0.99	1.99
PA2704	probable transcriptional regulator	-0.99	1.99
PA5549	glmS,glucosamine--fructose-6-phosphate aminotransferase	-0.99	1.99
PA5024	conserved hypothetical protein	0.99	1.98

PA3954	hypothetical protein	-0.99	1.98
PA0606	agtD,AgtD	0.98	1.98
PA2549	conserved hypothetical protein	-0.98	1.98
PA0177	probable purine-binding chemotaxis protein	0.98	1.98
PA4488	magE,MagE	0.98	1.98
PA1035	hypothetical protein	-0.98	1.97
PA4365	lysE,Lysine efflux permease	0.98	1.97
PA4762	grpE,heat shock protein GrpE	0.98	1.97
PA0276	hypothetical protein	-0.98	1.97
PA4499	psdR,Pseudomonas dipeptide regulator, PdsR	-0.97	1.97
PA3183	zwf,glucose-6-phosphate 1-dehydrogenase	-0.97	1.96
PA1410	probable periplasmic spermidine/putrescine-binding protein	0.97	1.96
PA0439	probable oxidoreductase	0.97	1.96
PA1784	hypothetical protein	-0.97	1.96
PA4507	hypothetical protein	-0.97	1.95
PA1512	hcpA,secreted protein Hcp	-0.96	1.95
PA5367	pstA,membrane protein component of ABC phosphate transporter	0.96	1.95
PA4321	hypothetical protein	0.96	1.95
PA4739	conserved hypothetical protein	-0.96	1.95
PA3064	pelA,PelA	-0.96	1.94
PA2259	ptxS,transcriptional regulator PtxS	-0.96	1.94
PA2080	kynU,kynureninase KynU	0.96	1.94
PA1600	probable cytochrome c	0.95	1.94
PA2239	pslI,PslI	0.95	1.93
PA4558	probable peptidyl-prolyl cis-trans isomerase, FkbP-type	0.95	1.93
PA2232	pslB,PslB	0.95	1.93
PA5159	multidrug resistance protein	0.95	1.93
PA3351	flgM,FlgM	-0.95	1.93
PA3890	opuCB,OpuC ABC transporter, permease protein, OpuCB	-0.95	1.93
PA5113	hypothetical protein	0.95	1.93

Appendix F: Metabolites identified in interactions with *P. aeruginosa* and *S. aureus*

Molecular Weight	# Replicates for PA2 vs SA4	# Replicates for PA4 vs SA2	Chemical Formula	Possible Name	Database ID			
					ChemSpider	mzCloud	PAMDB	KEGG
137.048	4/6	6/6	C7 H7 N O2	Aminobenzoic acid / Anthranilic acid	5369, 7141, 21106146, 4963, 471845, 21111785, 106, 9695869, 953, 76947, 222, 4514255, 58563, 21106144, 13863774	806, 593, 224, 113, 219, 244, 181, 3273	PAMDB000262	C01004, D01811, C00568, C00108
187.096	1/6	3/6	C7 H13 N3 O3	5-guanidino-3-methyl-2-oxopentanoic acid	27471432	n/a	n/a	n/a
225.097	1/6	1/6	n/a	n/a	n/a	n/a	n/a	n/a
261.111	2/6	1/6	C13 H15 N3 O3	Trp-Gly / Gly-Trp	49445, 92825, 231453	3112	n/a	C18864
519.181	1/6	1/6	n/a	n/a	n/a	n/a	n/a	n/a
657.502	1/6	1/6	n/a	n/a	n/a	n/a	n/a	n/a

Molecular Weight	# Replicates for PA2 vs SA2	# Replicates for PA4 vs SA4	Chemical Formula	Possible Name	ChemSpider ID
297.267	1/6	1/6	C18 H35 N O2	UNII:OUT5YHB7BO	77719, 167832, 8011589, 8014930, 4444423
368.365	1/6	2/6	C24 H48 O2	Lignoceric acid	4471748, 35013963, 35013962, 4471749, 4445732, 35015041, 4471746, 10724